

PROCEEDINGS
OF
ASIAN COSMIC RAY SYMPOSIUM
ON
SECONDARY COSMIC RAYS

Department of Physics
University of Hong Kong
20–23 December 1976

UNIVERSITY OF HONG KONG
LIBRARY



*This book was a gift
from*
Organizing Committee,
Asian Cosmic Ray Symposium on
Secondary Cosmic Rays,
Hong Kong

PREFACE

This volume constitutes the proceedings of an Asian regional symposium on the Secondary Cosmic Radiation held in Hong Kong from December the 20th to 23rd 1976. The symposium was sponsored by the departments of physics in the University of Hong Kong, the Chinese University of Hong Kong and the Department of Applied Sciences of Hong Kong Polytechnic, and had as its aims to discuss, on the one hand new results and future developments in the field of secondary cosmic ray research, and on the other the role that secondary cosmic rays could play in the teaching of high energy physics in institutes and universities which lack the sophisticated equipment generally necessary in this field.

About 30 scientists took part in the four day event. Scientific sessions were held at the University of Hong Kong, except on December the 23rd when the venue moved to the Chinese University campus at Shatin, and a total of 36 papers were presented.

The organising committee wishes to express its thanks to the authorities in the two universities and the polytechnic for their support, and to the following companies for their generous financial support which contributed in no small measure to the success of the symposium:

Cable and Wireless Ltd.
Hand Seng Bank Ltd.
Schmidt and Co. (H.K.) Ltd.
Dow Chemical Pacific Ltd.
Stephen S.F. Hui.
Nissei Sangyo Co., Ltd.
Patrick Trading Corporation.
Semiconductor Devices Ltd.
Harvey Main and Co., Ltd.

Thanks are also due to the secretarial and technical staff of the department of physics, University of Hong Kong, for their valuable efforts in support of the symposium, and especially to Miss T. Villa Carlo and Mrs. L. Liu for their assistance in the compilation of the proceedings.

Finally a grant from the Committee for Scientific Coordination, Hong Kong, towards the production of these proceedings is gratefully acknowledged.

Organising Committee

Professor A.J. Lyon (H.K.U.), Chairman.

Dr. L.S. Chuang (C.U.H.K.)

Dr. K.S. Lau (H.K. Polytechnic)

Dr. P.K. MacKeown (H.K.U.), Secretary.

Dr. L.K. Ng (H.K.U.)

1st March 1977.

CONTENTS

Opening Address	G.J. Bell. 1
Measurements of the Energy Spectrum of Vertical Cosmic Ray Muons at Sea Level with Emulsion Chamber.	
M. Akashi, Z. Watanabe, I. Ohta, A. Misaki, K. Mizutani, K. Kasahara, T. Yuda, I. Mito, T. Shirai, T. Taira, N. Tateyama, M. Shibata, K. Taira, S. Torii and Y. Takahashi..	4
Analysis of Data from a Cosmic Ray Muon Magnetic Spectrograph.	
S.K. Chan and K.S. Lau.	5
A Muon Telescope for the Measurement of the Spectra and Zenith Angle Dependence of Slow Muons.	
L.S. Chuang and M. Wada.	25
Calculation of Muon Momentum Spectra at Sea Level.	
K. Murakami, S. Sagisaka, A. Inoue, Y. Mishima and K. Nagashima.	34
Predicted and Recently Observed Muon Spectra at Sea Level (Read by title only).	
C.R. Paul, N.L. Karmakar and N. Chaudhuri.	44
Dao Scaling Model and Sea Level Cosmic Ray Muon Spectrum from Goodard Space Flight Group Measured Primary Proton Spectrum. (Read by title only).	
D.P. Bhattacharyya, R.K. Roychoudhury and D. Basu...	50
Sea Level Muon Spectrum Derived from GSFC Measured Nucleon Spectrum using CKP Model. (Read by title only).	
Kalpana Sarkar, D.P. Bhattacharyya and D. Basu.	57
Measurements of Deep Underground Intensities of High Energy Muons.	
K. Mizutani and I. Ohta.	64
An Analysis of Energy Spectrum of Muon.	
H. Komori	65
Analysis of Predicted and Observed Energy Loss Rate of Cosmic Ray Muons Penetrating Great Depths in Rock and Water. (Read by title only).	
C.R. Paul, N.L. Karmakar and N. Chaudhuri.	70
Average Energies and Differential Energy Spectrum of Muons at Various Depths.	
A. Misaki and J. Nishimura	73

Electromagnetic Interactions of Cosmic Ray Muons at Low Transfer Energies.	
S.Y. Lau and L.K. Ng.	74
Nuclear Interaction Cross Section of Cosmic Ray Muons from the Results of the Accelerator Experiments.	
T. Kitamura.	81
Muon Interactions in Mutron Calorimeter.	
T. Aoki, S. Higashi, K. Honda, S. Iida, Y. Kamiya, H. Kawashima, T. Kitamura, K. Kobayakawa, S. Mikamo, Y. Minorikawa, K. Mitsui, S. Miyake, Y. Muraki, I. Nakamura, Y. Ohashi, A. Okada, S. Ozaki, H. Shibata, T. Takahashi and Y. Teramoto.	94
Monte Carlo Simulation of Mutron Calorimeter.	
K. Mitsui, A. Okada and M. Shibata.	95
Cerenkov Radiation from a Shower Developed in the Deep Water.	
J. Nishimura.	96
The Experimental Determination of Charge Ratio of Cosmic Ray Muons in 0.2 - 0.8 GeV/c Momentum Range at a Low Latitude Station. (Read by title only).	
K.P. Singhal	111
Computation of the Muon Charge Ratio of Cosmic Rays at Large Zenith Angles.	
L.K. Ng and C.H. Poon.	112
A System for Measuring the Muon Charge Ratio in Small Air Showers.	
C.C. Lai, S.H. Leung, S.K. Leung, S.W. Fong and L.K. Ng ...	117
Possible Structure in the Muon Charge Ratio at Large Zenith Angles.	
P.K. MacKeown.	126
Arrival Direction Dependence of Muon Charge Ratio.	
S. Higashi, K. Honda, S. Iida, Y. Kamiya, Y. Kawashima, T. Kitamura, K. Kobayakawa, S. Mikamo, Y. Minorikawa, K. Mitsui, S. Miyake, Y. Muraki, I. Nakamura, Y. Ohashi, A. Okada, S. Ozaki, H. Shibata, S. Shibata, T. Takahashi and Y. Teramoto.	133
Charge Ratio of Cosmic Ray Pions in the Atmosphere (Read by title only).	
D.P. Bhattacharyya, R.K. Raychoudhury and Kalpana Sarkar	141

Electrons and Muons in Large Air Showers observed at Chacaltaya and the Energy Spectrum of Primary Cosmic Rays from 10^{16} eV to 10^{19} eV.	
C. Aguirre, G.R. Mejia, T. Kaneko, P.K. MacKeown, K. Suga, F. Kakimoto, Y. Mizumoto, K. Murakami, K. Nishi, M. Nagano, K. Kamata, Y. Toyoda, H. Yoshii.	147
E.A.S. Simulations in the Primary Energy Range 10^{12} eV - 10^{16} eV.	
A.K. Lee.	160
On the Correlation between the Optical Cerenkov Pulses and the Radio Pulses from Extensive Air Showers.	
D.C. Goswami and K.M. Pathak.	177
Studies on Optical Cerenkov Radiation in Association with Radio Pulses in Extensive Air Showers.	
D.C. Goswami and K.M. Pathak.... ..	188
Charge Ratio of Electrons in Extensive Air Showers.	
S.W. Fong and L.K. Ng.	197
Some Experiments Conducted in the University of Singapore on Cosmic Ray Muons with Cerenkov Liquid Scintillation Counters.	
M. Huq.	204
Numerical Solution of Integro Differential Equation - Early Development of Cascade Shower.	
A. Misaki and I. Mito.	216
A Computer Experiment in Cosmic Ray Physics - Monte Carlo Simulation of Cascade Shower.	
E. Konishi, A. Misaki and G. Watanabe.... ..	217
Akeno Air Shower Project.	
K. Kamata.	218
Energy Spectra of Splash Albedo Electrons of Cosmic Radiations. (Read by title only).	
S.D. Verma.	226
Resource Letter on Cosmic Ray Experiments in the Undergraduate Laboratory.	
K.B. Luk.	227
On the Teaching of Cosmic Ray Physics for Undergraduate Studies in a Private University in Japan.	
M. Ohta.	234

Updating a Research Laboratory for Social Demand (A case in Nuclear Sciences).	
L.S. Chuang.	241
Fundamental Idea which is derived from the Concept of Collaboration among Asian Countries.	
A. Misaki, Y. Muraki and I.Ohta.	253
List of Participants.	x
Author index.	xii

SECTION A

OPENING ADDRESS

Gordon J. Bell, OBE, AE, JP,
Chairman, Committee for Scientific Coordination, Hong Kong-

Ladies and Gentlemen,

I am most grateful to the organizing committee of this symposium for asking me to say a few words at the opening of your discussions on Secondary Cosmic Rays.

I have been asked to do so in my capacity as Chairman of the Hong Kong Committee for Scientific Co-ordination. This committee is the focal point for science in Hong Kong and is composed of scientists from Government, both local universities and the Polytechnic. I like to think of it as a nucleus from which one day will grow an Academy of Science.

In addition to giving this meeting its best wishes and every encouragement the Committee hopes to be able to assist in publishing your proceedings.

There is another reason why I am pleased to be here to-day. As a physicist myself I am delighted to be present at the opening of what I think is the first international gathering of physicists in Hong Kong. When I first became associated with the Physics Department of this University some 27 years ago, the number of active physicists in the Territory did not amount to two figures. In the last thirteen years we have not only seen the growth of this department and of Government science but we have also seen the birth of the Chinese University and the Polytechnic. I am therefore delighted to see that workers in the field of cosmic rays from all three academic institutions have joined together to organise this meeting.

We seem now to have attained a critical mass of physicists by which, I do not mean that they are about to be dispersed in an uncontrolled explosion but, rather, that they are now adequate in numbers to achieve this first step in what I hope will be a controlled growth of meetings and symposia in the years to come.

It is not often that we in Hong Kong are hosts to an international meeting which discusses esoteric problems far removed from the practicalities of everyday life. The pressures here are such that more mundane matters must take priority if we are to make fast headway to improve the standard of life of the over 4 million souls in this small territory. However, as part of the process of raising the quality of life of the people, we have in recent years seen considerable progress made by Government, institutions and dedicated individuals in providing facilities and entertainment in the arts. We now have a regular and successful Arts Festival, a professional symphony orchestra and much greater activity in the arts generally. Pure science as an educational and cultural activity is also growing but, by its very nature, rather less noticeably. Apart from the steady increase in the number of scientific symposia held here, there is an increasing number of science based exhibitions and increasing activity amongst the specialist scientific societies. However, some central meeting hall and lecture facilities are still greatly needed. The Urban Council is currently building a planetarium in the Cultural Complex and their plans for a science museum are well advanced. It is to be hoped that the momentum gained in providing these cultural facilities will be increased in the next few years.

I have always urged that the main thrust of research in physics in Hong Kong should be in the field of geophysics. So many other specialisations in physics require enormous sums of money to be spent on equipment if work on the frontiers of knowledge is to be undertaken. However, in geophysics we can make considerable contributions to science by making relatively inexpensive measurements here at Hong Kong at Latitude 22 N Longitude 114 E. I am very pleased that much of the ionospheric, magnetic, meteorological and cosmic ray activities are making progress in this direction.

It is about 75 years ago that the first hints of the existence of a non-terrestrial penetrating radiation were first revealed and the hunt for cosmic rays initiated. The study of cosmic rays is unique in ranging over the greatest possible scale from the astronomical to the sub-nuclear. Practitioners of nuclear physics are usually thought of as consuming a disproportionate share of science funds to build ever larger accelerators. Their colleagues who approach the subject through cosmic rays, using nature's own accelerators are often forgotten. Yet it is they who can be said to have started the study of elementary particles through their discovery of the positron in cosmic radiation.

I notice that you intend also to discuss the role of cosmic rays in the teaching of physics. As in so many scientific fields today our knowledge changes so rapidly that it is constantly necessary to examine what should be taught and how.

It only remains for me to wish you every success in your deliberations and to hope that our visitors enjoy their stay in Hong Kong and, finally, to declare this symposium open.

Measurements of the Energy Spectrum of Vertical Cosmic Ray Muons
at Sea Level with Emulsion Chamber.

M. Akashi and Z. Watanabe (Hirosaki University, Hirosaki, Japan),
I. Ohta (Utsunomiya University, Utsunomiya, Japan), A. Misaki and
K. Mizutani (Saitama University, Urawa, Japan), K. Kasahara and
T. Yuda (Cosmic Ray Laboratory, University of Tokyo, Tokyo,
Japan), I. Mito (Shibaura Institute of Technology, Tokyo, Japan),
T. Shirai, T. Taira and N. Tateyama (Kanagawa University,
Yokohama, Japan), M. Shibata (Yokohama National University,
Yokohama, Japan), K. Taira (Sagami Institute of Technology,
Fujisawa, Japan), S. Torii (Kyoto University, Kyoto, Japan) and
Y. Takahashi (Osaka University, Osaka, Japan).

The energy spectrum of vertical cosmic ray muons has been measured with the emulsion chamber exposed at shallow depth underground. The emulsion chamber of the present observations is constituted by nuclear emulsion plates, X-ray films and lead plates.

The energy spectrum of oblique muons was measured with the emulsion chamber arranged horizontally of the total amount of exposure of 61.6 ton years. The results gave indirectly the energy spectrum of vertical muons at sea level in the energy range 1 TeV to 10 TeV. The present results have been performed with the emulsion chamber arranged vertically of the amount of exposure of 12.7 ton years. The results of the vertical intensities of cosmic ray muons at sea level are not inconsistent with the results given indirectly from oblique muons, of the energies around 1 TeV.

ANALYSIS OF DATA FROM A COSMIC RAY MUON

MAGNETIC SPECTROGRAPH

S.K. Chan,

Department of Physics, University of Hong Kong, Hong Kong,

K.S. Lau,

Department of Applied Sciences, Hong Kong Polytechnic,

Hong Kong, and

E.C.M. Young,

Department of Physics, University of Hong Kong, Hong Kong.

Abstract

Analysis of data obtained with the cosmic ray solid iron magnetic spectrograph at Hong Kong has been carried out. The method of fitting the muon trajectories, determination of the muon momentum and the various corrections to the basic data are described. The corrected intensities are used to fit a phenomenological expression of the form $A_{\pi} E_{\pi}^{-\gamma}$ for the differential pion production spectrum, based on the appropriate diffusion equation. The resulting best fit yields: $A_{\pi} = 0.21 \pm 0.01$ and $\gamma = 2.68 \pm 0.01$ when the kaons to pions ratio K/π is set at 0.15.

In this paper the procedures of converting the basic data from a solid iron magnetic spectrograph into absolute muon intensities are reported. The resulting vertical muon differential and integral spectra are discussed.

The spectrograph

The solid iron magnetic spectrograph at Hong Kong (Lau et al, 1971) has been modified by improving its timing and spatial resolutions in an aim to measure absolute intensities. Four plastic scintillation counters are used as the triggering elements, and five trays of high pressure neon flash tubes (ext. dia. 7.5 mm and wall thickness 1.05 mm) are used as the track location devices. The muon trajectories are recorded on film, and by subsequently scanning the film the events are reconstructed.

Over-all height	560 cm
Zenith angle	0-4.5 degrees
Acceptance for infinite momentum	11.48 cm ² -sr
Magnetic flux density	16.58±0.15 kilogauss
Field line integral, $\int Bdl$	2.5x10 ⁶ gauss-cm
Maximum detectable momentum	497 GeV/c
Momentum cut-off	2.40 GeV/c
Dimension of magnet	150x120x75 cm ³
Power dissipation of magnet	0.7 KW
Counting rate of spectrograph	70 particles per hour

Parameters of the spectrograph.

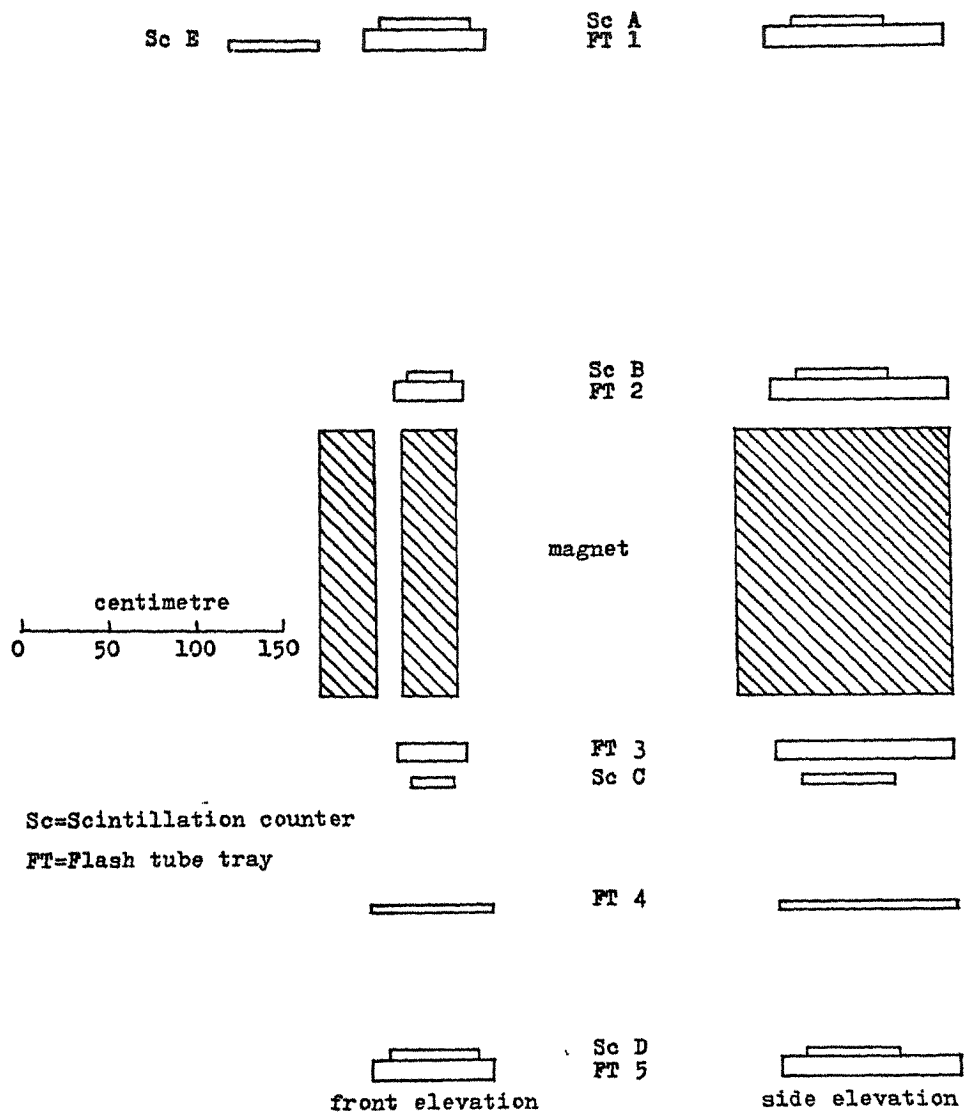


Fig. 1 Schematic diagram of the spectrograph.

The least squares fit of the muon trajectories and the angular resolution of the spectrograph

Muon trajectories above and below the magnet are found by the method of least squares fit to the excited flash tubes. The uncertainty in the position of traversal of a particle through an excited tube is taken into account by introducing into the theory of fitting a probability

$P(\Delta)d\Delta$ = Probability that the particle crosses the horizontal diameter of an excited tube at position Δ to $\Delta+d\Delta$ as shown below.

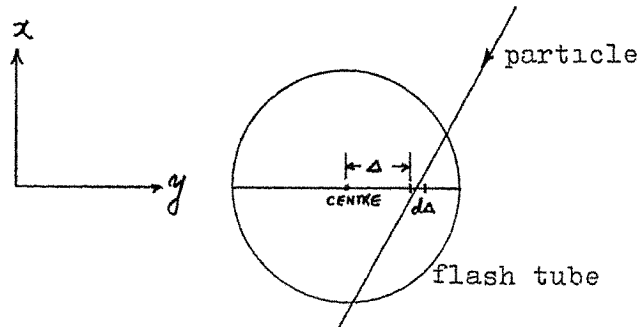


Fig.2 Traversal of a particle through a tube at Δ to $\Delta+d\Delta$ from the centre

Thus to fit a straight line of the form $y = a + bX$ through k excited flash tubes, we require that

$$D = \sum_{i=1}^k \int_{-r}^r P(\Delta) [\delta y_i(\Delta)]^2 d\Delta \quad (1)$$

is a minimum. $\delta y_i(\Delta)$ is the deviation from the best line of a point measured Δ horizontally from the centre of the i th excited tube. To allow for some ambiguous knock-on electrons, r will be greater than the flash tube radius.

Assuming $P(\Delta)$ is a symmetrical function, the calculation gives

$$a = \frac{\sum x_i^2 \sum y_i - \sum x_i \sum x_i y_i}{k \sum x_i^2 - (\sum x_i)^2} \quad (2)$$

$$b = \frac{k \sum x_i y_i - \sum x_i \sum y_i}{k \sum x_i^2 - (\sum x_i)^2} \quad (3)$$

where the summation is from 1 to k .

Thus the uncertainty in the position of traversal of a tube by the particle does not affect the fitting of the incident and emergent trajectories. However, the error of the gradient (b) does depend on this uncertainty. Since the angle of deflection by the magnet depends on the gradients of the incident and emergent trajectories, the traversal uncertainty thus has an effect on the angular resolution of the spectrograph. It can be proved that

the standard error of the gradient (b) is

$$S_b = \sqrt{\frac{D}{k-2} \cdot \frac{k}{k \sum x_i^2 - (\sum x_i)^2}} \quad (4)$$

and the standard error of the angular deflection (ϕ) is

$$S_\phi = \sqrt{\left(\frac{S_{b_1}}{1+b_1^2}\right)^2 + \left(\frac{S_{b_2}}{1+b_2^2}\right)^2} \quad (5)$$

where b_1, b_2 are the gradients of the incident and emergent trajectories respectively, and S_{b_1}, S_{b_2} are their standard errors.

The value of D depends only on the integral

$$\int_{-r}^r \Delta^2 P(\Delta) d\Delta \quad \text{which can be interpreted as the variance of the distribution of}$$

the y - coordinates of the centres of the excited tubes about the muon track. This integral has been evaluated experimentally by selecting some 1020 single events which correspond to muon momentum greater than 15GeV/c, the effect of multiple scattering is thus negligible for these events. We fit the best straight lines through the excited

tubes in each event; the deviations of the y-coordinates of the centres of the flash tubes about the fitted lines are found for each excited tube and for each event selected. The standard deviation of the distribution of the y-coordinates of the centres of some 21,220 excited tubes about their best lines is evaluated to be 0.196 ± 0.001 cm. Thus

$$\int_{-r}^r \Delta^2 p(\Delta) d\Delta = 0.0384 \pm 0.0004 \text{ cm}^2$$

Taking this integral into account, the m.d.m. of the spectrograph is 500 GeV/c.

Determination of the muon momentum

The trajectory of the muon inside the magnetic volume is a spiral of decreasing radius of curvature. However, by fitting the incident and emergent trajectories, the deflection (ϕ) due to the magnetic field can be computed directly irrespective of the trajectory inside the magnet.

$$\phi = \tan^{-1} b_2 - \tan^{-1} b_1 \quad (6)$$

To ensure that the spiral trajectory is within the magnetic edges, an effective width of the magnet is defined. For small zenith angles of the incident muons,

the effective width is greater than the physical width
by 2W,

$$W = h \left(\tan \frac{\phi}{2} - \tan \frac{\phi}{4} \right) \quad (7)$$

where h is the half-height of the magnet. The fitted trajectories should therefore intersect near the middle of the magnet and within this effective width.

After testing for the validity of the fitted tracks, the momentum (P) of the muon can be evaluated by numerically iterating on the computer the equation

$$P = \frac{\alpha(P) l}{1 - \exp\left(\frac{-\alpha(P) l}{300B}\right)} \quad (8)$$

$\alpha(P)$ is the momentum loss per unit length at the momentum P, l is the total path length inside the magnet and B is the flux density.

Methodological corrections to the basic data to obtain the absolute differential spectrum

The basic data consist of the running time of the spectrograph, the total number of particles incident on the spectrograph during its running time and the photographic records of a major portion of these particles.

The correction applied to the basic data can be classified into two categories - the corrections to the running time and the corrections to the total number of particles.

The corrections to the running time include:-

- (i) The resolving-times of the scintillation counters and the coincidence circuit.
- (ii) Dead-time of the electromagnetic register used to record the counts, and
- (iii) Paralysis-time on the coincidence-gate due to the anti-shower scintillation counter (E)

The corrections to the total number of particles include:-

- (i) Correction due to the efficiencies of the counters.
The efficiency for single muon events is 0.9618 ± 0.0054 .

- (ii) Correction due to the contamination of shower events.

The shower-reducing device has already removed the majority of the showers or multiple-muons incident on the spectrograph; however, due to the inefficiency of the device there is still a small number of shower or multiple-muons which have triggered the spectrograph.

- (iii) Correction due to impurities in the muon beam.

The possible major contaminations in the muon beam after traversing through the magnet are protons and pions. The differential spectra of proton and pion at sea-level due to Brooke et al (1964, 1973) have been used to predict the total number of these particles incident on the spectrograph during its total running time.

When the width of the pulses at the coincidence gate is equal to 150 ns the variation of the arrival time of the pulses at the gate is found to produce no loss of counts, and chance coincidence is insignificant.

(iv) Correction due to sampling of analysed events.

After applying the above corrections to the basic data, the effective running time (T) of the spectrograph and the total number (N) of single-muons that have entered into the solid angle of the spectrograph are found. Now of these N single-muon events we will only be able to analyse a major portion and obtain a momentum distribution from it. If this portion is assumed to be a random sample of the grand total, then it is necessary to normalize the momentum distribution of the sample to a total number of N .

The normalized distribution of muons are then subjected to the momentum dependent corrections which include:-

(v) The correction due to particles scattered out or into the solid angle of the spectrograph by the magnetic field.

When a muon of momentum P enters into the solid angle of the spectrograph, the probability $f_1(P)$ that it is accepted by the instrument can be found by simulating particles through it on a computer. $1/f_1(P)$ is the correction factor for this effect.

(vi) The correction due to particles scattered out or into the solid angle of the spectrograph by multiple scatterings in the magnet.

The acceptance probability $f_2(P)$ at the momentum P due to multiple scatterings in the magnet can also be found by simulation on the computer as for magnetic scatterings. However multiple scatterings differ from magnetic scatterings in that the latter occur only in the plane perpendicular to the magnetic field while the former occur in all directions. $1/f_2(P)$ is the correction factor for this effect.

(vii) The correction due to momentum uncertainty.

Owing to the steepness of the muon spectrum, the momentum uncertainty has the effect of flattening it. The error of the momentum arises from two sources — the error due to multiple scatterings in the magnet and

the error due to the track location by the flash tubes. To facilitate computation, Allkofer's differential spectrum (1971) is converted into the deflection spectrum. Particles in a deflection interval are considered to be distributed in a Gaussian manner with mean equal to the mean deflection of the interval, and standard deviation equal to the r.m.s. value of the standard deviations due to multiple scatterings in the magnet and spatial resolution by the flash tubes. By comparing the number of particles originally in an interval with the sum of particles scattered into this interval from all the intervals, we thus obtain a correction factor $f_3(P)$ for this effect.

The correction factors $1/f_1(P)$, $f_2(P)$ and $f_3(P)$ are shown in Table 1.

MOMENTUM INTERVAL GeV/c	MEAN MOMENTUM P GeV/c	$\frac{1}{f_1(P) \cdot f_2(P)}$	$f_3(P)$
4 - 5	4.47	5.556	1.1688
5 - 6	5.47	2.481	1.0287
6 - 7	6.48	1.795	1.0053
7 - 8	7.48	1.493	0.9970
8 - 9	8.48	1.370	0.9913
9 - 10	9.48	1.289	0.9838
10 - 20	13.59	1.190	0.9697
20 - 30	24.11	1.072	0.9302
30 - 40	34.34	1.049	0.9343
40 - 50	44.47	1.035	0.9126
50 - 60	54.56	1.020	0.9090
60 - 70	64.62	1.017	0.9122
70 - 80	74.67	1.013	0.9152
80 - 90	84.70	1.010	0.9091
90 - 100	94.73	1.005	0.8939
100 - 150	119.51	1.000	0.8698
150 - 200	171.04	1.000	0.8578
200 - 300	238.33	1.000	0.8391
300 - 400	341.68	1.000	0.7715
400 - 500	443.51	1.000	0.6937

Table 1 The Momentum dependent correction factors

Since there are three trays of flash tubes below the magnet, most burst-production events in the magnet are included for analysis by using the two lower trays of flash tubes to fit the emergent trajectories. For this reason, the correction due to interactions in the magnet is neglected.

The data

The results of this paper are based on two sets of data. Set (I) was collected in 1972 by Lau et al and the other, set (II) was collected in 1975 by Chan et al. The latter set (II) of basic data is corrected for all the necessary corrections discussed above to obtain the absolute vertical differential muon spectrum in the range 4 - 500 GeV/c. The former Set(I) of data is corrected for the loss of particles due to magnetic and multiple scatterings, and for the effect of momentum uncertainty; it is then converted to intensities by normalizing at the point 13.59 GeV/c to the measured absolute spectrum. The two differential spectra are combined by weighing factor according to the numbers of collected particles in the respective momentum intervals where the spectra are normalized.

Momentum In- terval GeV/c	Mean mo- mentum GeV/c	Differential intensities $cm^{-2} \cdot sr^{-1} \cdot s^{-1} \cdot (GeV/c)^{-1}$			% error of average
		(I)	(II)	weighed average	
4 - 5	4.47	6.42×10^{-4}	6.30×10^{-4}	6.37×10^{-4}	2.4
5 - 6	5.47	4.30×10^{-4}	4.28×10^{-4}	4.29×10^{-4}	2.1
6 - 7	6.48	2.99×10^{-4}	3.15×10^{-4}	3.05×10^{-4}	2.0
7 - 8	7.48	2.59×10^{-4}	2.50×10^{-4}	2.56×10^{-4}	2.1
8 - 9	8.48	1.92×10^{-4}	1.83×10^{-4}	1.89×10^{-4}	2.3
9 - 10	9.48	1.50×10^{-4}	1.49×10^{-4}	1.50×10^{-4}	2.5
10 - 20	13.59	6.43×10^{-5}	6.43×10^{-5}	6.43×10^{-5}	1.2
20 - 30	24.11	1.72×10^{-5}	1.50×10^{-5}	1.64×10^{-5}	2.1
30 - 40	34.34	7.30×10^{-6}	6.31×10^{-6}	6.92×10^{-6}	3.3
40 - 50	44.47	3.24×10^{-6}	2.97×10^{-6}	3.14×10^{-6}	4.8
50 - 60	54.56	1.83×10^{-6}	1.55×10^{-6}	1.72×10^{-6}	6.4
60 - 70	64.62	1.11×10^{-6}	1.13×10^{-6}	1.12×10^{-6}	8.0
70 - 80	74.67	7.44×10^{-7}	7.59×10^{-7}	7.49×10^{-7}	9.7
80 - 90	84.70	4.69×10^{-7}	4.20×10^{-7}	4.50×10^{-7}	12.5
90 - 100	94.73	3.23×10^{-7}	3.59×10^{-7}	3.37×10^{-7}	14.3
100 - 150	119.51	1.30×10^{-7}	1.82×10^{-7}	1.50×10^{-7}	9.4
150 - 200	171.04	5.32×10^{-8}	2.61×10^{-8}	4.28×10^{-8}	17.7
200 - 300	238.33	1.63×10^{-8}	2.08×10^{-8}	1.80×10^{-8}	18.9
300 - 400	341.68	3.99×10^{-9}	1.03×10^{-8}	6.42×10^{-9}	30.2
400 - 500	443.51	1.79×10^{-9}	2.64×10^{-9}	2.12×10^{-9}	50.0

Table 2 The measured vertical muon differential intensitie

Results

In a theoretical analysis based on an expression $A_\pi E_\pi^{-\gamma}$ for the differential pion production spectrum in the appropriate diffusion equation, we have shown that the muon intensity at sea-level is given by the phenomenological form

$$I(E_\mu) = W_\mu A_\pi (E_\mu + \Delta E)^{-\gamma} \cdot \left(\frac{r_\pi^{\gamma-1} B_\pi}{E_\mu + \Delta E + B_\pi} + \frac{K r_k^{\gamma-1} B_k}{E_\mu + \Delta E + B_k} \right) \quad (10)$$

where $I(E_\mu)$ = muon intensity at sea-level at the energy E_μ ; W_μ = survival probability of muons from production to sea-level, and is given by Rossi (1952);

ΔE = energy loss from production to sea-level;

$B_\pi = 89.07 \text{ GeV}/c$; $B_k = 458.20 \text{ GeV}/c$; $r_\pi = 0.76$;

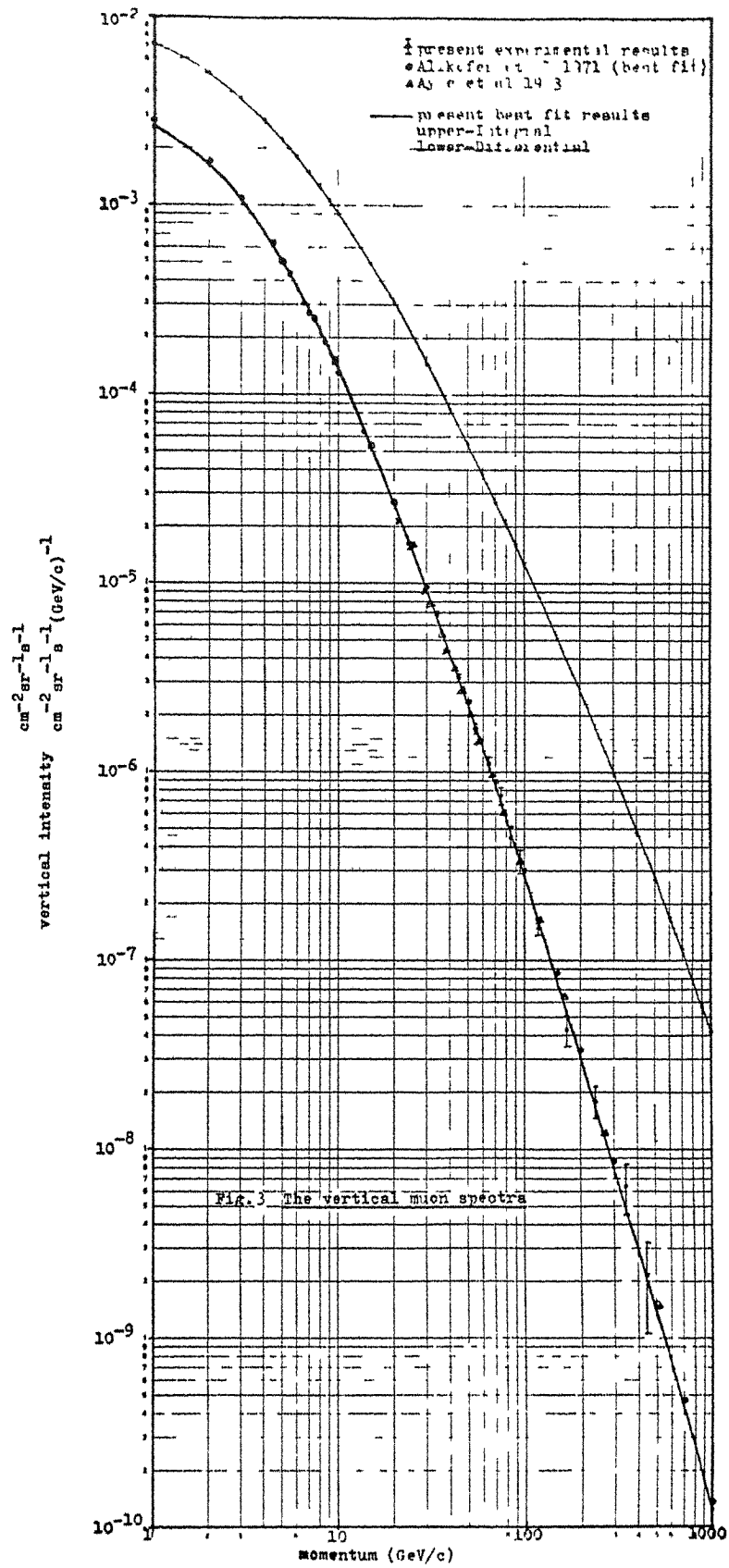
$r_k = 0.52$; and K = charged kaons to pions ratio.

The weighed average intensities in Table 2 are used to fit the above expression by the maximum likelihood technique. On the basis of recent accelerator measurements, K is set equal to 0.15 while A_π and γ are unknown parameters to be adjusted. The resulting best fit yields:

$$A_\pi = 0.21 \pm 0.01$$

$$\gamma = 2.68 \pm 0.01$$

From these best fit parameters, the differential



and integral intensities at sea-level are calculated at standard momenta. In Figure 3, both best fit spectra are presented together with the experimental data and some previous results. We see that within statistical limits, good agreement is obtained with the previous results of Allkofer et al (1971) and Ayre et al (1973).

Discussion

In Table 3, the best fit intensities are compared with the results of two independent absolute measurements in Hong Kong; the results of Ayre et al (1973) and Rossi's point are also shown.

Authors	Momentum GeV/c	Differential intensity $\text{cm}^{-2}\text{sr}^{-1}\text{s}^{-1}(\text{GeV}/\text{c})^{-1}$	Relative difference with pre- sent results
Rossi et al (1948)	1.00	2.45×10^{-3}	-8.6%
Lau et al (1973) Hong Kong	1.20	$(2.82 \pm 0.21) \times 10^{-3}$	14.6%
Authors	Momentum GeV/c	Integral intensity $\text{cm}^{-2}\text{sr}^{-1}\text{s}^{-1}$	Relative difference with pre- sent results
Lau et al (1973) Hong Kong	1.10	$(6.73 \pm 0.025) \times 10^{-3}$	- 2.5%
Ayre et al(1973) Durham	3.5 7.1	2.85×10^{-3} 1.34×10^{-3}	-11.8% - 8.2%
Kong et al (1975) Hong Kong	4.81 5.485	$(2.59 \pm 0.10) \times 10^{-3}$ $(1.95 \pm 0.07) \times 10^{-3}$	11.2% 3.0%

Table 3 Comparison of intensities

It is evident from the table that the present results do indicate that Rossi's point has been under-estimated, but not to such an extent as some 20% as reported by Allkofer et al (1970,1971). Disagreement with the results of Lau et al (1973), Kong et al (1975) and Ayre et al (1973) may be inherent to the different methods used, and the different solar activity periods of measurements. In fact, we are now comparing their absolute intensities with the best fit values which are results of some averaging procedures in assuming A_{π} , γ and K be constant over the whole momentum range. This may also be a cause of the discrepancy.

Finally we conclude that in view of the paucity of data in the high momentum region, the present results may be considered to be consistent with the previous spectrum measurements of Allkofer et al (1971) and Ayre et al (1973). In this respect, the present work can be regarded as a support for the validity of these previous measurements.

Acknowledgement

The authors wish to thank Dr. P.K.MacKeown for his valuable suggestions in connection with this work.

References

- Allkofer, O.C., Dau, W.D., Jokisch, H., 1970, Proc. VIth Inter-american Seminar on Cosmic Rays, La Paz, 4, 937
- Allkofer, O.C., Carstensen, K., Dau, W.D., 1971, Proc. 12th Int. Conf. on Cosmic Rays, Hobart, 4, 1314.

- Ayre, C.A., Baxendale, J.M., Deniel, B.J., Hume, C.J.,
Thompson, M.G., Whalley, M.R., and Wolfendale,
A.W., 1973, Proc. 13th Int. Cosmic Ray Conf.,
Denver, 3 , 1754.
- Brooke, G., and Wolfendale, A.W., 1964, Proc. Phys.
Sec., 83 , 843.
- Brooke, G., 1973, "Cosmic Rays at Ground Level", Ed. by
A.W. Wolfendale, London, Inst. of Phys., Chapter 3.
- Kong, D.F.L., Lau S.Y., and Ng, L.K., 1975, 14th Int.
Cosmic Ray Conf., München, MN 1.1 - 2.
- Lau, K.S., Ng, L.K., and Young, E.C.M., 1971, 12th Int.
Cosmic Ray conf., Hobart, 4 , 1587.
- Rossi, B., 1948, Rev. Mod. Phys., 20 , 537
- Rossi, B., 1952, "High-energy Particles", Prentice-Hall,
Page 157.
- Lau, S.Y., Ng, L.K., Young, E.C.M., 1973, 13th Int.
Cosmic Ray Conf., Denver, 3, 1809.

A MUON TELESCOPE FOR THE MEASUREMENT OF THE SPECTRA AND
ZENITH ANGLE DEPENDENCE OF SLOW MUONS

L. S. CHUANG

Department of Physics, The Chinese University of Hong Kong,
Hong Kong

M. WADA

Cosmic Ray Laboratory, The Institute of Physical and Chemical
Research, Tokyo, Japan

An attempt is made to construct a simple muon telescope, using plastic scintillators, for the measurement of the spectrum and zenith angle dependence of slow muons at sea level. Studies for the proper use of the muon telescope for this purpose, and determination of the correction factors for an absolute determination of the intensity of the muons stopped in the lower scintillator and then decayed, are presented. Confirmation for the correct measurement of the event is also discussed.

1. Introduction

Measured spectrum and zenith angle dependence of slow muons at sea level and underground has been of great interest for comparison with the results of theoretical calculations. Disagreement between the results of different workers using different experimental methods¹, however, urges further investigation with better statistics.

Taking into consideration the better statistics attainable from a large sensitive area, the thickness effect, and ease of adjustment for obtaining the open angles, an attempt is made to construct a simple muon telescope, using plastic scintillators, for the measurement of the spectrum and zenith angle dependence of slow muons at sea level.

2. Construction of the detector

The detector consists of two units, each of them comprising a plastic scintillator of dimensions 1m x 1m x 0.05m and a 5" photomultiplier tube, of type RCA-8055 with the maximum spectral response at 4400 Å, fixed in a light-tight iron case as shown in fig. 1. The whole system is installed in a room where the air temperature is kept within 20 ± 1 °C. The detectors are aligned vertically with the faces of the scintillators set horizontally. Separation of the detectors can be made easily by lifting the upper unit while the lower one remains, seated permanently, on a support; for instance, with the separations of 0.09-, 0.53-, 0.98- and 1.42-m the equivalent open angles are $85^{\circ}8'$, $62^{\circ}5'$, $45^{\circ}34'$ and $35^{\circ}9'$ respectively. At each open angle, iron plates of desired thickness can be placed successively in between the detectors to achieve the muon-energy range of interest; for instance, in addition to the roof thickness of 13 cm of concrete plus a 5 cm thick plastic scintillator, an iron plate of 0.084m thickness will bring the maximum muon-energy to 80 g/cm^2 of air equivalent.

The counting system is shown diagrammatically, together with the detector system, in fig. 1. Signals from the photocathodes are amplified and separately fed to the single channel pulse height analyzers which can be operated either as a discriminator or as a pulse height analyzer. The shaped pulses, of 12 nsec in rise time, from the single channel analyzer outputs are then fed to the separate inputs of a logic circuit in which double coincidence/triple coincidence/coinc-anti-coinc logic can be manipulated with variable delay time and coincidence time duration. The minimum time delay acceptable to the logic circuit, however, is 0.7 μ sec due to the inherent characteristics of the amplifier and the pulse height analyzer systems used.

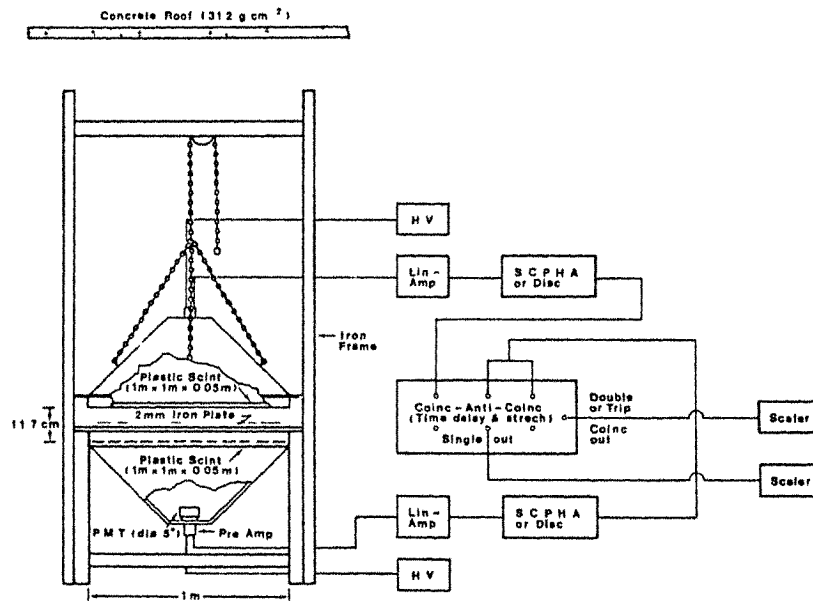


Fig. 1. The detector and the counting system.

Calibration for the timing of the logic circuit is made using a double pulse generator and an oscilloscope. An accuracy of better than 0.1% is attainable in setting the delay time. Calibration for the timing is repeated from time to time throughout the period of measurement.

3. Methods of measurement

Measurements for the triple coincidence events will then be made for each setting of the open angles and the various iron absorber thicknesses.

With the high voltages and the threshold energies set at the optimum values, the signals produced simultaneously in the upper and the lower detectors are delayed for 1.0 μ sec and then given a coincidence pulse duration of 0.9 μ sec. The second pulse which succeeds the first one, from the lower scintillator, in reaching the logic circuit will be shaped to a pulse of duration 0.1 μ sec. If this second pulse is generated within the time duration of 1.0 μ sec from the reception of the first signal by the logic circuit (i.e. the coincidence pulse duration plus the second pulse width), a triple coincidence count, which is an event of the present interest, will result. In order to avoid the errors which might arise from the day-and-night variation of the cosmic-ray intensity, measurements will have to be made at regular intervals.

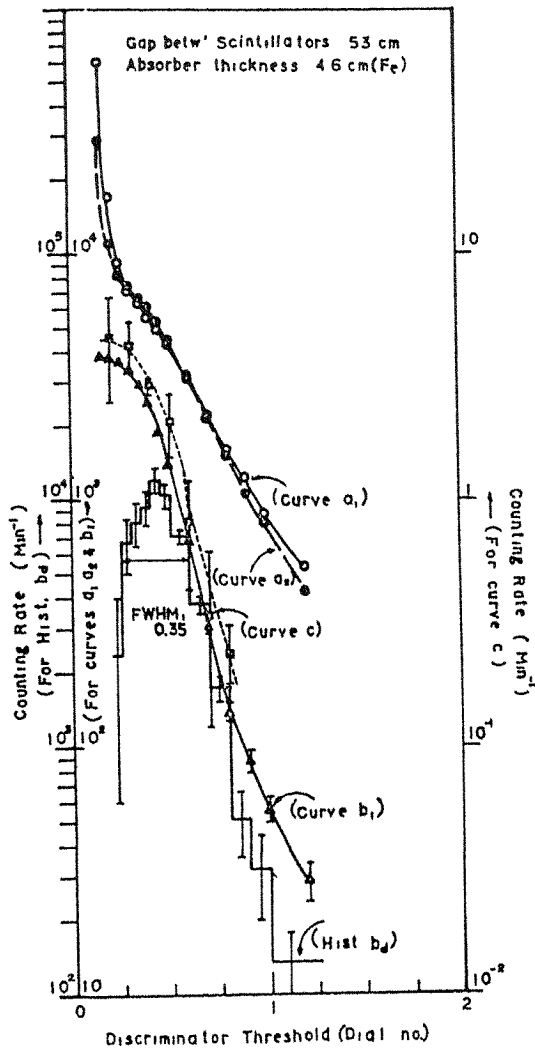


Fig. 2. Pulse height distributions: Curves a_1 and a_2 are for the lower and the upper detector, respectively; Curve b_i is for double coincidence counting and operated in "integral" mode; Curve b_d is differentiated from curve b_i ; Curve c is for triple counting.

Before the measurement for the triple coincidence events, which are of primary importance, the following measurements have to be made to make sure that a proper use of the telescope is made:

(a) Counting rate as a function of the threshold energy as shown by the curves a_1 and a_2 , for the lower and the upper detector, respectively, in fig. 2. (b) Double coincidence counting rate, resulting from the simultaneous events in the upper and the lower detectors, as a function of the threshold energy which is the same in both detectors; as the curve b_i which is plotted for an "integral" mode of measurement, and the histogram b_d , which

is differentiated from the curve b_1 , in fig. 2, and (c) Triple coincidence counting rate as a function of the threshold energy, which is the same in both detectors, as the curve c in fig. 2.

It is seen from the curves a_1 and a_2 that the high voltages applied to the two detectors were adjusted for an optimum value so that the pulse height distributions in the two detectors are almost identical. The peak in the histogram b_d corresponds to an energy loss of 11 MeV in the scintillator. The similarity between the curves b_1 and c is interpreted as meaning that almost all of the decay electrons have been detected.

4. Correction factors

For the determination of an absolute intensity of the muons stopped in the lower scintillator and then decayed, from the measured delayed triple coincidence counts, the following correction factors are necessary: (a) A correction factor f_d to account for the events of interest which are not measured due to a limited coincidence time interval setting. In the present experiment, from the fraction of time covered in a single measurement, f_d is expressed by:

$$f_d = \frac{1}{\tau} \int_{t_1 = 1.0 \text{ } \mu\text{sec}}^{t_2 = 2.0 \text{ } \mu\text{sec}} \exp(-t/\tau) \cdot dt \quad (1)$$

where $\tau = 2.15 \text{ } \mu\text{sec}$ is the accepted mean life time of a muon,

and $t_1 = 1.0 \text{ } \mu\text{sec}$ and $t_2 = 2.0 \text{ } \mu\text{sec}$ are the starting and the ending time, respectively, of the coincidence time duration. Accordingly, $f_d = 0.239$ in the present experiment. It should be noted, however, that the coincidence time duration used presently is an optimum one with regard to the comparativity of the increase of the counting rate of interest and the accompanying accidental coincidence rate as a result of the increase in the coincidence time duration; (b) A correction factor f_T to account for the events of interest which are not measured due to unnecessary discrimination of the real pulses as a result of too high setting of the threshold energy. To cover the whole range of pulses produced by the events of interest, the threshold energy must be set at a level at which the real pulses are all acceptable to the counting circuit. From the curve b_i of fig. 2 it is seen, in this special case, that an 100% counting of the double coincidence events is possible if the threshold level is set below 0.2 of the dial reading. The correction factor f_T , 0.4 in the present measurements, for a given geometry of the measurement, can therefore be determined by taking the ratio of the double coincidence counting rates for the threshold level with which the triple coincidence events are measured and that with which 100% counting of the events is possible. It is noted from the curve a of fig. 2 that too low setting of the threshold level will introduce unduly high noise pulse into the counting circuit and result in an abnormally high

accidental coincidence counting. To overcome this difficulty without sacrificing the counting statistics, an optimum threshold level is chosen in such a way that the standard deviation for a single delayed triple coincidence count is a minimum.

5. Confirmation of the method

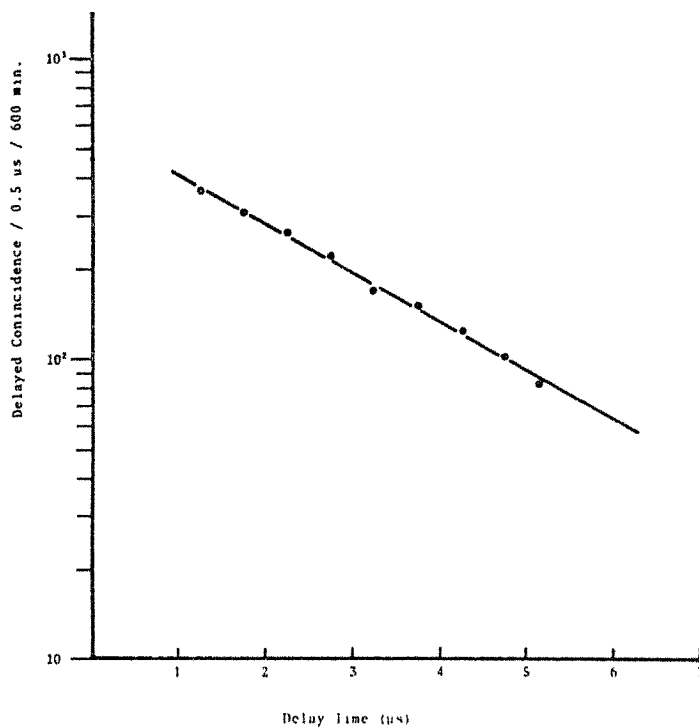


Fig. 3. The number of triple coincidence counting vs delay time.

To confirm that the muons detected are those of the present interest, i.e. muons stopped in the lower scintillator and decayed, analysis of the number of triple coincidence counting versus the delay-times was attempted. In this, the

events were analyzed in 0.5 μ sec bins. A straight line with a slope equivalent to the mean life time of muons, 2.15 μ sec, is drawn. The excellent agreement, within the experimental error, between the accepted decay curve and that of the presently measured one, shown in fig. 3, is a sure indication that the measured events are those of muons stopped in the lower scintillator and then decayed.

References

- L. Del Rosario and J. Davila-Aponte, Phys. Rev. 88 (1952)998.
J.R. Moroney and J.K. Parry, Aust. J. Phys. 7 (1954)423.
S. Fukui, T. Kitamura and Y. Murakami, J. Phys. Soc. Japan 10 (1955)735.
S. Kaneko, T. Kobozal and M. Takahata, J. Phys. Soc. Japan 10 (1955)915.
A. Subramanian et al, Nuovo Cim. 7 (1958)110.
D.W. Coates and W.F. Nash, Aust. J. Phys. 15 (1962)420.
P.J. Hayman and A.W. Wolfendale, Proc. Phys. Soc. 80 (1962)710.
R.J.R. Judge and W.F. Nash, Nuovo Cim. 35 (1965)999.
O.C. Allkofer and R.D. Anderson, Nuovo Cim. 51 (1967)329.
O.C. Allkofer, R.D. Anderson and W.D. Dau, Can. J. Phys. 46 (1968)301.
D.P. Bhattacharyya, Z. Phys. 234 (1970)17.

Calculation of Muon Momentum Spectra at Sea Level

K.Murakami, S.Sagisaka*, A.Inoue, Y.Mishima**
and K.Nagashima***

The Institute of Physical and Chemical Research, Tokyo

* Department of Physics, Shinshu University, Matsumoto

** Department of Physics, Ehime University, Matsuyama

*** Department of Physics, Nagoya University, Nagoya
Japan

Muon momentum spectra at sea level were calculated for the incident zenith angles of 0° and 75° by numerical integration of the equations of hadron cascades in the atmosphere. In the calculation on nuclear interactions, the recent data of accelerator experiments are introduced and Feynman's scaling is assumed to hold over the whole energy region. The calculations were carried out up to primary energy of 10^7 GeV and the results were extrapolated for the higher energy region. Concerning inelastic cross sections of nucleon, pion and kaon, the calculations were made not only for the constant cross sections but also for the energy-dependent ones. The absolute muon fluxes thus calculated are in good agreement with the momentum spectra measured at sea level over the momentum region except of high momenta. In high momentum region above 100 GeV/c, the calculated spectra are a little steeper than the observed spectra.

One-dimensional development of air shower also was computed. As several authors already discussed about air showers expected from scaling hypothesis, the discrepancy from observed properties of air shower is very distinct also in the present calculation. Possibilities to dissolve this discrepancy are discussed.

Introduction

During last four years several authors have tried to explain muon momentum spectra observed at sea level or underground by the assumption that Feynman's scaling is valid in nuclear interactions over energy range concerned. Some of them have successfully confirmed that the outline of muon spectrum is in agreement with the expectation from the scaling hypothesis. For modulation study also, response functions of muon observed in a certain condition have been calculated with the same assumption. Although our main purpose is to calculate the response functions applicable for various conditions such as altitude, underground depth, incident direction and so on, the comparison of the calculated results with muon momentum spectra measured at sea level is

really desired in order to see whether the procedure of calculation is suitable to actual particle transport in the atmosphere or not. In the previous papers (Murakami et al, 1976), we were concerned in muon spectra at zenith angle of 0° and 75° , and then the numerical integrations of hadronic cascade equations were made with the assumption of constant inelastic cross sections. The comparison with measurements (Allkofer et al, 1971 and Carstensen et al, 1975) showed that the absolute muon fluxes thus calculated are in good agreement with the momentum spectra measured at sea level over the momentum region except of high momenta. In high momentum region above 100 GeV/c, the calculated spectra are a little steeper than the observed spectra. As accelerator experiments of proton-proton and hadron-nucleus revealed that the hadronic interaction cross sections are increasing with incident energy, so we here adopted more rigorous cross sections of nucleon, pion and kaon increasing with logarithm of incident laboratory energy for the present calculation. Contrary to our anticipation, the difference in muon fluxes at sea level between constant and energy-dependent cross sections is very slight and insignificant. In high altitude, the difference is recognizable.

The calculations were carried out up to primary energy of 10^7 GeV. In addition to the calculation of muon flux, one-dimensional development of air shower also was computed for the discussion on the relation of muon spectrum to air shower. As several authors already discussed about air showers expected from scaling hypothesis, the discrepancy from the observed characters of air shower is very distinct also in the present calculation. Gaisser et al (1973), Fishbane et al (1974), Gaisser (1974), Wdowczyk and Wolfendale (1973) and Mason et al (1975) have suggested a possibility of predominance of Fe or heavier nuclei in primaries above 10^6 GeV to dissolve the discrepancy. There is, however, a fear that this predominance may contradict muon spectrum around 1 TeV/c. Another possibility will be discussed to dissolve the problem.

Calculations

The calculations are made for muons arriving at concerned atmospheric depths through nucleon and pion cascades and decay processes from primary protons of given energies. For muons from primaries of $Z \geq 2$, the calculated results from proton primary were superposed for the simplicity, although recent accelerator experiments show the effect of two-nucleons ball in collision of He incidence.

The cascade equations of nucleons and charged pions are as follows, where the production of energetic nucleon by incident pion is neglected.

$$\frac{dN(E,y)}{dy} = -\frac{N(E,y)}{\lambda_N(E)} + \int_E^{E_0} \frac{F_{NN}(E,E')}{\lambda_N(E') \cdot E} \cdot N(E',y) \cdot dE'$$

$$\frac{d\pi(E,y)}{dy} = -\left\{ \frac{1}{\lambda_N(E)} + \frac{\xi_\pi(y)}{E \cdot y} \right\} \pi(E,y) + \int_E^{E_0} \frac{F_{N\pi}(E,E')}{\lambda_N(E') \cdot E} \cdot N(E',y) \cdot dE'$$

$$+ \int_E^{E_0} \frac{F_{\pi\pi}(E,E')}{\lambda_\pi(E') \cdot E} \cdot \pi(E',y) \cdot dE'$$

E : Particle total energy in laboratory system.
 E_0 : Primary proton energy.
 y : Path from the top of the atmosphere, $g \cdot cm^{-2}$.
 $N(E,y)$: Nucleon number defined in $N(E,y)dE$.
 $\pi(E,y)$: Charged pion number.
 λ_N : Nuclear interaction m.f.p. of nucleon in air.
 λ_π : Nuclear interaction m.f.p. of pion in air.
 $\xi_\pi(y)/(E \cdot y)$: Decay probability of charged pion in US standard atmosphere.

$F_{1,2}(E_2, E_1)/E_2$ in the equations gives particle number per unit energy of particles at the final stage of the interaction by an incident particle (E_1). According to the recent data in accelerator experiments, the followings are provided.

1) $F_{NN}(E, E')/E$: Nucleon to nucleons. From the ISR experiments of p-p collision (Erne, 1973), the differential cross section, $d^2\sigma/dx_\parallel dp_\perp$, can be represented approximately to be proportional to $\exp(-4.3 p_\perp)$ and to be almost constant in Feynman's variable x_\parallel for both forward and backward directions in c.m.s.

2) $F_{N\pi}(E, E')/E$: Pion production by nucleon. The invariant cross section was quoted from the distribution of π^0 in proton-carbon collision (Einhorn, 1974).

$$E^* \frac{d^3\sigma}{dp^3} \propto (1 - X_R)^4 \cdot (p_\perp^2 + 0.86)^{-4.5}, \quad X_R = 2 \left\{ (p_\parallel^{*2} + p_\perp^2) / s \right\}^{1/2}$$

Asterisks mean quantities in c.m.s. and s is Feynman's scaling parameter. The cross section is normalized to the multiplicity of charged pions cited from the experiments of p-p collision (Giacomelli 1973).

$$\langle n_{\pi^\pm} \rangle = -4.3 + 1.71 \ln s + 3.7 \cdot s^{-1/2}$$

3) $F_{\pi\pi}(E, E')/E$: Pion to pions. This term includes pion production as well as a leading pion. The differential cross section of a leading pion is assumed to be of the same functional form as $F_{NN}(E, E')/E$ for forward direction. For pion production, the same function as $F_{N\pi}(E, E')/E$ was adopted.

Although the above expressions of $F_{1,2}/E$ are derived from the experiments in energy region from 50 GeV to 250 GeV or to 2 TeV, the numerical integrations of the equations were carried out consistently over the range of E_0 from a few GeV to 10^7 GeV by assuming that the expressions still hold at both low and high energies. The reason why the calculations are extended to low energy primary is that the empirical response function of ground meson detector has possibility to include an ambiguity due to the derivation from small latitude effect of 15 %. To see the fitness of the above expressions, the energy conservation in laboratory system between incident and outgoing particles was examined. It seems that the energy is well conserved over the wide range of incident particle energy.

From pion decay to survival muon, the following equations are solved.

$$\text{Muon production : } \frac{dM(E,y)}{dy} = \int_E^{E(\frac{m_\pi}{m_\mu})^2} \frac{\xi_\pi}{y} \cdot \Pi(E',y) \frac{dE'}{p'^2} \left\{ 1 - \left(\frac{m_\mu}{m_\pi} \right)^2 \right\}^{-1}$$

$$\text{Muon's survival probability : } \frac{dP_\mu}{dy} = - \frac{\xi_\mu}{E \cdot y} \cdot P_\mu(E,y)$$

$$\text{Muon's ionization loss : } E = E_f + \beta (y_f - y)$$

$M(E,y)$: Produced muon number.

m_π and m_μ : Rest masses of pion and muon, respectively.

$P_\mu(E,y)$: Survival probability of muon.

$\xi_\mu/(E \cdot y)$: Muon decay probability in US standard atmosphere.

β : Ionization loss rate.

Suffix f means observation level.

The effect of kaons on muon number was taken into account only for the first generation of kaons by nucleons and pions. The effect by kaons is supposed to become important at TeV or more, compared with muons produced by pions. In the present calculations, the assumptions on kaons are as follows.

Branching ratio of $k \rightarrow \mu$: 63.5 %.

Invariant cross section of kaon production (presumed from the paper by Badhwar et al, 1975) :

$$E^* \frac{d^3\sigma}{d^3p^*} \propto (1-x_k)^3 \exp(-4p_L)$$

Multiplicity of kaons (Giacomelli, 1973) :

$$\langle n_{K^\pm} \rangle = -1.02 + 0.24 \ln S + 1.45 \cdot S^{-1/2}$$

The energy transfer to kaons in nuclear interaction is as much as 5% of incident nucleon energy. This surplus energy transferred to kaon gives little error into the results.

Speaking of interaction m.f.p., λ_i ($i = N, \pi, k$), we carried

out the calculations for four sets of λ_i , as shown in the following.

- i) $\lambda_{N_0} = 80 \text{ g}\cdot\text{cm}^{-2}$, $\lambda_{\pi_0} = 120 \text{ g}\cdot\text{cm}^{-2}$, $\lambda_{K_0} = 150 \text{ g}\cdot\text{cm}^{-2}$.
- ii) λ_i normalized to λ_{i_0} at 10 GeV.
- iii) λ_i normalized to λ_{i_0} at 10^2 GeV.
- iv) λ_i normalized to λ_{i_0} at 10^3 GeV.

$$\text{Normalization : } \lambda_i = \lambda_{i_0} \cdot \frac{(1 + 0.044 \ln E_{\text{normalization}})}{(1 + 0.044 \ln E)}$$

The calculations are made for the combinations of various parameters.

Primary energy : 3 GeV to 10^7 GeV.

Zenith angle : 0° and 75° .

Atmospheric depth : 320, 550, 720, 940, 1030 $\text{g}\cdot\text{cm}^{-2}$.

Primary spectra were given as follows, according to Ryan et al (1972).

$$\text{Proton : } j_p(E_0) dE_0 = 2 \cdot 10^4 \cdot (E_0 + 1.034)^{-2.75} (\text{m}^2 \cdot \text{sr} \cdot \text{sec} \cdot \text{GeV})^{-1}$$

$$Z \geq 2 \text{ (He equivalent) : } j_Z(E_0) dE_0 = 1.45 \cdot 8.6 \cdot 10^2 (E_0 + 0.244)^{-2.77}$$

E_0 : Total energy per nucleon.

Muon momentum spectra

The calculated spectra are compared with the spectra observed at zenith angles of 0° and 75° (Allkofer et al, 1971 and Carstensen et al, 1975). Fig.1 shows the spectrum of vertically incident muons calculated for $\lambda_i(E)$ normalized at 10^2 GeV. Because the calculated result for each set of m.f.p. actually coincides with others and the difference of muon flux among four sets of m.f.p. is insignificant (less than 5%). The effects of difference in assumed m.f.p. are recognized in altitude variation of hadrons and accordingly in muons at high altitude. It seems that the values λ_π and λ_K relative to λ_N

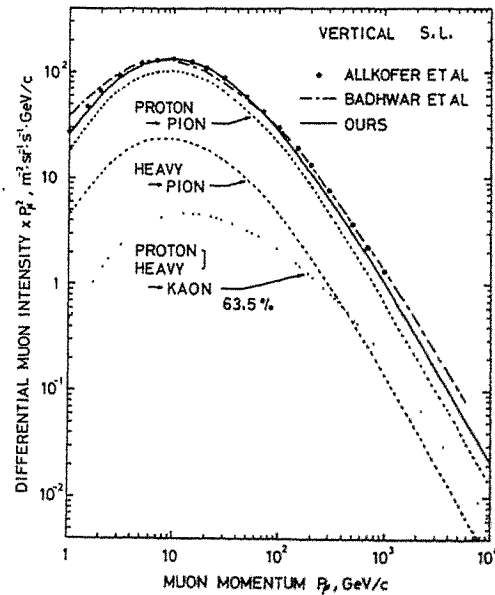


Fig. 1

is more important for sea level muons.

As shown in Fig.1, the absolute flux calculated here is in fairly good agreement with experimental points determined by Allkofer et al (1971), except of high momentum region. In high momentum region above 100 GeV/c, the difference of flux corresponds to that in the index of spectrum as much as about 0.1. Recently one of nice explanations has been done by Badhwar et al (1975). In Fig.1, one can see good agreements between measured points and their calculation over high momentum region. They have solved the pion and kaon cascade equations with the assumption of constant cross sections, presuming nucleon cascade and taking account of rising cross section in the incidence of nucleon.

Kiel group (Carstensen et al, 1975) have carried out the measurement of momentum spectra of muons arriving in large zenith angles. Our present calculation for 75° is compared with their measurement, as shown in Fig.2. The calculated spectrum is the result for m.f.p. normalized at 100 GeV, because of the same reason as the case of vertical muons. In the present calculation the roundness of isobar level at high altitude was taken into account. The effect of this roundness appears obviously in high momentum region (about 10 % at 1 TeV/c). Around 20 GeV/c the excess of calculated flux is largest and it is as much as 40 %. The excess is of large amount and is beyond the preciseness of experiment. Although the outline of the spectrum is explainable by the present calculation, there is an obvious difference in the slope of the spectrum between the calculation and observation , as Allkofer et al (1976) pointed out.

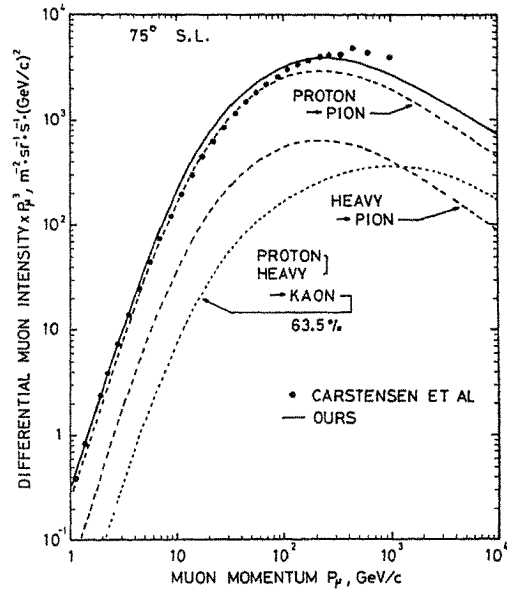


Fig.2

Air shower

In the previous work (Sagisaka et al, 1976), we

calculated air shower frequency of small size, which has been observed in Nagoya and Mt. Norikura, assuming constant m.f.p. In the present calculation, one-dimensional development of shower is calculated with the assumption of energy-dependent m.f.p. normalized to those at 100 GeV. Assuming that neutral pions are of half an amount of produced charged pions and that the energy of neutral pion is shared equally between two photons, the development in the Approximation B given by Snyder (1949) (Greisen, 1956) was used for the shower initiated by photons above 50 GeV. For showers initiated by photons from 500 MeV to 50 GeV, the results of simulated showers computed by Messel and Crawford (1969) were used. Regarding electron size, ionization loss is assumed to be 10 MeV in detector for single particle incidence. Fig.3 and Fig.4 show the development of shower size and the dependences of particle size on primary energy, respectively.

The tendencies of long attenuation length of electron size and small ratio of muon size to electron size for primary proton above 10^6 GeV are similar as those pointed out by Gaisser (1974) and Fishbane et al (1974).

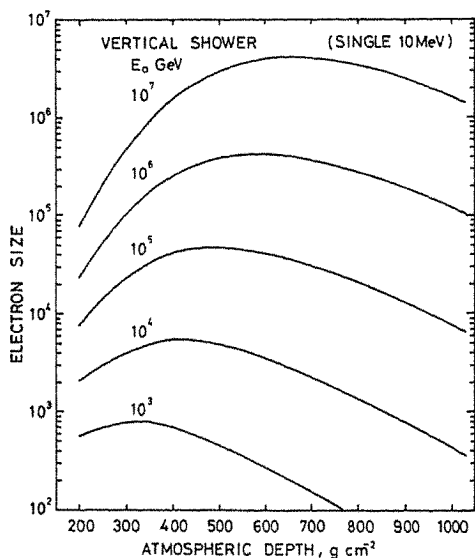


Fig. 3

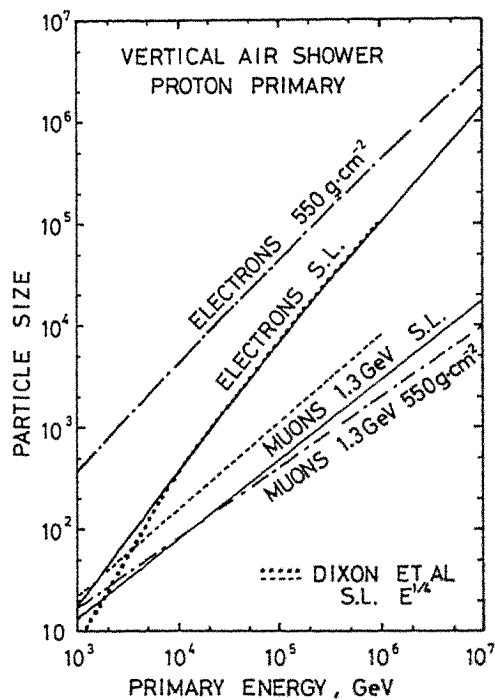


Fig. 4

Discussion

Concerning the limit of Feynman's scaling hypothesis, many authors have, so far, discussed on muon momentum spectrum, muon charge ratio and underground intensity, or on air shower development, the ratio of muon size to electron size and the fluctuation of muon number. In this section, the discussion is concentrated in relation to muon momentum spectra and air shower particle size.

From the observed vertical muon flux, Allkofer et al (1971) and Ayre et al (1973) have estimated the index of parent pion production spectrum, and Dau et al (1975) and Allkofer et al (1976) have shown the index for 75° estimated in the similar method. They all showed that the indices of pion production spectra are the values very close to 2.6, that is different from the indices of primary spectra obtained by Ryan et al (1972). The present calculations by assuming scaling also show almost the same results at high muon momentum for vertical muons as well as largely inclined muons. In a word, it seems certain that the flux of high momentum muons at sea level expected from scaling is insufficient.

On the other hand, when we assume the scaling holds up to very high energy region, it can be seen clearly that the ratio of muon size to electron size at sea level as well as mountain is conclusively of small value and shower particles are attenuating very slowly in showers initiated by primary protons above about 10^6 GeV. If the primary composition does not so much change still in primaries above 10^6 GeV, the above tendencies mean that the abundance of neutral pions produced by scaling hypothesis is too much and low energy muons in shower are very few. In other words, it seems that the average energy of pions in shower is too high in the case of scaling hypothesis. As seen in Fig.4, the assumption of high multiplicity of secondaries, $E^{3/4}$ -law (Dixon et al, 1973), may dissolve the above problem about air shower. But, by this assumption, the muon momentum spectrum at sea level is expected to become a little steeper than the case of scaling, and then, the discrepancy from the observation becomes larger. As described in Introduction, predominance of heavier nuclei in primaries also can give complements for insufficient muon size and slow attenuation of electron size in air shower of large size. It, however, must be expected that this kind of predominance brings too big amount of high momentum muons into muon momentum spectrum. Because, if the index of energy spectrum of iron primary is of 2.2 or 2.4 and if more than 80 % of primaries at $3 \cdot 10^5$ GeV is made up by Fe group, as Mason et al (1975) suggested, the amount of these heavier primaries must be comparable or more even at 10^{4-5} GeV, compared with proton or helium flux.

Now it will be tried to speculate another possibility in order to bring more amount of high momentum muons into muon spectrum and simultaneously to reduce the number of high

energy neutral pions in air shower development. If we could assume that average charged-to-neutral ratio of produced pions increases rapidly with incident energy above 10^4 GeV or more, high energy neutral pions will be reduced and the average energy of pions also will be reduced in air shower development. Moreover, there is a possibility to increase high energy muon in muon momentum spectrum. In this case, it will be necessary that the charged-to-neutral ratio depends on incident energy in order to approximately keep the distribution function of secondaries in laboratory system derived from scaling hypothesis.

Conclusion

Absolute muon momentum spectra at sea level calculated by the scaling hypothesis are in good agreement with measurements in zenith angles of 0° and 75° . It, however, is a little obscure why high momentum muons are insufficient in the calculation, compared with the measured fluxes.

In relation to air shower region in which there seems to be a limit of scaling, an idea that charged-to-neutral ratio of produced pions increases with incident energy may be one of the possibilities to dissolve the problems in muon momentum spectrum as well as the properties of air shower development which arise in the case of scaling hypothesis.

Acknowledgements

The authors like to express thanks to Dr. T. Kitamura in Cosmic Ray Laboratory, The University of Tokyo and Dr. K. Kobayakawa in Kobe University for their valuable discussions. For the present calculations, the facilities of the computer in The Institute of Physical and Chemical Research were provided.

References

- Allkofer, O.C., K. Carstensen and W.D. Dau, 1971, Phys. Letters, 36B, 425.
Allkofer, O.C., K. Carstensen, W.D. Dau, H. Jokish and H.J. Mayer, 1976, Proc. 2nd Intern. C.R. Symp., Japan, 26.
Ayre, C.A., J.M. Baxendale, B.J. Daniel, C.J. Hume, M.G. Thompson, M.R. Whally and A.W. Wolfendale, 1973, Conf. Papers 13th Intern. C.R. Conf., Denver, 3, 1754.
Badhwar, G.D., S.A. Stephens and R.L. Golden, 1975, Conf. Papers 14th Intern. C.R. Conf., Munich, 6, 2077.

- Badhwar, G.D., S.A. Stephens and R.L. Golden, 1975, Preprint.
- Carstensen, K., H. Jokish, H.J. Meyer, W.D. Dau, C. Grupen,
O.C. Allkofer and W. Stamm, 1975, Conf. Papers
14th Intern. C.R. Conf., Munich, 6, 2082.
- Dau, W.D., K. Carstensen and H. Jokish, 1975, Conf. Papers
14th Intern. C. R. Conf., Munich, 6, 1931.
- Dixon, H.E., J.C. Earnshaw, J.R. Hook, G.J. Smith and K.E. Turver,
1973, Conf. Papers 13th Intern. C.R. Conf.,
Denver, 4, 2473.
- Einhorn, M.B., 1974, FERMILAB-CONF.-74/74-THY/EXP.
- Erne, F.C., 1973, KEK-73-10, (National Lab. High En. Phys.,
Japan).
- Fishbane, P.M., T.K. Gaisser, R.H. Mauer and J.S. Trefil, 1974,
Phys. Rev. D 9, 3083.
- Gaisser, T.K., R.H. Mauer and C.J. Noble, 1973, Conf. Papers
13th Intern. C.R. Conf., Denver, 4, 2652.
- Gaisser, T.K., 1974, Jour. Franklin Inst., 208, 271.
- Giacomelli, G., 1973, NAL-PUB-73/74-EXP.
- Greisen, K., 1956, Prog. Cosmic Ray Physics, III, edited by
J.G. Wilson, North-Holland Pub. Co., Amsterdam.
- Messel, H. and D.F. Crawford, 1969, Electron-Photon Shower
Distribution Function, Pergamon Press.
- Murakami, K., S. Sagisaka, A. Inoue, Y. Mishima and K. Nagashima,
1976, Proc. 2nd Intern. C.R. Symp., Japan,
13 and 21.
- Sagisaka, S., K. Murakami, K. Nagashima and A. Inoue, 1976,
Proc. 2nd Intern. C.R. Symp., Japan, 183.
- Ryan, M.J., J.F. Ormes and V.K. Balasubrahmanyam, 1972, Phys.
Rev. Lett., 28, 985 and 1497(E).
- Wdowczyk, J. and A.W. Wolfendale, 1973, Conf. Papers 13th
Intern C.R. Conf., Denver, 3, 2336.
- Mason, G.W., J.W. Elbert, G.H. Lowe, J.L. Morrison and V.S.
Narasimham, 1975, Conf. Papers 14th Intern.
C.P. Conf., Munich, 8, 2943.

PREDICTED AND RECENTLY OBSERVED MUON SPECTRA AT SEA LEVEL

C.R. Paul, N.L. Karmarkar and N. Chaudhuri

Department of Physics, North Bengal University, Darjeeling, India.

Abstract

An evaluation of recently measured muon spectra at sea level has been made using an exactly calculated muon spectrum as reference. It is concluded that the significant differences that can be distinguished among existing sea level muon spectrum measurements are not expected to arise between the expected spectra from the conventional fireball type model for hadron interactions and those from the scaling model based on the Feynman scaling hypothesis.

1. Introduction

A reassessment of new measurements of muon spectra at ground level has been made in the light of the theoretically expected spectra on the basis of a rigorous treatment in a model, to be referred to as MC model, by Maeda and Cantrell^{1,2}. This model for the generation of muon spectra based on a fireball type model of high energy hadron interactions takes into account many effects in the process of generation of muons in the atmosphere which are neglected in the older CKP³ and CE⁴ models. Some of the more recent calculations of muon spectra using the Feynman predictions referred to as the Feynman scaling hypothesis⁵ have been examined against the calculated MC model spectra taking into account the inherent uncertainty in some of the parameters adopted in such calculations.

2. Calculation of muon spectra

The muon spectra have been calculated from both the differential spectra of pions and kaons produced in hadron-nucleus collisions. In the formalism of Maeda¹ the differential intensity of produced pions at an atmospheric depth, x , with zenith angle between θ and $\theta + d\theta$ is given,

in the usual notation, by

$$n_{\pi}(E_{\pi}, x, \theta) = \int_0^x \frac{J_{\pi}}{L_i} e^{-D} \sec\theta(x') dx'$$

$$D(E_{\pi}, x', \theta) = \int_0^{x'} \frac{\sec\theta(x'')}{L_a} dx'' + \int_{x'}^x \frac{1}{L} + \frac{b_{\pi}}{E_{\pi}(x'')\rho(x'')} \sec\theta(x'') dx''$$

The differential energy spectrum of muons at the production depth x is given by

$$n_{\mu}(E_{\mu}, x, \theta) = \int_{E_{\mu}}^{E_{\mu}\gamma^2} \frac{b_{\pi} \sec\theta}{E_{\pi} \rho(x)} P(E_{\pi}) n_{\pi}(E_{\pi}, x, \theta) dE_{\pi}$$

A muon thus produced at depth x at zenith angle θ with energy E_{μ} has a probability $W(E_o, x_o, x, \theta)$ to survive down to a depth x_o where its zenith angle is θ_o and energy E_o , given by

$$W(E_o, x_o, x, \theta) = \exp\left[- \frac{m_{\mu} c^2}{\tau_{\mu} c^2} \int_x^{x_o} \frac{\sec\theta(x')}{E_{\mu}} \frac{dx'}{\rho(x')} \right]$$

The differential muon spectrum at this observation level, x_o , is given by

$$i_{\mu}(E_o, x_o, \theta_o) = \int_0^{x_o} n_{\mu}(E_{\mu}, x, \theta) W(E_o, x_o, x, \theta) dx$$

Maeda used generalised Chapman functions to express the above expression for the intensity. The corresponding expression for muon differential spectra from kaon-decay may be obtained by replacing all the pion parameters. In the numerical calculations the production spectrum of pions is taken to be of the form

$$J_{\pi} \tau_{\pi} A_{\pi} (3.2 + E_{\pi})^{-\gamma_{\pi}}$$

The pion spectrum constant A_{π} and γ_{π} obtained in the previous investigations as summarised recently⁶ are in the ranges

$$A_{\pi} \approx 0.20 - 0.25$$

$$\gamma_{\pi} \approx 2.6 - 2.7$$

We have chosen $A_\pi = 0.25$ and $\gamma_\pi = 2.7$

The parameters used in the computation of the spectrum are the same as those adopted in the previous calculations^{1,2}. The energy dependence of the nucleon interaction mean free path of hadrons as calculated by Wayland et al² has also been taken into account.

3. Evaluation of the recent muon spectral data

The recently published experimental muon spectra at sea level have been included in the analysis for an evaluation with reference to the calculated MC model spectrum. The calculated spectral intensities are the weighted sums of the pion decay and kaon decay muon intensities assuming a ratio of 0.15. Some representative values of the differential spectra for 0° and 85° are shown in table 1, to indicate the status of the available data. The statistical errors are in the range of 3 - 15%, the lowest being in the vertical measurements up to a muon momentum of 520 GeV/c, Ayre et al⁷. The error range in the large angle measurements extends up to a maximum of 12% at 2000 GeV/c in the investigation of Leipuner et al⁸.

For measurements at zero degrees zenith angle^{6,7,9} the measured spectra show broad agreement with the MC model muon spectra. The difference is about 30% around 20 GeV/c and 20% around 200 GeV/c. At larger zenith angles most of the measured data are somewhat lower than the MC model spectrum up to about 100 GeV/c. Above about 400 GeV/c the fit of the measured spectrum with expectations appears to be satisfactory, although the data points at different zenith angles appear to overlap. The above evaluation of data is somewhat different from that obtained in previous works, (see for example Abdel - Monem et al¹⁰), where simplifications were introduced in the calculation involving production spectra and interaction characteristics of muon parents, and the propagation characteristics of muon parents and muons in the atmosphere.

The use of the scaling hypothesis of Feynman gives a pion production spectrum, (see for example Ramana Murthy and Subramanian¹¹, somewhat similar to the pion production spectrum used in the CKP, CE and MC model calculations. The pion production spectrum in the MC model differs from

Table 1

Zenith Angle (degrees)	Momentum (GeV/c)	Author	Experimental Intensity ($\text{cm}^{-2}\text{s}^{-1}\text{Sr}^{-1}\frac{\text{GeV}^{-1}}{c}$)	Theoretical (MC model) Intensity ($\text{cm}^{-2}\text{s}^{-1}\text{Sr}^{-1}\frac{\text{GeV}^{-1}}{c}$)	Difference From MC Model Value (%)
0°	1.2	Allkofer et al. ⁹	2.90×10^{-3}	2.90×10^{-3}	0
	2.		1.75×10^{-3}	1.55×10^{-3}	-13
	3.		7.80×10^{-4}		+18
	5	Nandi & Sinha ⁶	3.80×10^{-4}	3.60×10^{-4}	-6
	10		1.40×10^{-4}	1.60×10^{-4}	+14
	19		2.80×10^{-5}	4.10×10^{-5}	+30
	47		3×10^{-6}	4.20×10^{-6}	+30
	120		2×10^{-7}	2.65×10^{-7}	+25
	165	Ayre et al. ⁷	6.50×10^{-8}	9×10^{-8}	+28
	565		1.50×10^{-9}	1.65×10^{-9}	+9
1130	Nandi & Sinha ⁶	1.10×10^{-10}	1.20×10^{-10}	-18	
85°	12		4×10^{-6}	3×10^{-6}	-33
	15		3.60×10^{-6}	2.80×10^{-6}	-29
	21		2.50×10^{-6}	2.28×10^{-6}	-10
	32		1.55×10^{-6}	1.64×10^{-6}	+6
	52		7×10^{-7}	9×10^{-7}	+22
	93	Allkofer et al. ¹⁴	2.35×10^{-7}	3.50×10^{-7}	+33
	180		5.20×10^{-7}	1.00×10^{-7}	+48
	360		1.01×10^{-8}	1.80×10^{-8}	+44
	660		1.80×10^{-9}	2.40×10^{-9}	+25
	1200		4×10^{-10}	5×10^{-10}	+20

that based on the scaling model by about 10%, the scaling based result being higher in the lower energy range around 10 GeV and the spectrum in the MC model being higher near 100 GeV. Some inconsistencies are noticed in the predicted muon spectra obtained recently in scaling based calculations. For example Volkova et al.¹² obtained muon spectra which show a lack of agreement with those obtained by Abdul-Monem et al.¹⁰ when compared with recent measurements included in the present analysis. This and similar inconsistencies¹³ do not point to any improvement of the situation of interpretation of the observed sea level muon spectra using the scaling hypothesis. The theoretical error arising only from uncertainties in high energy scaling collision parameters may be $\pm 20\%$ in the computed muon spectra.

There are a number of uncertainties in the muon spectral calculations with any chosen model arising both from the systematic errors in meson parent interaction and absorption mean free paths (L_1 , L_a), and the meson interaction mean free path (L), and in measurements over a spread of 1 - 4 orders of magnitude in muon momentum. For example, the effect of the generation of pions by pions may increase the pion interaction mean free path by about 50% of the adopted value of 120 gms/cm², and the uncertainty of normalization of magnetic spectrograph data over the whole range of momentum implies some systematic error in the measurements.

References

1. K. Maeda : *Fortschritte der Physik*, 21, 113 (1973), *J. Geophys. Res.* 69, 1725 (1964)
2. W.G. Cantrell, Dissertation, Texas A & M. University (1969),
W.R. Sheldon, W.G. Cantrell and N.M. Duller : *Phys. Rev. Letters* 22, 312 (1969),
J.R. Wayland, W.G. Cantrell, N.M. Duller, P.J. Green : *Nucl. Phys.* B32, 527 (1971).
3. G. Cocconi, L.J. Koester and D.H. Perkins : UCRL Report 10022, 167 (1962), *Nucl. Phys.* B28, 371 (1971).
4. G. Brooke, P.J. Hayman, Y. Kamiya and A.W. Wolfendale : *Proc. Phys. Soc.* 83, 853 (1964).
5. R.P. Feynman : *Phy. Rev. Letters*, 23, 1415 (1969).

6. B.C. Nandi and M.S. Sinha : J. Phys. A5, 1384 (1972).
7. C.A. Ayre, J.M. Baxendale, B.J. Daniel, C.J. Hume, M.G. Thomson, M.R. Whalley, and A.W. Wolfendale : Proc. 13th Int. Conf. on Cosmic Rays, Denver, Vol. 3, 1754 (1973).
8. L. Leipuner, R. Larsen, L. Smith, R. Adair, B. Higgs, H. Kasha and R. Kellong : Proc. 13th Int. Conf. on Cosmic Rays. Denver Vol. 6, 1771 (1973).
9. O.C. Allkofer, K. Carstensen and W.D. Dau : Phys. Letters, 36B, 425 (1971).
10. M.S. Abdel-Monem, J.R. Benbrook, A.R. Osborne, and W.R. Sheldon : Proc. 14th Int. Conf. on Cosmic Rays, Munich, Vol. 6, 2048 (1975), and other references in this volume.
11. P.V. Ramana Murthy and A. Subramanian : Proc. Indian. Acad. of Sci., Vol. 76, A1 (1972).
12. L.V. Volkova and G.T. Zatsepin : Proc. 13th Int. Conf. on Cosmic Rays, Denver, Vol. 3, 2356 (1973).
13. R. Adair, H. Kasha, R. Kellog : Proc. 13th Int. Conf. on Cosmic Rays, Denver, Vol. 3, 2356 (1973).
14. O.C. Allkofer, K. Carstensen, W.D. Dau, E. Fahnders and R. Sobania : Proc. 13th Int. Conf. on Cosmic Rays, Denver, Vol. 3, 1748 (1973), Proc. 14th Int. Conf. on Cosmic Rays, Munich, Vol. 6, 2082 (1975).

DAO SCALING MODEL AND SEA LEVEL COSMIC MUON SPECTRUM FROM
GODDARD SPACE FLIGHT GROUP MEASURED PRIMARY COSMIC RAY PROTON SPECTRUM

D.P. Bhattacharyya, R.K. Roychoudhury and D. Basu

Indian Association for the Cultivation of Science,
Jadavpur, Calcutta-32, India.

A new type of scaling model for $p + p \rightarrow \pi^- + X$ inclusive reactions, proposed by Dao et al. (1974), has been applied to derive the sea level muon spectrum. The primary nucleon spectrum data of the Goddard Space Flight Group were taken as input. It is found that the sea level muon spectrum depends explicitly on the average value of the Feynman variable $\langle x \rangle$, whose most probable value is estimated to be 0.18.

1. Introduction

Some time ago Dao et al. (1974) studied the single particle distributions in proton-proton collisions at 300 GeV/c and proposed a new type of scaling, which is different from the usual Feynman (1969) scaling, for inclusive reactions $p + p \rightarrow \pi^- + X$. The fundamental difference between the conventional scaling hypothesis and new type of scaling proposed by Dao et al. is the following :

According to the Feynman scaling hypothesis the structure function $f = E(d^3\sigma/d^3p)$ is explicitly independent of s , the square of center of mass energy, for large values of s . In the scaling model of Dao et al. f depends on s through the parameters $\langle x \rangle$ and $\langle p_T \rangle$, the average value of the Feynman variable x and transverse momentum p_T of the secondary particle, respectively.

In the present paper we have derived the pion production spectrum from the primary cosmic ray nucleon spectrum of the Goddard Space Flight Cosmic Ray Group (Ryan et al. 1972). The sea level muon spectrum has been calculated with the conventional pion-atmospheric diffusion model described in our previous paper (Bhattacharyya et al. 1976). The calculated result has been compared with the magnetic spectrograph data of the Durham Group (Ayre et al. 1975).

2. Theoretical aspects

Ryan et al. (1972) have measured the energy spectrum of primary cosmic ray protons at Goddard Space Flight Centre, Maryland, and found that the data follow a power law of the form

$$N(E_p) dE_p = 2.0 E_p^{-2.75} dE_p \dots\dots\dots (1)$$

where E_p is the proton energy expressed in GeV and the intensity $N(E_p) dE_p$ is in $(\text{cm}^2 \text{ sec Sr GeV})^{-1}$ units. Assuming the nucleon to proton flux ratio at the top of the atmosphere to be 1.33, the calculated primary nucleon spectrum has been plotted in Fig. 1. Recently the Durham Group (Ayre et al. 1975) obtained the precise sea level cosmic ray muon spectrum in the momentum range 20 - 500 GeV/c. Their result is also presented in Figure 1.

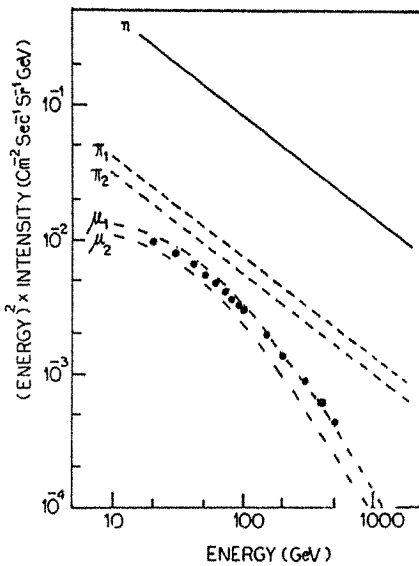


FIG 1

Figure 1.
The primary nucleon spectrum (n) - full curve; derived pion spectrum after Dao model (π_1) - broken curve, after Feynman scaling model (π_2) - chain curve. Calculated sea level muon spectra after Dao spectrum - μ_1 , scaling model - μ_2 . Sea level magnetic spectrograph data - ● Ayre et al. (1975).

3. Method of Calculation

The Feynman scaling hypothesis (Feynman 1969) suggests that in high energy p-p collisions the differential cross section for the production of a charged particle in Lorentz invariant form tends to a

limit given by

$$\lim_{s \rightarrow \infty} E(d^3\sigma/d^3p) = f(x, p_T) \dots\dots\dots (2)$$

where s is the square of the center of mass energy; E, p, p_T are the energy, momentum and transverse momentum, respectively of the secondary pions in the center of mass system, $x = 2p_L/\sqrt{s}$, where p_L is the longitudinal component of p parallel to the momentum p_{inc} of the incident particle.

At high energy $p_T \ll p_L$, hence the equation can be written as

$$d\sigma = \pi f(x, p_T) \frac{dx}{x} dp_T^2 \dots\dots\dots (3)$$

The probability of producing a secondary pion of energy E in the interaction of a primary nucleon of energy E_p with a target nucleon is given by

$$\pi(E, E_p) dE = \frac{d\sigma}{\sigma_{in.}} \frac{\pi}{\sigma_{in.}} \int_{p_T} E(d^3\sigma/d^3p) \frac{dx}{x} dp_T^2 \dots (4)$$

where $\sigma_{in.}$ is the total inelastic interaction cross section leading to pion production.

Dao et al. (1974) proposed the following formula for the experimental data at momenta 13, 21, 28.5 and 300 GeV/c for $p + p \rightarrow \pi^- + X$ reactions

$$\frac{d\sigma}{dp_T} = \frac{\sigma_{in.}}{\langle p_T \rangle} a (p_T/\langle p_T \rangle)^c \exp(-b p_T/\langle p_T \rangle) \dots\dots\dots (5)$$

$$\frac{d\sigma}{dp_L} = \frac{\sigma_{in.}}{\langle p_L \rangle} k \exp(-r[p_L/\langle p_L \rangle] - q[p_L/\langle p_L \rangle]^2) \dots\dots (6)$$

where $a = 6.23, b = 2.37, c = 1.37, k = 0.91, r = 0.83$ and $q = 0.03$. The χ^2 fits to the data per degree of freedom are 104/109 and 134/100 respectively. Taking $x = 2p_L/\sqrt{s}$ we have calculated from (5) and (6) the following formula for the Lorentz invariant cross section

$$E(d^3\sigma/d^3p) = \frac{A\pi\sigma_{in.}}{2p_T\langle p_T \rangle} \frac{x}{\langle x \rangle} (p_T/\langle p_T \rangle)^c \exp(-b p_T/\langle p_T \rangle) \exp(-r x/\langle x \rangle) \dots\dots (7)$$

where $A = a k/\pi = 1.81$.

Expression (7) is an approximate formula and is valid for $p_L \ll p_T$. It is to be noted that this result is different from that obtained from the usual scaling hypothesis because $\langle x \rangle$ and $\langle p_T \rangle$ are, in general, dependent on the variable s . In the present case we assume that $\langle p_T \rangle$ does not change significantly in the integration region over x . Using the relation (7) and integrating over p_T we get

$$\pi(E, E_p) dE = \frac{A\pi\Gamma(c+1)}{b^{c+1}} \exp(-r x/\langle x \rangle) \frac{dx}{\langle x \rangle} \dots\dots\dots (8)$$

Taking the nucleon spectrum of the following form

$$N(E_p) dE_p = B E_p^{-\gamma} dE_p \dots\dots\dots (9)$$

we get the production spectrum of charged pions at the top of the atmosphere

$$\begin{aligned} \pi(E_\pi) dE_\pi &= \int_{E_\pi}^{\infty} B E_p^{-\gamma} \frac{A\pi\Gamma(c+1)}{\langle x \rangle b^{c+1}} \frac{x}{E} \exp(-r x/\langle x \rangle) dE_p dE_\pi \\ &= \frac{A\pi B E_\pi^{-\gamma} \Gamma(c+1) dE_\pi}{b^{c+1} \langle x \rangle} \int_0^1 x^{\gamma-1} \exp(-rx/\langle x \rangle) dx \\ &= \frac{N(E_\pi) A\pi\Gamma(c+1)}{b^{c+1}} \frac{\Gamma(\gamma)}{r^\gamma} \langle x \rangle^{\gamma-1} dE_\pi \dots\dots\dots (10) \end{aligned}$$

where $A = 1.81$. It is assumed that at high incident energies E_p , $x = E_\pi/E_p$, for $p_T \ll p_L$ in the laboratory system.

The usual diffusion equation (Bhattacharyya et al. 1976) for the propagation of charged pions in the atmosphere allowing for loss of pions by interaction and decay, and gain by production in nucleon-nucleon collisions can be written as

$$\frac{\partial n_\pi(E,t)}{\partial t} = -n_\pi(E,t) \left(\frac{1}{\lambda_\pi} + \frac{B_\pi}{Et} \right) + \frac{\pi(E)}{\lambda_n} \exp(-t/\Lambda) \dots\dots\dots (11)$$

where $n_{\pi}(E,t) dE$ is the number of charged pions having energies between E and $E + dE$ at an atmospheric depth t ($/gcm^{-2}$), λ_{π} and λ_n are the interaction mean free path of pions ($120 g/cm^2$) and nucleons ($90 g/cm^2$), B_{π} is the critical energy of pion decay ($118 GeV$), Λ is the absorption free path of nucleons in air ($120 g/cm^2$). The muon spectrum can be calculated from the pion production spectrum by the following relation

$$\begin{aligned} \mu(E) dE &= \int_{t=0}^{1033} n_{\pi}(E,t) \frac{B_{\pi} r}{Et} r^{\gamma-1} dt dE \\ &= \frac{\pi(E) \Lambda r^{\gamma-1} B_{\pi} h(E) y(E)}{\lambda_n (B_{\pi} r + E)} dE \dots\dots\dots (12) \end{aligned}$$

where r is the energy degradation factor in a $\pi \rightarrow \mu$ decay, γ is the exponent of the differential energy spectrum of primary cosmic ray nucleons expressed as a power law, and is taken to be 2.75; $h(E)$ is a function depending on μ -e decay and energy losses of muons in the atmosphere and $y(E)$ is the correction factor depending on the kaon to pion ratio (K/π) at production. The derived sea level muon spectrum has been plotted in the Fig. 1 along with the pion spectrum for the best fit value of $\langle x \rangle = 0.18$. The derived muon spectrum agrees with the spectral shape of the experimental spectrum. The calculated spectrum contains a statistical fluctuation of approximately 12% which comes from the primary nucleon spectrum of Ryan et al. (1972) and errors in the different input parameters.

Using the primary cosmic ray spectrum of Grigorov et al. (1971), (cited by Hook and Turver 1974), and the sea level muon spectrum of Altkofer et al. (1971) as input the variation of $\langle x \rangle$ with secondary pion energy has been studied by us in our earlier work (Bhattacharyya et al. 1975) in which we suggested that $\langle x \rangle$ follows an asymptotic relation of the following form

$$\langle x \rangle = 0.08015 + 0.0922 E_{\pi}^{-0.25} - 0.008 E_{\pi}^{-0.5} \dots\dots (13)$$

At high energies $\langle x \rangle \approx 0.1$, but the GSFC nucleon spectrum gives a good fit to the muon spectrograph data of Durham Group (Ayre et al. 1975)

for $\langle x \rangle \approx 0.18$. This value is also supported by the most probable value of the machine data presented by Bertin et al. (1972) and Albrow et al. (1973), for $p + p \rightarrow \pi^- + X$ inclusive reactions. There is no significant intranuclear cascading for the value of x (≈ 0.16). Recently Wilson (private communication) has pointed out that data of Grigorov et al. (1971) at 1000 GeV has a discrepancy. In the measurement of Grigorov et al. (1971) there were some instrumental difficulties. The asymptotic values of $\langle x \rangle$ estimated after the data of Grigorov et al. are not supported by the machine measurements of Bertin et al. (1972) and Albrow et al. (1973).

Conclusion

Using the scaling model proposed by Dao et al. the primary cosmic proton spectrum was obtained in terms of the average value of the Feynman scaling variable x . A comparison with the data obtained by Ryan et al. yields the value $\langle x \rangle = 0.18$ and this is consistent with the sea level muon spectrum data of Allkofer et al. and previous machine experiments.

Acknowledgements

The authors express their thanks to Professor J.G. Wilson, University of Leeds, England for many useful suggestions.

References

1. Albrow M.G. et al, 1973, Nucl. Phys. B51, 388; Ibid B56, 2333.
2. Allkofer O.C., Carstensen K. and Dau W.D., 1971, Phys. Lett. 36B, 425.
3. Ayre C.A. et al., 1975, J. Phys. G : (Nucl. Phys.) 1, 984.
4. Bertin A. et al., 1972, Phys. Lett. 38B, 260.
5. Bhattacharyya D.P., 1975, J. Phys. G : (Nucl. Phys.) 1, 773.
6. Bhattacharyya D.P., Roychoudhury R.K. and Basu D., 1976, J. Phys. G : (Nucl. Phys.) 2, 689.
7. Dao F.T. et al., 1974, Phys. Rev. Lett. 33, 389.
8. Erlykin A.D., Ng. L.K. and Wolfendale A.W., 1974, J. Phys. A : (Math., Nucl. Gen.) 7, 2059.
9. Feynman R.P., 1969, Phys. Rev. Lett. 23, 1415.
10. Grigorov N.L. et al., 1971, Proc. 12th Int. Conf. on Cosmic Rays, Hobart (Hobart : University of Tasmania) Vol. 5, pp. 1746.

11. Hook J.R. and Turver K.E., 1974, J. Phys. A : (Math., Nucl. Gen.) 7, 765.
12. Ryan M.J., Ormes J.F. and Balasubrahmanyam V.K., 1972, Phys. Rev. Lett. 28, 985.
13. Wdowczyk J. and Wolfendale A. W., 1973, J. Phys. A : (Math., Nucl. Gen.) 6, 1594.
14. Wilson J.G., Private Communication (1976).

SEA LEVEL MUON SPECTRUM DERIVED FROM THE GSFC MEASURED
NUCLEON SPECTRUM USING CKP MODEL

Kalpana Sarkar (Miss), D.P. Bhattacharyya and D. Basu
Indian Association for the Cultivation of Science,
Jadavpur, Calcutta-700032,
India.

The sea level muon spectrum is estimated from the Goddard Space Flight Centre Group measured nucleon spectrum by using the model of Cocconi, Koester and Perkins (CKP). The derived muon spectrum agrees well with the magnetic spectrograph data of Ayre et al. (1975) when the energy dependence of pion inelasticity (K_{π}) in the CKP model is assumed in the pion energy range 10 - 500 GeV.

1. Introduction

Knowledge of the pion production spectrum at the top of the atmosphere and ground level muon spectra is of interest to cosmic ray phenomenology and particle astronomy.

It is assumed that the primary cosmic ray particles are directly accelerated in the cosmic ray sources, and the secondary nuclei are predominantly produced by spallation reaction of the primaries in the atmosphere. Moreover, the cosmic ray primaries comprising mainly charged particles (mainly protons) penetrate into the earth's atmosphere, collide with air nuclei and produce secondary components within a mean depth of 100 g/cm² of air. The majority of these products reaching ground level are mainly pions which decay into longer lived muons. The measured spectra of primary cosmic ray nucleons and ground level muons through the process of cosmic ray propagation in the atmosphere can be used to test the nature of the interaction models. The muon spectrum can also indicate the portion of energy transferred by nucleons to muons. Hook and Turver (1974) have reviewed the primary cosmic ray spectrum from the theoretical and experimental aspects. Erykin et al. (1974) have calculated the flux of primary cosmic ray nucleons by using the CERN Intersecting Storage Ring data and have found that the calculated primary nucleon

spectrum is rather accurate below 1000 GeV energy. In general the galactic cosmic radiation is composed of mainly protons and some other nuclei have been fairly reviewed by Daniel et al. (1974). Ryan et al. (1972) have measured at Goddard Space Flight Centre the fluxes of different primary cosmic ray particles by means of balloon flight ionization calorimeter experiments.

In the present paper we shall study the agreement of the pion production spectrum derived from the primary nucleon spectrum of Ryan et al., (1972), using the model of Cocconi, Koester and Perkins, (1961, to be referred to as CKP), with the experimental sea level muon spectrum. Attention has been paid to the energy dependence of the pion inelasticity (K_π). The conventional procedure of the pion atmospheric diffusion equation has been used in this work. The calculated sea level muon spectrum has been compared with the magnetic spectrograph data of Ayre et al. (1975).

2. Theoretical aspects

(i) Pion production spectrum derived from the measured nucleon spectrum at the top of the atmosphere :

The empirical relation formulated by Cocconi, Koester and Perkins (1961) from the data of pions emitted in p-low Z element interactions shows that the number of pions emitted (one sign) in the forward direction in the C system, $N(E_\pi)$, follows the relation

$$N(E_\pi) dE_\pi = \frac{A}{T_p} \exp(-E_\pi/T_p) dE_\pi \dots\dots\dots (1)$$

where E_π is the pion energy in the L system, A is the mean multiplicity of pions of one sign emitted in the forward direction in the C system, and T_p is the mean pion energy, and they obey the Fermi law of the form

$$\langle n_c \rangle = 1.80 E_p^{1/4} \dots\dots\dots (2)$$

which shows that $A = 0.45 E_p^{1/4} \dots\dots\dots (3)$

where the nucleon energy E_p is expressed in GeV units.

From the CKP model the differential pion production spectrum $P(E_\pi) dE_\pi$ can be calculated from the primary nucleon spectrum of the form

$$N(E_p) dE_p = B E_p^{-\gamma} dE_p \dots\dots\dots (4)$$

by the following relation

$$P(E_\pi) dE_\pi = \frac{2 dE_\pi}{[1 - (1 - K_\pi)^{\gamma-1}]} \frac{3a^2 B}{K_\pi} \int_{3E_\pi}^{\infty} E_p^{-\gamma-0.5} \exp\left(-\frac{3aE_\pi}{K_\pi E_p^{0.75}}\right) dE_p \dots\dots\dots (5)$$

where K_T = nucleon inelasticity; K_π = pion inelasticity;
 $a = 0.45$; γ = exponent of the primary nucleon spectrum with scaling factor B.

The primary cosmic ray nucleon spectrum of Ryan et al. (1972) gives values of B and γ equal to 2.66 and 2.75, respectively.

(ii) Sea level muon spectrum $\mu(E) dE$ derived from the pion spectrum $P(E) dE$ at the top of the atmosphere :

The usual diffusion equation for the propagation of charged pions in the atmosphere gives the pion intensity $n_\pi(E, t)$ at energy E and $E+dE$ at an atmospheric depth t g-cm² from the following relation (Bhattacharyya et al. 1976).

$$n_\pi(E, t) = \frac{P(E)}{\lambda_\pi} \exp(-t/\Lambda) \frac{t}{1+B_\pi/E} \dots\dots\dots (6)$$

where λ_π = interaction free path of pions in the atmosphere
 $= 120$ g/cm²;
 λ_n = interaction free path of nucleons in air = 90 g/cm²;
 Λ = absorption free path of nucleons in air = 120 g/cm²;
 B_π = critical energy for pion decay = 118 GeV.

The above expression is valid for the pions arising from nucleon collisions alone. The muon contribution from the pions originating in pion collisions is very small and this contribution is neglected. The sea level muon spectrum $\mu(E) dE$ can be estimated from the pion production spectrum at the

top of the atmosphere by the following expression

$$\begin{aligned} \mu(E) dE &= \int_{t=0}^{10^{33}} n_{\pi}(E, t) \frac{B_{\pi} r}{Et} r^{\gamma-1} dt \\ &= \frac{P(E) \Lambda r^{\gamma-1} B_{\pi} h(E) y(E)}{\lambda_n (B_{\pi} r + E)} dE \quad \dots\dots\dots (7) \end{aligned}$$

where r = the energy degradation factor in a π - μ decay;

γ = the exponent of the differential energy spectrum of primary cosmic ray nucleons expressed as a power law, = 2.75;

$h(E)$ is a function depending on μ - e decay and energy losses of muons in the atmosphere;

$y(E)$ is a correction factor for the kaon-pion ratio (K/π) at production.

3. Results and discussion

The primary cosmic ray nucleon spectrum at the top of the atmosphere is estimated by Ryan et al. (1972) at the Goddard Space Flight Center, Maryland (on assuming the nucleon to proton flux ratio at the top of the atmosphere to be 1.33) and is plotted in Fig. 1. This nucleon spectrum has been used to derive the pion production spectrum at the top of the atmosphere.

O'Brien (1969) has interpolated the values of nucleon inelasticity for the nucleon production $K_{\pi} = 0.422$. The energy dependence of pion inelasticity (K_{π}) is assumed in such a manner (Fig. 2) so that the derived sea level muon spectrum is in agreement with the experimental results. The values of the functions $h(E)$ and $y(E)$ have been taken from the work of Ramana Murthy and Subramanian (1972). The best fit pion spectrum is shown in the Fig. 1 (broken curve) along with the calculated sea level muon spectrum (chain curve) and magnetic spectrograph data of the Durham Cosmic Ray Group (Ayre et al. 1975).

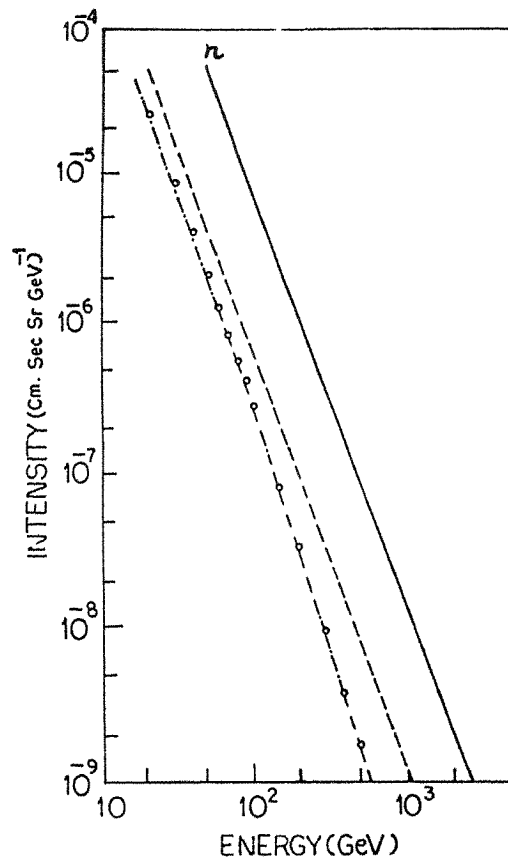


Figure 1. The spectra of primary nucleons (n) measured by Ryan et al. (1972); derived pion spectrum - broken curve; calculated sea level muon spectrum - chain curve; Magnetic spectrograph data - O Ayre et al. (1975.)

From the CKP model the primary energy E_p can be expressed as a function of secondary pion energy E_π and pion inelasticity K_π by the relation

$$E_p = (3aE_\pi/K_\pi)^{1/(1-\alpha)} \quad \text{where } \alpha = 0.25 \quad \dots\dots (8)$$

From this relation we get the value of E_π for $E_p = 1500$ GeV and $K_\pi = 0.35$ is about 62 GeV. So the machine data cannot provide any information about K_π above pion energy range 62 GeV.

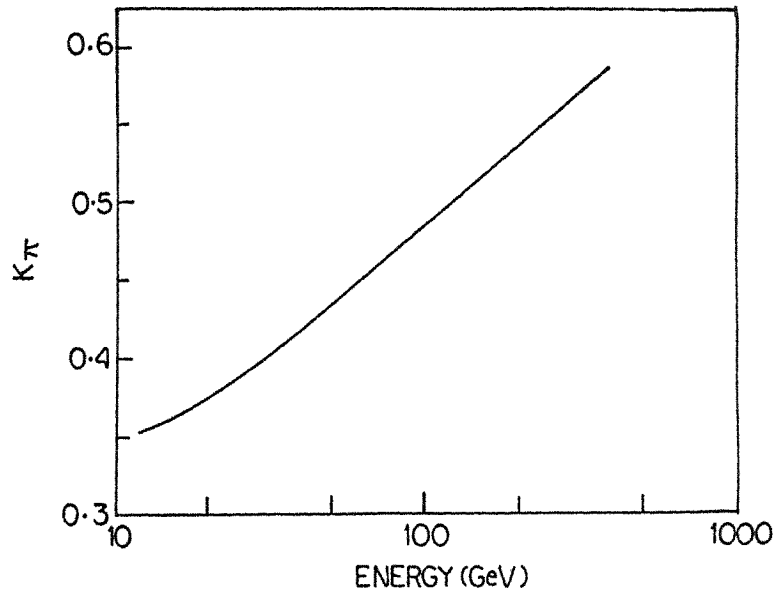


Figure 2. The pion inelasticity K_{π} estimated from the cosmic ray data has been plotted as a function of pion energy.

5. Conclusion

The CKP model can be used to derive the sea level muon spectrum from the measured primary nucleon spectrum of Ryan et al. (1972) when the energy dependence of pion inelasticity is assumed in the pion energy range 10 - 500 GeV. This fact is supported by CE model of Brooke et al. (1964). The increase of pion inelasticity with pion energy suggests that the secondary pions share more energy from the primary nucleons at high energies.

References

1. Ayre C.A. et al., 1975, J. Phys. G : Nucl. Phys. 1, 584.
2. Bhattacharyya D.P., 1972, Z. Physik 257, 292.
3. Bhattacharyya D.P., 1975, J. Phys. G : (Nucl. Phys.) 1, 773.
4. Bhattacharyya D.P., Roychoudhury R.K. and Basu D., 1976, J. Phys. G : (Nucl. Phys.) 2, 689.
5. Brooke G., Hayman P.J., Kamiya Y. and Wolfendale A.W., 1964, Proc. Phys. Soc. 83, 853.

6. Cocconi G., Koester K. and Perkins D.H., 1961, Lawrence Radiation Laboratory Report, High Energy Study Seminars, B. No. 28, pt. 2.
7. Daniel B.J. et al., 1974 J. Phys. A: (Math., Nucl. Gen.) 7, L20.
8. Erlykin A.D., Ng. L.K. and Wolfendale A.W., 1974, J. Phys. A : A : (Math., Nucl. Gen.) 7, 2074.
9. Grigorov N.L. et al., 1971 Proc. 12th Int. Conf. on Cosmic Rays, Hobart (Hobart : University of Tasmania) Vol. 5, p.1746.
10. Hook J.R. and Turver K.E., 1974, J. Phys. A :(Math., Nucl. Gen.) 7, 765.
11. Hook J.R. and Turver K.E., 1974, J. Phys. A:(Math., Nucl. Gen.) 7, 765.
12. O'Brien K., 1969, Nucl. Instrum. & Meth. 72, 93.
13. Ramana Murthy P.V. and Subramanian A., 1972, Proc. Ind. Acad. Sci. 76, 1.
14. Ryan M.J., Ormes J.F. and Balasubrahmanyam V.K. 1972 Phys. Rev. Lett. 28, 985.

Measurements of Deep Underground Intensities of High Energy Muons.

K. Mizutani

Department of Physics, Saitama University, Urawa, Japan

and

I. Ohta

Faculty of Education, Utsunomiya University, Utsunomiya, Japan.

The exposure of the emulsion chamber deep underground has been started in order to measure the energy spectrum of muons deep underground.

With the emulsion chamber exposed deep underground, it is possible to observe the showers induced by muons of high energies and to measure the energy spectrum of muons deep underground. This spectrum would be certainly important cues for examining the attenuation of high energy muons in the ground by comparing with other data; muon spectra at sea level and intensities of muons more deep underground.

Preliminary results based on the emulsion chamber of about 2 ton of lead are presented. This exposure has been performed at vertical depth of 850 hg/cm^2 underground in Okutadami Road Tunnel.

An Analysis of Momentum Spectrum of Muon

H. Komori

Physics Laboratory, Tokyo University of Fisheries,
4-5-7 Konan, Minato-ku, Tokyo 108, Japan

A lot of muon momentum spectra at sea level have been measured. A typical vertical spectrum¹⁾ at the present stage is, for instance, an observation of MARS spectrograph at Durham. They have shown that the differential spectrum is well represented by the logarithmic polynomial

$$p^3 N(p) = -0.524 + 0.366(\ln p) - 0.0445(\ln p)^2 + 0.0008(\ln p)^3 \quad (1)$$

where p is in GeV/c and $N(p)$ is in $s^{-1}cm^{-2}sr^{-1}(GeV/c)^{-1}$ for $p=7-500$ GeV/c. However, the expression may seem not to be obtained under considerations of the observation error of individual momentum and of the momentum width for each category.

We have applied a method of "Statistical Adjustment of Data"²⁾ to an analysis of their experimental data. It is assumed that the differential momentum spectrum has a form of $a((p+b)c/m_{\mu}c^2)^{-\gamma} dp$. Under considerations of 0.586 cm as the RMS value of the category-zero acceptance which corresponds to the MDM of 670 GeV/c, the distribution, $f(\Delta_i)$, of true displacement Δ_i will be given by the following³⁾,

$$f(\Delta_i) = K \left[\exp\left(-\frac{(\Delta_i - \Delta)^2}{2\sigma_{\Delta}^2}\right) + \exp\left(-\frac{(\Delta_i + \Delta)^2}{2\sigma_{\Delta}^2}\right) \right],$$

where σ_{Δ} and Δ represent standard deviation, which is taken as 0.586 cm, and apparent displacement, respectively.

A result of the analysis is as follows,

$$a = 551.37 \pm 0.27 \quad (\text{particles/cm}^2 \text{s sr (GeV/c)})$$

$$b = 5.32 \pm 0.12 \quad (\text{GeV/c})$$

$$\gamma = 3.09 \pm 0.09, \quad \text{for } 67.9 \geq p \geq 21.3 \text{ GeV/c,}$$

and

$$a = 5705.56 \pm 0.51 \quad (\text{particles/cm}^2 \text{s sr (GeV/c)})$$

$$b = 15.04 \pm 0.58 \quad (\text{GeV/c})$$

$$\gamma = 3.39 \pm 0.14, \text{ for } 442 \leq p \leq 76.6 \text{ GeV/c}$$

where the above standard error for each parameter does not contain any effects from propagation of errors of another terms.

The upper and lower values of muon spectrum shown in the Figures 1 and 2 have been obtained from 95% confidence level estimated the effect of propagation of all errors which appeared in three parameters a, b and γ . Fig.1 represents a confidence region of the calculated muon spectrum and does the experimental data. Fig.2 shows a comparison between the present estimated spectrum multiplied by p^3 and a result of the equation (1) given by MARS group. There should be ninety-five percent of number of true values in the confidence region of Figures 1 and 2.

Using the upper and the lower limits of the present muon spectrum, we can obtain a width of the exponent of power law spectrum of pion energy E_π employing the procedure of Bull et al⁴), as the following;

$$N(E_\pi) dE_\pi \propto E_\pi^{-(2.46--2.47)}, \text{ for } 20 \leq E \leq 70 \text{ GeV/c},$$

and

$$N(E_\pi) dE_\pi \propto E_\pi^{-(2.35--2.56)}, \text{ for } 80 \leq E \leq 500 \text{ GeV/c}.$$

Thompson and Whalley⁵) very recently, have obtained that the best representation of the data given by the equation (1) will be expressed by

$$N(E_\pi) dE_\pi \propto E_\pi^{-(2.637 \pm 0.014)}, \text{ for } 30 \leq E \leq 100 \text{ GeV}$$

and

$$N(E_\pi) dE_\pi \propto E_\pi^{-(2.540 - 0.036)^{+0.039}}, \text{ for } 100 \leq E \leq 700 \text{ GeV},$$

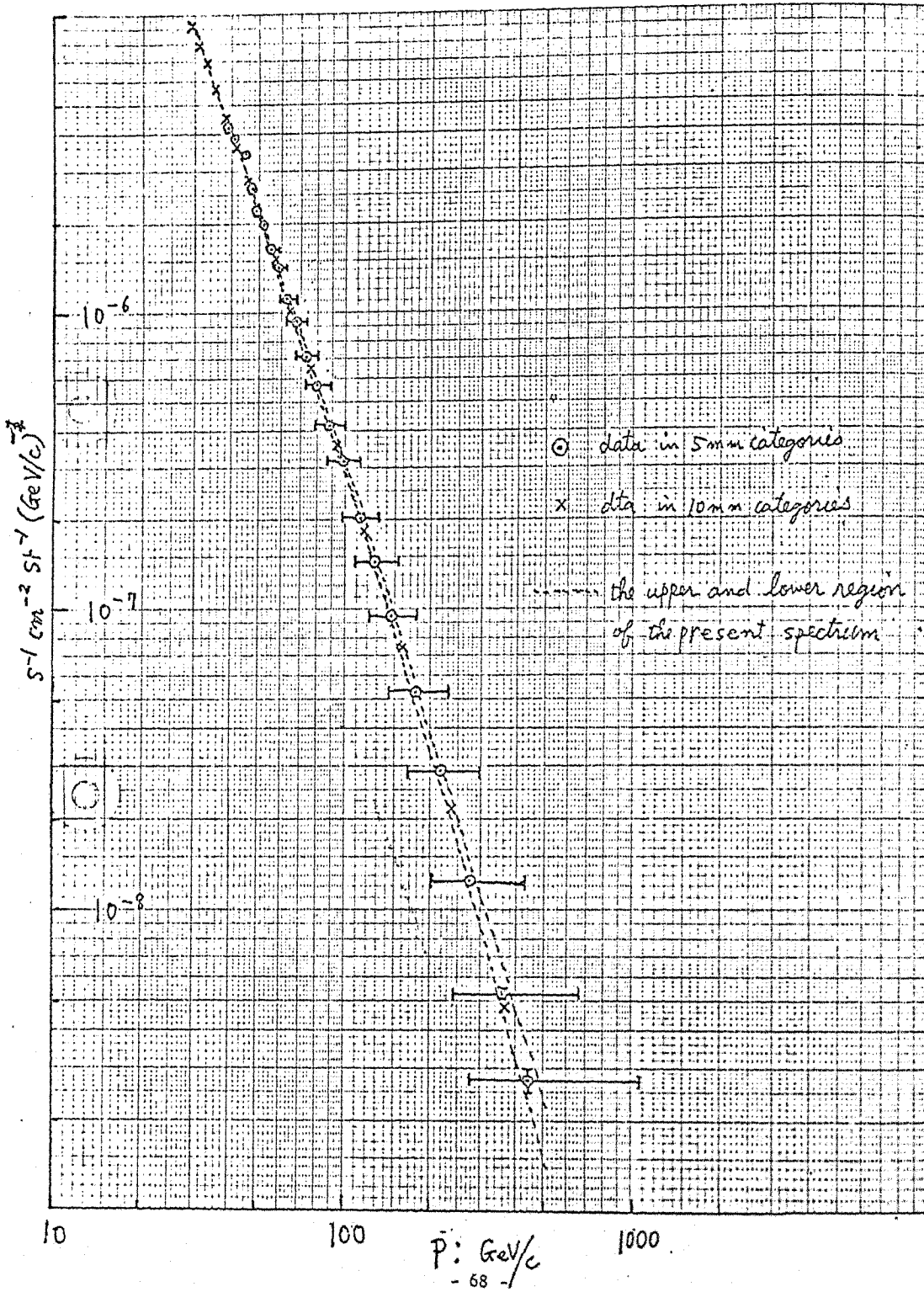
where the effect of the $K_{\mu 2}$ decay are also considered. They have concluded that γ of the exponent of power law spectrum of pion energy decreases over the range of E_π , 30--700 GeV. However, if we take into account the uncertainty of γ of the

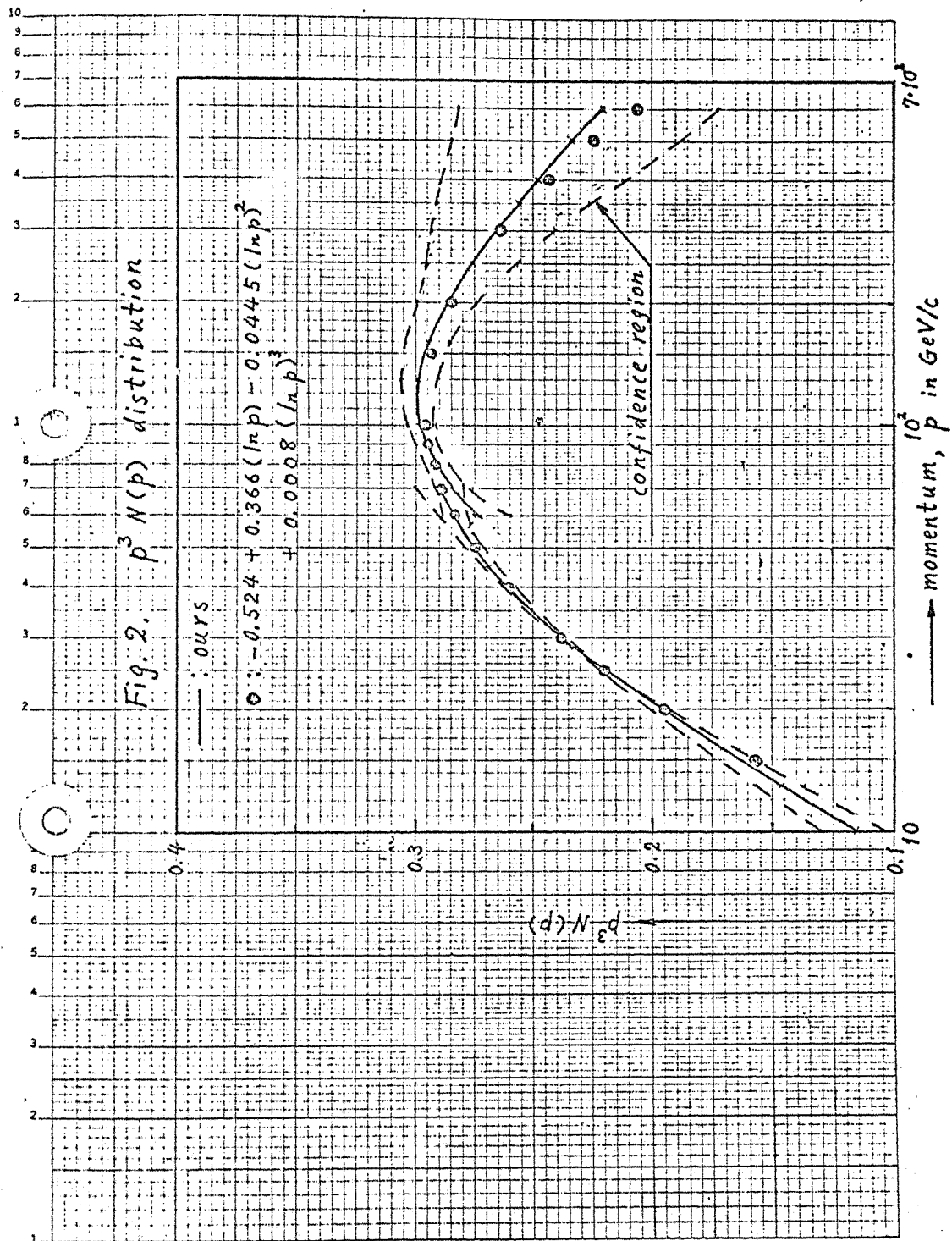
pion spectrum, we may not be able to say such a conclusion.

REFERENCES

- 1) C.A.Ayre, J.M.Baxendale, C.J.Hume, B.C.Nandi, M.G.Thompson and M.R.Whalley, J.Phys.G.1, 584(1975).
- 2) W.E.Deming, "Statistical Adjustment of Data", Willey and Sons Publ.Inc.
- 3) P.J.Hayman and A.W.Wolfendale, Proc.Phys.Soc., 80, 710(1962).
- 4) R.M.Bull, W.F.Nash and B.C.Rastin, Nuovo Cimento, XLA, 365 (1965).
- 5) M.G.Thompson and M.R.Whalley, J.Phys.G,1, L48(1975).

Fig. 1 differential momentum spectrum





ANALYSIS OF PREDICTED AND OBSERVED ENERGY LOSS RATE OF
COSMIC RAY MUONS PENETRATING GREAT DEPTHS IN ROCK AND WATER

C.R. Paul, N.L. Karmakar and N. Chaudhuri

Department of Physics, North Bengal University, Darjeeling, India.

Abstract

The cosmic ray muon high energy interaction behaviour is examined in a comparison of the observed absolute intensities in great underground and underwater depths with those expected from the recently measured sea-level energy spectra of muons and the refined theoretical energy loss rate data. It is concluded that the energy loss rates as predicted by the recent calculations of different interaction mechanisms can adequately account for the high energy muon interaction behaviour. For the muon-nuclear inelastic interaction process, it is not necessary to assume a value of photo-nuclear absorption cross section higher than the value of $125\mu\text{b/nucleon}$ adopted in the present work.

1. Introduction

The very high energy interaction behaviour of muons has been studied using the absolutely measured sea-level vertical muon spectrum and the deep underwater and underground muon intensities. The theoretically predicted energy loss rate formulae adopted in previous investigations have been computed accurately with a view to showing that the different adopted energy loss rates in the earlier analyses of underground muons lead partly to disagreeing conclusions (see for example Bazer-Bachi et al¹ in such analyses. Starting from the very carefully measured muon spectra at sea-level, and new theoretical results for some of the energy loss rate processes, the integral muon intensities at various underwater and underground depths have been derived and a comparison made with the available muon absolute intensity data at depths down to $\sim 10^4$ hg/cm² (standard rock). The present analysis may be considered as a useful adjunct to previous such works²⁻⁵, where the adopted sea level muon vertical spectra and their underground intensities are subject to large uncertainties.

2. Evaluation of Energy Loss Rate

The most recent underground and underwater absolute muon intensity data have been taken in the analysis. For each of the depths of observation the depth of penetration by muons has been converted to equivalent depth of standard rock. The minimum initial energy at sea-level of a muon in the vertical beam which just reaches a particular depth of underground and underwater has been computed by using the theoretically expected total energy loss rate with a constant photo-nucleon absorption cross section of $125\mu\text{b/nucleon}$ for the muon-nuclear interaction process. The expected integral muon intensity for this lower limit of muon energy for the particular depth in question was taken from the measured vertical sea-level spectrum (Ayre et al⁶). Above 1 TeV the measured spectrum extrapolated to higher energies using an $E^{-\gamma}$ type variation with $\gamma = 2.7$ has been used. The recent spectrograph measurements⁸ are consistent with $\gamma = 2.6$ up to 1 TeV. Above 500 GeV energy loss through bremsstrahlung and muon-nuclear interactions with characteristic fluctuations are important. The corrections for such fluctuations^{3,9} have been taken into account in the analysis. A comparison of the expected intensities with the observed values, as a function of minimum mean muon energies corresponding to the various depths of observation, indicates that the present state of the theory of interaction processes can adequately account for the propagation of the sea-level muon fluxes deep underground and underwater. It is not necessary to assume any increase in the photo-nucleon total absorption cross section with muon energy as suggested by some previous workers (see for example Chowdhuri and Saxena¹⁰.)

3. Discussion and Conclusion

The present analysis is consistent with the theoretically expected total fractional energy loss rate (due to bremsstrahlung direct electron pair production, muon-nuclear interaction process) values of 3.26 at 100 GeV, 4.1 at 1000 GeV and 4.55 at 30,000 GeV as against a constant value of 5.10 over the whole energy range in the analysis of Meyer et al¹¹ and O'Brien¹². Within the uncertainties of measurements, a change in the value of this quantity at muon energies above 100 GeV by about 5% gives rise to much larger discrepancies than observed between the expected and

observed underground muon intensities. The value of the collision loss rate, which is important for muon energies up to 500 GeV, has also been taken higher by Meyer et al. and O'Brien than the exactly calculated values. It is therefore concluded that sea-level and underground muon intensity measurements in the vertical direction cannot provide evidence in favour of anything new in the interaction behaviour of super high energy muons.

References

1. A.R. Bazer-Bachi, G. Vedrenne, W.R. Sheldon and J.R. Benbrook : Proc. 14th Int. Conf. Cosmic Rays (Munich) Vol. 6 1880 (1975).
2. P.J. Hayman, N.S. Palmer, and A.W. Wolfendale : Proc. Roy. Soc. A275 391 (1963), and references quoted therein.
3. K. Kobayakawa : IL Nuovo Cimento, B47, 156 (1967).
4. M.G.K. Menon and P.V. Ramana Musthy : Prog. Elem. Part. and Cosmic Rays (North Holland, Amsterdam) Vol. 9, 163 (1967).
5. R.K. Adair and H. Kasha : Proc. 13th Int. Conf. Cosmic Rays (Denver) Vol. 3, 1740 (1973).
6. C.A. Ayre, J.M. Baxendale, B.J. Daniel, C.J. Hume, M.G. Thomson, M.R. Whalley and A.W. Wolfendale : Proc. 13th Int. Conf. on Cosmic Rays, Denver, Vol. 3, 1754 (1973).
7. B.C. Nandi and M.S. Sinha : J. Phys. A5 1384 (1972).
8. O.C. Allkofer, K. Carstensen and W.D. Dau : Phys. Letts. 36B, 425 (1971).
9. K. Kobayakawa : Proc. 13th Int. Conf. of Cosmic Rays (Denver) Vol. 5, 3156 (1973).
10. B. Choudhuri and Y.C. Saxena, Pramana, Vol. 5, Nos. 3, 162 (1975).
11. B. S. Meyer, J.P.F. Sellschop, M.F. Crouch, W.R. Kropp, H.W. Sobel, H.S. Gurr, J. Lathrop, and F. Reines : Phys. Rev. D1, 2229 (1970).
12. K.O'Brien : Phys. Rev. D5, 597, (1972).

Average Energies and Differential Energy
Spectrum of Muon at various Depths

Akeo Misaki and Jun Nishimura*

Department of Physics, Saitama University,
Urawa, Japan.

*Institute for Aeronautical Science, University of
Tokyo, Komaba, Tokyo, Japan.

Abstract

Average Energies and Differential energy spectrum of muon are calculated at both various exponents of incident muons and various depth according to Nishimura's theory.

ELECTROMAGNETIC INTERACTION OF COSMIC RAY MUONS
AT LOW TRANSFER ENERGIES

S.Y. Lau* and L.K. Ng
Physics Department
University of Hong Kong

Abstract

An experiment was performed to investigate the electromagnetic interactions of cosmic ray muons concentrating on the knock-on process. A total of 1408 interaction events with transfer energies between 0.1 GeV and 2 GeV were collected and analysed. Good agreement in the interaction cross-sections measured with the theories was found apart from the higher value around $E_t = 1\text{ GeV}$. The overall ratio of the detected to the expected results was found to be 1.07 ± 0.03 . The charge asymmetry as a function of transfer energy and that of muon energy were also checked. The asymmetry was found to be insignificant.

Introduction

In a number of cosmic ray experiments dealing with the electromagnetic interactions of muons in matter (e.g. Allkoter et al (1971), Ayre et al (1971) and Osborne et al (1975)), a discrepancy between theories and experiments was found in the range of transfer energies around 1 GeV where the knock-on process was predominant. The discrepancy was that the cross-section for positive muons measured was larger than expected. This difference was reflected in a larger total interaction cross-section and in the existence of a positive excess of the muon cross-sections.

The purpose of this experiment was to study the knock-on process in the interactions with transfer energies from 0.1 GeV to 2.0 GeV to see whether the discrepancy mentioned could be substantiated. Individual muon charges and energies were also measured for more refined analysis.

The experiment involved a burst calorimeter consisting of 6 iron plates (2.15 radiation lengths) and 6 plastic scintillators interleaved together. Above the calorimeter was a vertical magnetic

*Now in the Applied Science Department, Hong Kong Polytechnic.

spectrometer which measured individual muon charges and energies up to 500GeV. Detailed description of the set-up was given elsewhere (S.Y. Lau et al (1975)).

Analysis on the interaction probability distributions

In this experiment, the energy spectra of the positive and negative muons were obtained, together with the burst events in the calorimeter. The energy transfer in each interaction in the calorimeter was determined by the burst size development. A total of 1408 interaction events, each with transfer energy greater than 0.1 GeV, were collected and analysed. The experimental values for the interaction probability as a function of the transfer energy is shown in figure 1. They are compared with the expected values calculated from the measured incident muon spectrum. The calculation was similar to Bhabha (1938), Petrukhin et al (1968) and Kohonliu et al (1970). The agreement is fairly satisfactory. There are only two intervals, 0.4 - 0.5GeV and 0.8 - 1.0GeV, which have values about one standard deviation away from the expected curve. It is also interesting to compare the experimental points with the expected curves calculated from muons of energy 8GeV and from muons of energy 15GeV, which are respectively the median energy and the mean energy of the incident muons. These curves are also shown in the same figure. The agreement is even better, showing that the deviation may be due to the small error in the muon spectrum itself, since corrections for the multiple scattering in the magnet and for the MDM uncertainty of the spectrometer have not been applied to individual muons.

For the purpose of a finer analysis, the interaction probability was plotted as a function of muon energy for each of four given values of the energy transfer as shown in figure 2. These four values are the median points of the energy transfer in the ranges of 0.1 - 0.2GeV, 0.2 - 0.3GeV, 0.3 - 0.6GeV and 0.6 - 2.0GeV respectively. The muon energies given in brackets on the horizontal axis are the median energies of the bins calculated from the detected muon spectrum. Since large bursts with transfer energies around 1GeV and above are seldomly produced by low-energy muons, the first data point on the 1GeV curve was chosen at 4.5 GeV instead of 3.8GeV. It can be seen that the agreement for $E_t < 10\text{GeV}$ is excellent. Above this energy, the points fluctuate. In particular, the point with $E_t = 1\text{GeV}$ and $E_\mu = 27\text{GeV}$ has a higher interaction probability when it is compared with the equivalent points in the same muon-energy bin.

It should be noted that, among the events with E_t below 2GeV and E_μ between 5GeV and 90GeV, more than 95% belong to the knock-on events. Therefore, mixing of other events due to bremsstrahlung and direct pair production is very small.

Analysis on the charge asymmetry ratio

The charge symmetry ratio δ is defined as the ratio of the interaction cross-section (N_μ^+) of positive muons to that (N_μ^-) of the negative muons, and is dependent on the energy transfer, i.e.

$$\delta(>E_t) = \frac{N_\mu^+(>E_t)}{\rho N_\mu^-(>E_t)}$$

where the muon charge ratio ρ was obtained from this experiment. Figure 3 shows how the measured δ with transfer energies $E_t > 0.1\text{GeV}$ varies with the muon energy. In this case, the burst events due to different charged muons were divided among themselves into muon energy cells and each cell is represented by the median muon energy. It can be seen that within the present statistical accuracy, no significant change of the asymmetry ratio with muon energy is present.

The charge asymmetry δ can also be conveniently expressed as the charge excess η . Taking the differential cross-sections $\sigma_\mu^\pm(E_t)$ instead, we have the plots as shown in figure 4. Apart from the points with $E_\mu < 5\text{GeV}$, where large fluctuation occurs, the results are quite consistent with the zero value.

Discussion

The significantly higher interaction cross-section between transfer 0.8GeV energies and 1.0GeV seems to support the results of Deery et al (1961), Kearney et al (1965), Chaudhuri et al (1965) and Allkofer et al (1971). The peaking is seen from figure 2 to have been produced by muon of energy greater than 20GeV, and hence it has not been observed with muons of $E_\mu < 15\text{GeV}$ in the machine experiments. Figure 5 gives a comparison among the various data. Further discussion was given elsewhere (S.Y. Lau (1976)).

Reference

1. Allkofer, O.C., Grupen, C. and Stamm, W.,
Phys. Rev. D. 4, 638 (1971)
2. Backenstons, G, Hyans, B.D., Knop, G., Marin, P.C. and Stierlin, V.
3. Bhabha, H.J., Proc. Roy. Soc., A 164, 257 (1938)
4. Chaudhuri, N. and Sinha, M.S., Nuovo Cimento 35, 13 (1965)
5. Dery, R.F., and Neddermeyer, S.H., Phys. Rev. 121, 1803 (1961)
6. Kearney, P.D., and Hazen, W.E., Phys. Rev. 138, 173 (1965)
7. Kirk, T.B.W., and Neddermeyer, S.H., Phys. Rev. 171, 1412 (1968)
8. Kokoulin, R.P., and Petrukhin, A.A., Proc. 11th Int. Conf. on
Cosmic Rays, Budapest 1969, Acta Phys. Hung, 29, suppl. 4,
277 (1970)
9. Lau S.Y. Ph. D. Thesis, Hong Kong University (1976)
10. Lau S.Y., Fong S.W., Chan S.K., MacKeown and L.K. Ng,
Proc. 14th Int. Conf. on Cosmic Rays, Munchen, 6, 1979, (1975).
11. Petrukhin, A.A., Shestakov, S.S., Cand. J. Phys., 46, 377 (1968).
12. Roc. B.P., and Ozaki, S., Phys. Rev. 116, 1022 (1959).

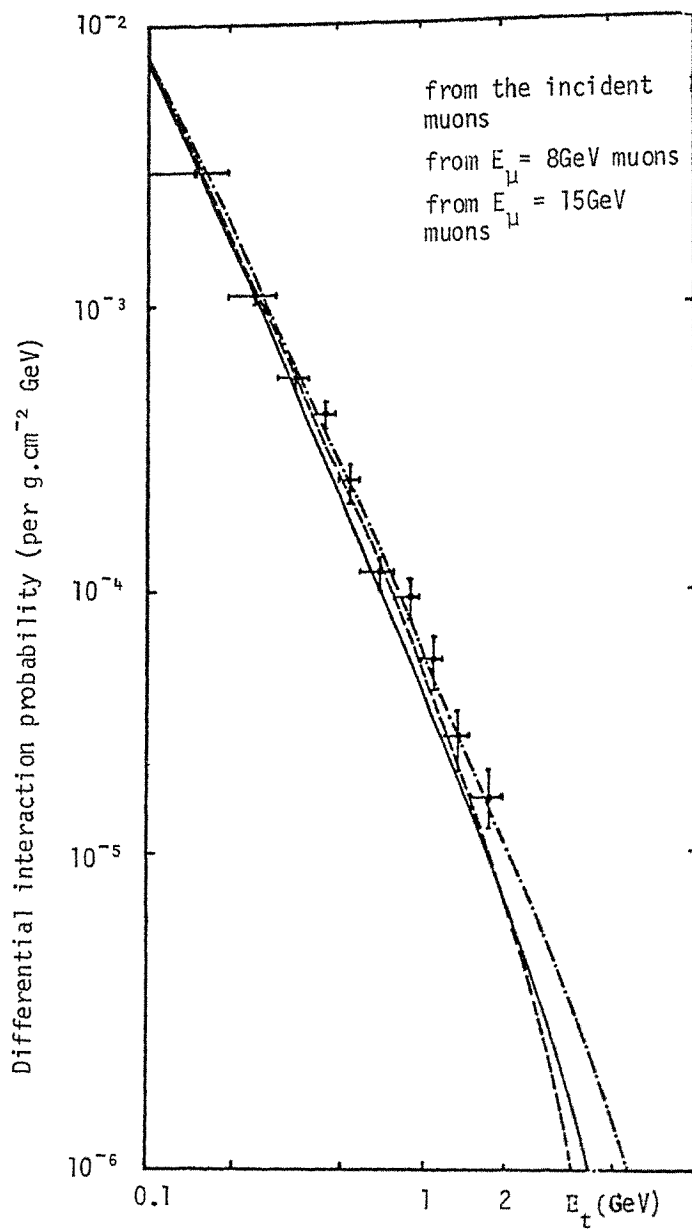


Fig.1. Comparison of detected total interaction cross-section with calculated values at different energy transfer. The vertical bars indicate the statistical uncertainty. The horizontal bars indicate the interval of consideration.

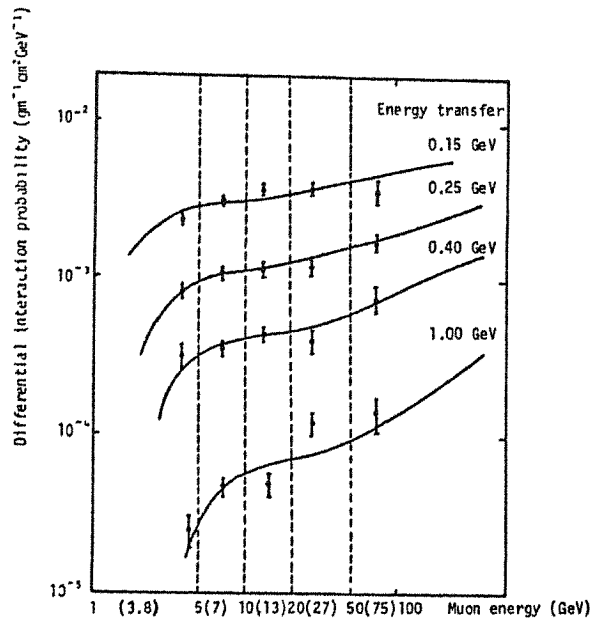


Fig.2 Interaction probability as a function of the muon energy for different values of the energy transfer. The muon energy given in brackets are the median energies of the bins.

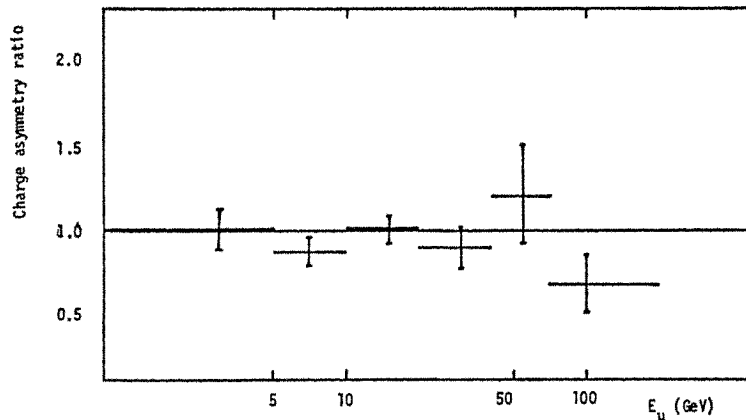


Fig.3. The dependence of the measured charge asymmetry ratio on muon energy.

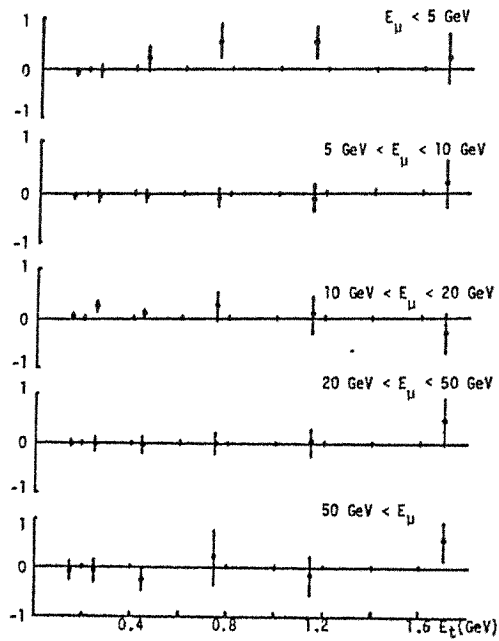


Fig.4. Dependence of the measured charge excess of differential cross-section on muon energy and energy transfer.

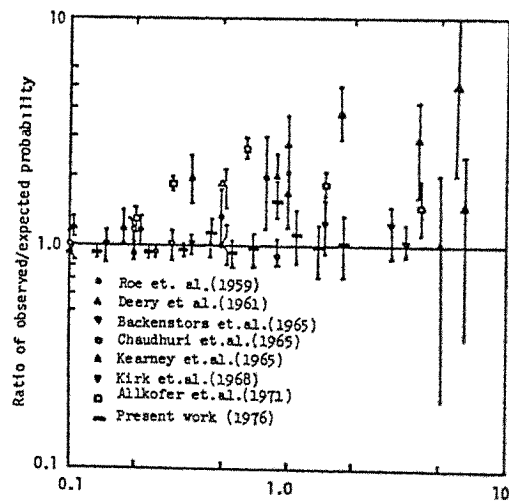


Fig.5. Results on knock-on process Energy transfer (GeV)

Nuclear Interaction Cross Section of Cosmic Ray Muons
estimated from the results of the accelerator experiments

Takashi Kitamura

Cosmic Ray Laboratory,
 University of Tokyo,
 JAPAN

1) Introduction

Theoretical expressions for nuclear interactions of cosmic ray muons (called deep inelastic scattering of high energy muons in fields of high energy physics) have been given by a lot of investigators¹⁾ extending from the classical treatment of Weizsäcker-Williams expression to recent Hand expression²⁾ and Drell-Wallecka expression³⁾. In Cosmic ray muon field, however, recent experimental results obtained with inelastic scattering of leptons in accelerators are not much utilized yet.

In this paper, we shall apply the Drell-Wallecka expression to cosmic ray muons fields, using values of the structure functions W_1 and W_2 which have been obtained from the experimental results of inelastic scattering in accelerator electrons and muons beams. So, we shall compare and discuss it with other cross section expressions which are presently been using in cosmic ray muons fields.

2) Recent expressions for nuclear interaction cross sections which are been using in cosmic ray muons fields.

We shall describe two typical expressions which presently are used in cosmic ray fields. One is DKMN expression which has been derived by Kobayakawa et al⁴⁾. The Drell-Wallecka expression being used in inelastic lepton scattering by high energy people has been based on this expression. The expression is

$$\frac{d^2\sigma}{dq^2 d\nu} = \frac{\alpha}{8\pi^2} \frac{1}{E_0 - m^2} \frac{1}{q^4} \left[L' (q^2 - m^2)^2 + L \left\{ (E_0 + (E_0 - \nu)^2) q^2 - 2m^2 \nu^2 - q^4/2 \right\} \right], \quad 1)$$

where q^2 : squared 4-dimensional momentum transfer,

ν : transfer energy,

E_0 : incident muon energy,

m : muon mass,

α : fine structure constant.

L and L' are structure functions and are related with the structure functions for W_1 and W_2 in the Drell-Wallecka expression as follows,

$$\begin{aligned} W_2 &= 2c q^2 \cdot L, \\ W_1 &= \frac{2c (q^2 - 2m^2)}{q^2} \left\{ \nu^2 L + (q^2 - 2m^2) L' \right\}, \quad 2) \end{aligned}$$

$$\text{with } c = 1/32\pi^3 \alpha A,$$

A: a converted constant.

For satisfying the Bjorken scaling⁵⁾, afterwards, Chin improved⁶⁾ the forms as follows,

$$L = \frac{4\pi}{\nu} \sigma_{\pi N} \left(\frac{\Lambda^2}{\Lambda^2 + q^2} \right),$$

$$L' = 0,$$

with $\Lambda^2 = 0.269 (\text{GeV}/c)^2$, 2)

At the München conference, Borog and Petrukhin⁷⁾ gave the following expression using Hand expression.

$$\frac{d\sigma}{d\nu} = \frac{\alpha}{\pi} \sigma_{\pi N} \frac{1}{\nu} \left\{ \nu - 1 + \left[1 - \nu + \frac{\nu^2}{2} \left(1 + \frac{2m^2}{\Lambda^2} \right) \right] \right. \quad 3)$$

Here $\nu = \nu/E_0$ and M is a nucleon mass. Referring the experimental results⁸⁾ for a region of $5 < K = \nu - \frac{M^2}{2M} < 8.3$ GeV of accelerator electron and muon beams, they decided a value of $0.4 (\text{GeV})^2$ as Λ^2 . In analysis of experimental results of cosmic ray muons, an integral form of the total cross section are rather convenient^{for} comparisons among them, because of few occurred frequencies. In order to discuss these expressions of Chin and Petrukhin et al, their intergral ones of total cross section are shown in Fig.1 for three cases of transfer energies 10 GeV, 100 GeV and 1000 GeV. In this calculations, each value of real photon cross section, σ_{γ} was taken as $1.25 \times 10^{-28} \text{ cm}^2/\text{nucleon}$ for Chin and $1.0 \times 10^{-28} \text{ cm}^2/\text{nucleon}$ for Petrukhion et al as they did. These values and energy dependences of cross sections give rather different behaviours.

In order to decide which expression more reasonable is, we shall get their values of so-called b-term which is given by

$$b_n = \frac{N}{E_0} \int_{\nu_{\min}}^{\nu_{\max}} \int_{q_{\min}^2}^{q_{\max}^2} \nu \frac{d^2\sigma}{dq^2 d\nu} dq^2 d\nu, \quad 4)$$

where N is the Avogadro number. Their upper and lower limits of the integrations are determined by kinematics limits of the nuclear interactions and given by the following expression.

$$\nu_{\max} = E_0 \left\{ 1 - \frac{M}{2E_0} \left(1 + \frac{m^2}{M^2} \right) \right\} \approx E_0 \left(1 - \frac{M}{2E_0} \right),$$

$$\nu_{\min} = m_{\pi} + (q^2 + m_{\pi}^2)/2M \approx m_{\pi}$$

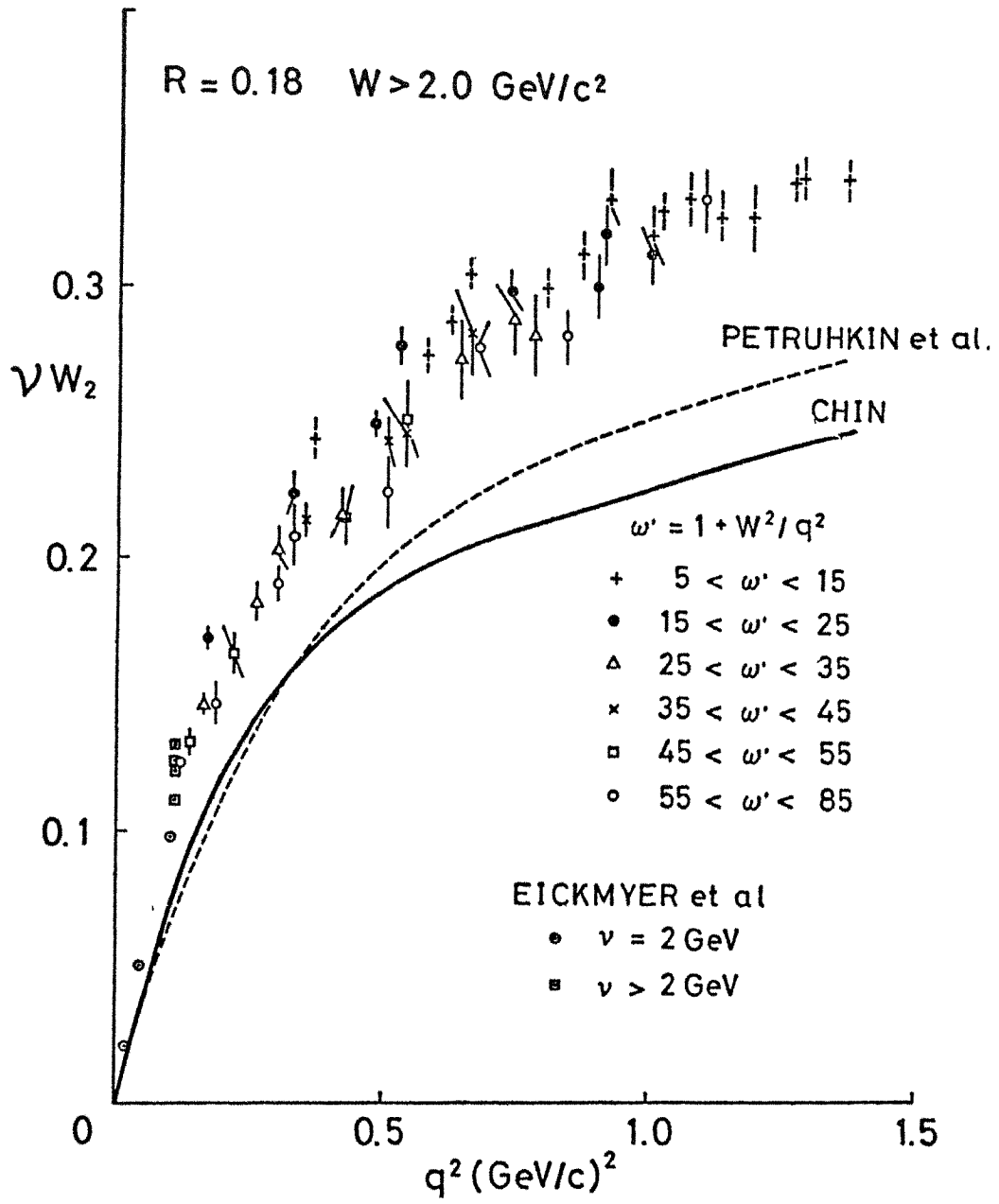
$$q_{\max}^2 = 2M(\nu - m_{\pi}) - m_{\pi}^2 \approx 2M\nu$$

$$q_{\min}^2 = m^2 \nu^2 / E_0 (E_0 - \nu). \quad 7)$$

Their calculated values of b_n -term are shown in the table.

	b_n -value (at 1000 GeV muon energy)
Chin	$4.67 \times 10^{-7} \text{ cm}^2/\text{g}$ (with $= 1.25 \times 10^{-28} \text{ cm}^2/\text{nucleon}$)
Petrukhin et al	$4.48 \times 10^{-7} \text{ cm}^2/\text{g}$ (with $= 1.0 \times 10^{-28} \text{ cm}^2/\text{nucleon}$)

Fig. 1



The measured value of b_n -terms is obtained from a comparison between the observed muon energy spectrum at sea-level with the observed range spectrum below ground and by subtracting the energy loss of electromagnetic interactions of muons from the difference between both spectra. The measured value is given as nearly constant with a value of $(4 \sim 5) \times 10^{-7} \text{cm}^2 \text{g}^{-1}$ in a region of 100 GeV to 2 TeV of muons⁹⁾. From the table, thus, the value for b_n -terms obtained from both expressions seems to be consistent with the measured value.

To have more discussions, we shall compare the behaviour of Λ^2 -value of Petrukin et al with the accelerator data in Fig.2. Although they took a form of the total cross section as $\sigma_{TW} \frac{1}{1 + \frac{1}{2} \nu^2 / \Lambda^2}$ with $\Lambda^2 = 0.4 (\text{GeV}/c)^2$ for a region of $5 \leq K(=) \frac{\nu^2}{2M} \leq 8.3$ GeV, some data satisfying the region which have been obtained with the observation of Eickmeyer et al¹⁰⁾ are deviated from the form of Petrukin et al as shown in Fig.2.

In order to compare the structure function W_2 used by the expressions of Chin and Petrukin et al with the data of accelerator experiments, furthermore, we shall estimate those values of both expressions. The value for W_2 in the expression of Chin is obtained from the expression (2) and when an approximation of

$$\varepsilon = \Gamma_\ell / \Gamma_t = \left\{ 1 + 2 \left(1 + \nu^2 / q^2 \right) \tan^2 \frac{\theta}{2} \right\}^{-1} \approx 1$$

is valid for the expression of Petrukin et al, the value of W_2 is obtained by

$$W_2 = \frac{1}{4\pi^2 \alpha} K \frac{q^2}{q^2 + \nu^2} (\sigma_t + \sigma_\ell). \quad 6)$$

Here, Γ_t : flux of transversely polarized virtual photons,

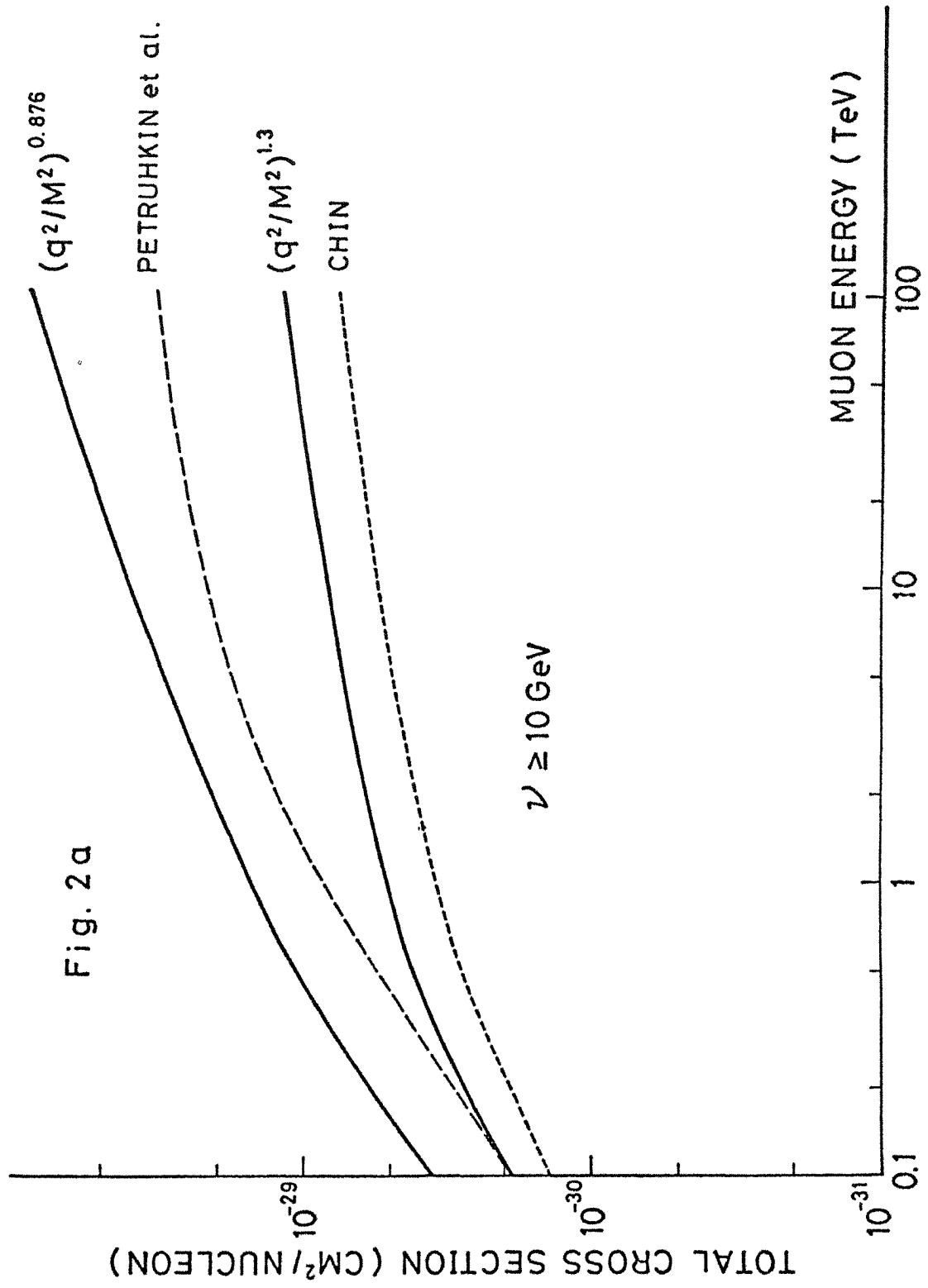
Γ_ℓ : flux of longitudinally polarized virtual photons,

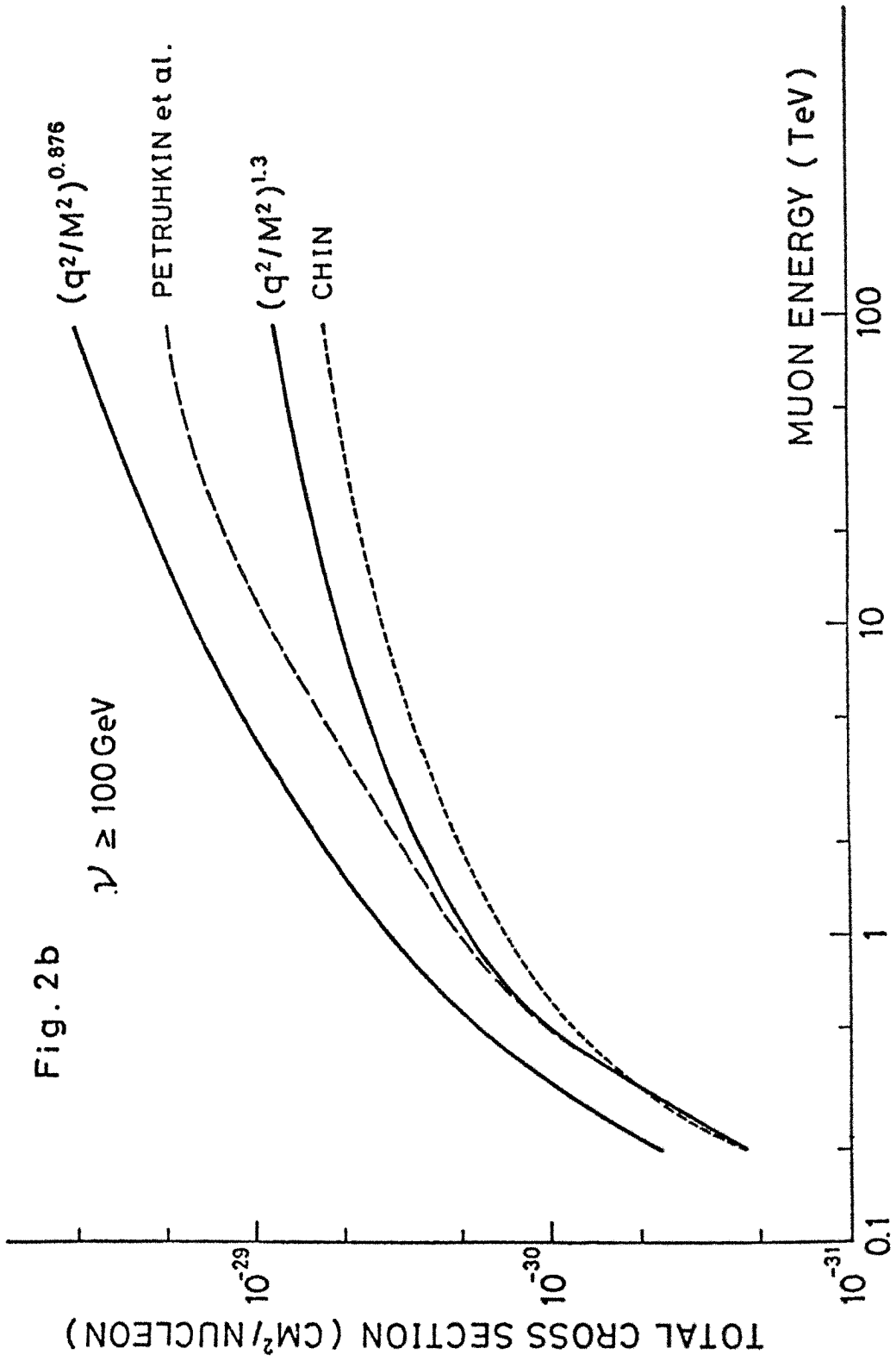
σ_t : total cross section of transversely polarized virtual photons,

σ_ℓ : total cross section of longitudinally polarized virtual photons.

Taking into considerations the above approximation, but, this W_2 -value may give the maximum one. Behaviours of νW_2 obtained from both expressions are plotted in Fig.3 as the horizontal axis of q^2 .

For comparisons, the experimental data of interactions in a case of missing mass $W \geq 2 (\text{GeV}/c)^2$ obtained by SLAC electron beam¹¹⁾ are plotted together with them. For a region of $q^2 \leq 0.12 (\text{GeV}/c)^2$, the recent experimental results with transferred energies, ν , of 2.0 to 8.45 GeV obtained by Eickmeyer et al are also added. These values seem to be connected rather smoothly with the other values of $q^2 > 0.12 (\text{GeV}/c)^2$ and also not contradicted with the data of 12 GeV muons cited by Petrukin et al within rather large statistical errors though.





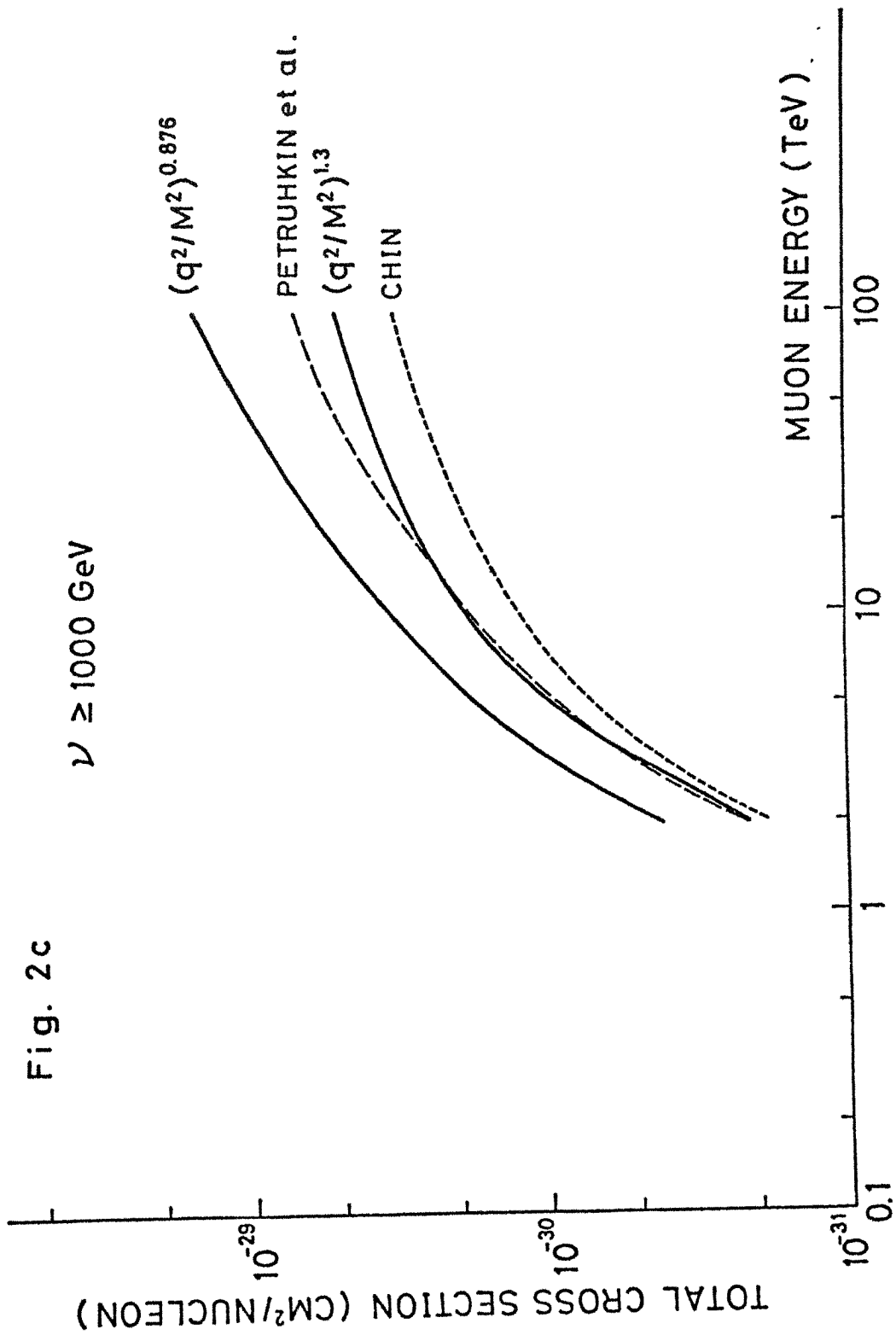
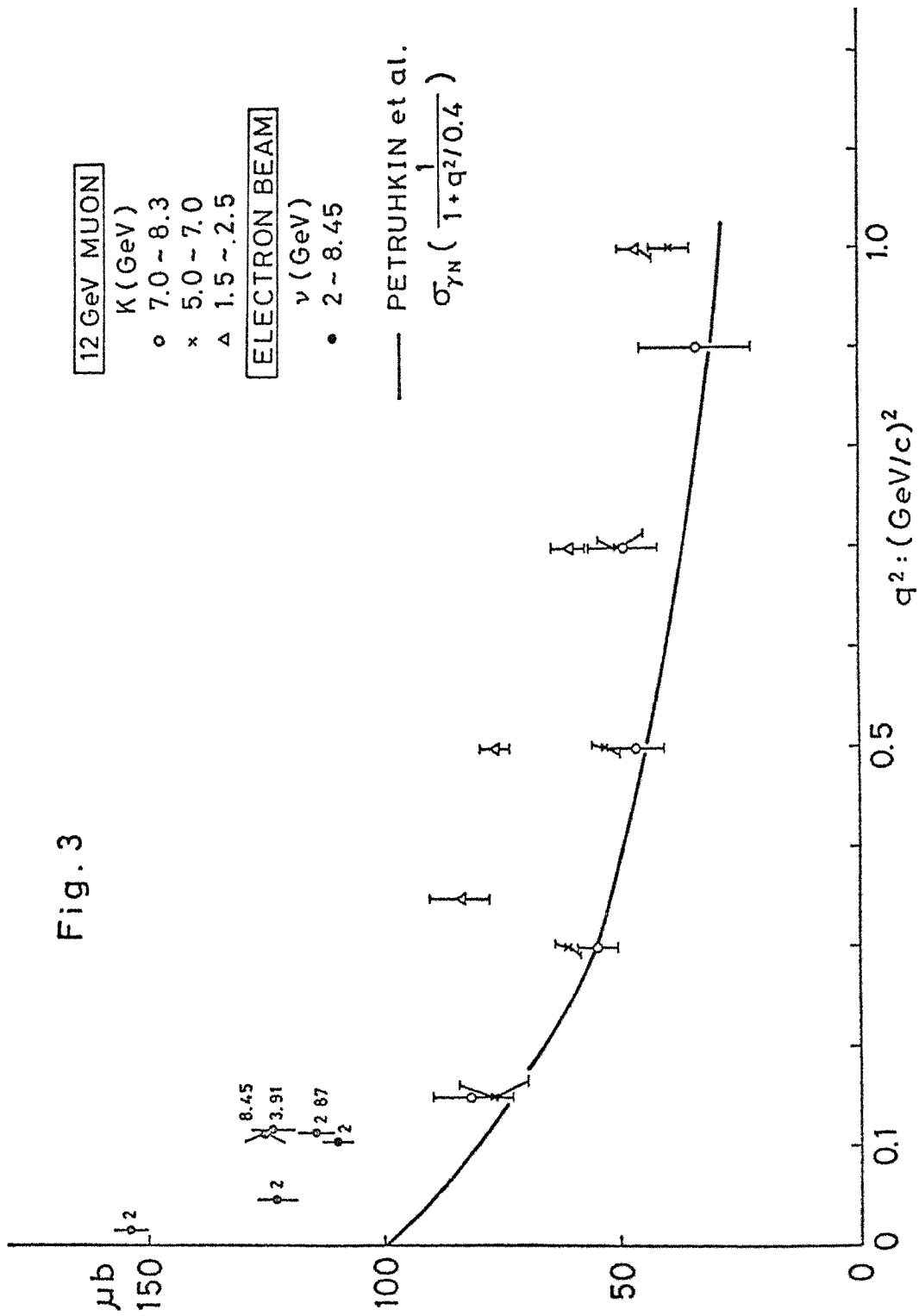


Fig. 3



From the figure, it is found that both expressions of Chin and Petrukin et al have rather smaller values of structure function νW_2 than the accelerator data have given.

3) The present expression for cross section

In the above paragraph, it was known that values of structure function νW_2 in both expressions of Chin and Petrukin et al are very small compare with the experimental data of the electron beam of accelerator. At these energy region, it is very hard to consider that there would be some differences between characters of muons and electrons. Therefore, we shall try to get the expression for cross sections to have the structure function that is consistent with the accelerator data. Using the experimental results of $R = \sigma_2/\sigma_1 = 0.18^{11)}$ which has shown by the accelerator electron beam, one can get the following expression by substituting W_2 for W_1 .

$$\frac{d^2\sigma}{d^2q^2 d\nu} = \frac{4\pi\alpha^2}{q^4} \frac{E'}{E_0} \left[W_2 \cos^2 \frac{\theta}{2} + 2W_1 \sin^2 \frac{\theta}{2} \right] \\ \approx \frac{4\pi\alpha^2}{q^4} \frac{E'}{\nu} \frac{E'}{E_0} \left[1 + \frac{1}{1+R} \left(\frac{E_0}{E'} + \frac{E'}{E_0} - 2 \right) \right] \nu W_2, \quad (7)$$

where $\nu = E_0 - E'$,
 $R = \sigma_2/\sigma_1$.

To be consistent with the experimental results of shown at Fig.3, the following expressions for W_2 are given as

$$\begin{aligned} \nu W_2 &= 0.34 && \text{in } q^2 \geq 1.4 \text{ (GeV/c)}^2, \\ \nu W_2 &= 0.307 (q^2/M^2)^{0.259} && \text{in } 1.4 > q^2 \geq 1.0 \text{ (GeV/c)}^2, \\ \nu W_2 &= 0.308 (q^2/M^2)^{0.276} && \text{in } 1.0 > q^2 \geq 0.6 \text{ (GeV/c)}^2, \\ \nu W_2 &= 0.324 (q^2/M^2)^{0.467} && \text{in } 0.6 > q^2 \geq 0.12 \text{ (GeV/c)}^2, \\ \nu W_2 &= 0.716 (q^2/M^2)^{0.872} && \text{in } 0.12 > q^2 > 0 \text{ (GeV/c)}^2. \end{aligned} \quad (8)$$

Using the expressions (7) and (8), we shall get the total cross section with larger transferred energies than ν as follows,

$$\sigma(>\nu) = \pi\alpha^2 \left[6.462 (\ln E_0/\nu) - \frac{E_0 - \nu}{E_0} + 2.851 \left(\frac{E_0^2 - \nu^2}{E_0^2} \right) - 0.723 \left(\frac{1}{\nu} - \frac{1}{E_0} \right) + \frac{0.110}{E_0^2} \ln E_0/\nu \right] \quad (9a)$$

in $q^2 \geq 0.12 \text{ (GeV/c)}^2$,

$$\sigma(>\nu) = \pi\alpha^2 \left[173.648 (E_0/\nu)^{0.256} + 69.406 (\nu/E_0)^{0.744} - 237.109 + 32.802 \{ (E_0 - \nu)/E_0 - \ln E_0/\nu \} - 19.329 (\nu/E_0)^{1.744} + 1.757 (\nu/E_0)^{2.744} + 13.899 (\nu/E_0)^2 \right] \quad (9b)$$

in $0 < q^2 < 0.12 \text{ (GeV/c)}^2$.

Here, each energy is expressed by a unit of GeV. In this case, however, a calculation of the b_n -value using the expression (8) for νW_2 give a value of the b_n - term as $2.98 \times 10^{-6} \text{ cm}^2/\text{g}$ at 1000 GeV muon energy which is very large compared with the measured value

mentioned in the previous paragraph. This contradiction is too large so as to be explained by the difference between the total cross sections of proton and neutron in the nucleus of rock matter that has been observed by Eickmeyer et al. In general, the value of b_n - term is mostly determined with only values of νW_2 in a region of very small q^2 -values as ≤ 0.1 (GeV/c)². So, if the another expression of $1.66 (q^2/M^2)^{1.3}$ for νW_2 is adopted in a region of $0.12 > q^2 > 0$ (GeV/c)², the b_n -value in this case is obtained as $\sim 5.0 \times 10^{-7}$ cm²/g which does not contradict with the measured value. In the case of this expression of $1.66 (q^2/M^2)^{1.3}$ for νW_2 , the total cross section is given by

$$\begin{aligned} \sigma(\nu) = \pi\alpha^2 [& 13.828 \{ b_n E_0/\nu - (E_0 - \nu)/E_0 + 5.859 (E_0^2 - \nu^2)/E_0^2 \\ & - 8.336 + 4.600 (\nu/E_0)^{0.6} - 2.967 (\nu/E_0)^{1.6} \\ & - \frac{5.747}{E_0^{2.3}} \int_{\nu}^{E_0} \nu^{1.6} / (E_0 - \nu)^{0.3} d\nu \quad \text{in } 0 < q^2 < 0.12 \text{ (GeV/C)}^2 \end{aligned} \quad (10)$$

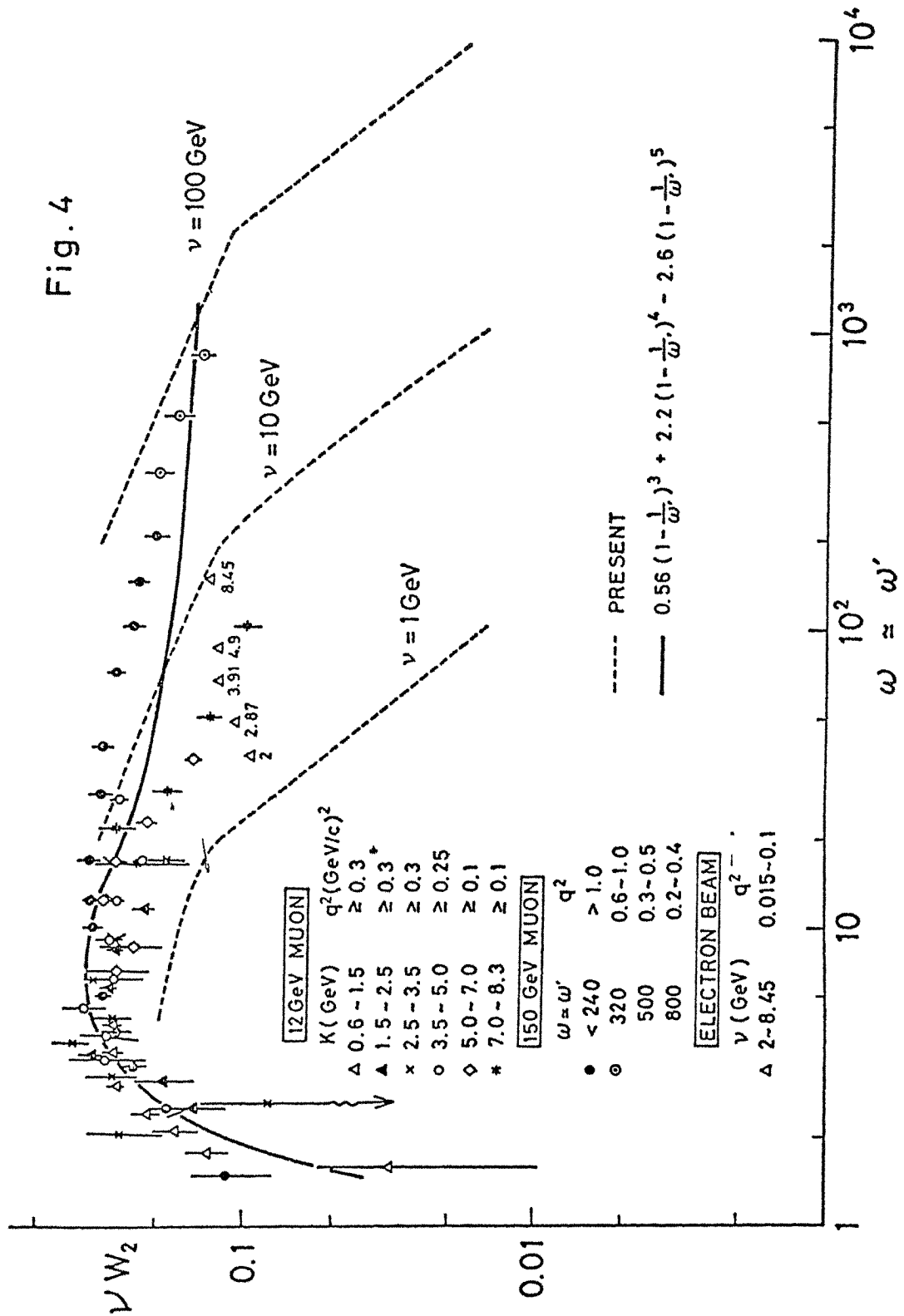
In three cases of $\nu \gg 10$ GeV, 100 GeV and 1000 GeV, two behaviours of the total cross section are plotted with a real line of $(q^2/M^2)^{0.876}$ for the expression (9a)+(9b) and a real line of $(q^2/M^2)^{1.3}$ for the expressions (9a)+(10). From the figure, it is clear that dependences of incident muon energy E_0 of the real lines of $(q^2/M^2)^{0.876}$ and $(q^2/M^2)^{1.3}$ are similar as those of Chin and Petrukhin et al, respectively, however the absolute value seem to be about two times larger.

4) Discussions

From the experiments of electron beam, it has been known that the behaviours of νW_2 are valid for scaling by a parameter of, say, $\omega = 2M\nu/q^2$ or $\omega' = \frac{W^2}{q^2} + 1 = \frac{M^2 + 2M\nu}{q^2}$. For example, the behaviour has been given with the following experienced law¹²⁾,

$$\nu W_2(\omega') = 0.56 (1 - 1/\omega')^3 + 2.2 (1 - 1/\omega')^4 - 2.6 (1 - 1/\omega')^5, \quad (11)$$

which is drawn in Fig.4. Very recently, the observation of muon beam with 150 GeV of Fermi NAL¹³⁾ has shown to be similar with the expression as seen from the figure. However, the data of 12 GeV muons at SLAC seem to be deviated from the curve in a region of $\omega > 20$. Also, the data with transferred energies of 2 GeV to 8.45 GeV of Eickmeyer et al show some deviations from the curve as plotted in the same figure. This illustrates that values in a region of $q^2 < \text{a few tenth (GeV/c)}^2$ cannot be expressed by the expression of scaling. This situation becomes very clear when values of the present expression (9a)+(10) for νW_2 are plotted in the same figure.



The dotted curves of three cases with $\nu=1$ GeV, 10 GeV and 100 GeV begin to be deviated from $q^2 \sim (0.1 \sim 0.2) (\text{GeV}/c)^2$.

In experiments of cosmic ray muons, almost interactions observed have rather small q^2 values even in cases of very large transferred energies. So, we consider that the present expression should be valid for the total cross section of cosmic ray muon interactions in large ω values. Also, it is very interested the different values between two cross sections of $(q^2/M^2)^{0.872}$ and $(q^2/M^2)^{1.3}$. Although the case of $(q^2/M^2)^{0.872}$ is obtained from the observation at very small q^2 of electron beam, it is contradicted with the measured value of b_n -term. In these connection, it is most necessary to check the present expression for cross section by using an observation of MUTRON⁴⁾.

References

- 1) For example, Y.Minorikawa: CKJ report-17 (Cosmic Ray Lab. Tokyo University) (1974).
- 2) L.N.Hand: Phys. Rev. 129 1834 (1963).
- 3) S.D.Drell and J.D.Walecka: Ann. Phys. 28 18 (1964).
- 4) K.Daiyasu, K.Kobayakawa et al: J. Phys. Soc. Japan Supple A3 344, 367 (1962).
- 5) J.D.Bjorken: Phys. Rev. 179 1547 (1969).
- 6) S.Chin: Dr. Thesis (Osaka City University) (1973).
- 7) V.V.Borog and A.A.Petukhin: Proc. 14th I.C.R.C. 6 1949 (1975).
- 8) T.J.Braunstein, W.L.Lakin et al: Phys Rev. D6 106 (1972).
- 9) For example, K.Kobayakawa: Proc. 13th I.C.R.C. 5 3156 (1973).
- 10) J.Eickmeyer et al: Phys.Rev. Lett. 36 289 (1976).
Phys Letters 63B 104 (1976).
- 11) For example, B.C.Barish: CALT-68-477 (1974).
- 12) E.D.Bloom et al: Phys. Rev. D4 2901 (1971).
- 13) Y.Watanabe, L.N.Hand et al: Phys. Rev. Lett. 35 898 (1975).
L.W.Mo et al: Phys. Rev. Lett. 37 4 (1976).
- 14) T.Kitamura, K.Mithui et al: Proc. 13th I.C.R.C. 3 1962 (1973).

Figure Captions

- Fig. 1. Integral values of total cross sections of Chin (a broken line), Petruhkin et al (a chain line) and the present (a real line) in three cases of $\nu \gg 10$ GeV, $\gg 100$ GeV and $\gg 1000$ GeV.
- Fig. 2. Comparisons of values for νW_2 in cases of Chin and Petruhkin et al with the accelerator data.
- Fig. 3. Comparisons of cross sections used by Petruhkin et al with the accelerator data.
Values of attached to the dark circle indicated the transfer energy.
- Fig. 4. Experimental results of the accelerator muon beam in a function of $\omega \approx \omega'$. A real curve is given by an experimental law (11) estimated from the experimental results of the accelerator electron beam. Dotted lines show the curves drawn by the expressions (9a)+(10) with $\nu=1, 10$ and 100 GeV. Values of attached to the triangle indicate the transfer energy.

Muon Interaction in Mutron Calorimeter

T.Aoki, S.Higashi, K.Honda, S.Iida, Y.Kamiya, H.Kawashima,
T.Kitamura, K.Kobayakawa, S.Mikamo, Y.Minorikawa, K.Mitsui,
S.Miyake, Y.Muraki, I.Nakamura, Y.Ohashi, A.Okada, S.Ozaki,
H.Shibata, T.Takahashi, and Y.Teramoto

Cosmic Ray Laboratory, University of Tokyo,
Tanashi, Tokyo 188, Japan (representative address)

Abstract

The calorimeter of Mutron is under test operation, which is made of 12 iron plates (3m x4m x12cm) with proportional chambers or spark chambers inserted between them. The aim of this calorimeter is to study muon interaction up to Tev region. Preliminary results will be presented.

Monte Carlo Simulation of Neutron Calorimeter

K.Mitsui, A.Okada, M.Shibata

Cosmic Ray Laboratory, University of Tokyo,
Tanashi, Tokyo 188, Japan (representative address)

Abstract

According to a Monte Carlo simulation, nuclear interactions of muons in the calorimeter can be separated from the other electromagnetic interactions, because of the difference of longitudinal development of showers between them.

The efficiency of the separation is about 90 % in case of 100 GeV transfer energy without any consideration of experimental errors.

Cerenkov Radiation from a Shower Developed in the Deep Water

Jun Nishimura

Institute of Space and Aeronautical Science,
University of Tokyo,
Komaba, Tokyo, Japan

1. Introduction

Recent development of technology in the Oceanography has opened the wide possibilities to observe the cosmic ray phenomena occurring in the deep sea water. Thus the "DUMAND"⁽¹⁾ project is proposed to observe μ meson and neutrino interactions in the deep sea water.

Spectrum of high energy μ mesons arising from the cosmic ray interactions in the atmosphere have been studied by magnetic spectrometers, by emulsion chamber technics, by observing the flux at deep underground and by the Horizontal Air Shower observation to explore the characteristics of the interactions at extremely high energy region. High energy neutrino interaction is also studied at deep underground. These neutrinos are considered to be produced by the cosmic ray interactions in the atmosphere. But recently it is proposed higher flux of neutrino of cosmical origin than that of cosmic rays exists beyond 10 TeV region⁽²⁾.

Inspite of these many observations, it is quite desirable to find an efficient way to observe these rare events at extremely high energy region.

In this respect, Soviet group⁽³⁾ have proposed to observe the Cerenkov Radiation from an electron shower produced by these μ mesons and neutrinos in the deep water.

The Cerenkov Radiation from an electron shower developing in the water has a different feature from those observed in the Extensive Air Showers. Thus it is necessary to have the accurate knowledge of lateral distribution of Cerenkov photons from the shower to see the feasibility of such an experiment.

In this paper, first, the characteristics of the Cerenkov Radiation from an electron shower developing in the water are discussed. Next, the analytical solution of the lateral distributions of these photons are derived.

The mathematical treatment is based on the three dimensional cascade theory in the App. B.⁽⁴⁾, and the solution is derived without using other approximations.

The numerical evaluation of the analytical solution are made, and the results are shown for a different incident energies as well as at a different depth from the starting point of the electron shower. The results are compared to those given by Soviet group.

Referring to these results the possibilities to observe high energy μ mesons and neutrino interactions in the deep sea water are discussed in this paper.

2. Characteristic of the lateral distribution of the water Cerenkov Radiation from an electron shower

The characteristics of the Cerenkov Radiation from the shower developing in the water have widely been studied by Soviet people⁽³⁾. Referring to their works, some basic quantities related to the water Cerenkov Radiation are shown in the Table 1.

Table 1
Basic Quantities for the Water Cerenkov Radiation

	N	Eth	θ_c	photons*/cascade unit
water	1.33	.778 MeV	41°19'	6.15 x 10 ³
air**	1.00027	22.8 MeV	1°20'	1.27 x 10 ⁴

* water 3500 Å - 5000 Å
air 3500 Å - 6000 Å

** 1 atmospheric pressure

As shown in the Table, the water Cerenkov Radiation from a shower is characterized by high refractive index and thus by the large Cerenkov cone angle. Thus the lateral distribution of the Cerenkov Radiation from an electron shower is determined by this large Cerenkov angle and the angular distributions of the shower electrons at each depth as shown in Fig.1. The degree of each contribution to the lateral spread can be evaluated by comparing the Cerenkov cone angle and angular spread of shower electron.

The angular spread of shower electrons is calculated by using the angular distribution given in the three dimensional cascade theory in App. B. (4)

The angular distribution is

$$\pi(E_0, E, \theta, t) = -\frac{1}{8\pi^2 L} \iiint ds dp dq \left(\frac{E_0}{E}\right)^s \left(\frac{\epsilon}{E}\right)^p \left(\frac{\epsilon^2}{K^2}\right)^{-p-1} \frac{\Gamma(p+1)\Gamma(-p)}{s+2p+q} \mathcal{M}(s, p, q, t), \quad (1)$$

where E_0 , E , ϵ and K^* are the incident energy, the energy of shower electrons, the critical energy and the scattering energy. \mathcal{M} is given as the solution of the difference equation in the reference (4).

The mean square deviation angle is thus given by

$$\langle \theta^2 \rangle = \frac{\int_0^\infty \theta^2 \pi 2\pi \theta d\theta}{\int_0^\infty \pi 2\pi \theta d\theta} \quad (2)$$

The numerical results are shown in Table 2, together those given by other authors.

* 1 cascade unit = 36 gr/cm²

$\epsilon = 73$ MeV, $K = 19.3$ MeV, in the water

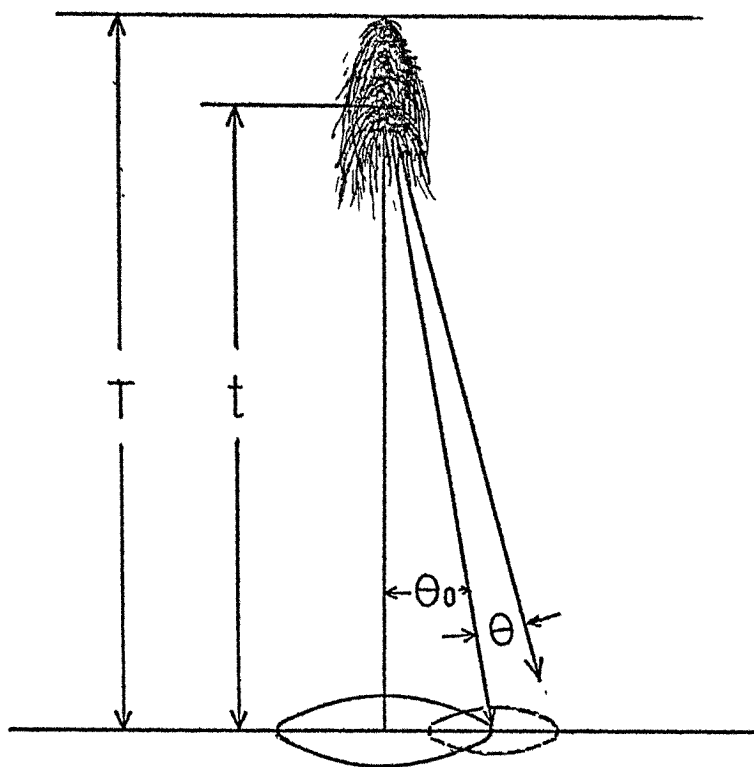


FIG.1 CERENKOV CONE AND SCATTERED ELECTRON

Table 2

Average Scatted Angle of Shower Electron

E	$\langle \theta \rangle$	$\langle \theta^2 \rangle^{1/2}$	$\langle \theta^4 \rangle^{1/2}$
≥ 0	23°45'	∞	∞
≥ 1 MeV	14°32'	34°30'	60°37'
≥ 2 MeV	13°14'	26°54'	47°07'
≥ 5 MeV	11°04'	18°05'	33°08'
App A	4°42'	6°36'	10°01'
Ivanenko		36°40'	
Chudakov		15°~20°	

The results show the average deviation angle of shower electron is comparable to the Cerenkov cone angle. Since these angles are as large as 40°, lateral spread of the radiation at the observation place becomes comparable to the distance from the starting place of the electron showers. This is quite a different feature compared to the case of Extensive Air Shower, in which the lateral distribution of the Cerenkov photons are essentially determined by the angular spread of shower electrons.

Comparison is made for the Cerenkov photon density at the observation place, for showers of the same energy developing in the water and atmosphere.

Table 3

Comparison of Cerenkov Photon Densities
for a Shower of the Same Energy

Effect Due to	E_{th}	Emissivity	Lateral Spread	Total
Water	3	1	$10^2 \sim 10^4$	$10^2 \sim 10^4$
Air	1	2	1	1

From the figures in the Table 3, the Cerenkov photon densities are expected to be as large as $10^{2\sim 4}$ times of that EAS, if the shower of the same energy is developing in the water. This means if the apparatus is able to observe the Cerenkov Radiation from EAS of 10^{16} eV, the same photon density is expected for the showers of 10^{12} eV in the water.

The detectors placed with a suitable separation such as an EAS array cover the large detection area. Besides these, by the large amount of overlying producing material for the interaction, the observation of the Cerenkov Radiation gives us an efficient way to observe the feature of interaction of high energy μ mesons and neutrinos compared to other detection method.

3. Derivation of the lateral distribution of water Cerenkov Radiation

As described in the proceeding section, the lateral distribution of the water Cerenkov Radiation from an electron showers are determined by the combination of the contribution of the Cerenkov cone and the angular spread of the shower electron at each depth.

The lateral distribution of the Cerenkov photons at the depth T emitted by an electron at the height of t, t+dt from the observation point T is given by*,

$$2\pi g(r')r'dr' = \alpha \cdot \delta\left(\theta_0 - \frac{r'}{t}\right) \frac{dr'}{t} dt \quad (3)$$

if one ignore the scattering of the emitting electrons and absorption by water for the photons. T, t and r' are measured in cascade unit of water and α the number of photons produced per one cascade unit.

$$\begin{aligned} * \quad \alpha &= \frac{2\pi e^2}{\hbar c} \left(1 - \frac{1}{n^2\beta^2}\right) \left(\frac{1}{\lambda_{\min}} - \frac{1}{\lambda_{\max}}\right) \text{ photons/cm} \\ &= 7.18 \cdot 10^5 \left(\frac{1}{\Lambda_{\min}} - \frac{1}{\Lambda_{\max}}\right) / \text{c.u.} \quad \text{in the water,} \end{aligned}$$

where Λ is measured in 1000 Å unit.

The angular distribution** of the total shower electrons is given by putting E to 0 in the formula (1), and

$$\Pi(E_0, \theta, T-t) = \frac{-1}{4\pi^3} \iint ds dp \left(\frac{E_0}{E}\right)^s \left(\frac{E^2 \theta^2}{K^2}\right)^{-p-1} \Gamma(2p+s) \Gamma(p+1) \pi^*(s, p, T-t). \quad (4)$$

The lateral distribution of the Cerenkov Radiation $G(r) 2\pi r dr$ is derived by combining the both distributions given by (3) and (4).

The distribution is given by,

$$G(\vec{r}) = \int_0^T dt \int g(\vec{r}') \Pi(\vec{r} - \vec{r}') d\vec{r}', \quad (5)$$

where θ in the formula (4) is replaced by $\frac{r'}{t}$. Because of the axial symmetry of both function g and Π , the Hankel transformation with respect to r is applied to the formula (5). The Hankel transform of g and Π yields

$$\begin{aligned} H_g &= \alpha J_0(s\theta_0 t) \\ H_\Pi &= -\frac{1}{4\pi^3} \iint ds dp \left(\frac{E_0}{E}\right)^s \left(\frac{K^2 s^2 t^2}{4E^2}\right)^p \Gamma(-p) \Gamma(2p+s) \pi^* \end{aligned} \quad (6)$$

Thus the essential part of the inverse transformation is given by

$$\Gamma(-p) \int_0^\infty J_0(s\theta_0 t) J_0(sr) \left(\frac{K^2 s^2 t^2}{4E^2}\right)^p s ds \quad (7)$$

This is the Weber - Shafheitlin integral and is given by⁽⁵⁾

$$\Gamma(p+1) \left(\frac{E^2}{K^2}\right)^{-p-1} \frac{t^{2p}}{(r^2 + \theta_0^2 t^2)^{p+1}} \cdot \frac{E^2}{K^2} F\left(\frac{p}{2} + \frac{1}{2}, \frac{p}{2} + 1, 1; \frac{4\theta_0^2 t^2 r^2}{(r^2 + \theta_0^2 t^2)^2}\right), \quad (8)$$

** If one is necessary to have the angular distributions of electrons with energy higher than a certain value (E_c), the formula (2) is also valid if one replace $\pi(s, p, t)$ by $\pi^*(s, p, E_c, t)$ in the same formula.

where F is the Hypergeometric function.

Then the lateral distribution is given by

$$G = -\frac{\alpha}{4\pi^3} \int_0^T \frac{dt}{t^2} \iint ds dp \left(\frac{E_0}{\epsilon}\right)^S \left(\frac{\epsilon^2}{K^2}\right) \left(\frac{\epsilon^2(r^2 + \theta_0^2 t^2)}{K^2 t^2}\right)^{-P-1} \Gamma(2P+S) \Gamma(P+1) \pi^* F \quad (9)$$

By using the transformation of Hypergeometric function.

$$\begin{aligned} & F\left(\frac{1}{2} + \frac{P}{2}, 1 + \frac{P}{2}, 1; \frac{4\theta_0^2 t^2 r^2}{(r^2 + \theta_0^2 t^2)}\right) \\ &= \left(\frac{r^2 + \theta_0^2 t^2}{|r^2 - \theta_0^2 t^2|}\right)^{2P+1} F\left(-\frac{1}{2} - \frac{P}{2}, -\frac{P}{2}, 1; \frac{4\theta_0^2 t^2 r^2}{(r^2 + \theta_0^2 t^2)^2}\right), \end{aligned}$$

one get another representation of the lateral distribution.

The result is

$$G = \frac{-\alpha}{4\pi^3} \int_0^T \frac{dt}{t^2} \iint ds dp \left(\frac{E_0}{\epsilon}\right)^S \left(\frac{\epsilon^2}{K^2}\right) \left(\frac{\epsilon^2 R^2}{K^2 t^2}\right)^{-P-1} \frac{|r^2 - \theta_0^2 t^2|}{(r^2 + \theta_0^2 t^2)} \Gamma(2P+S) \Gamma(P+1) \pi^* F, \quad (10)$$

where

$$R = \frac{|r^2 - \theta_0^2 t^2|}{\sqrt{r^2 + \theta_0^2 t^2}}.$$

The physical meaning of the expression (10) is better understood than that of (8), since R is a certain average value of the distance from the observation point to the annual ring determined by the Cerenkov cone. In fact the formula (10) is more appropriate to the numerical evaluation than the expression of (8) as shown in the next section.

To see the consistency of this solution, the total flux of the Cerenkov photon is calculated by putting $T = \infty$ and integrating over the area, $\int_0^\infty G 2\pi r dr$, being proved to be coincide with αZ_π , where Z_π is the track length of the shower.

The formula (10) can be reduced to be a simple form at the limiting cases of r to 0 and to ∞ .

At the point of shower axis, we have

$$R = \theta_0 t, \quad \frac{|r^2 - \theta_0^2 t^2|}{r^2 + \theta_0^2 t^2} = 1 \quad \text{and} \quad F\left(-\frac{1}{2} - \frac{P}{2}, -\frac{P}{2}, 1; 1\right) = 1,$$

and the formula (10) becomes

$$G = \frac{-d}{4\pi^3} \int_0^T \frac{dt}{t^2} \iint dS dp \left(\frac{E_0}{E}\right)^S \left(\frac{E}{K}\right)^2 \left(\frac{E^2 \theta_0^2}{K^2}\right)^{-p-1} \Gamma(2p+S) \Gamma(p+1) \pi c^*.$$

This is just the superposition of the Cerenkov Radiation from the shower electron having deviation angle of θ_0 , as is simply expected by the physical reason.

Far beyond the shower axis, we have

$$R = r, \quad \frac{|r^2 - \theta_0^2 t^2|}{r^2 + \theta_0^2 t^2} = 1 \quad \text{and} \quad F\left(-\frac{1}{2} - \frac{p}{2}, -\frac{p}{2}, 1; 1\right) = 1.$$

Then we have again a simple expression of the formula (10), representing again the superposition of Cerenkov Radiation from the electron with deviation angle of $\frac{r}{t}$.

4. Numerical results

Numerical evaluation of the formula (10) is made in the following way.

The Hyper Geometric Function F in the formula (10) is slowly varying function of p except at very near the place of $r = \theta_0 t^*$. Using this feature of F , the evaluation of the integral with respect to p is first performed. In the place of integral of p , we have an angular distribution such as

$$\frac{1}{2\pi i} \int dp \Gamma(2p+S) \Gamma(p+1) \left(\frac{E^2 R^2}{K^2 t^2}\right)^{-p-1} \pi c^* F = \frac{f\left(S, \frac{ER}{KE}\right)}{\left(\frac{ER}{Kt}\right)^{2-S}} \cdot F(p = \bar{p}),$$

* At $r = \theta_0 t$,

$$F\left(-\frac{p}{2} - \frac{1}{2}, -\frac{p}{2}, 1, 1\right) = \frac{\Gamma\left(\frac{1}{2} + p\right)}{\Gamma\left(\frac{1}{2} + \frac{p}{2}\right) \Gamma\left(1 + \frac{p}{2}\right)}$$

and has a pole at $p = -\frac{1}{2}$.

where \bar{p} is determined by the saddle point method, namely

$$\Psi(p+1) + 2\Psi(2p+s) - 2 \ln \frac{\epsilon R}{Kt} + \frac{m^{*'}}{m^*} = 0 .$$

Then integration with respect to s is performed by the saddle point method, and finally the integral of t is performed by numerical way. In this calculation, m^* is used for the energy of 1 MeV as the lower limit of the shower electrons to emit the Cerenkov Radiation.

The results for the incident energy of 10^{10} eV, 10^{11} eV, 10^{12} eV and 10^{13} eV at a different depth is shown in Fig.2 and 3, where attenuation mean free path in the sea water is assumed to be $20 \text{ m}^{5)}$, and λ between 3500 \AA and 5000 \AA . Starting from the shower axis, the photon density increases up to the distance corresponding to the Cerenkov cone, and decays rather rapidly with increasing the distance. The photon density changes almost in proportion to E_0 / T^2 as is expected. The place of hump shifts almost in proportion to the depth T , but the proportion is slightly dependent on T , because Cerenkov Radiation comes on the average at the place near the shower maximum, thus the lateral displacement of the hump is proportional to $T - T_{\text{max}}$.

5. Discussions

Shape of the lateral distribution calculated by Soviet group is compared to ours given in Fig.2 and 3. Both results agree well with each other, in spite of the different approxiamtions used by each authors. However, slight differences are seen between both results. For an example, the ratio of the photon density at the hump to that shower axis is about 7 in our case, while their result gives a value of about 5.

As to the detection of these Cerenkov Radiation, the lower limit for the detection is tentatively assumed to be 10^2 photons / m^2 at the shower axis. The maximum depth from the starting point for the detection is thus obtained using the calculated results for different incident energies. The depth increses with incresing the shower

LATERAL DISTRIBUTION of CERENKOV PHOTONS
for A SHOWER of DIFFERENT ENERGY

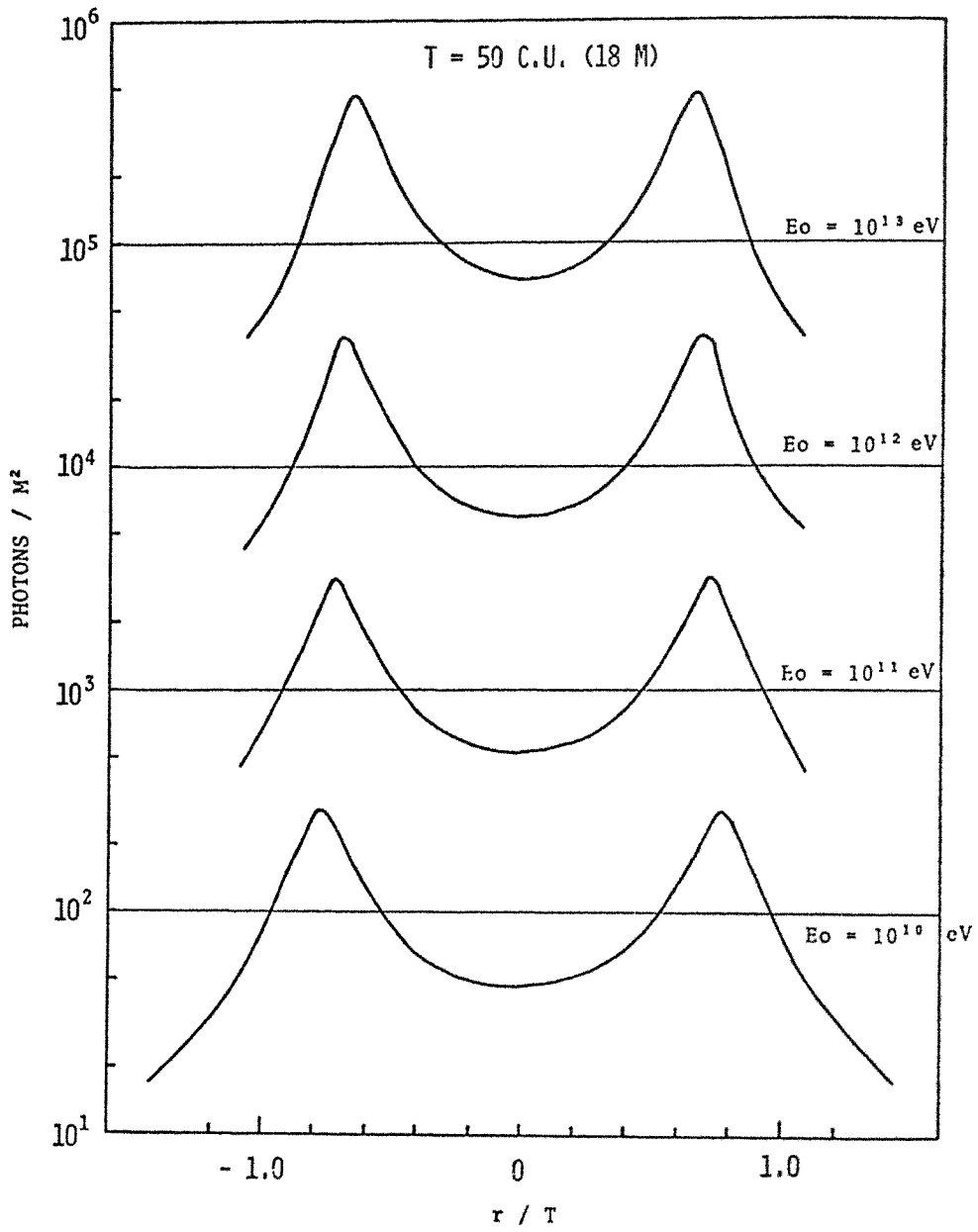


FIG. 2

LATERAL DISTRIBUTION of CERENKOV PHOTONS
at DIFFERENT DEPTH

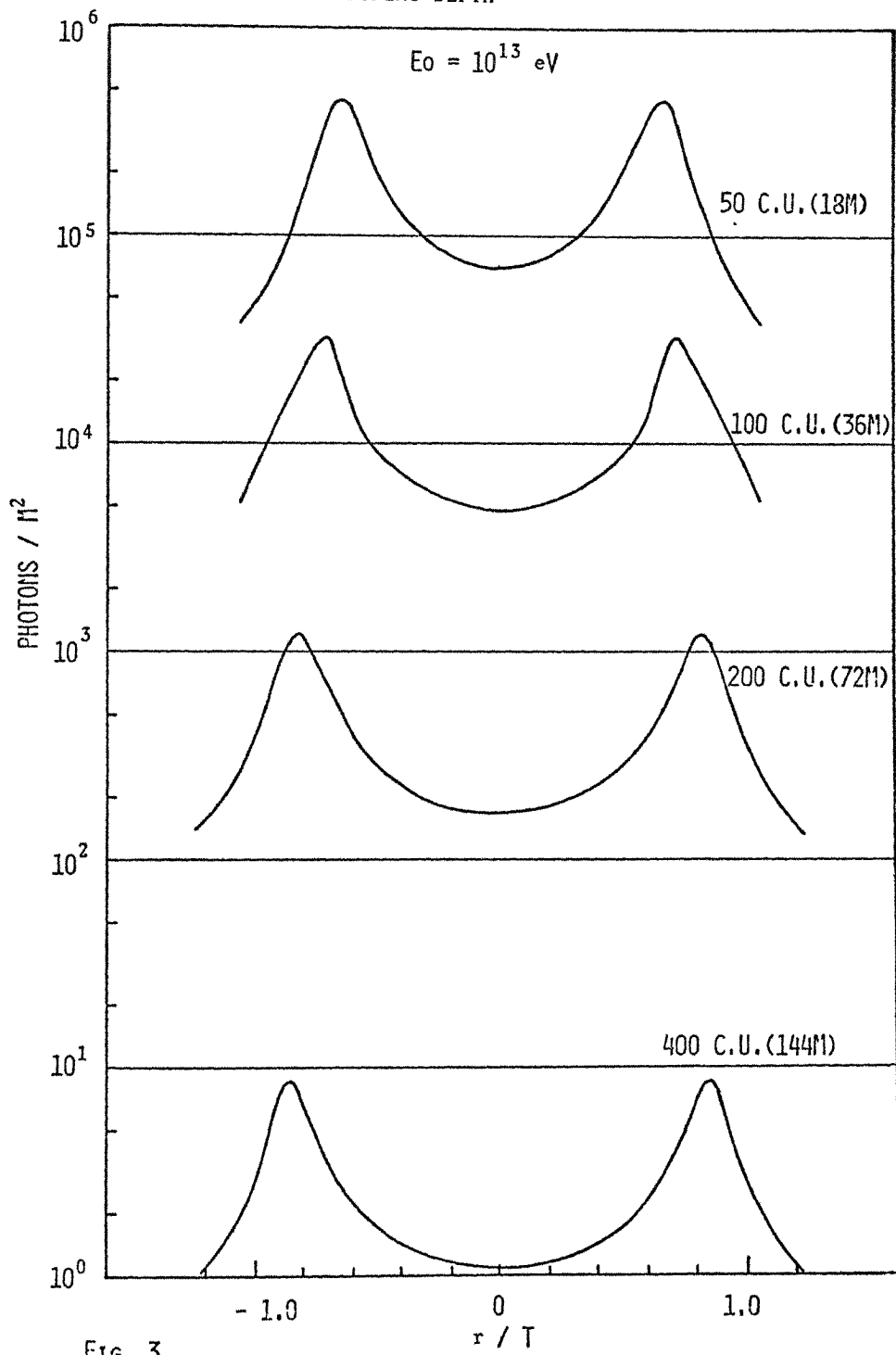


FIG. 3

energies, and the results are shown in Table 4*.

Table 4

Limiting Depth for 100 Photons/m²

E ₀	10 ¹⁰ eV	10 ¹¹ eV	10 ¹² eV	10 ¹³ eV	10 ¹⁴ eV
T	15 m	30 m	50 m	80 m	110 m
W = πT ³	1.1·10 ⁴ ton	8.5·10 ⁴ ton	3.9·10 ⁵ ton	1.6·10 ⁶ ton	4.2·10 ⁶ ton
E.C.C.		2·10 ⁴ ton	8·10 ⁴ ton	3·10 ⁵ ton	8·10 ⁵ ton
H.A.S.					5000 ton

W : Effective Weight of Producing Material.

E.C.C. : Corresponding Amount of Pb for Bremsstrahlung

H.A.S : Detection Area 1000 m²

Effective Thickness 500 gr/cm²

These Cerenkov Radiations spread within a circle of radius of about T, and the effective amount of water for producing the interactions by μ-mesons and neutrinos are estimated as about πT³. The amount is some order of 10⁶ tons for the shower of energy beyond 10¹³ eV. If it is compared to the case of E.C.C., the amount corresponds the order of 10⁵ tons of Pb for the case of μ meson bremsstrahlung.

H.A.S. is also considered to be quite efficient to detect the high energy μ meson bremsstrahlung. The effective amount of material for producing bremsstrahlung in this case is estimated by assuming

Detection Area : 10³ m²

Effective Depth : 500 gr/cm²,

yielding about 5·10³ tons.

* The estimate in reference (3) is optimistic, because they assume the photons are uniformly distributed within a circle of radius of $T \cdot \{(\theta_0)^2 + \theta^2\}^{1/2}$.

From these figures, it is seen to observe the Cerenkov Radiation in the water is quite efficient way compared to other observation method to detect the rare events arising from the μ mesons and neutrinos at extremely high energy region.

Once the lateral distribution of the Cerenkov Radiation is observed in the water, the distance between the hump gives us the information of the depth where the shower is initiated. Next the total photon flux is estimated by integrating the lateral distribution of the observed photons as usually adopted in the analysis of E.A.S.. From the total photon flux, the incident energy of shower is estimated, thus referring to the information of the starting depth, the probability of the occurrence of such an event is estimated.

These features are usefull to explore the flux as well as interaction of μ mesons and neutrinos at extremely high energy, and it is quite desirable to perform such an experiment in DUMAND project as is suggested by Soviet group.

References

- (1) Deep Underwater Mu-meson And Neutrion Detection.
- (2) Work shop; DUMAND, Hawaii, 1976.
- (3) L.V.Volkova and G.T.Zatsepin ;
Proc. 14th. Int. on Cosmic Rays, Munchen, 6,2120, 1975.
A.E.Chudakov; Work shop, DUMAND, Hawaii, 1976.
I.P.Ivanenko, V.V.Makarov and I.A.Hein ;
Preprint 98, P.N.Levedev Physical Institute, 1976.
- (4) J.Nishimura;
Hand.bd.Physik. 46/2, Springer Verlag. 1967.
- (5) R.Zaneveld ; Work shop, DUMAND, Hawaii, 1976.

SECTION B

THE EXPERIMENTAL DETERMINATION OF CHARGE - RATIO OF
COSMIC-RAY MUONS IN 0.2 - 0.8 GeV/C MOMENTUM RANGE AT
A LOW LATITUDE STATION

K.P. SINGHAL*

Department of Physics
Gujarat University
Ahmedabad 380 009
INDIA

ABSTRACT

An experiment to determine the charge-ratio of cosmic-ray muons based on the method of delayed coincidences was conducted at Ahmedabad. The apparatus consisted of three scintillation counters. Muons in a certain momentum range were brought to rest in an absorber and their decay product electrons were registered in different time channels depending upon their arrival after the stoppage of parent muons.

Two different absorbers, one of high atomic number (lead) and another of low atomic number (graphite) were used as stopping materials. Both positive and negative muons decay freely in the latter absorber while only positive muons decay in the former, negative ones being captured by the lead nuclei. The charge-ratio is found to be nearly one with a slight indication of an increase with increase of the momentum. The implications of the results are discussed.

* formerly at PHYSICAL RESEARCH LABORATORY, AHMEDABAD

Computation of the Muon Charge Ratio of Cosmic Rays
at Large Zenith Angles

L.K. Ng and C.H. Poon

Physics Department, Hong Kong University

Abstract

The muon charge ratios of cosmic rays at 60° and 80° zenith angles were computed in terms of their energies. The energy range covered was from 10 GeV to 1.5×10^4 GeV, which enabled a direct comparison with a large number of the accumulated experimental data. The calculation was based on the scaling hypothesis, using up-to-date parameters. Corrections for the energy loss and the survival probability through the atmosphere were rigorously treated. With the assumption of constant primary mass composition, the charge ratios found were in good agreement with the more recent experimental data and were essentially independent of muon energy at high energies.

Introduction

The cosmic-ray muon charge ratio has been calculated by various authors using different models. Unfortunately, their results do not completely agree with one another. It is important to obtain a satisfactory theoretical prediction, for, as pointed out by Erlykin et al (1974), if we assume the model to be correct, a discrepancy between theory and experiment may mean either a failure of the scaling hypothesis (Feynman (1969)) or a change in the relative number of neutrons and protons in the primary spectrum.

Several years ago, Frazer et al (1972) followed the approach of Barrett et al (1952) and, incorporating the scaling hypothesis, made an estimate of the vertical muon charge ratio in the high energy limit, based on the then available laboratory data. The value obtained (1.56) was high compared with the experimental data. Recently, this method was generalized (Ng et al (1976)) to give the response function at different zenith angles, and the result compared satisfactorily with other calculations in the case of vertical propagation. We have therefore applied this method to recompute the muon charge ratio using more up-to-date parameters, and, in order to compare with most of the recent data, propagation at zenith angles 60° and 80° have been considered.

Method of Computation

To define the notations given, a brief description of the method of calculation is necessary. Let the proton, neutron and the charged pion fluxes in the atmosphere be represented by $\mathcal{P}(E, l)$, $\eta(E, l)$ and $\pi^\pm(E, l)$ respectively. The diffusion equations are as follows:

$$\frac{\partial \mathcal{P}}{\partial l} = -\frac{\mathcal{P}}{\lambda_N} + \frac{1}{\lambda_N E} \int_E^\infty dE' \left(\mathcal{P}(E', l) \tilde{f}_{pp}\left(\frac{E}{E'}\right) + \eta(E', l) \tilde{f}_{pn}\left(\frac{E}{E'}\right) \right) \dots (1)$$

$$\frac{\partial \eta}{\partial l} = -\frac{\eta}{\lambda_N} + \frac{1}{\lambda_N E} \int_E^\infty dE' \left(\mathcal{P}(E', l) \tilde{f}_{pn}\left(\frac{E}{E'}\right) + \eta(E', l) \tilde{f}_{pp}\left(\frac{E}{E'}\right) \right) \dots (2)$$

$$\frac{\partial \pi^\pm}{\partial l} = -\frac{\pi^\pm}{\Lambda_\pi} - \frac{B_\pi \pi^\pm}{E \gamma} + \frac{1}{\lambda_N E} \int_E^\infty dE' \left(\mathcal{P}(E', l) \tilde{f}_{p\pi^\pm}\left(\frac{E}{E'}\right) + \eta(E', l) \tilde{f}_{n\pi^\pm}\left(\frac{E}{E'}\right) \right) \dots (3)$$

where $\tilde{f}_{pp}(x)$ is the single-particle distribution of a p-air collision producing a proton (plus anything), and $\tilde{f}_{pn}(x)$, $\tilde{f}_{p\pi^\pm}(x)$ are similar distributions, i.e.

$$\tilde{f}_{pp}(x) = \frac{x}{\sigma_{p-air}} \int_0^\infty \frac{d^2 \sigma_{pp}}{d\alpha dP_T} dP_T,$$

with $x = E/E'$ according to the scaling hypothesis. In equations (1), (2) and (3), we have already used the charge symmetry results for strong interactions, i.e.

$$\tilde{f}_{pp} = \tilde{f}_{nn}, \quad \tilde{f}_{pn} = \tilde{f}_{np}, \quad \text{and} \quad \tilde{f}_{p\pi^\pm} = \tilde{f}_{n\pi^\mp}.$$

Also, λ_N is the nucleon interaction mean free path, and Λ_π , the pion attenuation length. B_π is the expression $m_\pi c H / v_\pi$ where H is the scale height. Finally, $\mathcal{P}(E, l)$ and $\eta(E, l)$ satisfy the following boundary condition,

$$\mathcal{P}(E, 0) + \eta(E, 0) = \frac{dN}{dE} = N_0 E^{-\gamma} \dots (4)$$

for all zenith angles.

According to the ideas of limiting fragmentation (Benecke et al (1969)) the distributions for $x > 0$ are independent of the target nucleus.

The solutions to equations (1), (2) and (3) are then,

$$\mathcal{P}(E, l) = \left(\frac{1}{2} N_0 e^{-\frac{l}{\lambda_N}} + \frac{1}{2} \Delta_0 e^{-\frac{l}{\lambda_N}} \right) E^{-\gamma} \dots (5)$$

$$\eta(E, l) = \left(\frac{1}{2} N_0 e^{-\frac{l}{\lambda_N}} - \frac{1}{2} \Delta_0 e^{-\frac{l}{\lambda_N}} \right) E^{-\gamma} \dots (6)$$

and

$$\pi^\pm(E, l) = \frac{1}{2} \frac{N_0}{\lambda_N} E^{-\gamma} \left\{ (Z_{p\pi^\pm} + Z_{n\pi^\pm}) e^{-\frac{l}{\lambda_N}} \sum_{n=0}^{\infty} \frac{(-l/\lambda_1)^n}{n!(n+1+\frac{B_\pi l}{E \gamma})} \pm (Z_{p\pi^\pm} - Z_{n\pi^\pm}) \frac{\Delta_0}{N_0} e^{-\frac{l}{\lambda_N}} \sum_{n=0}^{\infty} \frac{(-l/\lambda_1)^n}{n!(n+1+\frac{B_\pi l}{E \gamma})} \right\} \dots (7)$$

Here, $\frac{\Delta_0}{N_0}$ is the charge composition in the primary pectrum,

$$\Lambda_1 = (\Lambda_N^{-1} - \Lambda_\pi^{-1})^{-1} \quad \text{and} \quad \Lambda'_1 = (\Lambda_N'^{-1} - \Lambda_\pi^{-1})^{-1},$$

with $\Lambda_N = \lambda_N(1 - Z_{pp} - Z_{p\pi})$ and $\Lambda_N' = \lambda_N(1 - Z_{pp} + Z_{p\pi})^{-1}$,

$$\text{where} \quad Z_{AB} = \int_0^1 dx \quad x^{\gamma-2} \tilde{f}_{AB}(x) \quad \dots(8)$$

As a consequence of the the assumed scaling property, Z_{AB} 's are constants independent of energy and atmospheric depth.

Similar expressions are obtained for the kaon fluxes $K^\pm(E, l)$, with Λ_1, Λ'_1 in equation (7) replaced by

$$\Lambda_2 = (\Lambda_N^{-1} - \Lambda_K^{-1})^{-1} \quad \text{and} \quad \Lambda'_2 = (\Lambda_N'^{-1} - \Lambda_K^{-1})^{-1}$$

respectively, in addition to other obvious changes.

The muon differential spectrum at production due to pions is then

$$\mu_\pi^\pm(E, l) = \frac{1}{2} \frac{N_0}{\lambda_N} \frac{E^{-\gamma}}{(1 - \frac{m_\pi^2}{m_N^2})} e^{-\frac{l}{\Lambda_\pi}} \int_1^{\frac{m_N^2}{m_\pi^2}} ds \quad s^{-(\gamma+1)} \left\{ (Z_{p\pi^+} + Z_{p\pi^-}) \cdot \sum_{n=0}^{\infty} \frac{(-l/\Lambda_1)^n}{n!(1+(n+1)\frac{SEY}{B\pi l})} \pm (Z_{p\pi^+} - Z_{p\pi^-}) \frac{\Delta_0}{N_0} \sum_{n=0}^{\infty} \frac{(-l/\Lambda'_1)^n}{n!(1+(n+1)\frac{SEY}{B\pi l})} \right\} \dots(9)$$

That due to kaons is expressed similarly, except that a factor $\beta_{K\mu}$ (branching ratio of the $K \rightarrow \mu$ decay) must be included).

We have computed the sea-level muon differential spectrum after including the survival probability and the energy loss factors, and after integrating over the atmospheric depth, the muon charge ratio is then given by

$$R(E) = \frac{\mu_\pi^+(E)_{\text{sea-level}} + \mu_K^+(E)_{\text{sea-level}}}{\mu_\pi^-(E)_{\text{sea-level}} + \mu_K^-(E)_{\text{sea-level}}}$$

The values for the parameters used in the computation are largely the same as in Ng et al (1976). In particular, the distributions \tilde{f}_{pp} , $\tilde{f}_{p\pi^\pm}$ and \tilde{f}_{pK^\pm} are obtained from Elbert et al (1975), and $\tilde{f}_{p\pi}$ is taken to be $0.77 \tilde{f}_{pp}$. The parameters λ_N, Λ_π and Λ_K are taken to be 80, 120 and 150 gcm^{-2} respectively. The primary spectrum is estimated from the data of Erlykin et al (1974). For the primary energies greater than 10^3 GeV ,

$$\frac{dN}{dE} \propto E^{-2.70} \quad \text{nucleons } \text{m}^{-2} \text{s}^{-1} \text{sr}^{-1} (\text{GeV/nucleon})^{-1}$$

with the charge composition $\frac{\Delta_0}{N_0} \approx 0.74$, which is also the value used by Frazer et al (1972).

Results and Discussions

The results of our calculations are given in figures 1 and 2, together with some recent experimental data (Ashley et al (1976) and (1973), Iida (1975), Leipuner et al (1973) and Burnett et al (1973)). It is seen that the theoretical charge ratio at each of the zenith angles 60° and 80° rises very slowly at lower energies and flattens off at higher energies. For the muon energy range 50 GeV - 10^4 GeV shown in the figures, good agreement with the experimental data is obtained. This agreement indicates that scaling should hold at energies as high as 10^4 GeV and that there is no necessity to assume a varying charge composition for the primary spectrum at these energies. In this respect, one should bear in mind that the muon spectrum is relatively insensitive to changes in the values of $\tilde{f}_{p\pi^\pm}(x)$ for $x \approx 0$, so that the muon charge ratio is not a sensitive test of the scaling behaviour at $x \approx 0$.

For muon energies below 50 GeV, it is seen that the theoretical curves are below the experimental values. One possible explanation is that the actual distributions $f_{p\pi^\pm}(E_\pi)$ for the parent pions may not scale at these energies. The ratio $Z_{p\pi^+}/Z_{p\pi^-}$ should then be higher than the corresponding value at large energies. Consequently, the low-energy values of the charge ratio should be higher than what is given in the present calculation.

Reference

1. Ashley G.K. et al (I), private communication (1976).
2. Ashley G.K. et al (II), Proc. 13th Int. Conf. on Cosmic Rays Denver, 3, 1828 (1973).
3. Barrett P.H. et al, Rev. Mod. Phys. 24, 133 (1952).
4. Benecke J., Chou T.T., Yang C.N. and Yen E., Phys. Rev., 188, 2159(1969).
5. Burnett et al, Phys. Rev. Lett., 30, 937(1973).
6. Elbert J.W. et al, Phys. Rev. D, 12, 660(1975).
7. Erlykin A.D., Ng L.K., and Wolfendale A.W., J. Phys. A Math Nucl Gen, 7, 2059(1974).
8. Feynman R.P., Phys. Rev. Lett., 23, 1415(1969).
9. Frazer W.R. et al, Phys. Rev. D, 5, 1653(1972).
10. Iida S., Nuovo Cimento, 26B, 559(1975).
11. Leipuner L. et al, Proc. 13th Int. Conf. on Cosmic Rays Denver, 3, 1771(1973).
12. Ng L.K., Poon C.H. and Wolfendale A.W., Proc. 2nd Int. Cosmic Ray Symp., on High Energy Cosmic Ray Modulation, Tokyo, 7 (1976).

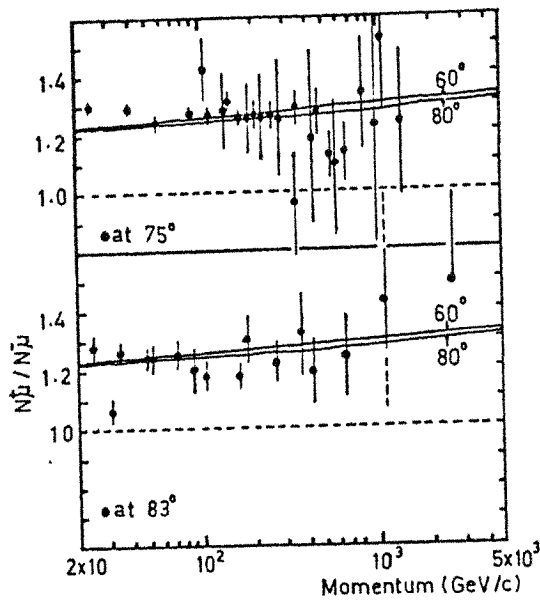


Figure 1 Comparison of the present calculated muon charge ratios with the experimental data at 75° and 83° zenith angles from Iida, Leipuner et al and Burnett et al.

— present calculated curves at 60° and 80° respectively.

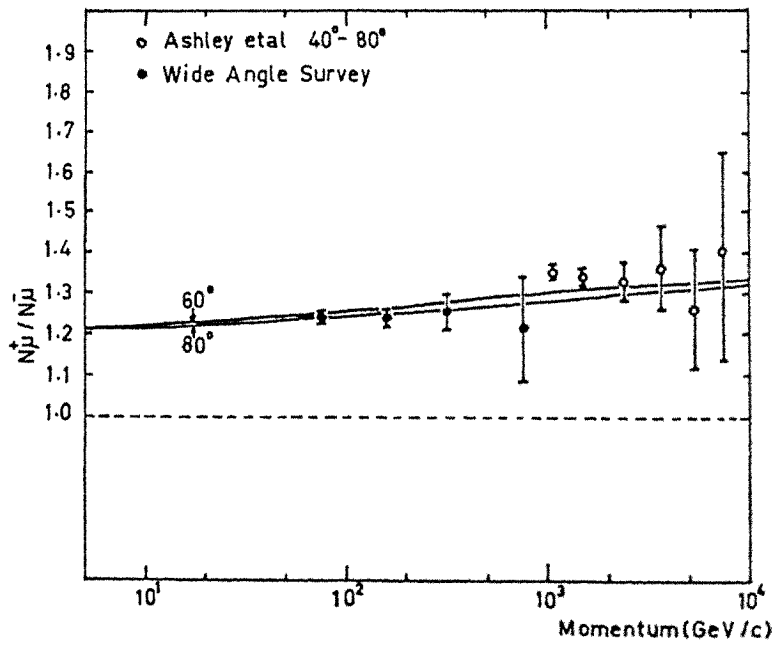


Figure 2 Comparison of the present calculated muon charge ratios with the experimental data from Ashley et al (I) and the wide angle survey compiled by Ashley et al (II).

— present calculated curves at 60° and 80° respectively.

A System for Measuring the Muon Charge Ratio
in Small Air Showers

C.C. Lai, S.H. Leung, S.K. Leung, S.W. Fong and L.K. Ng
Physics Department, Hong Kong University

ABSTRACT

A new experimental system for measuring the muon charge ratio in small air showers was discussed. It consisted of a small-air-shower array of 4 counters together with an automatic recording muon spectrograph. The system is able to measure the particle densities of electron showers as well as the energies and charges of the associated muons. A microprocessor and a magnetic tape are used for initial processing and recording. The dead time per event is about 8 milliseconds.

Introduction

The study of the muon momentum spectrum and the charge ratio in extensive air showers is important, since it gives informations on the production height of the shower particles and on the mass composition of the primaries. The production height, which can be calculated from the momentum spectrum and the core distance, is essential for determining the longitudinal development of extensive air showers (Burger et al (1975)). Comparison of the observed muon charge ratio with the theoretical charge ratio based on a model gives a method for predicting the primary mass composition or the multiplicity law (Earnshaw et al (1971)).

Several experiments have been done to measure the various aspects of EAS muons, e.g. the angular characteristics, the momentum spectrum, the lateral distribution, and the charge ratio. However, not much data has been accumulated to give sufficiently good statistics particularly for the charge ratio, and only a small number of experiments have in fact involved in spectral and charge-ratio measurements. This is because such measurements are very laborious and time consuming in the recording and analysis by using the standard photographic method.

In the present system, automatic recording and analysis is enhanced to reduce the workload and to enable continuous operation. The interest here is centred at small showers due to the limitation of the shower arrays.

The System

The detection system consists of a small shower array and a muon magnetic spectrograph. The former is intended for estimating the core

location and the shower size, and the latter for finding the muon momentum and the charge. The whole system is placed in an air-conditioned hut with a thin roof of about 2 gm-cm^{-2} .

The shower array is now under operation, while the spectrograph is under modification to achieve automatic recording and analysis. The present shower array is suitable for measuring showers of sizes between 10^{12} eV and 10^{14} eV. More stations will be added to the array in later dates.

For each event detected by the system, the data recorded are first condensed by a microprocessor, which also acts as a buffer storage, and are then sent to a digital magnetic tape recorder. The tape is finally transferred to a large computer for analysis. Thus the system can record the events continuously, and the analysis becomes much less laborious as in the case of photographic recording.

Detailed description of the system is divided into the following three parts:

The Shower Array

The small shower detection array is composed of four plastic scintillation counters, each of effective area $50 \times 50 \text{ cm}^2$. They are arranged at the upper four corners of the temperature-controlled hut, with a diagonal separation of 5.87 m, centre-to-centre, as shown in figures 1(a) and (b). Each plastic scintillator is enclosed in a thin wooden box as shown in figure 1(c). A cone made of thin sheets of galvanised iron coated internally with a layer of aluminium foil is used as a reflector. Its vertical height is 40 cm against a square base of $50 \times 50 \text{ cm}^2$. Except the top surface of the scintillator, the rest are painted with a good diffused reflector (TiO).

A 5-inch photomultiplier tube (Du Mont 6364) is used for each counter, from which two signal outputs are taken. Triggering signals are obtained from the anode of the tube, and linear signals from the first dynode. The former signals are used to generate control or master pulses for the processing of respective events. The latter signals produce the particle densities. Vertical single muons are used for the calibration of the signal amplitudes.

The array has been in operation for more than a year working in conjunction with the study of electron-positron ratio in small air showers (Fong and Ng (1977)).

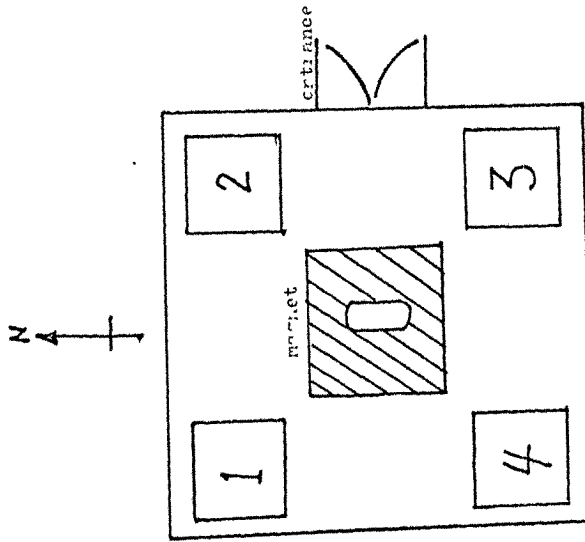


Fig. 1 (a)
Plan view of the shower detection array.
(not to scale)

1 : 4 boxes of scintillators.

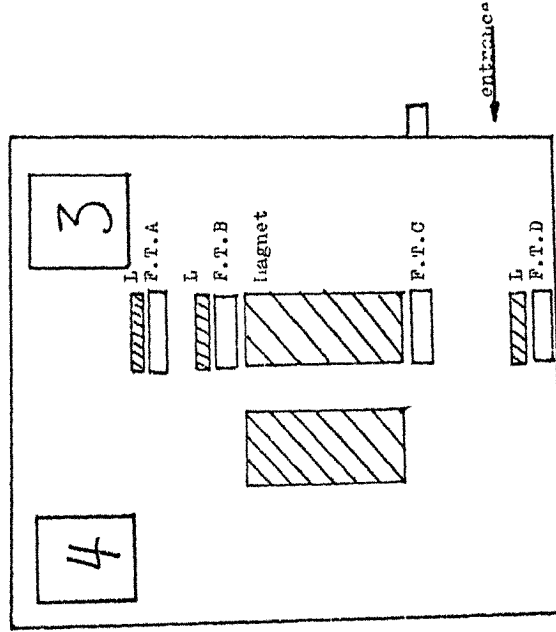


Fig. 1 (b)
Side view of the shower detection array and the arrangement of the Flash-tube Trays.
(not to scale.)

L : Plates of lead to cut off electrons
F.T.A : 4 Flash-tube Trays.

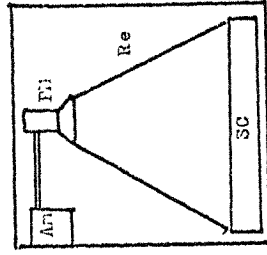


Fig. 1 (c)
Inside a box
(not to scale.)

Am : Amplifier.
Pi : Photomultiplier tube
Re : Reflector
SC : Scintillator

The Muon Spectrograph

The muon magnetic spectrograph consists of a 3-ton iron magnet, a scintillation counter and four trays of flash tubes, three of which are covered by 5 cm of lead and the fourth by the magnet iron to remove the unwanted electron tracks in the shower. The geometry of the set-up is as shown in figure 2.

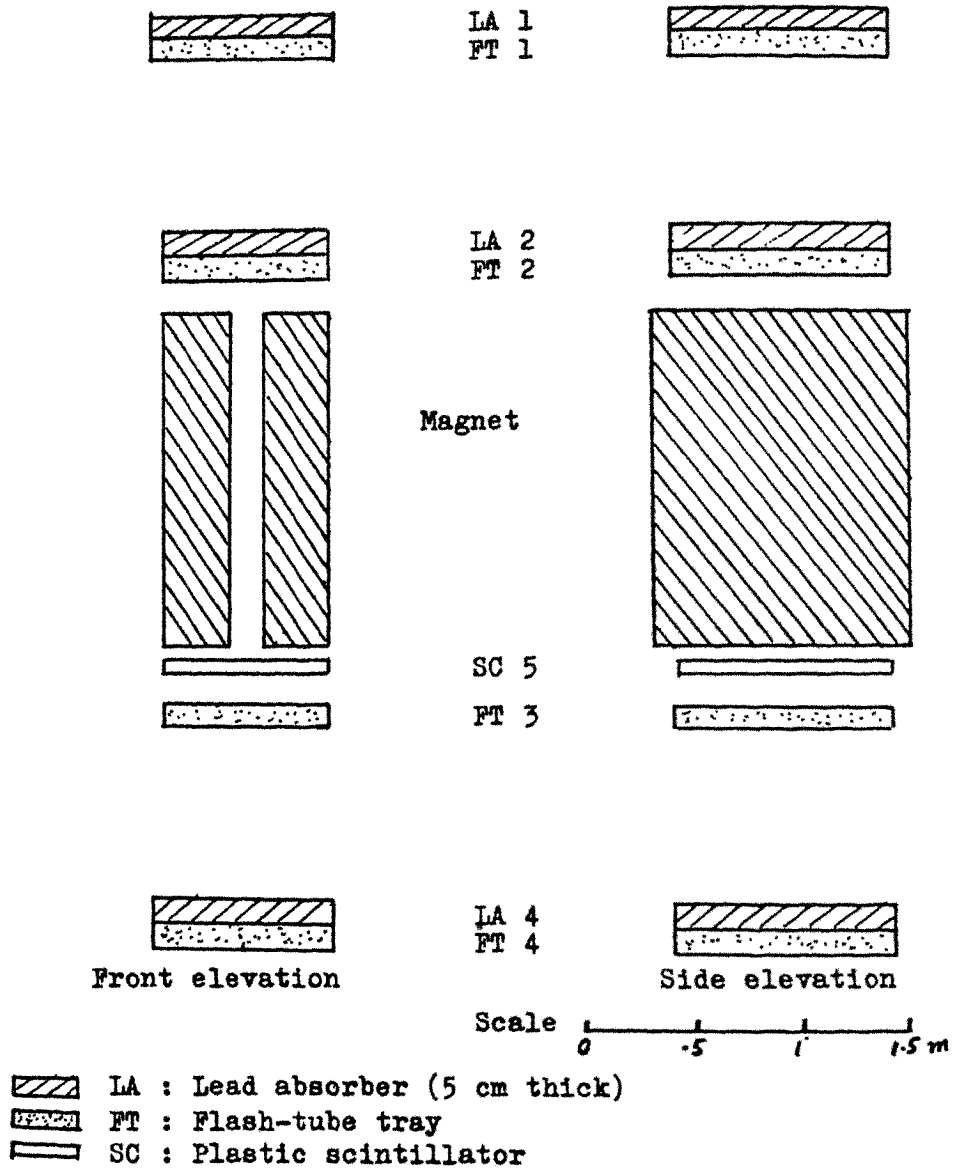


Figure 2 Systematic diagram of the magnetic spectrograph.

Each wound arm of the magnet has a height of 1.50 m and horizontal area of $0.55 \times 0.275 \text{ m}^2$, and its internal magnetic field is 16.6 Kilogauss.

With the geometry shown in figure 2, the acceptance of the spectrograph at zero field is about $25 \text{ cm}^2 \text{sr}$, and the MDM is about 300 GeV/c.

The flash tubes used are of length 1 m and external diameter 7.5 mm, and of gas pressure 2.4 atmospheres. Each tray consists of 6 layers of flash tubes arranged alternatively in the number of 65 and 64 tubes per row in a rigid perspex frame.

The scintillation counter SC5 is required to indicate the passage of at least one muon through the spectrograph. A signal from this counter in coincidence with the triggering signals from the shower array tells the arrival of a shower accompanied by at least one muon through the spectrograph. Hence the flash-tube trays are triggered by the coincidence signal, and give rise to the visual track of the muon.

Information from the flash-tube trays during the passage of a muon is not recorded visually but electronically using the method adopted by Ayre et al (1969). This is done by picking up the electromagnetic signal from one end of each flash tube (while firing) by a simple probe. The emission of the electromagnetic signals from flash tubes has been described by Ayre et al (1972).

In the present system, the arrangement for picking up the signals is shown in figure 3. The observed waveform of the signal is shown in figure 4. The initial sharp pulse shown is due to the UHT signal operating on the flash-tube trays, and hence appearing in all the tubes. This initial signal is rejected during latching as described later.

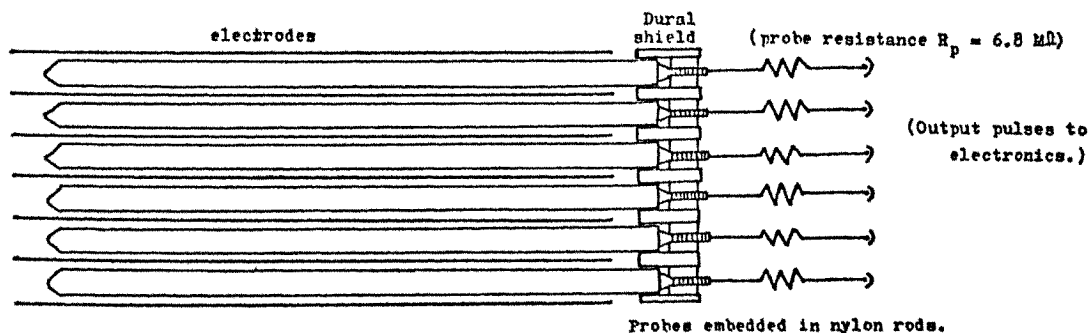


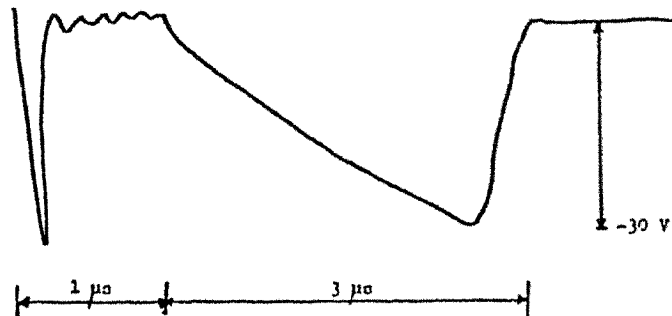
Fig. 3 A Flash tube Tray (64 columns with 6 flash-tubes per column).

Fig. 4 Preliminary observation of a pulse from the probe
 (probe resistance = 6.8 M Ω)
 (high tension pulse up to -10 kV)

(a) Pulse from a non-flashing tube.



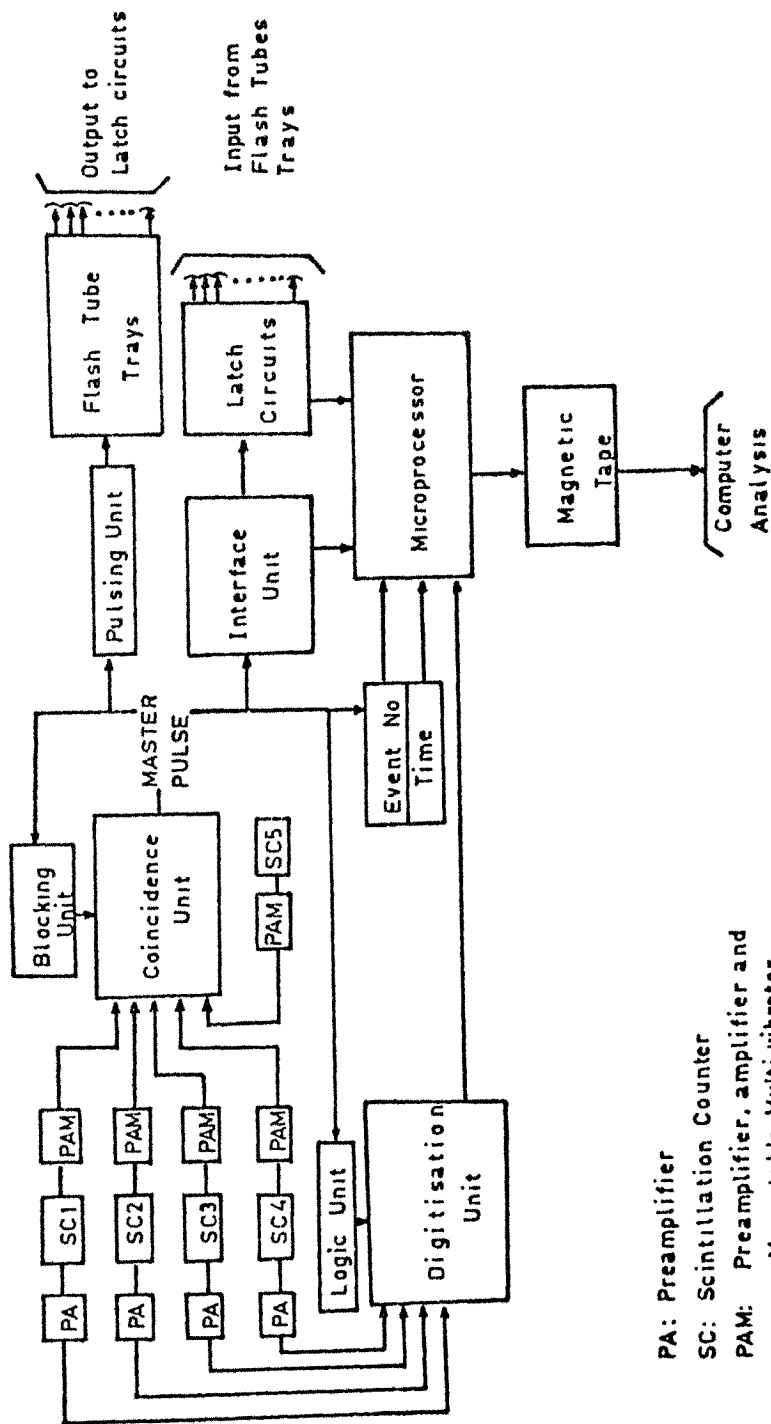
(b) Pulse from a flashing spurious tube.



The Electronic Circuits

A block diagram for the electronics involved is shown in figure 5. It can be seen that an event is defined by the coincidence of the signals from the five scintillators SC 1 - 5. The Master Pulse so obtained starts the processing of that event. It blocks its own input gate for a period of 8 milliseconds during which the processing is taking place. It triggers the Pulsing Unit to give a UHF pulse for the flash-tube trays. It initiates the operation of the Interface Unit, which controls the inputs of the Microprocessor. It advances the event number by 1. And finally, it enables the Digitization Unit.

The linear outputs from the shower counters SC 1 - 4, which yield the shower densities, are connected through linear preamplifiers to the Digitization Unit. Four 10-bit analogue-to-digital converters are used in the Unit together with four sample-and-hold amplifiers. The dynamic range of each channel is therefore about 10^3 . The digitization process is done by



PA: Pre-amplifier

SC: Scintillation Counter

PAM: Pre-amplifier, amplifier and Monostable Multi-vibrator.

Fig. 5 Block Diagram of Electronic System

first holding the peak amplitude of each pulse by the sample-and-hold amplifier, and then allowing the ADC to digitize the amplitude. In order to eliminate the interference due to the UHF signal, 'holding' is only allowed to take place after the unwanted UHF interference has subsided, i.e. after 3 microseconds. The data from the four ADC's are then fed into the microprocessor together with other data.

The Pulsing Unit used to generate UHF pulses contains a spark gap and high voltage capacitors, which shape the pulses to a width of less than a few microseconds.

Signal outputs from the flash tubes are connected to the Latch Circuits which are basically controlled flip-flops. As has been shown in figure 4, the fluctuations in the first microsecond due to a UHF pulse have to be rejected. This is done by delaying the time when latching sets in, that is the flip-flops are allowed to change state only after the initial fluctuations have vanished. The command signal for each latching to take place is obtained from the Interface Unit. With about 1600 flash tubes used, the same number of flip-flops is required in the Latch Circuits. It is clear that the Latch Circuits acts as a temporary storage for the flash-tube data. The data are then transferred 6 bits at a time to the microprocessor.

The Microprocessor is an expanded type of Motorola No. 68010, with 512 x 8 memory bits. It condenses the data received from the Latch Circuits and stores them together with those from the Digitization Unit, the Event No. and the Time. The whole set of data per event is then transferred to the magnetic tape, which in turn can be processed by a large computer.

The sequential activity of the Microprocessor is programmed and the inputs are controlled by the Interface Unit.

Discussions

The present system provides a straightforward way of measuring the momentum and charge of muons in small air showers. It has a number of important advantages over the standard system using photographic recording:

- (i) It eliminates the tedious processes of film development and dark-room scanning;
- (ii) It reduces the dead time per event from 2 secs (required for film winding) to 8 milliseconds;
- (iii) It provides instant checking of individual events by directly printing out the data from the microprocessor using a teletype printer; and
- (iv) It avoids frequent interruption due to film loading and

unloading, and hence is much preferable for continuous operation.

As the shower array is small, most of the showers detected should be in the energy range of 10^{12} - 10^{14} eV. This is the range where the spectrometer data and the EAS data meet, and hence it is important in bridging the two types of measurements. It should also be noted that so far not much work has been done in this range of energies.

Reference

- Ayre C.A. and Thompson M.G., Nucl. Inst. and Meth. 69, 106 (1969).
Ayre C.A., Thompson M.G., Walley M.R., and Young E.C.M., Nucl. Inst. and Meth., 103, 49 (1972).
Burger J., Bohm E., and Suling M., Proc. 14th Conf. on Cosmic Rays, Munchen, 8, 2784 (1975).
Earnshaw J.C., Machin A.C., Oxford K.J., Pickersgill D.R. and Turver K.E., Proc. 12th Int. Conf. on Cosmic Rays, Hobart, 3, 1086 (1971).
Fong S.W. and Ng L.K., present proceedings (in press).

POSSIBLE STRUCTURE IN THE MUON
CHARGE RATIO AT LARGE ZENITH ANGLES

P.K. MacKeown

Department of Physics, University of Hong Kong.

Abstract

The asymmetry of the cosmic ray hadron flux with respect to local zenith angle at a point in the atmosphere is evaluated. The combined effect of this asymmetry with the observed p_{\perp} dependence of the charge excess of mesons in p-p interactions at accelerator energies on the cosmic ray muon charge excess at large zenith angles at sea level is estimated. It is concluded that even at the lowest muon energies the effect is so small that it will be swamped by Coulomb scattering, and in most practical cases geomagnetic deflection.

Introduction

It is well known that the predicted muon charge ratio in the vertical direction at sea level is essentially determined by the x dependence of the charge excess of the secondary mesons produced in hadronic collisions, where x is the energy scaling variable, and only the mean value of the p_{\perp} distribution of these mesons plays a role. This is because over the solid angle region of nucleons contributing to the vertical flux the variation of both the nucleon intensity and its charge excess, $\sim e^{-\text{const} \text{Sec } \zeta}$ where ζ is the angle between the nucleon and meson trajectories, is insignificant. At large zenith angles however the penetration depth in the atmosphere depends more sensitively on direction, and accordingly the nucleon flux. Furthermore the charge excess of mesons in nucleon collisions shows, at a fixed value of x , a dependence on p_{\perp} , as can be seen from figs. 1a and 1b. These figures show some data on the charge excess per particle, π mesons and K mesons respectively, as a function of x and p_{\perp} in p-p collisions abstracted from Alper et al. (1973), ($\sqrt{s} = 30.6$ and 52.8 GeV), Baker et al. (1974), ($E_0 = 200, 300$ GeV), and Cronin et al. (1975) ($E_0 = 200, 300, 400$ GeV) - the latter two sets of data having been reduced by the authors from p-Be and p-W collisions respectively. In general the charge excess increases with p_{\perp} at a given x .

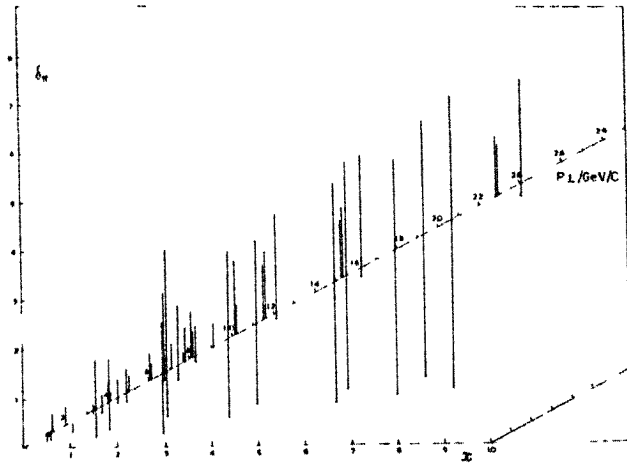


Fig. 1(a). The charge excess per pion in p-p collisions at accelerators as a function of x and p_{\perp} .

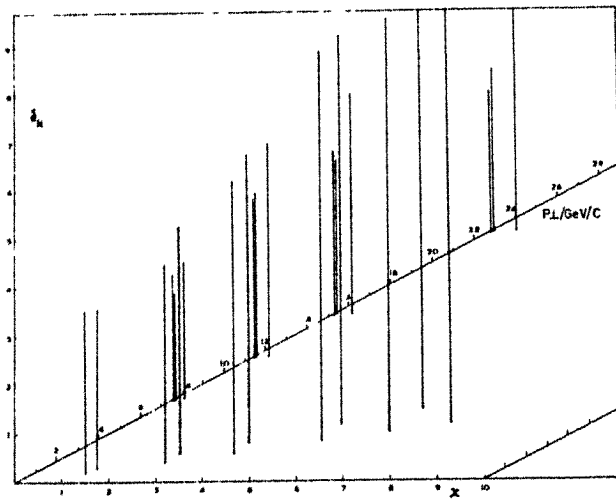


Fig. 1(b). The charge excess per K meson in p-p collisions at accelerators as a function of x and p_{\perp} .

Calculation of the Muon Flux

Because the local zenith angle, λ , at a point along a trajectory at large zenith angles depends on the radial depth, y ($/g\text{ cm}^{-2}$), at that point the integro differential equation for the propagation of the parents of the muons is rather intractable and the summation method of Maeda (1964, 1970) is used. Although this method excludes the production of mesons except by nucleons it has the advantage of offering greater physical insight into the processes involved. The notation is, in part, explained in fig.2. Assuming the meson and muon trajectory colinear, a muon incident at sea level, ($y = 1030\text{ g cm}^{-2}$), at

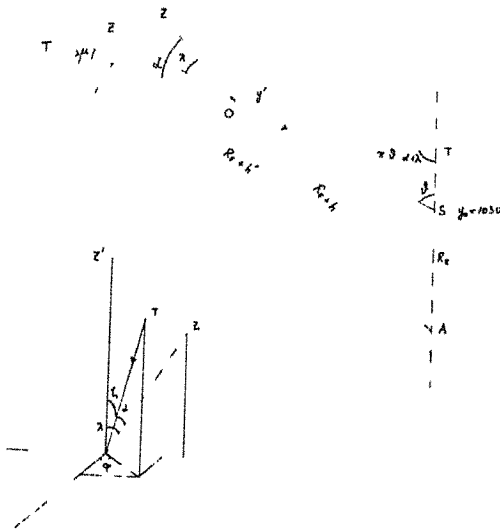


Fig.2. A muon incident at sea level (S) at 0 originated from a meson produced at a radial depth $y'(0)$, a product of the collision of a nucleon incident at an angle α to the zenith. A is the centre of the earth.

a zenith angle θ will arise from a meson produced in a nucleon-airnucleus interaction in dy' at y' , where the local zenith angle is λ , given by:

$$\lambda = \text{Cos}^{-1} \sqrt{1 - \frac{\text{Sin}^2 \theta}{(1 + h(y')/R_E)^2}}$$

$h(y')$ being the linear height of the level y' above the earth's surface and R_E the radius of the earth. The angle the meson makes with the trajectory of the nucleon producing it is denoted by ζ .

Nucleons giving rise to such a pion or K meson are incident in a range of local zenith angles α , $\lambda - \zeta \leq \alpha \leq \lambda + \zeta$, corresponding to the azimuthal angle, ϕ , of the emitted pion varying in $0-2\pi$ about the axes OZ' , where

$$\cos \alpha = \sin \lambda \sin \zeta \sin \phi + \cos \lambda \cos \zeta$$

The differential source spectrum of secondaries, ($m = \pi$ or K mesons, or prompt muons), produced by nucleons per unit vertical thickness at y' is

$$S_m^\pm(E, y') = \sum_{j=p,n} \int dE_0 d\Omega' \frac{\partial J_j}{\partial E_0 \partial \Omega'} \frac{1}{\lambda_i^{(j)} \cos \alpha} \frac{\partial m_j^\pm}{\partial E \partial \Omega}$$

where $\partial J_j / \partial E_0 \partial \Omega' (E_0, y', \alpha)$ is the differential spectrum of nucleons of type j incident at local zenith angle $\alpha(\zeta, \phi)$, $\lambda_i^{(j)}$ is the interaction length for such nucleons, $d\Omega' = \sin \zeta d\zeta d\phi$, and $\partial m_j^\pm / \partial E \partial \Omega$, the differential production spectrum of particles of type m^\pm in interactions of j type nucleons with air nuclei, is a function of E (or in the scaling limit, x) and ζ (through its p_\perp dependence).

Assuming a power law primary spectrum, and ignoring any energy dependence of the nucleon cross-section, we can write

$$\partial J_j / \partial E_0 \partial \Omega = A_j E_0^{-\gamma} e^{-\xi(y', \alpha)/\Lambda}$$

$\xi(y', \alpha)$ is the penetration depth to y' along the direction ζ, ϕ

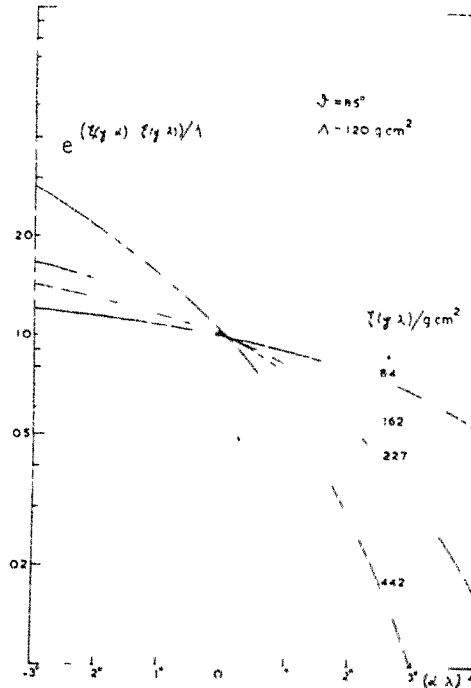
$$\xi(y', \alpha) = \int_0^{y'} dy'' / \cos \mu = \int_{h(y')}^{\infty} dh' \rho(h') / \cos \mu$$

where

$$\cos \mu = \sqrt{1 - \left(\frac{R_E + h(y', \phi)}{R_E + h'} \right)^2 \sin^2 \alpha}$$

For the case of $\theta = 85^\circ$ and several slant depths $\xi(y', \lambda)$ the α dependence of the ratio of the nucleon flux to the flux incident at $\alpha = \lambda$, assuming an attenuation length $\Lambda = 120 \text{ g cm}^{-2}$, is shown in fig. 3. As would be expected the sensitivity to direction increases with depth in the atmosphere.

Fig. 3. The ratio of the nucleon flux to that along the principal direction (λ) as a function of local zenith angle α for several penetration depths $\xi(\lambda)$, at $\theta = 85^\circ$.



Using this source spectrum the differential spectrum of mesons at a depth y , travelling along the direction θ is, after Maeda (1964):

$$j_m^\pm(E, y, \theta) = e^{-\xi(y)/\Lambda^{(m)}} \int_0^y dy' S_m^\pm(E(y-y'), y') e^{\frac{\xi(y')}{\Lambda^{(m)}} - B_m \int_{y'}^y \frac{\sec \lambda(y'') dy''}{y'' E(y-y'')}}.$$

From this the muon source spectrum can be evaluated, and, folding in the survival probability including energy loss, the sea level muon spectra found.

Results

Rather than carry out this calculation rigorously we can see that two separate effects are involved, namely the possibly different weightings of the p_1 values (and thus the charge excess per meson) due

to the angular distribution of the nucleons, and the nett nucleon charge excess at any level will be different from that at the same depth ξ in the vertical direction.

It can be seen from fig.3, $\theta = 85^\circ$, that there is an appreciable dependence of the nucleon flux on the local zenith angle of the nucleon, especially at greater depths in the atmosphere. The greatest effect would be expected for small values of $p_\perp(\zeta)$, because of the $\sim e^{-ap_\perp}$ damping term in the production spectrum, i.e. for small E_μ values (E_μ is the muon energy at sea level). But at these energies the dominant terms in the muon spectrum are the exponential absorption of the nucleons and the muon survival probability, and even for $E_\mu = 1 \text{ GeV}$ the bulk of the muons at 85° are produced at $\xi \lesssim 200 \text{ g cm}^{-2}$, ($y \lesssim 30 \text{ g cm}^{-2}$). At these depths, when averaged over azimuth ϕ , the mean nucleon intensity as a function of ζ will give rise to insignificantly different weighting of p_\perp values from the case of the vertical atmosphere at the corresponding depth ξ . Using an exponential p_\perp distribution with a mean of $0.4 \text{ GeV}/c$, for $\theta = 85^\circ$, $E_\mu = 1 \text{ GeV}$ the mean angle at which a pion comes off at $\xi = 277 \text{ g cm}^{-2}$ differs by much less than 1% from the case of a radial flux. This is because, when integrated over azimuth, the local zenith angle dependence of the nucleon intensity within 3° only differs from the radial case by $\sim 4\%$. Since the great majority of muons come from levels above this the effect is seen to be negligible.

The second, related, effect arises because of the variation of the charge excess in the nucleon beam with depth penetrated,

$$\delta_N(\xi) \equiv \frac{p-n}{p+n} = \delta_0 e^{-b\xi}$$

where δ_0 is the charge excess in the primary radiation, $b = 2 h_{pn}(\gamma-1)\lambda_1$; γ the index of the primary differential spectrum, and

$h_{pn}(s) = \int_0^1 du u^{s-2} f_{pn}(u)$. It can be shown that

$$h_{pn}(s) = 1 - \lambda_1/\Lambda - h_{pp}(s)$$

where $h_{pp}(s) = \int_0^1 du u^{s-2} f_{pp}(u)$, f_{pp} the invariant differential cross-section for p production in p - p collisions averaged over p_\perp . Taking

$\gamma = 2.7$ we find $h_{pp} = 0.15$, e.g. Garraffo et al. (1973), and taking $\lambda = 86 \text{ g cm}^{-2}$, $\Lambda = 120 \text{ g cm}^{-2}$ we find $b = .0031 \text{ g}^{-1} \text{ cm}^2$, i.e. a characteristic attenuation length of 320 g cm^{-2} . This is a very slow depth dependence, which combined with the small modification of the local zenith angle distribution within the angular region determined by the p_{\perp} distribution, noted above, will also produce negligible difference in the muon charge excess compared to the case where the p_{\perp} distribution is neglected.

Conclusions

It is concluded that, provided there is no dramatic increase in the mean transverse momentum of mesons with energy, there will be no p_{\perp} dependent variation of the sea level muon charge ratio at large zenith angles due to the p_{\perp} distribution which would be distinguishable above the smearing out caused by Coulomb scattering and geomagnetic deflection, which become important at these angles, Osborne (1966). The largest such effect will be due, as noted before, MacKeown and Wolfendale (1966), to the varying relative contributions of muons from π and K decay with zenith angle.

References

- Alper B. et al., Phys. Lett. 47B, 75 (1973).
 Baker W.F., et al., Phys. Lett. 51B, 303 (1974).
 Cronin J.W., et al., Phys. Rev. D11, 3105 (1975).
 Garraffo Z., Pignotti A. and Zgrablich G., Nucl. Phys. B53, 419 (1973).
 MacKeown P.K. and Wolfendale A.W., Proc. Phys. Soc., 89, 553 (1966).
 Maeda K., J. Geophys. Res. 69, 1725 (1964),
 Proc. 6th Interamerican Cosmic Ray Seminar,
 La Paz, 4, 847, (1970).
 Osborne J.L., Ph.D. Thesis, University of Durham, (1966).

Arrival Direction Dependence of Muon Charge Ratio

S. Higashi¹, S. Iida², Y. Kamiya², Y. Kawashima³, T. Kitamura, K. Kobayakawa⁴,
S. Mikamo⁵, Y. Minorikawa⁶, K. Mitsui, S. Miyake, Y. Muraki, I. Nakamura,
Y. Ohashi, A. Okada, S. Ozaki¹, H. Shibata³, S. Shibata², T. Takahashi¹
and Y. Teramoto¹

Cosmic Ray Laboratory, University of Tokyo, Tanashi, Japan

¹ Department of Physics, Osaka City University, Osaka

² Department of Physics, Nagoya University, Nagoya

³ Department of Physics, Okayama University, Okayama

⁴ Department of Physics, Kobe University, Kobe

⁵ High-Energy Laboratory, Tsukuba-Taihocho, Ibaragi

⁶ Department of Physics, Kinki University, Higashi Osaka

Abstract

There have been so many observations of the cosmic-ray muon charge ratio using cosmic-ray momentum spectrograph in recent years. The values of muon charge ratio at large zenith angles and low momenta depend strongly on the orientations of spectrograph axes because of the geomagnetic effect on cosmic-ray muons in the atmosphere. So that the values of charge ratio are varied with zenith angles and azimuthal angles. In the experiments so far performed, however, this geomagnetic effect seems not to be considered sufficiently.

In this report, the preliminary calculations of the geomagnetic effect on cosmic-ray muons in the atmosphere are given and derived their correction factors to the charge ratio. The result is compared with the experiments previously obtained by Nagoya Cosmic-ray Spectrometer. The expected charge ratio by Mutron will be given.

1. Introduction

The investigation of charge ratio of cosmic-ray muons at sea level brings important informations such as the momentum distribution, the multiplicity and the composition of parent particles to study the hadronic interactions produced by high-energy cosmic ray primary particles near the top of the earth's atmosphere.

On the basis of accelerator experiments, the cosmic-ray muon charge

ratio has recently been studied theoretically in terms of the hadronic scaling law (1) or the limiting fragmentation model (2)(3)(4)(5)(6)(7)(8)(9). Their analyses have given a consistent interpretation on the near constancy of the cosmic-ray muon charge ratio at high energies.

A number of muon charge ratio measurements at sea level have been performed so far (10)(11)(12)(13)(14)(15)(16)(17)(18)(19). Recently, Thompson (20) summarised those experimental data and showed that over the muon production energy range 2-1000 GeV the charge ratio is essentially constant and the majority of experiments are statistically compatible. Representative of the near-vertical experiments are the papers by Ayre et al. (6), Allkofer et al. (10), Nandi and Sinha (11) and representing experiments over a range of zenith angles are given by Burnett et al. (17). This result is consistent with prediction of the scaling hypothesis, as above described, and the charge ratio measurements are now extended to higher energy regions for finding where the manifestation of the scaling hypothesis is broken.

In the experimental values of low energy region, however, there have been several reports on the existence of discrepancies such as dips or rises (21)(22)(23)(24), especially a dip around 100 GeV (25) is noticeable. Those small variations, however, are not compatible each other although their statistical accuracies are fairly good. One of the reasons is that those data were measured by spectrographs setting in the different orientation of their axes, that is zenith angle and azimuthal angle. The zenith angle and azimuthal angle dependencies are both explained as a manifestation of the geomagnetic effect, so that measurements at large zenith angles and low energies are especially sensitive.

The aim of this report is to emphasize the importance of elimination of the geomagnetic effect on the charge ratio in the low energy region and to summarize those data from this point of view. Preliminary calculation of the motion of cosmic-ray muons in the atmosphere and the geomagnetic correction factors on the value of charge ratio are given here. The results are applied to the data obtained by Nagoya Cosmic Ray Spectrometer and "Mutron" which will be reported in this symposium.

2. Motion of cosmic ray muon in the atmosphere

It is assumed that the primary cosmic rays are uniformly distributed when they arrive at the top of the atmosphere. They produce hadrons by collisions with air nuclei and they decay into muons according to their life

time. Due to the earth's magnetic field, muons detected at sea level in the magnetic east-west plane will describe trajectories as shown in Fig. 1, the deflection of the positive and negative muons in the atmosphere being in opposite directions. Accordingly, as seen in Fig. 1, the positive muons trajectory is longer at the east side of the detector than at the west and when it has arrived at the detector the number in the west is larger than that in the east, for the survival probability of mesons depends on the length of their orbit. This relation is just reversed for the negative particles. At sea level, therefore, the charge ratio in the west is increased in comparison with the charge ratio at production and is decreased in the east.

3. Calculations of muon trajectory

In calculating the deflection of a cosmic-ray particle during its trajectory through the atmosphere, the following assumptions are taken into account.

- 1) The observed values of the geomagnetic field at Nagoya were used; the horizontal component, the declination and the dip are 0.305 gauss, 6 °W and 48.7°, respectively. The dip varies linearly along the direction of the earth's latitude.
- 2) Hadrons are produced at 100gcm^{-2} atmospheric depth along with the line of motion of the primary.
- 3) All hadrons decay into muons immediately.
- 4) The radius of curvature of the earth is 6368km and the surface of the earth is treated as spherical.
- 5) Muon loses its energy only in the collision with the air and Bethe's formula is used.
- 6) Energy dependence of the muon life time are taken into account.
- 7) All muon move with the light velocity.
- 8) The density of air depends only on the altitude and the scale height is the linear function of the atmospheric depth.

Under the assumptions described above, the equation of motion of the charged particle is given and calculated stepwise by Runge-Kutta-Gill method. Each step interval is taken 5km. A trajectory of muon having its initial conditions of energy E_0 , zenith angle Z_0 and azimuth A_0 is traced backwards along the line of motion from sea level to the upper atmosphere. In each step, the position of the particle, direction, air density of the atmosphere,

altitude, energy and survival probability are given and checked up. When the altitude is negative value, the calculation is stopped as a forbidden track. Also, when the residual track length of the particle reaches 100gcm^{-2} atmospheric depth along the track, the pursuit of the trajectory will be ceased.

The geomagnetic correction factor to find the charge ratio at production is derived using the survival probabilities given above. It is composed of three factors, representing the different energies at production, survival probabilities, and decay probabilities of the parents of the muons (assumed to be pions) of the two charges respectively. Writing $N(\mu^+)/N(\mu^-) = R$ and the subscripts i and p for incident and production, we have

$$R_i = R_p \left(\frac{E_{\mu^+}}{E_{\mu^-}} \right)^{-\gamma} \frac{S^+}{S^-} \frac{D_{\pi^+}}{D_{\pi^-}}$$

where E_{μ^+} , E_{μ^-} are the energies at production of positive and negative muons having an energy E at sea level. S^+ , S^- are the survival probabilities given above, and D_{π^+} , D_{π^-} are the decay probabilities for the parent pion, all these functions depending on the zenith angle, and γ is the exponent of the pion production spectrum assumed equal to 2.64. Now we put $\frac{D_{\pi^+}}{D_{\pi^-}} = 1$ because of the assumption (3) that all pions decay into muons. The geomagnetic correction factor is, therefore, represented as

$$\omega = \left(\frac{E_{\mu^+}}{E_{\mu^-}} \right)^{-2.64} \frac{S^+}{S^-}$$

The values of ω are shown in Fig. (2)(3).

4. Discussions

The axis of the Nagoya Cosmic-ray Spectrometer is placed horizontally in the local geomagnetic north-south direction, so that the particles coming from both directions are detected. The azimuthal range is $\pm 3.4^\circ$. It is clear from Figure (2) that the geomagnetic correction factor (ω) is 1 on an average over the azimuthal range of the spectrometer, so that the charge ratios observed in the north and the south of this spectrometer are considered to represent the values of the charge ratio at production.

Also, the geomagnetic correction factors for the charge ratio observed by Mutron are examined. The axis of Mutron is placed horizontally in the direction of 34° west (N-W) from the local geomagnetic north-south direction and the azimuthal range is $\pm 15.6^\circ$,

so that the particles coming from both directions, 34° west (N-W) and 146° east (S-E) from the geomagnetic north-south direction respectively, are detectable. As are shown in Fig. (3), the differences of ω 's are very big, especially for low energy particles. For example, the ω 's in the N-W and the S-E observed at 84° zenith with momentum 10 GeV/c are 3.5 and 0.25 respectively. Mutron has a momentum selector so that the muons having their momentum < 100 GeV/c is able to rejected. Therefore, the differences between the values of ω 's obtained in the both directions are not so serious. For example, the ω 's in the N-W and the S-E observed at 88° zenith with momentum 100 GeV/c are 1.35 and 0.75 respectively.

It is shown in Fig. (4) that the azimuthal distribution of the axes of the spectrographs directed in the large zenith angles. The numbers of the spectrographs observing in the west direction is excess those in the east direction. It should be noticed, therefore, the mean value of those experimental data is weighted in the western direction which gives higher value of charge ratio. Because of that Kiel spectrograph is directed in the east, its charge ratios in the energy range < 7 GeV appear as a negative excess. The geomagnetic correction for those data have done by Allkofer (26).

In the above discussions, the importance of the geomagnetic correction for the charge ratio of low energy region has been described. Our calculations are still continueing and we intend, in future, to give necessary geomagnetic correction factors for each spectrograph in order to refine the summary of those useful experimental results.

References

- (1) R. P. Feynman; Phys. Rev. Lett., 26, 1585 (1969)
- (2) J. Benecke, T. T. Chou, C. N. Yang and E. Yen; Phys. Rev., 188, 2159 (1969)
- (3) W. R. Frazer, C. H. Poon, D. Silverman and H. J. Yesian; Phys. Rev., D5, 1635 (1972)
- (4) G. Yekutieli; Nucl. Phys., B47, 621 (1972)
- (5) Z. Garraffo, A. Pignitti and G. Zgrablich; Nucl. Phys., B56, 419 (1973)
- (6) C. A. Ayre, J. M. Baxendale, B. J. Daniel, C. J. Hume, B. C. Nandi, M. G. Thompson, S. C. Wells, M. R. Whally and A. W. Wolfendale; Proc. 13th Int. Conf. on Cosmic Rays, Denver, 1822 (1973)
- (7) J. L. Morrison and J. W. Elbert; Proc. 13th Int. Conf. on Cosmic Rays, Denver, 1833 (1973)
- (8) A. Liland and H. Pilkuhn; Proc. 13th Int. Conf. on Cosmic Rays, Denver, 1841 (1973)

- (9) L. V. Volkova and G. T. Zatsepin; Proc. 13th Int. Conf. on Cosmic Rays, Denver, 2332 (1973)
- (10) O. C. Allkofer, K. Carstensen, W. D. Dau, E. Fahnders, W. Heinrich and H. Jokisch; Proc. 12th Int. Conf. on Cosmic Rays, Hobart, 1319 (1971)
- (11) B. C. Nandi and M. S. Sinha; Nucl. Phys., B40, 289 (1972)
- (12) M. S. Abdel-Monem, J. R. Benbrook, A. R. Sheldon, N. M. Duller and P. J. Green; Proc. 13th Int. Conf. on Cosmic Rays, Denver, 1811 (1973)
- (13) S. R. Baber, W. F. Nash and B. C. Rastin; Nucl. Phys., B4, 539 (1968)
- (14) L. Leipuner, R. Larsen, L. Smith, R. Adair, B. Higgs, H. Kasha and R. Kellogg; Proc. 13th Int. Conf. on Cosmic Rays, Denver, 1771 (1973)
- (15) R. W. Flint and W. F. Nash; Nucl. Phys., B33, 632 (1971)
- (16) G. K. Ashley, J. W. Keuffel and M. O. Larsen; Proc. 13th Int. Conf. on Cosmic Rays, Denver, 1828 (1973)
- (17) T. H. Burnett, L. J. LaMay, G. E. Masek, T. Maung, E. S. Miller, H. Ruderman and W. Vernon; Phys. Rev. Lett., 30, 937 (1973)
- (18) T. H. Burnett, L. J. LaMay, G. E. Masek, T. Maung, E. S. Miller, H. Ruderman and W. Vernon; Phys. Rev. Lett. 30, 110 (1973)
- (19) B. J. Bateman, N. M. Duller, P. J. Green and A. V. Jelinek; Proc. 13th Int. Conf. on Cosmic Rays, Denver, 1816 (1973)
- (20) M. G. Thompson; Cosmic Rays at Ground Level, edited by A. W. Wolfendale (International Scholarty Book Service, Portland, 1974), pp. 44-48
- (21) G. P. Tebb, W. F. Nash and C. A. Deacon; Proc. 12th Int. Conf. on Cosmic Rays, Hobart, 1340 (1971)
- (22) R. W. Flint and W. F. Nash; Proc. 12th Int. Conf. on Cosmic Rays, Hobart, 1346 (1972)
- (23) C. A. Ayre, M. A. Hamdau, C. J. Hume, M. G. Thompson, S. C. Wells, M. R. Whalley and A. W. Wolfendale; Proc. 12th Int. Conf. on Cosmic Rays, Hobart, 1364 (1972)
- (24) S. Kawaguchi, T. Sakai, H. Oda, H. Ueno and Y. Kamiya; Proc. 10th Conf. on Cosmic Rays, London, 941 (1965)
- (25) T. Kitamura; Proc. 14th Int. Conf. on Cosmic Rays, Rapporteur Talk (1975)
- (26) O. C. Allkofer; Proc. 2nd Int. Cosmic Ray Symposium, Tokyo (1976) in press

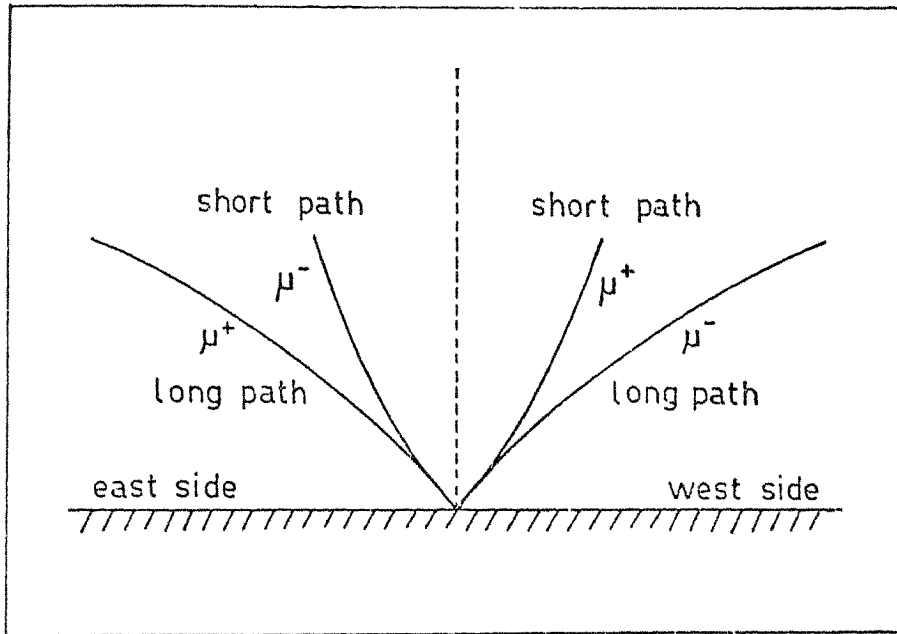


Figure 1. Muon trajectories in the East-West plane of the atmosphere.

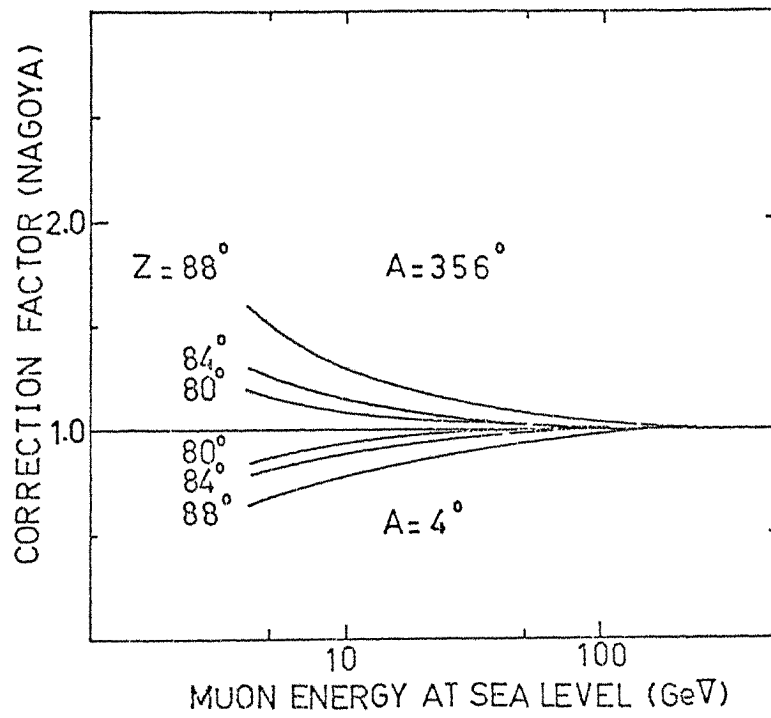


Figure 2. Geomagnetic Correction factors for the charge ratio (Nagoya Cosmic Ray Spectrometer)

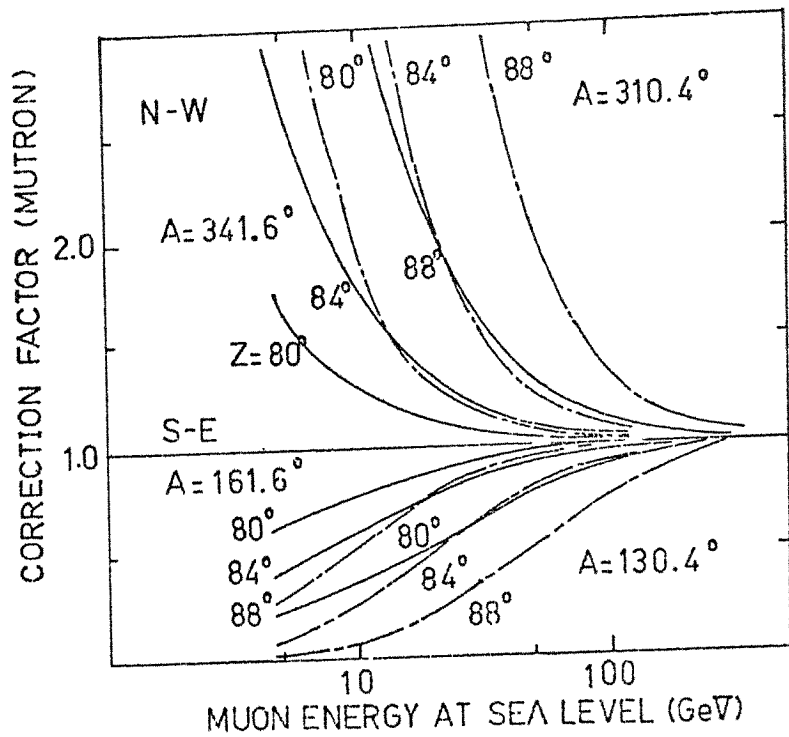


Figure 3. Geomagnetic Correction factors for Charge ratio (MUTRON)
 N (local geomagnetic)

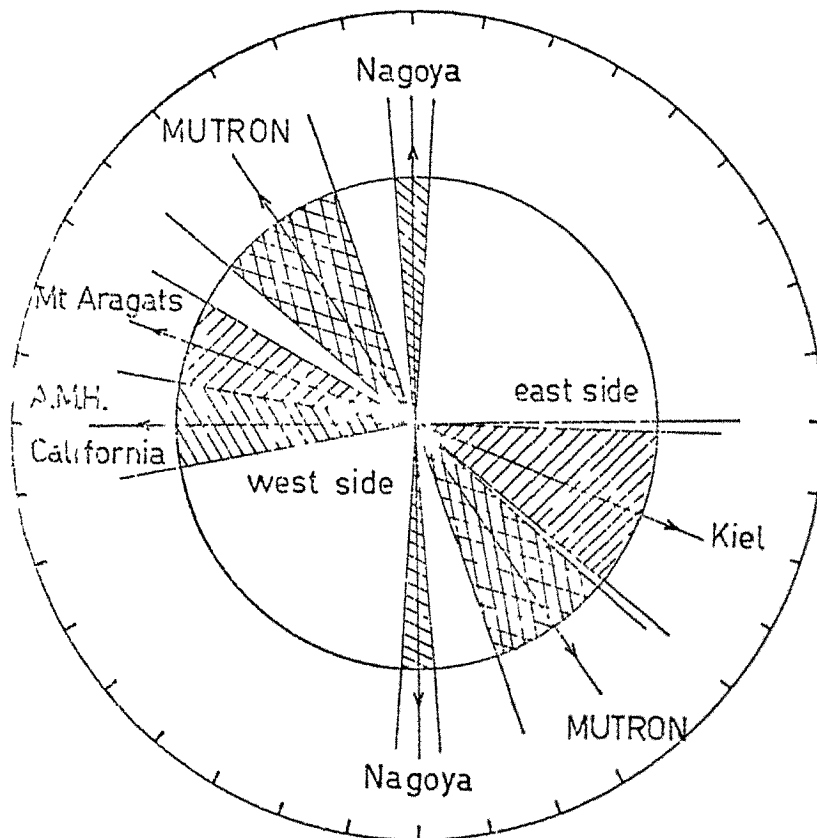


Figure 4. Orientation of large zenith angle spectrometer axes

CHARGE RATIO OF COSMIC PIONS IN THE ATMOSPHERE

D.P. Bhattacharyya, R.K. Roychoudhury and Kalpana Sarkar
Indian Association for the Cultivation of Science, Jadavpur,
Calcutta-700032. India.

It is found that the CERN Intersecting Storage Ring data on $p + p \rightarrow \pi^{\pm} + X$ reactions can be represented by a single scaling variable $\eta = 2p_T^2 x / [c' \ln(s/s_0)]$ for $0.075 \leq x \leq 0.3$ and $0.2 \leq p_T \leq 1.5$ GeV/c. The charge ratio of cosmic pions at the top of the atmosphere has been estimated by using this type of scaling variable and the primary nucleon spectrum of Grigorov et al. (1971).

1. Introduction

The charge ratio of the cosmic pion spectrum at the top of the atmosphere is of phenomenological importance in cosmic ray physics.

Earlier Frazer et al. (1972), Yekutieli (1972), Morrison and Elbert (1973), Adair et al. (1973), Yen (1973), Hume et al. (1973) and Erylkin et al. (1974) have calculated the charge ratio of pions originated from pp collisions.

In the present work we have fitted the Intersecting Storage Ring data of Capiluppi et al. (1974) for $p + p \rightarrow \pi^{\pm} + X$ reactions by our proposed new scaling variable (Roychoudhury and Bhattacharyya 1976). Using the primary cosmic ray spectrum of Grigorov et al. (1971) the charge ratio of pions at the top of the atmosphere has been estimated. The present result is compared with the values presented by different authors.

2. New scaling variable and the pion charge ratio at the top of the atmosphere

The CERN Intersecting Storage Ring data on inclusive reactions $p + p \rightarrow \pi^+ + X$ and $p + p \rightarrow \pi^- + X$, respectively are represented in Figures 1 and 2 as functions of a new scaling variable

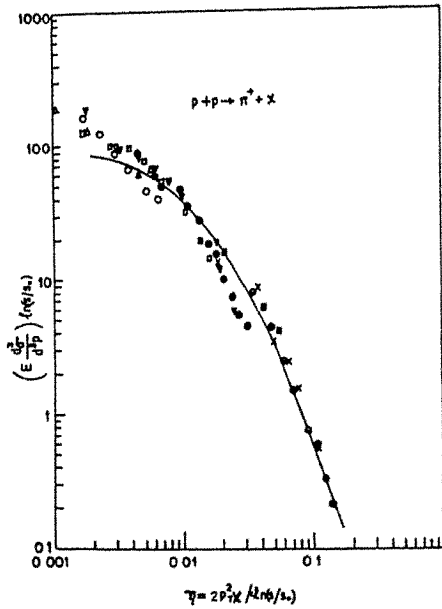
$$\eta = \frac{2p_T^2 x}{[c' \ln(s/s_0)]} \dots\dots\dots (1)$$

where $x = 2p_L/\sqrt{s}$, p_L is the center of mass longitudinal momentum of the detected particle and \sqrt{s} is the total center of mass energy; p_T is the center of mass transverse momentum. The new scaling variable is taken to be dimensionless by taking $c' \approx 1 \text{ (GeV/c)}^2$ and s_0 to be 1 GeV. The parametrization of the invariant cross section used in the present work is of the following form

$$E(d^3\sigma/d^3p) = A \exp(-a\eta + b\eta^2) \dots\dots\dots (2)$$

The fit in Fig. 1 for the positive pions corresponds to $A = 168.7$, $a = 113.9$, $b = 683.4$ and the fit to Fig. 2 corresponds to $A = 46.06$, $a = 85$ and $b = 510$ for negative pions.

Figure 1



The cross section data for $p + p \rightarrow \pi^+ + X$ reactions,

$$E(d^3\sigma/d^3p) \ln(s/s_0) \text{ vs } \eta = \frac{2p_T^2 x}{c' \ln(s/s_0)}$$

have been plotted from the work of Capiluppi et al. (1974). Solid curve shows the fit from the equation

(2). Experimental data :

- $\sqrt{s}=23.3 \text{ GeV}$ Δ for $x = 0.15$,
- \blacktriangle for $x = 0.3$; $\sqrt{s} = 30.6 \text{ GeV}$
- \square for $x = 0.15$, \blacksquare for $x = 0.3$;
- $\sqrt{s} = 44.6 \text{ GeV}$ ∇ for $x = 0.075$,
- \blacktriangledown for $x = 0.15$, \times for $x = 0.3$;
- $\sqrt{s} = 53 \text{ GeV}$ \circ for $x = 0.075$,
- \bullet for $x = 0.15$, \bullet for $x = 0.3$.

Figure 2

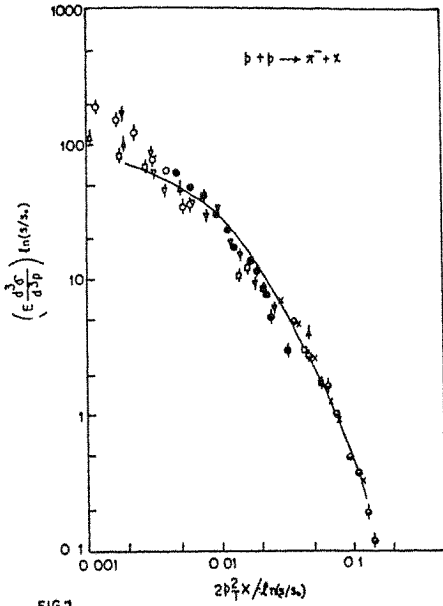


FIG 1

The cross section data for
 $p + p \rightarrow \pi^- + X$ reactions,

$$E(d^3\sigma/d^3p) \ln(s/s_0) \text{ vs } \eta = \frac{2p_T^2 x}{c' \ln(s/s_0)}$$

have been plotted from the work
of Capiluppi et al. (1974).
Solid curve shows the fit from
the equation (2). Experimental data :

- $\sqrt{s} = 23.3$ GeV, Δ for $x = 0.15$,
- \blacktriangle for $x = 0.3$; $\sqrt{s} = 30.6$ GeV
- \square for $x = 0.15$, \blacksquare for $x = 0.3$;
- $\sqrt{s} = 44.6$ GeV, ∇ for $x = 0.075$,
- \blacktriangledown for $x = 0.15$, \times for $x = 0.3$;
- $\sqrt{s} = 53$ GeV \circ for $x = 0.075$,
- \bullet for $x = 0.15$, \bullet for $x = 0.3$.

The pion nucleon flux ratio can be derived for p-p collisions
in the following way

$$P(E_\pi, E_p) dE_\pi = \frac{\pi}{\sigma_{in.}} \int_{p_T} f(x, p_T) \frac{dx}{x} dp_T^2 \dots \dots \dots (3)$$

where E_p is the primary nucleon energy and E_π is the secondary pion
energy in the laboratory system. For large E_p and not too small values
of x , x is given by

$$x \approx E_\pi / E_p \dots \dots \dots (4)$$

From (2) and (3) we find

$$P(E_\pi, E_p) dE_\pi = \frac{\pi A}{2\sigma_{in.}} \frac{dx}{x^2} I(\beta) \dots \dots \dots (5)$$

where $I(\beta) = \int_0^\beta \exp(-a^2/4b) \exp\{b(\eta - a/2b)^2\} d\eta \dots \dots \dots (6)$

The integral over η is cut off at some suitable value (actually $\beta = 0.1$ is sufficient for the data analysed here) $I(\beta)$ can also be expressed in the following form

$$I(\beta) = \frac{\exp(-a^2/4b)}{\sqrt{b}} [\exp(a^2/4b) D(a/2\sqrt{b}) + \exp\{b(\beta - a/2b)^2\} D\{\sqrt{b}(\beta - a/2b)\}] \dots (7)$$

where $D(x) = \exp(-x^2) \int_0^x \exp(t^2) dt \dots \dots \dots (8)$

Taking the hadron source spectrum of Grigorov et al. (1971), their result follows a power law of the following form

$$N(E_p) dE_p = N_0 E_p^{-\gamma} dE_p \dots \dots \dots (9)$$

where $N_0 = 2.54$ and $\gamma = 2.6$, E_p is expressed in GeV and the differential nucleon intensity $N(E_p) dE_p$ is expressed in units of $(\text{cm}^2 \text{ sec sr GeV})$, we get the pion-nucleon flux ratio in the top of the atmosphere by the following relation

$$\begin{aligned} \pi(E_\pi) dE_\pi &= \int P(E_\pi, E_p) N(E_p) dE_p dE_\pi \\ &= \frac{\pi A I(\beta)}{2\sigma_{in.}} N_0 E_\pi^{-\gamma} \int_0^1 x^{\gamma-3} dx dE_\pi \\ &= \frac{\pi A I(\beta)}{2(\gamma-2)\sigma_{in.}} N(E_\pi) dE_\pi \dots \dots \dots (10) \end{aligned}$$

3. Results and discussion

It is evident from relation (10) that the pion nucleon flux ratio decreases with an increase of σ_{in} with energy. Taking σ_{in} as 35 mb from the Intersecting Storage Ring data of Capiluppi et al. (1974) at a center of mass energy $\sqrt{s} = 52.8$ GeV, we get the flux ratios of charged pion-nucleon, at the top of the atmosphere, presented in Table - I.

Table - I

Charged pion to nucleon flux ratios estimated from the relation (10)

Flux	Ratio value
π^+/N	0.1037
π^-/N	0.0690

The calculated charge ratio of the pion spectrum (π^+/π^-) in the atmosphere is presented in Table - II, along with the results of different authors.

Table - II

π^+/π^- ratio determined by different authors are presented along with the present work.

Authors	Exponent of the integral spectrum	Pion charge ratio (π^+/π^-)
Frazer et al. (1972)	1.70	2.02
Yekutieli (1972)	1.70	2.06
Morrison and Elbert (1972)	1.70	1.46
Adair et al. (1973)	1.70	1.83
Yen (1973)	1.70	1.70
Hume et al. (1973)	1.60	1.72
Erlykin et al. (1974)	1.62	1.54
Present work	1.60	1.50

Our calculated charge ratio of cosmic ray pions at the top of the atmosphere agrees well with the results of Morrison and Elbert (1972) and Erlykin et al. (1974).

The authors express their thanks to Professor D. Basu, Director, Indian Association for the Cultivation of Science, Jadavpur, Calcutta for his interest in the work.

References

1. Adair R.K., Kasha H. and Kellogg R. 1973 Proc. 13th Int. Conf. on Cosmic Rays, Denver 3, 1822.
2. Capiluppi P., Giacomelli G., Rossi A.M., Vanni G. and Bussiere A., 1974 Nucl. Phys. B70, 1.
3. Erlykin A.D., Ng L.K. and Wolfendale A.W., 1974 J. Phys. A (Math., Nucl. Gen.) 7, 2059.
4. Frazer W.R. et al., 1972 Phys. Rev. D5, 1653.
5. Grigorov N.L. et al., 1971 Proc. 12th Int. Conf. on Cosmic Rays, Hobart (Hobart : University of Tasmania) Vol. 5, pp. 1746.
6. Hume C.J. et al., 1973 J. Phys. A (Math., Nucl. Gen.) 6, L63.
7. Morrison J.L. and Elbert J.W., 1973 Proc. 13th Int. Conf. on Cosmic Rays, Denver (Denver : University of Denver) Vol. 4, pp. 1833.
8. Roychoudhury R.K. and Bhattacharyya D.P., 1976 Can. J. Phys. 54, in press.
9. Yekutieli G., 1972 Nucl. Phys. B47, 621.
10. Yen E., 1973 Phys. Rev. D8, 1618.

ELECTRONS AND MUONS IN LARGE AIR SHOWERS OBSERVED AT CHACALTAYA (5,200m a.s.l.)

AND

ENERGY SPECTRUM OF PRIMARY COSMIC RAYS FROM 10^{16} eV to 10^{19} eV

C. Aguirre and G.R. Mejia, Instituto de Investigaciones Fisicas, Universidad Mayor de San Andres, LaPaz, Bolivia

T. Kaneko, Department of Physics, Okayama University, Okayama, Japan

P.K. MacKeown, Department of Physics, University of Hong Kong, Hong Kong

K. Suga, F. Kakimoto and Y. Mizumoto, Department of Physics, Tokyo Institute of Technology, Meguro, Tokyo, Japan

K. Murakami and K. Nishi, The Institute of Physical and Chemical Research, Itabashi, Tokyo, Japan

M. Nagano and K. Kamata, Institute for Cosmic Rays, University of Tokyo, Tanashi, Tokyo, Japan

Y. Toyoda, Department of Physics, Kobe University, Nada, Kobe, Japan

H. Yoshii, Department of Physics, Ehime University, Matsuyama, Japan

Abstract

Results are presented on the average lateral distributions of electrons and muons in large air showers observed at Mt. Chacaltaya (5,200m a.s.l.) in Bolivia. Results are also presented on the average longitudinal development of air shower electrons, the energy spectrum of primary cosmic rays determined from electron sizes and that determined from muon sizes in the same showers. The former spectrum is significantly higher than the latter one, and the discrepancy is explained by a possible existence of copious direct production of photons besides the production of charged and neutral pions at these high energies. The present spectra are also compared with energy spectra by other groups.

1. Introduction.

At the 13th International Cosmic Ray Conference in 1973 and at the 14th International Cosmic Ray Conference in 1975, we reported preliminary results on the average lateral distributions of electrons and muons in large air showers observed at Mt. Chacaltaya (5,200m a.s.l., 550gcm^{-2} atmospheric depth) in Bolivia, the average longitudinal development of air showers and the energy spectrum of primary cosmic rays from $5 \times 10^{16}\text{eV}$ to $2 \times 10^{19}\text{eV}$.^{1,2} Thereafter, we have refined the analyses including smaller showers and adding showers processed recently at the larger size region. P.K. MacKeown has made a series of simulation of air showers which is important for corrections to obtain the final results. And we have newly determined the energy spectrum of primary cosmic rays from muon sizes besides that from electron sizes in the same showers. At this Symposium, we present these results and propose the direct production of photons besides the production of charged and neutral pions to explain the discrepancy between the two energy spectra.

2. Experimental.

The experimental arrangement of detectors and the triggering requirements in recording air showers are already described.^{1,2} The characteristics of detectors important in the analyses are listed in Table I, together with the characteristics of four fast-timing 1.00m^2 unshielded scintillation detectors added in 1974 to expand the area of array from $300\text{m} \times 700\text{m}$ to $700\text{m} \times 700\text{m}$ as shown in Fig. 1.






Kind of detector	Number of Detectors	area of scintillator	thickness of scintillator	photomultiplier
F ₁ (fast-timing) 	12(I~XII)	0.87m^2	9.6cm	RCA6810A(2")
F ₂ (fast-timing) 	4(XIII~XVI)	1.00m^2	10.0cm	RCA6342A(2")
N 	20(1~20)	0.83m^2	7.5cm	DuMont6364(5") or RCA8055A(5")
n' 	8(1'~8')	$1/16\text{m}^2$	2.0cm	RCA8055A(5")
MU 	15	4m^2	5.0cm	DuMontK1328(16")

Table I

3. Lateral distribution of electrons.

We have determined the location of shower axis and the total number of charged particles (size N), fitting the densities recorded in unshielded detectors to the empirical lateral distribution function already described.² The distribution is represented by

$$\rho(R,N)/m^2 = \frac{C_1 N}{2\pi R_0^2} x^{s-2} (1+x)^{s-4.5} (1+C_2 x^{2.0}), \quad (1)$$

$$C_1 = 1/\left\{ \frac{\Gamma(s)\Gamma(4.5-2s)}{\Gamma(4.5-s)} + C_2 \frac{\Gamma(2.0+s)\Gamma(2.5-2s)}{\Gamma(4.5-s)} \right\},$$

$$C_2 = 0.100 + 0.125(\sec\theta-1),$$

$$3 \times 10^6 < N < 5 \times 10^9, \quad 0 < \theta < 60^\circ, \quad 0.1 R_0 < R < 3 R_0,$$

where R is expressed in m, $x=R/R_0$, R_0 is 155m and s is an age parameter smaller than 1.25. We determined the arrival direction, zenith angle (θ) and azimuth angle (ϕ), from relative delays of arrival times of shower front particles in the fast-timing detectors, taking into account the curvature of shower front.

As the transition effect of shower particles in scintillators is important to obtain the genuine lateral distribution, we have studied the transition effect by comparing densities recorded in detectors with different thickness of scintillator at the same distances from the axis. The recorded density (ρ_{rec}) is related to the incident density (ρ_{inc}) as $\rho_{rec} = \rho_{inc} \exp(-t \sec\theta/\lambda)$, where t is the thickness of scintillator and λ is 34.1cm independent of size between 10^7 and 10^9 and of x between 0.2 and 3.

We have also confirm the response of detectors to higher densities including the photomultiplier and amplifier by comparing densities recorded in detectors with different area of scintillator and with different window area of photomultiplier. In particular, we have paid attention to the long-lived fluorescence in the window glass of photomultiplier produced by scintillator light and Cerenkov light from electrons in the window glass and to the

after-pulse inside of photomultiplier for the highest densities.

After these considerations and refinements, we have obtained the genuine average lateral distribution of air shower particles expressed as

$$\rho/m^2 = \frac{1.03C_1 N}{2\pi R_0^2} x^{s-2} (1+x)^{s-4.5} (1+C_2 x^{2.0}) [1-0.20\exp\{-(\ln x+0.3)^2/0.50\}] \quad (2)$$

This lateral distribution is compared with the lateral distribution obtained by the Volcano Ranch group (corresponding to $\sec\theta = 1.49$ at Chacaltaya)³ and that adopted by the Yakutsk group (corresponding to $\sec\theta = 1.85$ at Chacaltaya)⁴, as shown in Fig. 2. As the lateral distributions within $1R_0$ are not accurately determined by these two groups, they may under-estimate the size of shower.

4. Lateral distribution of muons.

We have obtained the average lateral distribution of muons above $600x\sec\theta$ MeV for showers with sizes 10^7 - 10^9 and with $\sec\theta$ 1.0-1.4 from densities recorded in fifteen $4m^2$ shielded scintillation detectors. We have applied corrections for bursts produced by nuclear interactions of hadrons and bremsstrahlung of muons at distances within 100m from the axis and for the accidental incidences of particles unrelated to the shower at distances beyond 550m from the axis. The distribution between 60m and 600m from the axis is represented by

$$\rho(r,N) = (629 \pm 29) (N/10^8)^{1.03 \pm 0.04} r^{-0.75} \{1+r/r_0(N)\}^{-2.50}, \quad (3)$$

$$r_0(N) = (445 \pm 22) - (43 \pm 3) \log_{10}(N/10^8),$$

where r and r_0 are expressed in m and the average $\sec\theta$ is 1.17.

5. Effective areas and simulation of showers.

Dr. P.K. MacKeown of Department of Physics, University of Hong Kong has calculated the effective areas as a function of N , θ and s analytically

and by Monte Carlo method, to obtain the size spectra as a function of $\sec\theta$. Fluctuations in particle density determined experimentally, characterized by a standard deviation $\sigma(\rho) = \{\rho + (0.35\rho)^2\}^{1/2}$, have been considered in these calculations.

He has also generated simulated showers which correspond to the showers recorded by the scintillation detectors and has analysed these showers with the same procedure as that for recorded showers to estimate the systematic shifts of θ , ϕ , N , s and location of axis of analysed shower and to estimate the fluctuations of these parameters. The flow chart of this simulation of showers and the analysis is shown in Fig. 3. The results are used to apply corrections to the size spectra as a function of $\sec\theta$.

6. Longitudinal development of air shower electrons.

We have obtained the size spectra as a function of $\sec\theta$ with the effective areas mentioned in Section 5 as well as by the "variable area method. (VAM)". VAM is a method by which one can obtain the areas with trigger efficiencies of almost 100% and the intensities without calculation under the triggering levels of detectors and an information on the fluctuations in particle density. We plotted flux against area, counting the number of shower axes in a square whose center is situated at the center of array (N_{11}) and varying the area. We took the fluxes at the plateau for smaller areas as the intensity of showers. We have confirmed the availableness of this method with a Monte Carlo method. The size spectra by VAM corrected for the systematic shift of location of axis is in good agreement with the size spectra by the effective areas. We have corrected these size spectra for the systematic shift of N and the uncertainties in N and θ .

Then, we have obtained the longitudinal development by so-called

equi-intensity cuts of the integral size spectra at different zenith angles. The longitudinal developments are shown in Fig. 4, together with those obtained by the Volcano Ranch group (indicated by squares)⁵ and the Yakutsk group (indicated by triangles)⁶ for intensities of $10^{-10} \text{ m}^{-2} \text{ s}^{-1} \text{ sr}^{-1}$ and $10^{-13} \text{ m}^{-2} \text{ s}^{-1} \text{ sr}^{-1}$.

7. Energy spectrum of primary cosmic rays from electron sizes.

The electron size at maximum development (N_{max}) from a primary cosmic ray with a given energy (E_0) does not fluctuate much and is insensitive to the nature of the primary nucleus or the character of nuclear interaction, according to calculations by many authors. These results suggest that E_0 is $(1.6-2.0) \times 10^9 \text{ eV} \times N_{\text{max}}$. We have determined the energy spectrum of primary cosmic rays from the electron sizes at maximum development obtained in Section 6, multiplying $1.8 \times 10^9 \text{ eV}$ and correcting for the fluctuations in N_{max} at fixed primary energy although this fluctuation is not important. The energy spectrum is indicated by J_e in Fig. 5, and is expressed as

$$J_e (\geq E_0) = (1.84 \pm 0.34) \times 10^{-9} (E_0 / 10^{17} \text{ eV})^{-2.02 \pm 0.10} \text{ m}^{-2} \text{ s}^{-1} \text{ sr}^{-1}, \quad (4)$$

for $10^{16} \text{ eV} \leq E_0 \leq 10^{19} \text{ eV}$.

The lateral distribution within $0.1R_0$ has not been well determined in this experiment, although the apparent distribution is proportional to R^{-1} and the real distribution may be steeper than R^{-1} . Assuming the apparent distribution within $0.1R_0$, we have estimated a lower limit of the spectrum as indicated by J_e' in Fig. 5.

8. Energy spectrum of primary cosmic rays from muon sizes.

The average lateral distribution of muons corrected for the systematic shift and the uncertainty of size is expressed as

$$\rho_{\mu}(r, N) / \text{m}^2 = (660 \pm 40) (N / 10^8)^{1.14 \pm 0.04} r^{-0.75} \{1 + r / r_0(N)\}^{-2.50} \quad (5)$$

$$r_o(N) = (98 \pm 6) - (43 \pm 3) \log_{10}(N/10^8).$$

The lateral distribution of muons within 60m could not be determined due to much contamination of bursts from hadrons and muons. We estimated the extreme distributions within 60m as proportional to $r^{-0.4}$ and $r^{-1.5}$ and we have taken into account these uncertainties as errors when we obtained the muon size by integrating the lateral distribution. The muon size is represented by

$$N_\mu = (8.60 \pm 0.70) \times 10^5 (N/10^8)^{0.850 \pm 0.025} \quad (6)$$

The ratio of N_μ/N is 1.2×10^{-2} at the size of 10^7 and becomes smaller for larger sizes. Therefore, the size N is practically equal to the electron size.

We have obtained the integral muon size spectrum for $\sec\theta$ of 1.17 from N_μ in Equation (6) and the integral size spectrum for this zenith angle. The energy spectrum of primary cosmic rays is derived from the E_o to N_μ relation obtained theoretically at an atmospheric depth of $550 \text{gcm}^{-2} \times \sec\theta(1.17)$. We have used the results by Capdevielle⁷ and Dedenko⁸ for primary proton with $E^{1/4}$ -law multiplicity. The energy spectrum from the muon sizes thus obtained is indicated as J_μ in Fig. 5 and is expressed as

$$J_\mu(\geq E_o) = (2.90 \pm 0.50) \times 10^{-10} (E_o/10^{17} \text{eV})^{-1.99 \pm 0.16} \text{m}^{-2} \text{s}^{-1} \text{sr}^{-1}, \quad (7)$$

for $10^{16} \text{eV} \leq E_o \leq 10^{18} \text{eV}$. If the primary particles are heavier nuclei, the energy spectrum becomes lower than that for primary proton.

9. Comparison of the energy spectrum from electron sizes with that from muon sizes.

The energy spectrum from electron sizes is about 6 times higher in intensity or about 2.5 times higher in energy than that from muon sizes. And the energy spectrum from electron sizes by the lateral distribution proportional to R^{-1} within $0.1R_o$ is still higher than that from muon sizes. If one uses the E_o - N_μ relation by $E^{1/2}$ -law multiplicity,⁹ the energy spectrum from muon

sizes becomes lower in energy than that by $E^{1/4}$ -law multiplicity by a factor of 2.2. If one uses the E_0 - N_{μ} relation by $\ln E$ -law multiplicity,⁹ the energy spectrum becomes higher in energy than that by $E^{1/4}$ -law multiplicity by a factor of 2.6. The $\ln E$ -law multiplicity is not accepted at energies concerned in this experiment according to the publications¹⁰ from observations of air showers by several authors. Therefore, the discrepancy between the two spectra can not be explained by the conventional models of nuclear cascades in air shower as far as the one-dimensional electro-magnetic cascade theory under Approximation B is correct.

We propose the direct production of photons besides the production of charged and neutral pions at these energies to explain the discrepancy. The electron size at maximum development of shower from a photon with an energy E_0 is about $1.0 \times (E_0/10^9 \text{eV})$, while that from a nucleus with an energy E_0 is about $(0.5-0.6) \times (E_0/10^9 \text{eV})$. A brief estimate with this fact leads to about equal share of primary energy into the direct production of photons and the production of $\pi^{\pm}\pi^0$. The longitudinal development of air showers mentioned in this report suggests that the multiplicity of produced photons is fairly high and the energies of individual photons are 10^{-2} or 10^{-3} times lower than the primary energy. The real energy spectrum of primary cosmic rays may be in between the two spectra as expressed by $J_{\tau}(\geq E_0) = (1.0 \times 10^{-9}) (E_0/10^{17} \text{eV})^{-2.0} \text{ m}^{-2} \text{ s}^{-1} \text{ sr}^{-1}$ for $10^{16} \text{eV} \leq E_0 \leq 10^{18} \text{eV}$ and even for higher energies.

At the 14th International Cosmic Ray Conference at München, Antonov and Ivanenko¹¹ pointed out independently that the energy spectra around 10^{15}eV obtained from electron sizes in air showers are not consistent with the energy spectrum obtained by the satellite-borne ionization calorimeters¹² (indicated by G in Fig. 5) and both spectra are reconciled if the energy spectra from air showers are determined with a conversion from N_{max} to E_0 by $E_0 = (1.0 \times 10^9 \text{eV}) \times N_{\text{max}}$, and they suggested an existence of copious

direct production of photons with low energies.

10. Comparison of the energy spectra with these obtained by other groups.

Energy spectra of primary cosmic rays have been determined from electron sizes by the Volcano Ranch group¹³ (indicated by V in Fig. 5) and the Yakutsk group¹⁴ (indicated by Y in Fig. 5). These spectra are significantly lower than the present spectrum from electron sizes. Since the empirical formulas of lateral distributions by these groups show flatter distributions than ours near the axis as shown in Fig. 2, we reestimated the sizes by these groups with Equation (2). The examples are shown in Fig. 4 with arrows and strips. The longitudinal developments from these reestimated sizes are consistent with those presented in this report. Therefore, the discrepancy may be explained by the difference in the lateral distributions.

Energy spectra have been also determined by the Haverah Park group¹⁵ (indicated by H in Fig. 5) from energy loss in the deep water Cerenkov detector at a distance of 600m from the axis in which the main contribution is muons and by the Sydney group¹⁶ (indicated by S in Fig. 5) from muon sizes. The former is consistent with the present energy spectrum from muon sizes. The latter is lower than the energy spectrum by the Haverah Park group, but becomes consistent with the Haverah Park Spectrum by a conversion from N_{μ} to E_0 based on the same model of nuclear interactions.

Acknowledgements.

We wish to thank Messrs. A. Trepp, C. Ormachea, I. Geier, I. Saravia and Mrs. E. Maceda of the Instituto de Investigaciones Fisicas of the Universidad Mayor de San Andres in LaPaz, Staffs of the Institute of Physical and Chemical Research in Tokyo for their contribution to the construction and

operation of the equipment and the data analysis. We are also grateful to Messrs. M. Furugori and H. Yonezawa of the Tokyo Institute of Technology and Mrs. A. Inoue of the Institute of Physical and Chemical Research for their contribution to the data analysis.

This work is partly supported by the Universidad Mayor de San Andres, the organization of American States, the Japan Society of the Promotion of Sciences, Mitsubishi Foundation in Japan, the Ministry of Education of Japan, and the Japan International Cooperation Agency.

The computation is carried out at the computer centers of the Universidad Mayor de San Andres, the University of Hong Kong, the Tokyo Institute of Technology, the Institute for Nuclear Study of the University of Tokyo and the Institute of Physical and Chemical Research.

References.

- ¹ C. Aguirre et al., Conference Papers of the 13th International cosmic Ray Conference, Denver, USA 1973 (University of Denver, Denver, Colorado, USA , 1973) (hereafter referred to as CP13ICRC.) 4, 2592 (1973).
- ² T. Kaneko et al., Conference Papers of the 14th International Cosmic Ray Conference, München, Germany, 1975 (Max-Planck-Institute für Extraterrestrische Physik, München, Germany, 1975) (hereafter referred to as CP14ICRC.) 8, 2747 (1975), 8, 2695 (1975) and 12, 4343 (1975).
- ³ J. Linsley, CP13ICRC. 5, 3212 (1973).
- ⁴ O.S. Diminstein et al., CP14ICRC. 12, 4334 (1975).
- ⁵ J. Linsley, CP13ICRC. 5, 3207 (1973).
- ⁶ O.S. Diminstein et al., CP14ICRC. 12, 4325 (1975); D.D. Krasilnikov et al., CP14ICRC. 12, 4347 (1975).
- ⁷ J.N. Capdevielle, PhD thesis, Universite de Paris-Sud, Centre D'Orsay (1972).

- ⁸ L.G. Dedenko, CP14ICRC. 8, 2857 (1975).
- ⁹ G. Tanahashi, unpublished, private communication.
- ¹⁰ N.N. Kalmykov et al., CP14ICRC. 8, 3034 (1975); A.R. Clarke et al., CP14ICR 8 2699 (1975); N.N. Kalmykov and G.B. Khristiansen, CP14ICRC. 8, 2861 (1975); M.L. Barret, J. Phys. G. 2, L73 (1976).
- ¹¹ R.A. Antonov and I.P. Ivanenko, CP14ICRC. 8, 2708 (1975).
- ¹² N.L. Grigorov et al., Conference Papers of the 12th International Cosmic Ray Conference, Hobart, Australia, 1971 (University of Tasmania, Hobart, Tasmania, Australia, 1971) 5, 1746 (1971).
- ¹³ J. Linsley, Proceedings of the 8th International Conference on Cosmic Rays, Jaipur, India, 1963 (Tata Institute of Fundamental Research, Colaba, Bombay, India, 1963) 4, 77 (1963). Re-evaluation of the energy spectrum is given in CP13ICRC. 5, 3207 (1973) and in CP14ICRC. 2, 598 (1975).
- ¹⁴ O.S. Diminstein et al., CP14ICRC. 12, 4318 (1975); D.D. Krasilnikov et al., CP14ICRC. 12, 4347 (1975).
- ¹⁵ A.R. Clarke et al., CP14ICRC. 8, 2699 (1975); R.G. Brounlee et al., CP14ICRC. 8, 2709 (1975).
- ¹⁶ C.J. Bell et al., J. Phys. A. 7, 990 (1974).

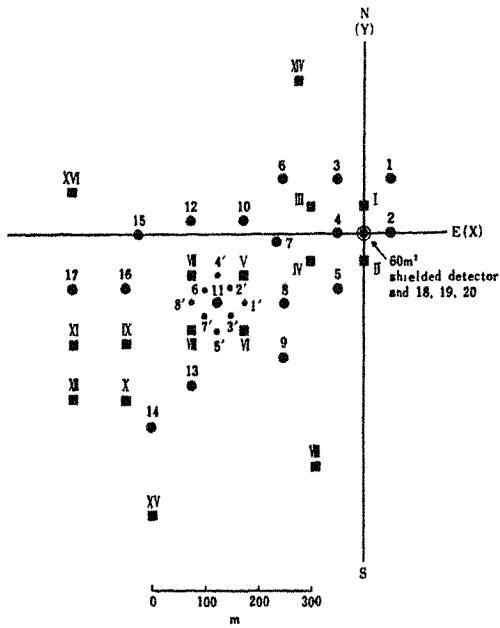


Fig. 1

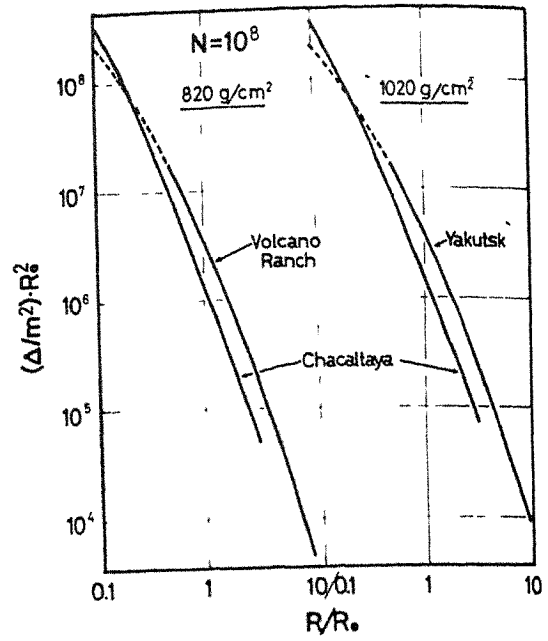


Fig. 2

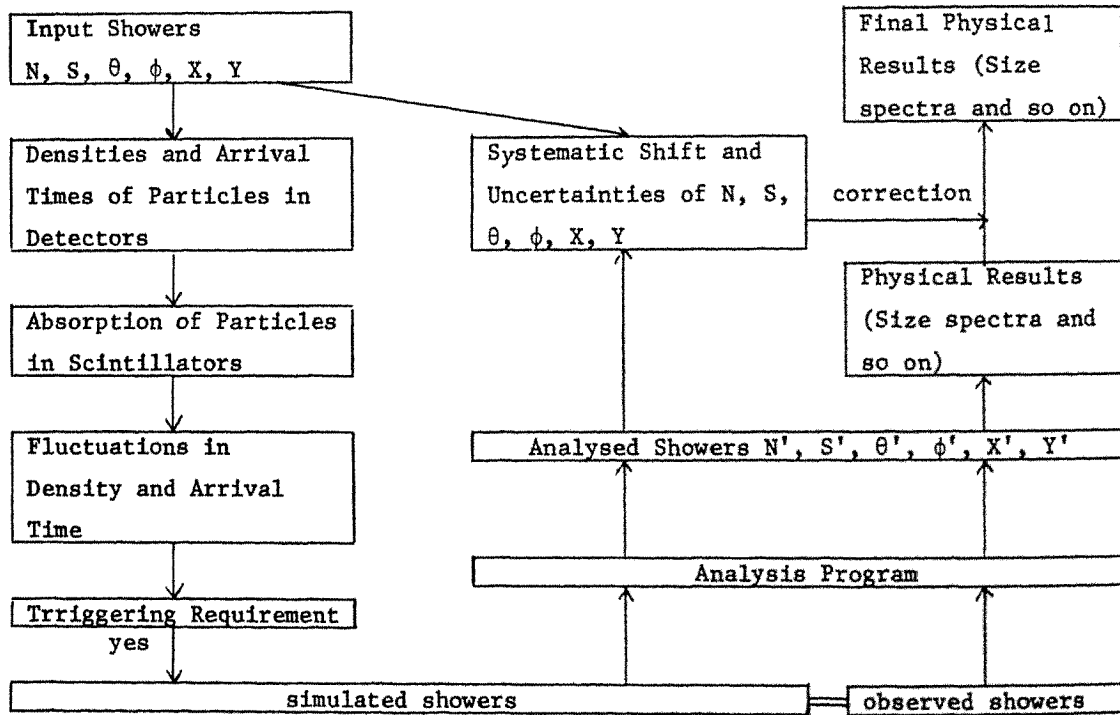


Fig. 3

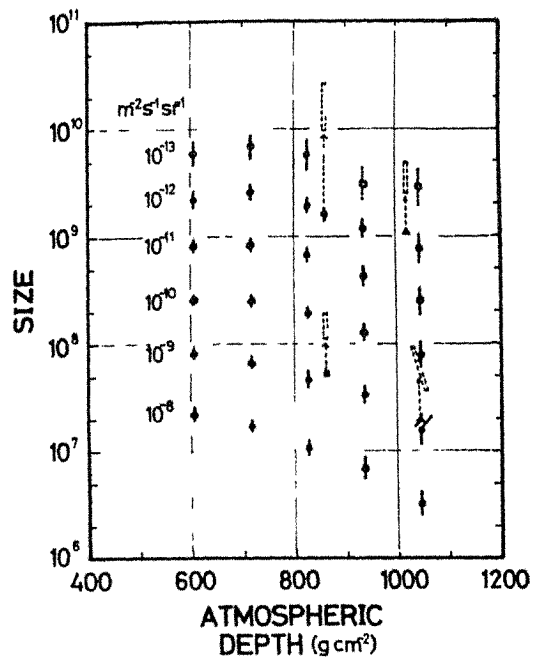


Fig. 4

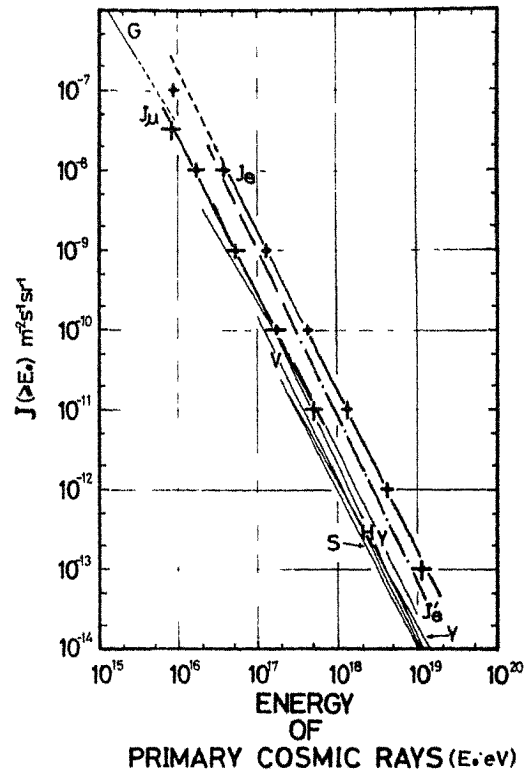


Fig. 5

E.A.S. SIMULATIONS IN THE PRIMARY ENERGY RANGE

$10^{13}\text{eV} - 10^{16}\text{eV}$

A.K. Lee

Department of Physics, University of Hong Kong

Introduction

The study of E.A.S. in the energy range $10^{14}\text{eV} - 10^{16}\text{eV}$ is of great interest in relation to particle physics and astrophysics. At present, the I.S.R. at C.E.R.N. can only accelerate protons up to $2 \times 10^{12}\text{eV}$ equivalent in the laboratory system. Studies of particle physics above 10^{13}eV still rely heavily on E.A.S. studies and any particle theories proposed for hadrons of energies above 10^{13}eV must be able to explain various E.A.S. phenomena in a consistent way. In fact some hypotheses, such as the reduction of interaction lengths of hadrons with increasing hadron energy, the scaling¹ and the limiting distribution² hypotheses etc., have constantly been incorporated in E.A.S. simulations to test their validity at post-I.S.R. energies. E.A.S. studies are also of great astrophysical interest in that they provide clues to the composition of primary cosmic rays, information on which is important in the investigation of the origin of cosmic rays.

For primary energies greater than 10^{14}eV , studies of the primary composition by the nuclear emulsion method run into great difficulty as the aperture required is very large. One still has to rely on E.A.S. studies for the information on primary composition. Unfortunately, E.A.S. parameters are usually sensitive both to the primary composition and to the details of the nuclear physics, and usually it is difficult to segregate the effects on the parameters due to each of them.

The present effort of simulation should focus on finding measurable quantities in E.A.S. which are sensitive to one of the effects and not the other, in order that information on the sensitivity of such quantities on one of the effects is gained. The present article is written with the above objectives in mind, and hundreds of vertical proton and Fe initiated

showers are simulated. Due to certain limitations, most of the muon and all of the hadron results are not presented.

The Model for Simulations

The particulars of our 'semiscaling' model are as follows :

- (A) The elasticity for N-air nucleus collisions is assumed to be 0.6.
- (B) The energy distribution for the 'fragmentation' pions in N-air nucleus interactions is given by a normalized scaling function obtained from I.S.R. data of Bertin et al³. The relation between the scaling variable x and a random number R (R < 1) is given by

$$x = 0.086 \ln (1.0175/(1.0175 - R))$$

and a cut off at x equal to 0.35 is adopted. The average number of such pions is independent of incident nucleon energy and is approximately 4.5. This idea is consistent with the experimentally observed constancy of the muon charge ratio.

- (C) The number of pionization pions is assumed to follow the multiplicity law $(2.4E_0^{1/4} + 2.25)$, which is the best fit to the experimental data between 100 and 10^4 GeV (Fishbane et al⁴), and the available energy is assumed shared among half of the pions, i.e. those emitted in the forward cone in the c.m.s. The inelasticity for these pions is assumed to be 0.05.
- (D) The leading particle effect is also assumed for pion-air nucleus collisions by assuming an elasticity of 0.6 for incident pions, (an inelasticity of 0.4). This is supported by the experimental studies of hadrons (mostly pions less than 100 GeV) by Vatcha et al⁵, who conclude that an inelasticity less than 0.5 is indicated. The probability for a secondary pion emitted with scaling variable x is given by

$$\frac{d\sigma}{dx} = A(s) \frac{f(x)}{\sqrt{x^2 + 4(m^2 + p^2)}/s}$$

where A(s) is a normalizing constant, f(x) is the scaling function, m, p and s are the mass, transverse momentum and the square of total energy in c.m.s. respectively. The scaling function is obtained from the accelerator data of Beaupre et al⁶.

- (E) The pion-air nucleus interaction length is assumed to be 70 gm/cm² and 120 gm/cm² for pions of energy greater than and less than 200GeV respectively.
- (F) The P-air nucleus interaction length is assumed to increase with increasing primary nucleon energy and assumes values 75, 70, 65, 60 gm/cm² at primary energies equal to 10¹³, 10¹⁴, 10¹⁵, 10¹⁶eV respectively.
- (G) The distribution in transverse momentum p of the produced pions assumed is the C.K.P. relation

$$f(p) = \frac{p}{p_0^2} \exp\left(-\frac{p}{p_0}\right)$$

with p₀ (half of the average value of the transverse momentum) equal to 0.2 GeV.

Method of Simulation

(A) The Electronic Component

The number of electrons at the observation levels due to γ rays from π⁰ decay is given by

$$N_e = \frac{0.31}{\sqrt{\beta}} e^{[t(1-1.5\ln r)]}$$

where $t = y/37.7$, and y is the thickness of air traversed by the γ ray in gm/cm², $\beta = \ln(E_\gamma/0.0842)$ and $r = 3t/(t + 2\beta)$. To obtain the lateral distributions of electron densities due to each π⁰, the shower age due to the π⁰ at the observation level in question is first calculated. The density of electrons per m² at a distance x from the shower axis in Moliere's units, r_1 , is given by

$$\Delta_e(x) = \frac{N_e}{r_1^2} C(s) x^{s-2} (x + 1)^{s-4.5}$$

where $C(s)$ is a normalizing constant depending on the shower age s . By adding up the contributions due to each π⁰, the resulting electron number and lateral distribution for the whole shower can be determined and the shower age ascertained. The positions of the assumed detectors are at 25m,

60m, 120m and 200m from the shower axis, and the effect of the transverse momentum of the π^0 is also included in the two dimensional electron simulations.

(B) The Muon Component

Our three dimensional muon simulations include p for charged pions, the effect of the earth's magnetic field and Coulomb scattering on the lateral distributions of the muons at various observation levels.

(C) The Fe Simulations

For Fe simulations, the fragmentation parameters are obtained from the works of Waddington et al⁷. The relative probabilities for Fe nucleus-air nucleus interactions giving fragments of L-nuclei ($Z = 4$), M-nuclei ($Z = 7.5$), LH- nuclei ($Z = 12$), He nuclei ($Z = 2$) are 0.127, 0.073, 0.073 and 0.727 respectively. The number of nucleons remaining in $Z > 2$ fragments in Fe-air nucleus collisions is allowed to fluctuate from 50% to 80%. This is consistent with the result of Waddington et al that the average number of protons released in an Fe-air nucleus collision is 8.2. The rest of the constituent nucleons are assumed to be released and the fraction of released nucleons taking part in N-air nucleus interactions is obtained from the works of Tomaszewski et al⁸, the remaining nucleons merely being shaken free and proceeding independently. The interaction lengths of $Z > 2$ fragments and Fe with air nuclei are given by the expressions of Cleghorn et al⁹. The treatment of further interactions of $Z > 2$ fragments with air nuclei is given as follows :

(I) He fragments -

For He fragments-air nucleus collisions, all the constituent nucleons of He are assumed to be freed and two of them take part in N-air nucleus interactions and the others merely being shaken free.

(II) $Z > 4$ fragments -

In the interactions of these fragments with air nuclei, about half of the nucleons are assumed to remain bound as He nuclei. The remaining nucleons being released and the portion of the released nucleons taking part in the interactions with air nuclei is again determined from the works of Tomaszewski et al.

In this way, the points of first interaction of constituent nucleons of an Fe nucleus can be determined.

General Simulation Results

(A) Shower Age Simulations

The variations of average shower age with primary (proton or Fe) energy at depths of 1030 and 550 gm/cm² are given in Fig. 1(a) - (d).

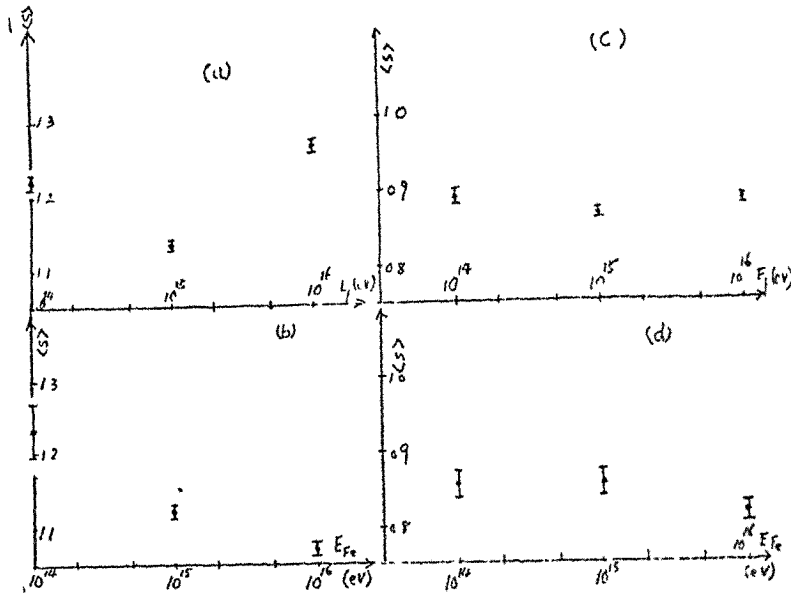


Fig. 1 Variation of average shower age with primary energy for
 (a) primary proton at sea level
 (b) primary Fe at sea level
 (c) primary proton at 550 gm/cm²
 (d) primary Fe at 550 gm/cm²

An interesting feature to be noted is that the predicted average shower age reaches a minimum value at a primary proton energy equal to 10^{15} eV. The reason for the rise in $\langle s \rangle$ for $E_p > 10^{15}$ eV is probably that for $E_p > 10^{15}$ eV, most of the interacting pions are of energy greater than 200 GeV and since a shortening of the interaction length of charged pions is assumed for $E_\pi > 200$ GeV, the shower develops faster and gives an older shower age.

This is consistent with the experimental results of Vernov et al¹⁰. who show experimentally that the average shower age reaches a minimum value for fixed shower sizes in the vicinity of 7×10^5 . These shower sizes correspond approximately to a primary proton energy of 10^{15} eV. Since the correlation of s and N_e at fixed primary proton energy is small, the shower age for average sizes in the vicinity of 7×10^5 should not be very much different from the corresponding value at a fixed primary proton energy of 10^{15} eV and this piece of information may as well indicate protonic nature of primary cosmic rays at $E_p \sim 10^{15}$ eV. The predicted average shower ages at sea level for Fe initiated showers show a monotonous decrease with increasing primary energy, while the predicted average shower ages at 550 gm/cm² remains practically constant over the range of primary energies considered. Fig. 2(a) - (d) show the predicted fluctuations of shower age without considering the Poissonian distributions of electrons.

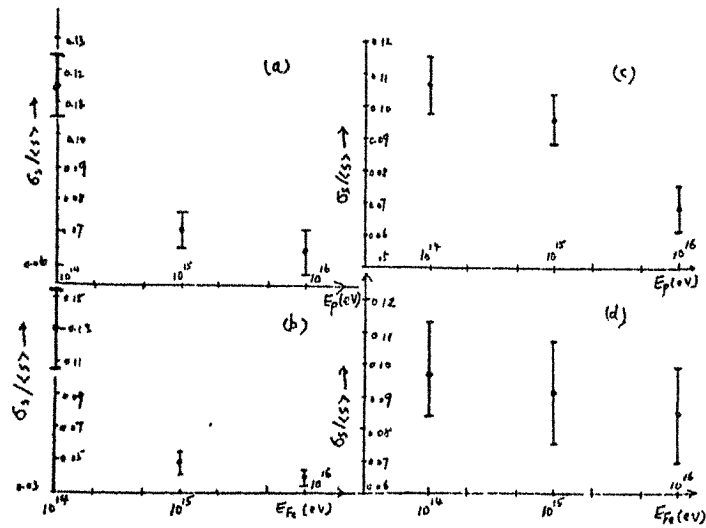


Fig. 2 Variation of $\sigma_s / \langle s \rangle$, the relative fluctuation of shower age with primary energy for
(a) primary proton at sea level
(b) primary Fe at sea level
(c) primary proton at 550 gm/cm²
(d) primary Fe at 550 gm/cm²

If the shower size is small (e.g. less than 10^5 particles), one must take into account the Poissonian distributions of electrons in comparing predicted shower age fluctuations with experimental ones. In fact, using the information on the detector areas at various distances from the center of the Moscow State University array (Vernov et al) and taking the Poissonian distributions of electrons into account, the fluctuation parameter, $\sigma_s/\langle s \rangle$, for Fe showers at 10^{15} eV increases from 0.0485 ± 0.0082 to 0.065 ± 0.0055 . For Fe showers at 10^{16} eV, the effect of Poissonian distributions of electrons is negligible and the predicted fluctuation parameters could be compared with experimental ones provided that all other systematic sources of fluctuations are duly corrected for. In order to compare the predicted fluctuation parameter with experiment at a fixed muon size $N_\mu(E_\mu > 10 \text{ GeV})$ of 1.4×10^4 (Vernov et al.), the distributions of shower ages of Fe primaries at 10^{15} eV and proton primaries at 10^{16} eV are investigated. The experimental value of the fluctuation parameter, 0.11 is clearly much larger than the corresponding values for Fe primaries at 10^{15} eV and proton primaries at 10^{16} eV, 0.065 and 0.0647 respectively. However if one mixes 50% Fe primaries at 10^{15} eV with 50% P primaries at 10^{16} eV, a maximum value of the predicted fluctuation parameter of 0.085 is obtained. One important point worth mention is that the average shower age at a fixed energy is sensitive to the assumed value of the elasticity for N-air nucleus collisions. The surprisingly young simulated average shower age at sea level supports the idea that N-air nucleus collisions are rather elastic.

(B) The Longitudinal Shower Development

The experimental data on longitudinal shower development in the lower atmosphere are derived from equi-intensity cuts of size spectra measured at different zenith angles in high-altitude experiments. The longitudinal development curve is sensitive to the details of the interaction model and to the primary composition used in the simulations. In general, the use of isobar or scaling models for pion productions in simulations lead to greater depth of maximum development than that using the C.K.P. model, and the development curve for Fe primaries is always steeper than the corresponding one for proton primaries. The shower development curves obtained in the present simulations are plotted in Fig. 3, for 10^{16} eV, for both P and Fe primaries while the plotted points are the data from Ref.(11).

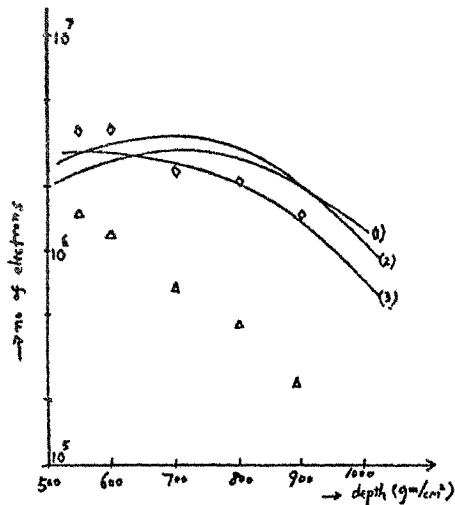


Fig. 3 Graphs of the number of electrons at various atmospheric depths for showers of average development under various assumptions: Curve 1 - proton primary. Curve 2 - proton primary + 'Gamaisation'. Curve 3 - Fe primary. Points \diamond and Δ are experimental data adapted from reference (11).

It is interesting to note that at 10^{16} eV, the rapid absorption of shower particles in the lower atmosphere and the small depth of maximum development can be explained by assuming all primaries to be as heavy as Fe. One thus tends to conclude that primaries at 10^{16} eV are heavy. However since the details of the interaction model employed can seriously affect the longitudinal shower development, such a conclusion must be considered as tentative. Fig. 4 is a graph of the variation of the depth of maximum development with primary energy for both P and Fe primaries.

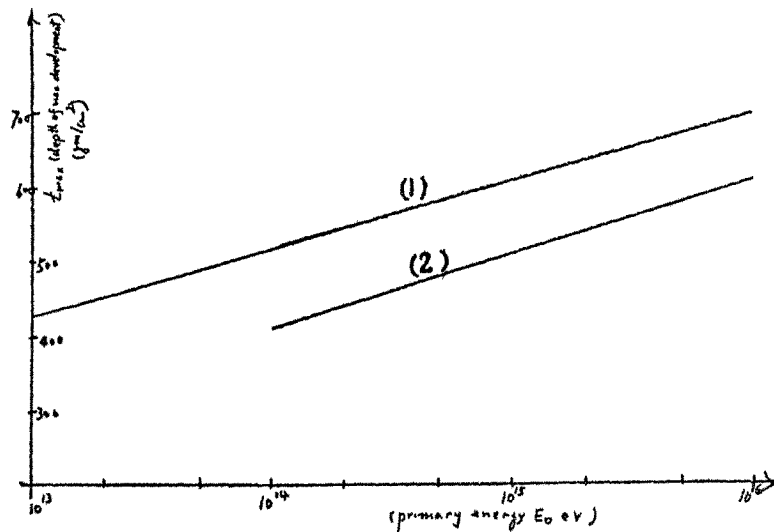


Fig. 4 Graph of the variation of the depth of maximum development with primary energy E_0 . Curve 1 - primary proton. Curve 2 - primary Fe.

Figs. 5 (a) - (b) are graphs of the variation of the electron fluctuation parameter $\sigma_N / \langle N_e \rangle$ at various primary energies with atmospheric depths for both P and Fe primaries.

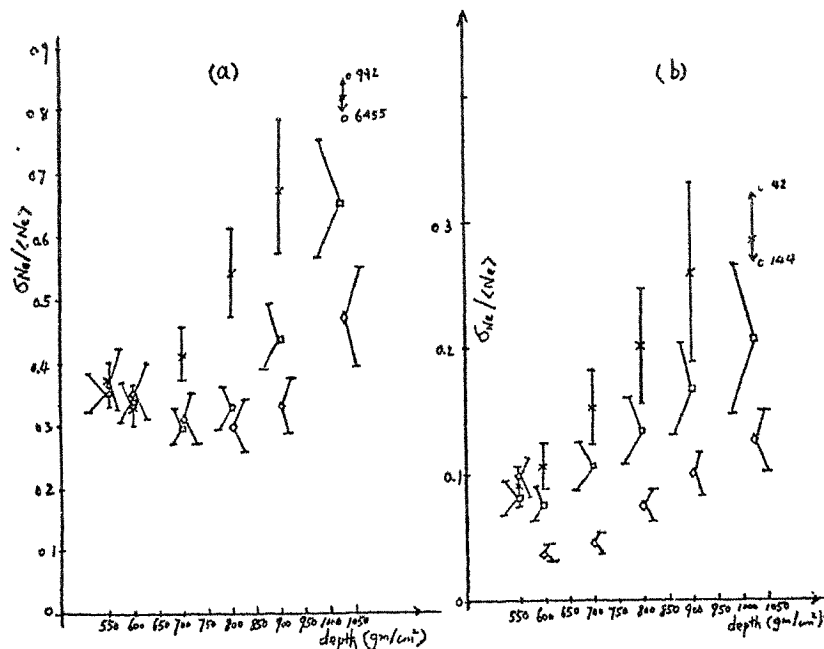


Fig. 5 Values of relative electron number fluctuation, $\sigma_N / \langle N_e \rangle$, for various depths and primary energies.
 (a) $\square E_p = 10^{14} \text{ eV}$, $\square E_p = 10^{15} \text{ eV}$, $\square E_p = 10^{16} \text{ eV}$
 (b) $\square E_{Fe} = 10^{14} \text{ eV}$, $\square E_{Fe} = 10^{15} \text{ eV}$, $\square E_{Fe} = 10^{16} \text{ eV}$.

(C) The effect of including 'Gamaisation' and variation of the average π^0 transverse momentum on shower development

The suggestion of direct gamma ray production in N-air nucleus collisions, termed 'Gamaisation', was first suggested by Nikolsky¹². The 'Gamaisation' model employed here involves the production of a single gamma ray having ~~5%~~ of the incident nucleon energy in N-air nucleus collisions involving incident nucleons of energy greater than or equal to 10^{15} eV . The effect of such an assumption is to increase the average shower age at levels of observation in the lower atmosphere and give greater depth of maximum development. The increase of the average shower age may be due to the fact that with the assumption of 'Gamaisation', the elasticity for N-air nucleus collisions reduces from 0.6 to 0.55 and thus showers develop faster and give older shower ages.

The development curve for an average development shower under such an assumption is shown in Fig. 3. It is seen that the position for proton primaries alone to explain the shower development is not very much improved.

The fractions of the total number of electrons derived from gamma rays at 700 and 550 gm/cm² are 21% and 25% respectively. The effect of the variation of average π^0 transverse momentum on average shower age and fluctuation of shower ages for $E_p = 10^{16}$ eV at 700 gm/cm² with 'Gamaisation', and $E_p = 10^{15}$ eV at 1030 gm/cm² without 'Gamaisation', are shown in Figs. 6(a) - (b) and Figs. 6(c) - (d) respectively. A prominent feature of these figures is the decrease of average shower age with the increase of average π^0 transverse momentum, while the effect on the fluctuations of shower age at the level is seen to be quite small. Figs. 6(c) - (d) show that the average shower age at sea level is not very sensitive to the mean transverse momentum for π^0 , while the shower age fluctuation parameter increases with increasing mean transverse momentum of the π^0 .

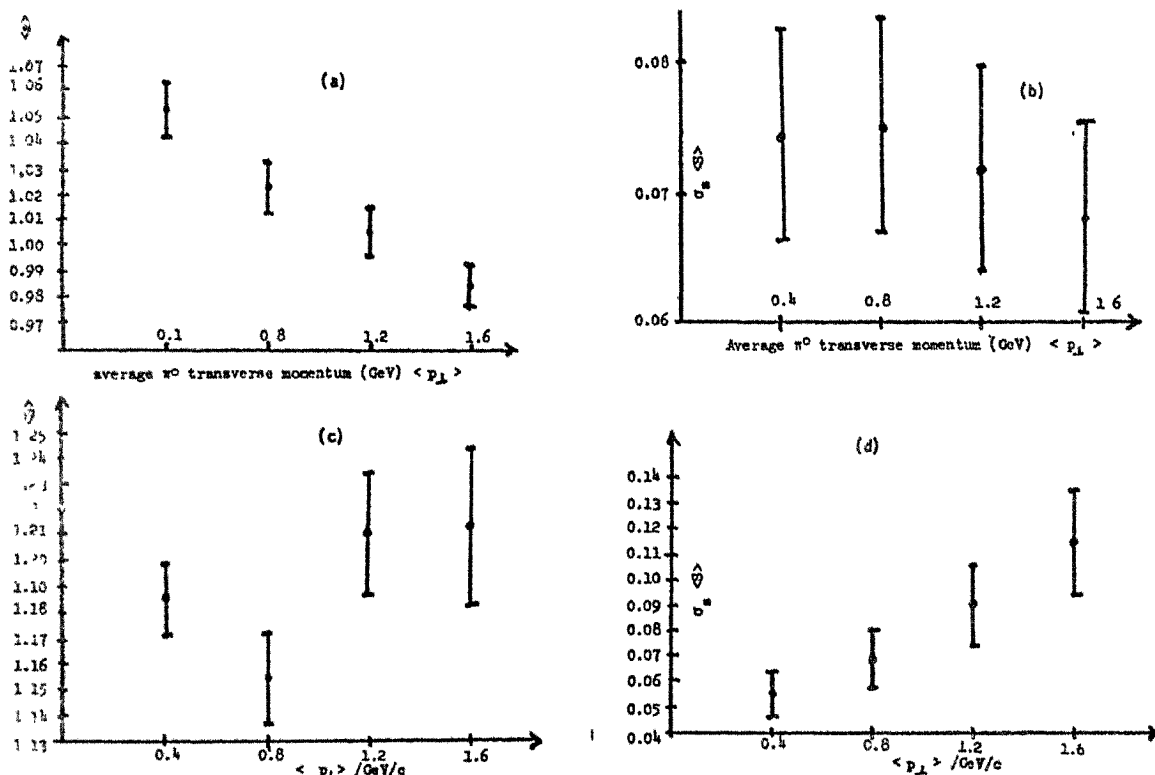


Fig. 6. Variation of (a) average shower age $\langle s \rangle$ and (b) its fluctuation $\sigma_s / \langle s \rangle$, with $\langle p_{\perp} \rangle$ for π^0 at 700 gm/cm² for $E_p = 10^{16}$ eV with 'Gamaisation'. Similarly for (c) and (d) with $\langle p_{\perp} \rangle$ for π^0 at 1030 gm/cm² for $E_p = 10^{15}$ eV without 'Gamaisation'.

(D) Showers at Fixed Size

The fixed size calculations are for vertical showers at sea level. The primary proton spectra assumed are $N(E_p) = (2.0 \pm 0.2) E_p^{\gamma}$ protons $\text{cm}^{-2} \cdot \text{s}^{-1} \cdot \text{Sr}^{-1}$ with $\gamma = -2.75$, and $N(E_p) = 0.64 E_p^{\gamma}$ protons $\text{cm}^{-2} \cdot \text{s}^{-1} \cdot \text{Sr}^{-1}$ with $\gamma = -2.60$. The former is the result of the Goddard Space Flight Center group (e.g. Ryan et al¹³.) for $E_p < 2 \times 10^{12}$ eV/nucleon. It is assumed that such a spectrum continues to higher primary energies. The latter is obtained by equating the differential intensity at $E_p = 2 \times 10^{12}$ eV to the former. The 'primary proton spectra' at fixed size range $10^6 - 10^{6.5}$ are presented in Fig. 7.

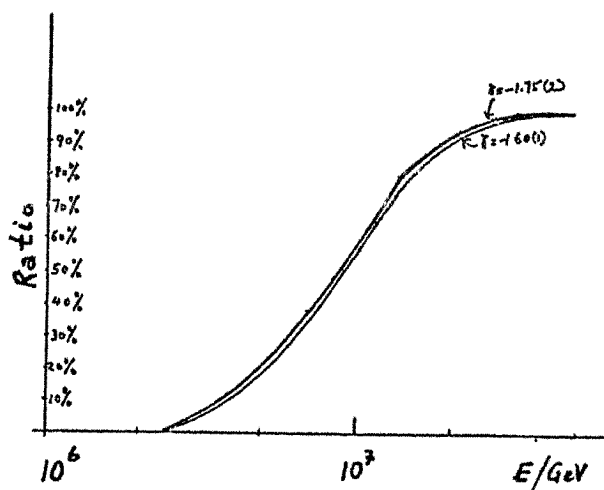


Fig. 7 The 'primary proton energy spectrum' in the size range of $10^6 - 10^{6.5}$ expressed in the ratio, (no. of protons of energy $< E$ in the size range/total no. of primary protons in the size range). Curve 1 and 2 are for the integral primary proton exponents equal to 1.6 and 1.75 respectively.

The variations of median primary proton energies with the mean sizes for different fixed size intervals are shown in Fig. 8. It is interesting to note the variations of the ratios of the number of Fe showers to that of P showers as one samples at fixed size with mean sizes for different size intervals under the assumption of a mixture of 50% proton and 50% Fe, by introducing the same primary spectrum for Fe in addition

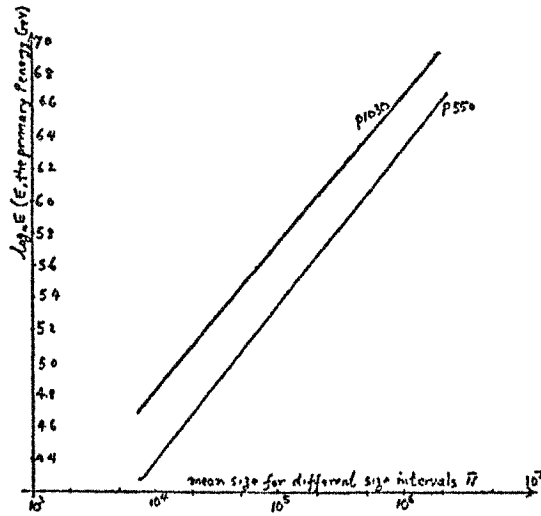


Fig. 8 The variation of median primary proton energy with size for various size intervals. $\gamma = -2.75$.

to that for P. This corresponds to an enhancement of the primary intensity by a factor of 2. The results are shown in table 1.

Table 1 : Variation of Fe/P ratio with shower size

fixed size range	Fe/P ratio for $\gamma = -2.75$	Fe/P ratio for $\gamma = -2.6$
$10^{3.7} - 10^4$	0.1138	0.1584
$10^4 - 10^{4.5}$	0.1281	0.1767
$10^{4.5} - 10^5$	0.1617	0.2187
$10^5 - 10^{5.5}$	0.2229	0.2923
$10^{5.5} - 10^6$	0.3063	0.3909
$10^6 - 10^{6.5}$	0.4210	0.5228

It can be seen that the ratio Fe/P increases with size as expected, as for larger sizes, the constituent showers are in general of greater energies, they fluctuate less and the upward fluctuation of proton showers of lower energies to the size in question is less pronounced.

The predicted E.A.S. number spectra are shown in Fig. 9 for the two assumed primary energy spectra under the assumptions of (a) 100% proton (b) 50% proton plus 50% Fe (c) 100% proton for $E_p < 1.1 \times 10^{15}$ eV and 50% P plus 50% Fe for $E_p > 1.1 \times 10^{15}$ eV. The differences in exponents for the assumed energy spectrum and size spectra are significant.

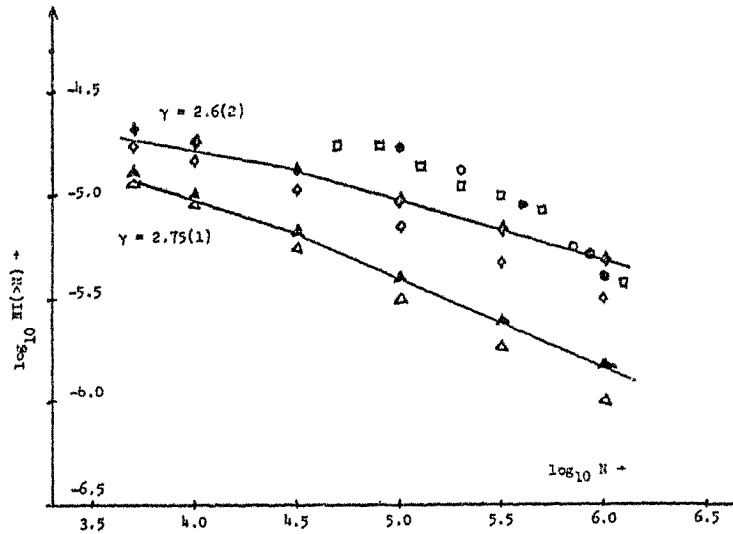


Fig. 9 The variation of integral shower size intensity expressed in $NI(>N)$ with size under various assumption: Δ - 100% P, \blacktriangle - 50% P + 50% Fe, Curve 1 - 100% P for $1.1 \times 10^6 \text{ GeV} > E_p$ and 50% P + 50% Fe for $E_p > 1.1 \times 10^6 \text{ GeV}$. The corresponding ones for the exponent of the integral primary spectrum equal to -1.6 are \diamond , \blacklozenge and curve 2 respectively. The experimental points indicated are due to \square , Kiel (Ref. 14), \bullet M.S.U. (Ref. 15), \circ M.I.T. (Ref. 16).

Fig. 10 shows the variations of $N_\mu(>E_\mu)/N_e$ with E_μ , the threshold muon energy, under various assumptions of primary composition, together with experimental points for $N_e \sim 10^6$, Ref. (17). It can be seen that the experimental data are consistent with the predicted curves under the assumption of 100% Fe. But the predicted curves seem too flat to explain the variation of $N_\mu(>E_\mu)/N_e$ with E_μ . The variations of the muon fluctuation parameter at fixed size, $\sigma_{N_\mu}/\langle N_\mu \rangle$, with mean sizes for different size intervals under various assumptions of primary composition

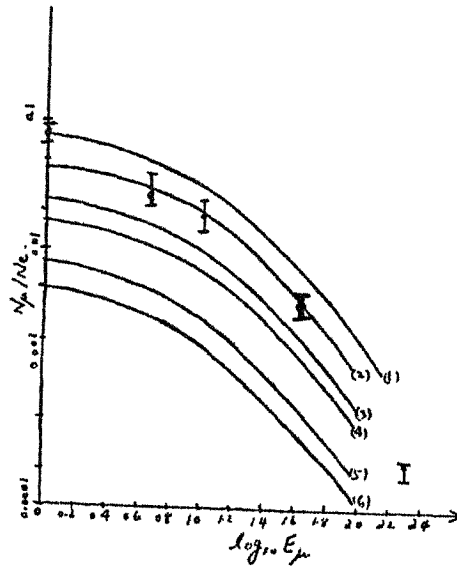


Fig. 10 Variation of $N_{\mu}(>E_{\mu})/N_e$ with E_{μ} for two fixed size ranges with the assumption of 1.75 for the exponent of the primary cosmic ray spectrum. The corresponding curves for 1.60 as exponent practically coincide with the curves indicated. Curve 1 - 100% Fe, size range $10^{5.5} - 10^6$. Curve 2 - 100% Fe, size range $10^6 - 10^{6.5}$. Curve 3 - 50% P + 50% Fe, size range $10^{5.5} - 10^6$. Curve 4 - 50% P + 50% Fe, size range $10^6 - 10^{6.5}$. Curve 5 - 100% P, size range $10^{5.5} - 10^6$. Curve 6 - 100% P, size range $10^6 - 10^{6.5}$.

and threshold muon energies are shown in Fig. 11. Also plotted on the graph are the data of Vernov et al. The predicted muon fluctuation parameters are obtained by identifying each primary proton energy at fixed size with a fixed number of muons. Thus the parameter $\sigma_{N_{\mu}}$ reflects the spread of primary proton energy at fixed shower size. The effect of the fluctuation of the number of muons at fixed primary proton energy on the fluctuation parameter can be neglected because $\sigma_{N_{\mu}}/\langle N_{\mu} \rangle$ at fixed primary energy at sea level and the correlation of N_e and N_{μ} at fixed energy are small (e.g. $\sigma_{N_{\mu}}/N_{\mu}$ at $E_p = 10^{15}$ eV is ~ 0.176) and the inclusion of this effect will raise the value of the fluctuation parameter by $\sim 10\%$.

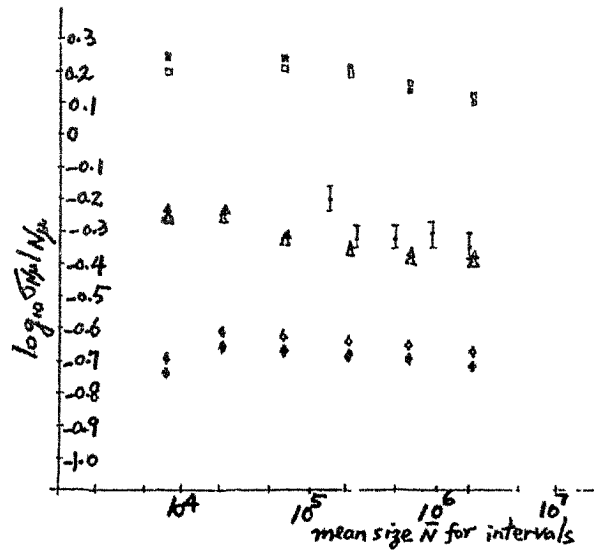


Fig. 11 Variation of $\sigma_{N_{\mu}}/N_{\mu}$ for showers at fixed size with mean size N for various size intervals under the assumption of 1.75 for the exponent of primary cosmic ray spectrum. The corresponding data for 1.6 as exponent practically coincide with the points indicated. \square - 50% P + 50% Fe, $E_{\mu} > 10\text{GeV}$. Δ - 100% P, $E_{\mu} > 10\text{GeV}$, \diamond - 100% Fe, $E_{\mu} > 10\text{ GeV}$. The corresponding black points are for $E > 1\text{ GeV}$.

Comparing the experimental points with predicted ones, one sees that the experimental muon fluctuation parameters at various fixed sizes indicate pure protonic nature of the primary beam.

Conclusions and Discussions

In the comparisons of the variation of average shower age with primary energy and the predicted $\sigma_{N_{\mu}}/\langle N_{\mu} \rangle$ at fixed shower size with experimental values, pure protonic nature of primary beam can be concluded provided that the present model of interactions and assumptions represent the true situation. The experimental shower age fluctuation parameter $\sigma_s/\langle s \rangle$ at sea level for $N_e \sim 10^5$, 0.09 (Vernov et al.), can be explained with a pure protonic beam of $E_p \sim 10^{15}\text{eV}$ provided the mean transverse momentum for π^0 is $\sim 1\text{ GeV}$. For Fe showers of the same size,

the assumption of increasing mean transverse momentum for π^0 is probably not valid because the neutral pions are of much lower energies. This is further evidence for the protonic nature of the primary beam at $N_e \sim 10^5$. The rapid absorption of shower particles in the lower atmosphere, the small depth of maximum development, and the high $N_\mu(>E_\mu)/N_e$ ratio can only be explained by assuming primary cosmic rays being as heavy as Fe. Introduction of 'Gamaisation' involving the production of a single gamma ray with the assumption of a beam of protonic primaries cannot explain the experimental data. However if one assumes multiple gamma ray productions and/or various other assumptions of particle physics such as the drastic decrease of π -air nucleus interaction length, the experimental $N_\mu(>E_\mu)/N_e$ ratio, rapid shower development and small depth of maximum development may be explained with a pure protonic beam. Our simulated charge to neutral ratios and the number of pions for a given primary proton energy are much higher than the experimental ones. These discrepancies may also be removed with such an assumption. However the assumption of drastic decrease of p-air nucleus interaction length as indicated by Jacob (18) may not be assumed as the assumption of which will give much older shower ages at observation levels.

Acknowledgements

The author wishes to express here his thanks to Dr. P.K. MacKeown for his guidance and some very useful discussions and also to Dr. E.C.M. Young for his constant help.

References

1. Feynman R.D., 1969 Phys. Rev. Lett. 23 1415.
2. Benecke J. et al., 1969 Phys. Rev. 188 2159.
3. Bertin A. et al., Phys. Lett. 41B No.2, 201-204, Phys. Lett. 38B, No.4, 260.
4. Fishbane P.M. et al., Phys. Rev. D19, 3083 - 3095 (1974).
5. Vatcha R.H. et al., J. Phys. A., 6, 1078 - 1089 (1975).
6. Beaupre J.V. et al., Phys. Lett. 37B, 432 (1971).
7. Waddington C.J. et al., Proc. 13th Int. Conf. on Cosmic Rays, Denver P2449.
8. Tomaszewski A. et al., J. Phys. A., 8, 1189-1192 (1975).
9. Cleghorn T.F., Can. J. Phys. 46, S572 (1968).
10. Vernov S.N. et al., Proc. 11th Int. Conf. on Cosmic Rays, Budapest 1969 P429-434.
11. Bradt H., Proc. 9th Conf. on C.R. 1965, 2, 715.
12. Nikolsky S.I., 1967, Sov. Phys. - JETP 24 535-45.
13. Ryan M.J. et al., 1972 Phys. Rev. Lett. 28, 985-8.
14. Samorski M., Dissertation, University of Kiel.
15. Vernov S.N. et al., 10th I.C.C.R., Calgary, Part A 345-396 (1967).
16. Clark G.W. et al., Phys. Rev. 122, 637-654 (1961).
17. DeBeer J.F. et al., Proc. Phys. Soc. 89, 567 (1966).
18. Jacob M. 1973 CERN Report TH-1639.

ON THE CORRELATION BETWEEN THE OPTICAL CERENKOV
PULSES AND THE RADIO PULSES FROM EXTENSIVE AIR SHOWERS

D.C. Goswami and K.M. Pathak

Department of Physics, University of Gauhati, Assam,
India.

Summary

Associated production of optical Cerenkov pulses and radio-pulses (at 30 and 44 MHz) from Extensive Air Showers (EAS) has been studied, using dipole antenna systems and an optical Cerenkov detector. Correlation between the two types of pulses has been investigated in detail. The statistical analyses indicate negative correlation between the two types of pulses.

It is surmised that the true mechanism responsible for the production of radio-pulses is predominantly the charge acceleration mechanism, although there is some small contribution from the low frequency end of Cerenkov radiation.

1. Introduction

Predictions of possibilities of emission of Cerenkov radiation¹ as well as radio-pulses² from extensive air showers (EAS) have opened new fields of study, and have attracted a good number of workers all over the world.

The optical pulses from EAS have been confirmed to be optical Cerenkov pulses due to relativistic charged particles in EAS^{3,4}. Radio pulses from EAS have also been detected at frequencies ranging from few MHz to about 550 MHz^{5,6,7,8}. There have been several theories put forward to explain the emission of radio-pulses for EAS. For instance, Askaryan⁹ showed that the normal Cerenkov radiation produced by the individual relativistic particles in an EAS was enhanced by phase coherence at the lower frequencies. According to Kahn and Lerche¹⁰, the contribution to the emission of radio frequency due to geomagnetic separation of the

charges in a shower front was greater than that from the normal Cerenkov radiation. Allan¹¹ analysed theoretically the radio-emission in an EAS due to the geomagnetic separation mechanism. Fuji and Nishimura¹² also studied theoretically the radio frequency emission in an EAS. They investigated the relative importance of Cerenkov radiation and emission due to charge acceleration from the particles in an EAS.

But it is interesting to note that in spite of intensive theoretical and experimental work, it has not been possible to date to determine unambiguously the relative roles of geomagnetic deflection and other processes in the observed radio frequency emission, or to pin point the production mechanism of the radio pulses. These findings prompted us to study the associated production of the radio pulses and the optical pulses from EAS. It is reasonable to expect that a correlation, or a lack of it, between the optical Cerenkov pulses and the radio pulses may lead to a better understanding of the production mechanism of the radio pulses. As it is now well established that the light pulses produced by EAS are due to optical Cerenkov radiation, a positive correlation between the optical and the radio pulses from EAS would lead one to conclude that the radio pulses are also due to the Cerenkov emission process, while a negative correlation between the two types of pulses would lead one to surmise that there may be some other process responsible for radio frequency emission.

For this purpose an experiment was carried out in the Gauhati University campus ($26^{\circ} 22'N$, $91^{\circ} 23'E$, and altitude $\sim 100m$) during the winters and autumns of 1972-74, mainly to study the associated production of optical Cerenkov pulses and radio pulses from EAS.

2. Experimental set up and data collection

The details of the experimental set up, procedure of collection of data, and the selection criteria were presented in a preceding paper, (submitted to Nuov. Cim.), which will hereafter be referred to as paper I.

As described in paper I, optical pulses were collected with the help of a Cerenkov detector comprising a parabolic reflector, a wide cathode, (125mm), photomultiplier tube, and the associated electronic

circuits. Radio pulses at 30 and 44 Mhz were collected by broad-side half-wave dipole arrays and a Hallicrafter VHF receiver.

3. Analyses of the data

3.1 Optical pulses

In paper I, the optical data of the present experiment were analysed in detail, and were confirmed to be optical Cerenkov pulses by comparing them with a theoretical curve generated by a primary-energy-independent general equation developed by the authors.

3.2 Radio pulses

The number of acceptable radio pulses collected at 30 and 44 Mhz were 38 and 125 respectively. Figs. 1 and 2 give the pulse height distributions of these pulses.



Figure 1. Radio pulse height distribution at 30Mhz.

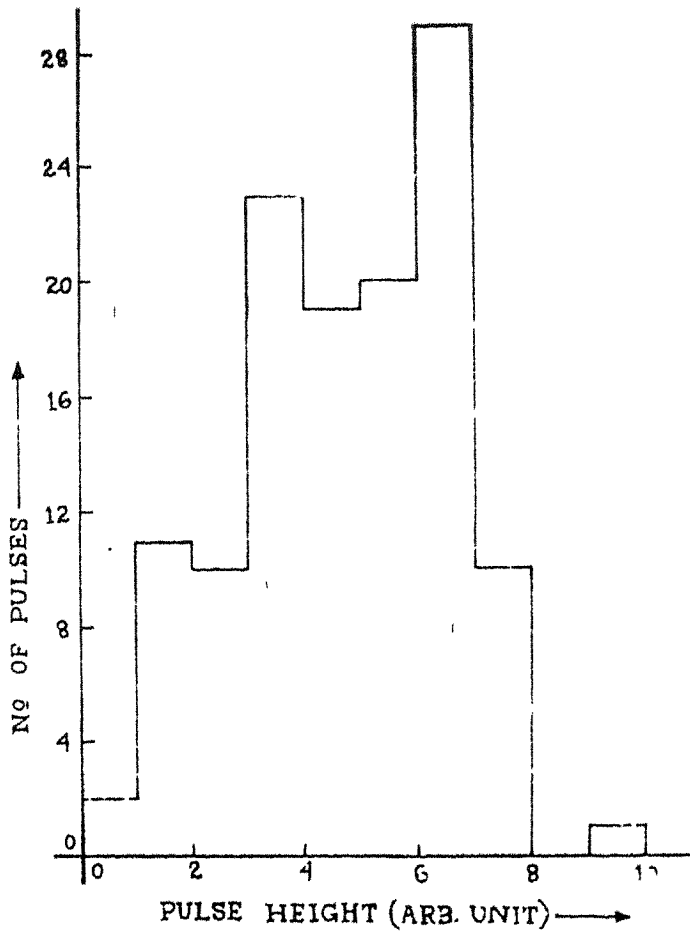


Figure 2 as Figure 1, at 44 MHz.

4. Correlation between the optical Cerenkov pulses and the radio pulses

For studying the relationship or the degree of association between the two groups of data, viz., the optical Cerenkov pulses and the radio pulses, the method of correlation has been applied using the 'product-moment' coefficient of correlation, r , given by¹³,

$$r = \frac{\Sigma xy}{\sqrt{\Sigma x^2 \times \Sigma y^2}} \dots\dots\dots (1)$$

where x and y are deviations from the actual means of the two distributions, and Σx^2 and Σy^2 are the sums of the squared deviations in x and y taken from the two means.

The coefficient of correlation is calculated by using the scattergram method, i.e. by arranging the data in the form of a diagram or chart of bivariate distribution as shown in Figs. 3, 5 and 7. The regression lines for both the pulse height distributions are also shown in Figs. 4, 6 and 8.

4.1 Correlation with 30 MHz Radio Pulses

At first a scattergram of the optical data and the simultaneously observed radio pulse data are plotted (Fig. 3). In the scattergram a 'tally' (/) is given in the appropriate square in accordance with the two characteristics, viz., the optical pulse height and the radio pulse height. Along the bottom of the diagram in the f_x row is tabulated the number of data in each radio pulse height interval; while along the right hand margin in the f_y column is tabulated the number of data in each optical pulse height interval. The frequency of each cell is also added and entered in the diagram. Thus the scattergram becomes a correlation table (Fig. 3). The correlation table is separately shown

		30MHz RADIO PULSE HEIGHTS→								f_y means	
		0.00-2.49	2.50-4.99	5.00-7.49	7.50-9.99	10.00-12.49	12.50-14.99	15.00-17.49	17.50-19.99		
OPTICAL PULSE HEIGHTS ↑	2.33-2.66	///								3	1.25
	2.00-2.33	/			/					2	6.30
	1.67-1.99	/								1	1.25
	1.34-1.66	/								1	1.25
	1.00-1.33	/								1	1.25
	0.67-0.99	///								5	1.25
	0.34-0.66	32								32	1.25
	0.00-0.33	12	//	//	/	/				18	3.10
f_x →		56	2	2	1	2					
means →		0.7	0.17	0.17	0.17	1.17					

Figure 3. Scattergram showing the paired pulse heights of the Optical Cerenkov pulses and the 30 MHz radio pulses.

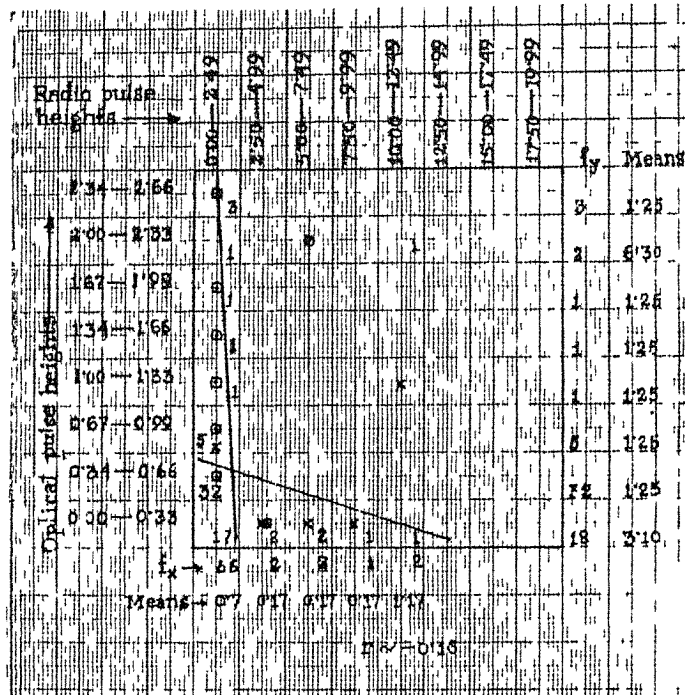


Figure 4. Correlation table for the optical Cerenkov pulse heights and the 30 MHz radio pulse heights.

on graph paper in figure 4. The means of the data in each column are then calculated and shown along the bottom. Similarly, the means of the data in each row are calculated and shown along the right hand margin. The means of the columns are then plotted graphically with small crosses and the means of the rows with small circles. Through the crosses and the circles two regression lines are drawn, giving more importance to those crosses and circles which correspond to more data.

The inclination of the regression lines from lower right to the upper left hand section of the diagram indicates that the correlation between the optical Cerenkov pulses and the 30 MHz radio pulses is negative. The product moment correlation coefficient calculated from the slope of the two lines comes out to be

$$r \approx -0.11,$$

which from the null hypothesis is not significant either at the 5% or at the 1% level, the standard significant values of r at these levels being 0.22 and 0.28 respectively.^{1,3}

The negative tendency of the degree of association between the optical and the radio pulses is depicted even when an expanded correlation table is formed with the first few cells at the bottom left hand corner of Figs. 3 and 4, where there is a greater concentration of data, as shown in Figs. 5 and 6.

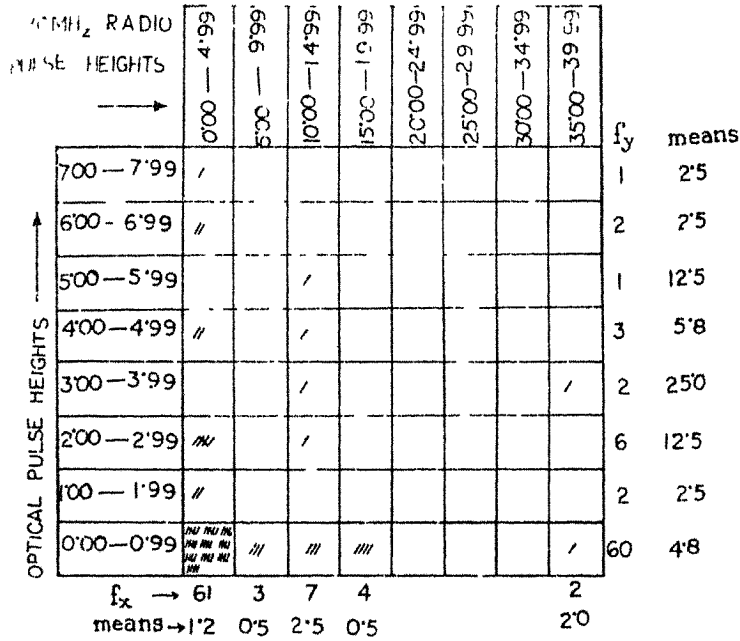


Figure 5. Extended Scattergram showing the paired pulse heights of the optical Cerenkov pulses and the 30 MHz pulses.

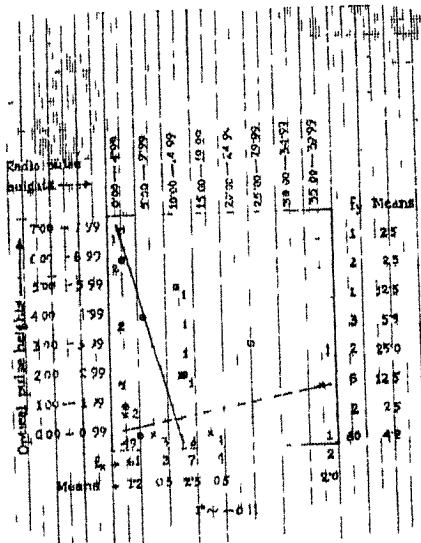


Figure 6. Correlation table for the data in Fig. 5.

4.2 Correlation with 44 Mhz Radio Pulses

In similar manner, a correlation table is formed (Figure 7.)

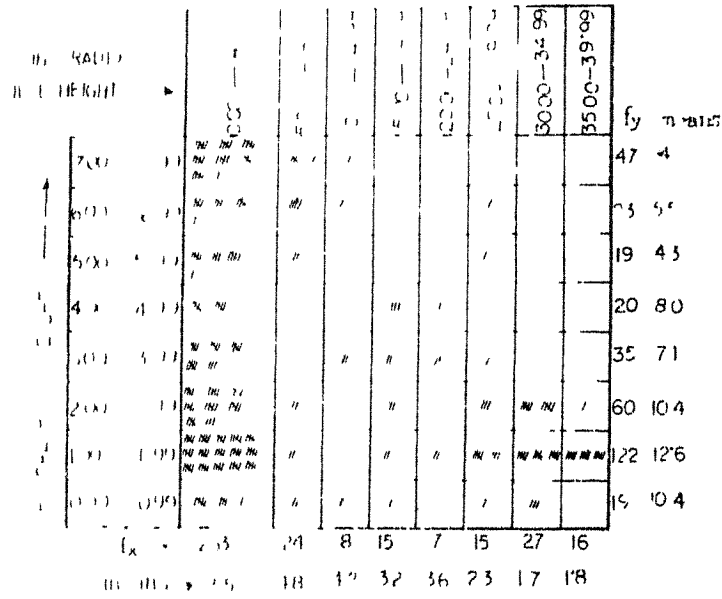


Figure 7. Scattergram showing the paired pulse heights of the optical Cerenkov pulses and the 44 Mhz radio pulses.

for the optical pulses and the simultaneously observed radio pulses at 44 Mhz. From the regression lines drawn as shown in Figure 8,

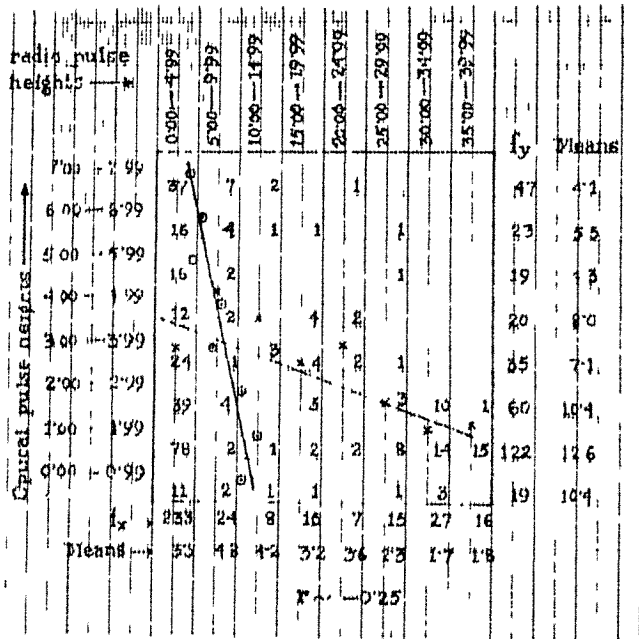


Figure 8. Correlation table for the optical Cerenkov pulse heights and the 44 Mhz radio pulse heights.

it is obvious that the correlation is negative. The coefficient of correlation is found to be

$$r \approx -0.25$$

which is significant at the 5% as well as the 1% level, the standard significant values of r at these levels being 0.098 and 0.128 respectively.¹³

5. Conclusion

Statistical analyses of the correlation between the emission of the two types of pulses i.e. radio and optical pulses, as detailed in the preceding section indicate negative correlation between the two types of pulses. The value of the product moment coefficient of correlation, r for the 30 MHz radio pulses and the simultaneously collected optical pulses is found to be ~ -0.11 , which is not significant. Again, the value of r for the 44 MHz radio pulses and the simultaneously collected optical pulses is found to be ~ -0.25 and this is a significant negative value of r .

The negativity of the product moment coefficient of correlation proves that the optical and the radio pulses have a negative degree of association, i.e., if the magnitude of one increases that of the other decreases.

The optical pulses from EAS are known for sure to be caused by Cerenkov radiation. This Cerenkov spectrum extends to the radio region also and for higher energy showers ($E > 10^{17}$ eV) the signal to noise ratio is substantial¹⁴ so as to make it detectable by broad-side antenna systems like the ones used in the present experiment. But if the radio pulses were due only to the Cerenkov mechanism, there should have been a positive correlation between the optical and the radio pulses from EAS. Because, the Cerenkov radiation loss is proportional to $\omega d\omega$, where ω is the band frequency and $d\omega$ is the bandwidth, any increase in the optical pulse height should have been accompanied by an increase in the pulse height of the corresponding radio pulses. But the results of the present experiment indicate that the correlation is negative, and that is why one will have to look towards some mechanism in addition to the Cerenkov mechanism for the emission of radio pulse from EAS.

One important point to be noted here is that although the coefficient is negative both with 30 and 44 MHz radio pulses, the negativity is less in the case of 30 MHz than with 44 MHz radio pulses. This means that the mechanism(s), whatever it (or they) might be predominate(s) over the Cerenkov contribution which is always there. This predominance is more at higher frequencies.

The above observation leads us to surmise that perhaps the true mechanism responsible for the production of radio pulses is predominantly the charge acceleration mechanism, as has been pointed out by Kahn and Lerche¹⁰ although there is some small contribution from the low frequency end of Cerenkov radiation.

In future, it may perhaps be useful to extend this work to higher radio frequencies to check the degree of predominance of the charge acceleration mechanism of emission of radio pulses over the Cerenkov mechanism.

Acknowledgements

The authors wish to thank the authorities of Gauhati University, Assam, India, for giving them laboratory facilities. They would like to thank Professor A.W. Wolfendale of Durham University, England, for his advice and valuable comments.

References

1. P.M.S. Blackett : Physical Society Gassiot Committee Report, 34 (1948).
2. P.M.S. Blackett and A.C.B. Lovell : Proc. Roy. Soc., London, Ser. A., 177, 183 (1940).
3. W. Galbraith and J.V. Jelley : J. Atmos. Terr. Phys., 6, 250 (1955).
4. N.M. Nesterova and A. Chudakov : Zh. Eksp. Teor. Fiz., 28, 384 (1955).
5. H.R. Allan : Nature, London, 225, 253 (1970).
6. H.R. Allan and J.K. Jones : Nature, 212, 129 (1966).
7. W.N. Charman : Nuo. Cim., 3, 845 (1970).
8. D.J. Fegan : Nature, 227, 156 (1970).
9. G.A. Askaryan : Sov. Phys. JETP, 14, 441 (1962).

10. F.D. Kahn and I. Lerche : Proc. Roy. Soc., A289, 206 (1966).
11. H.R. Allan : J. Atmos. Terr. Phys., 29, 1103 (1967).
12. M. Fuji and J. Nishimura : Proc. 12th Int. Conf. Cosmic Rays, Hobart, 2753.
13. H.E. Garret : Statistics in Psychology and Education, Vakils, Feffer and Simons, Bombay (1965).
14. K. Mahesh and B.N. Srivastava : Nucl. Instr. Methods, 60, 27 (1968).

STUDIES ON OPTICAL CERENKOV RADIATION IN ASSOCIATION
WITH RADIO PULSES IN EXTENSIVE AIR SHOWERS

D.C. Goswami and K.M. Pathak

Department of Physics, University of Gauhati
Assam, India.

Summary

Associated production of radio pulses and optical Cerenkov pulses from Extensive Air Showers (EAS) has been studied. In the present paper, an analysis of the optical Cerenkov pulse height distribution is given. A general equation is developed to generate the frequency distribution of the optical Cerenkov radiation from EAS assuming a direct proportionality between the pulse height and the intensity. The experimental results and the theoretical prediction are compared.

1. Introduction

The emission of light pulses by relativistic particles passing through the atmosphere was first predicted by Blackett in 1948¹. Observations of light flashes of very short duration superimposed on the background of night sky glow correlated with the passage of cosmic radiation in the atmosphere were first reported by Galbraith and Jelley in 1953². Later on they showed that these pulses did possess the properties of Cerenkov radiation^{3,4}. Theoretical works on this line are being continued in several laboratories^{5,6}.

More recently, radio pulses have also been detected from Extensive Air Showers (EAS). The possibility of emission of electromagnetic radiation at radio frequencies was first predicted theoretically by Askaryan in 1962⁷. He showed that the normal Cerenkov Radiation produced by the individual relativistic particles in an EAS was enhanced by phase coherence at the lower radio frequencies. Kahn and Lerche⁸ also studied the problem theoretically and concluded that the contribution to the emission at radio frequencies due to the geomagnetic separation of the charges was greater than that from the normal Cerenkov Radiation. Allan in 1967⁹, and Fujii and Nishimura in 1971¹⁰ also studied theoretically the radio wave emission from EAS.

In this paper data collected on the optical Cerenkov pulses are reported and their frequency distribution is shown.

2. Experimental arrangements

2.1 EAS detector.

Cosmic ray showers of energy in the energy region $> 10^{16}$ eV were detected at the rate of $\approx 4 \text{ h}^{-1}$ with an array of GM counter trays A_1 , A_2 and A_3 , (Fig.1), operated in coincidence. The master coincidence pulses were used to trigger a double beam 15 MHz oscilloscope.

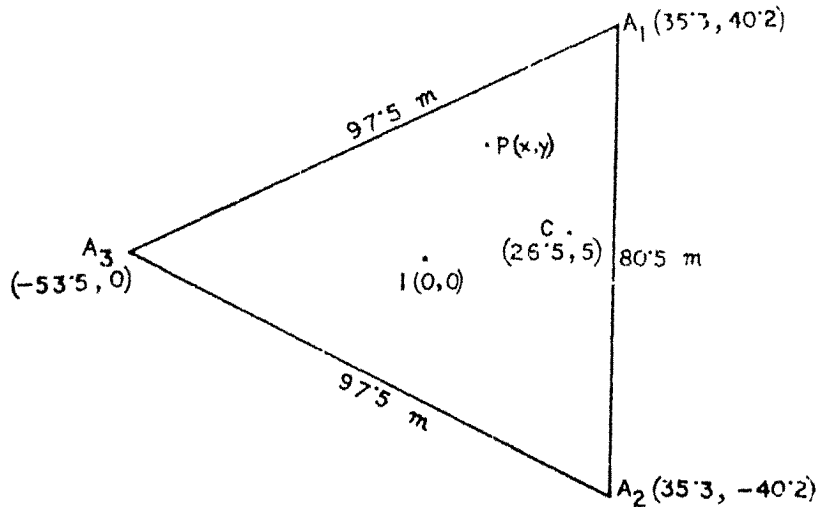


Fig.1. Geometry of the detecting system. I - circumcentre,
C - Cerenkov detector, area of each tray, $S = 0.48 \text{ m}^2$.
Co-ordinates are expressed in metres taking I as the origin.

2.2 Optical Cerenkov detector.

The optical detector used in the experiment consisted of a parabolic reflector of 76 cm diameter and 13 cm focal length pointing towards the zenith. A photomultiplier tube, (type EMI 9579 B) having a 125 mm diameter photocathode, placed at the focus received the light collected by the reflector. Although the Gauhati University campus is situated 12 Km away from the main city and the background illumination is not high, the whole system was kept inside a four-walled cell to avoid scattered light. The roof of the cell was removed and the optical detector was exposed during clear dry moonless nights when the optical experimenta was conducted. It may be pointed out here that the detector

collects light mainly from vertical showers within the cone of acceptance of the mirror system. The position of the optical detector is also shown in Fig.1.

Pulses from the photomultiplier tube, after sufficient voltage and power amplification, and after being suitably delayed (1.6 μ s), were displayed on one of the oscilloscope beams, the other beam being used for radio pulse display. The pulses were then simultaneously photographed on a fast film (ASA 400), the camera shutter being kept open during the experiment. After every triggering the film was advanced automatically.

3. Selection criteria

The following selection criteria were adopted in the analyses of the experimental results:-

i) Only those optical pulses which appeared at the particular position of the base line of the oscilloscope as were specified by the delay line were accepted as probable events.

ii) Only those pulses which had a signal to noise ratio greater than 3:1 were accepted as genuine.

4. Experimental results

The apparatus was run for 700 hours. During this time 417 acceptable optical Cerenkov pulses were observed. The pulses observed in the oscilloscope were typically of 0.5 μ s rise time (10% to 90% of peak value). Fig. 2 shows the facsimile of a typical Cerenkov pulse.

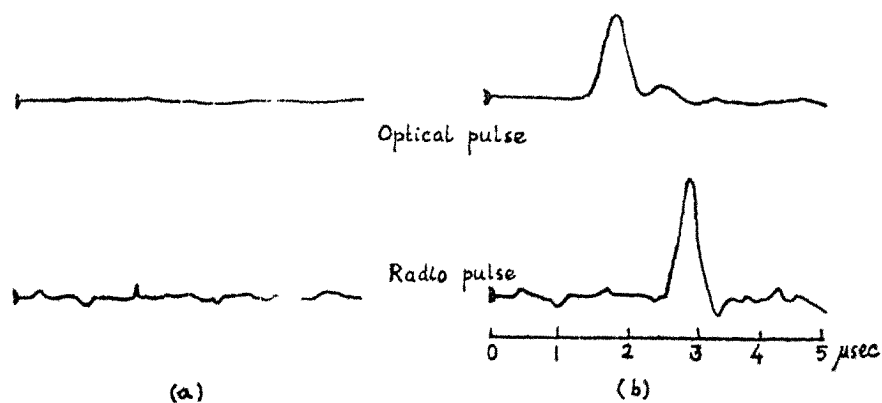


Fig.2. Facsimiles of the oscilloscope beams; (a) without and (b) with genuine pulses.

5. Theoretical pulse height distribution of optical Cerenkov pulses in EAS.

A general equation was developed to generate the frequency distribution of the optical Cerenkov pulses from EAS, as detailed below:

In an EAS detecting system like the one used in the present experiment the detection probability of a particular shower depends on the location of the shower axis and also on the primary energy. Again, for a particular position of the Cerenkov detector, the pulse height depends on the location of the axis and the energy of the primary. From these two considerations, one can eliminate the energy term and can integrate over all the locations of the shower axis, (vertical), to arrive at a relation between the number of showers, (vertical), detected and pulse heights.

Let a shower of primary energy E be incident at P(x,y) (see Fig.1) for which the densities at the detectors (trays A₁, A₂ and A₃) are Δ₁, Δ₂ and Δ₃ respectively. Then the probability that the shower is detected is given by Galbraith¹¹ as,

$$P = \prod_{i=1}^3 [1 - \exp (- \Delta_i S_i)] \dots\dots\dots(1)$$

where S_i = area of the i-th tray.

Now from the number spectrum the frequency of showers having total number of particles between N and N + dN is

$$K (N) dN = A N^{-\gamma-1} dN.$$

where¹², $\gamma = 1.53 + 0.0195 \ln (N/10^6)$
A = constant.

For showers of mean size of a few 10⁶ particles, and E ≥ 10¹⁶ eV, γ = 1.55. Therefore,

$$K (N) dN = A N^{-2.55} dN. \dots\dots\dots(2)$$

From Olbert's calculations¹³, the relation between the total number of particles at sea level and the primary energy is

$$N = 5 \times 10^{-13} E^{1.16} \dots\dots\dots(3)$$

where E is in eV.

So the frequency of EAS having primary energy between E and E + dE is,

$$n(E) dE = B E^{-2.80} dE \dots\dots\dots(4)$$

(B = constant)

The number per unit time of such showers having primary energy between E and E + dE falling on an area dx dy at (x, y) is

$$C dE dx dy = \prod_{i=1}^3 [1 - \exp (- \Delta_i S_i)] B E^{-2.80} dE dx dy \dots(5)$$

The density of particles at a distance R (metres) from the axis is

$$\Delta = N f (R) = 5 \times 10^{-13} E^{1.16} f(R) \dots\dots\dots(6)$$

where f(R) is taken,

$$f(R) = 1.75 \times 10^{-3} \frac{1}{R} \exp (- R/80)$$

$$\therefore \Delta_i = 8.75 \times 10^{-16} E^{1.16} \frac{1}{R_i} \exp (- R_i/80) \dots\dots\dots(7)$$

Again, on the assumption that the pulse height (H) is directly proportional to the intensity (I), i.e., H = KI (K = constant), and also from the theoretical calculation of Zatsepin and Chudakov¹⁴, one gets

$$I = D r^{-1} E^{+1} \quad (D = \text{Constant})$$

so that,

$$H = D_1 r^{-1} E \dots\dots\dots(8)$$

(D₁ = constant).

On eliminating E from equations (5), (7) and (8), and integrating for all positions of the shower axis, one gets

$$C(H) = \iint_{x y} \prod_{i=1}^3 [1 - \exp \{ -8.75 \times 10^{-16} (\frac{r}{D_1} \cdot H)^{1.16} \frac{1}{R_i} \exp (- \frac{R_i}{80}) S_i \}] \cdot B (\frac{r}{D_1} \cdot H)^{-2.80} \frac{r}{D_1} \cdot dH \cdot dx \cdot dy$$

or

$$C(H) = \iint_{x y} \prod_{i=1}^3 A_i [1 - \exp \{ - r^{1.16} (A_2 H)^{1.16} \frac{1}{R_i} \exp (- \frac{R_i}{80}) \}] \cdot r^{-1.80} \cdot (A_2 H)^{-2.80} dH \cdot dx \cdot dy$$

where A_1 , and A_2 are constants, and

$$R_1 = \sqrt{(x - 35.3)^2 + (y - 40.2)^2}$$

$$R_2 = \sqrt{(x - 35.3)^2 + (y + 40.2)^2}$$

$$R_3 = \sqrt{(x + 53.5)^2 + y^2}$$

$$r = \sqrt{(x - 26.5)^2 + (y - 5)^2}$$

Thus equation (9) gives the pulse height distribution where both C and H are relative.

It must be pointed out here that the approximation (rather oversimplified) that leads to equation (9) takes into account only vertical showers, and this procedure leaves a slight bias in favour of large showers.

6. Discussion and conclusions

As has been mentioned in the introduction, the ultimate aim of the present experiment was to investigate the simultaneous production of radio pulses and optical Cerenkov pulses in EAS. However, in the present paper, analysis of the optical pulses detected is chiefly undertaken.

First, the optical data collected in association with the 30 MHz and 44 MHz radio pulses are shown separately in Figs. 3 and 4. In order to compare the distribution with that predicted by equation (9), a grand pulse height distribution is drawn taking all the pulses together and is shown in Fig. 5.

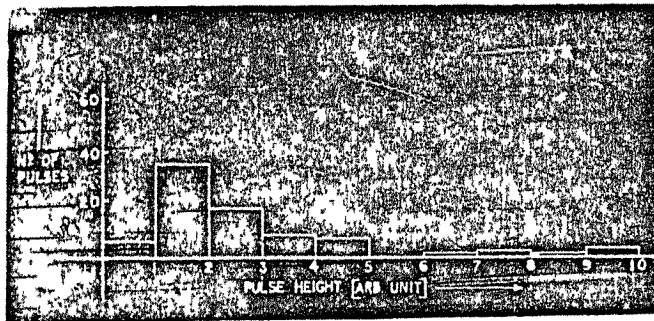


Fig.3 Pulse height distribution of optical Cerenkov pulses in association with radio pulses at 30 MHz.

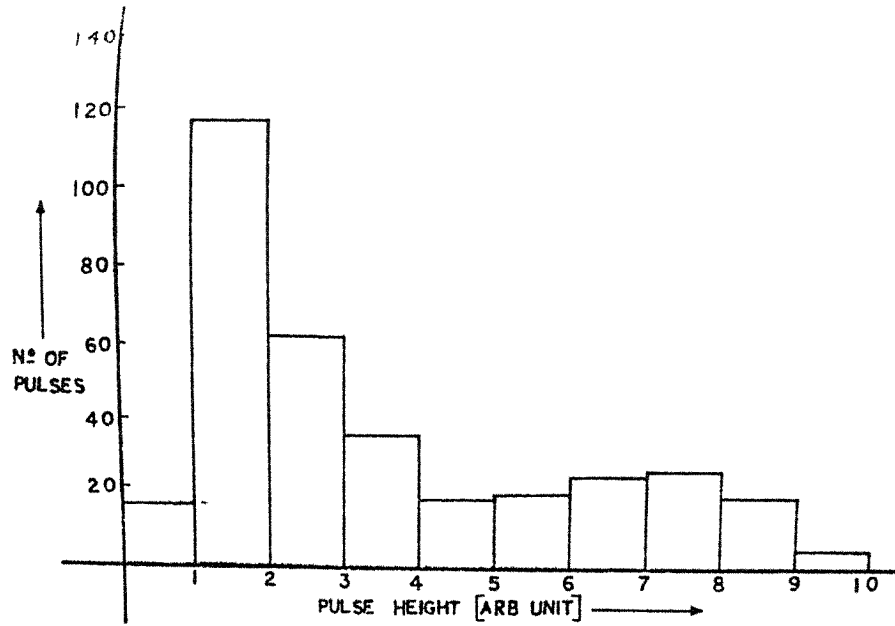


Fig.4 Pulse height distribution of optical Cerenkov pulses in association with radio pulses at 44 MHz.

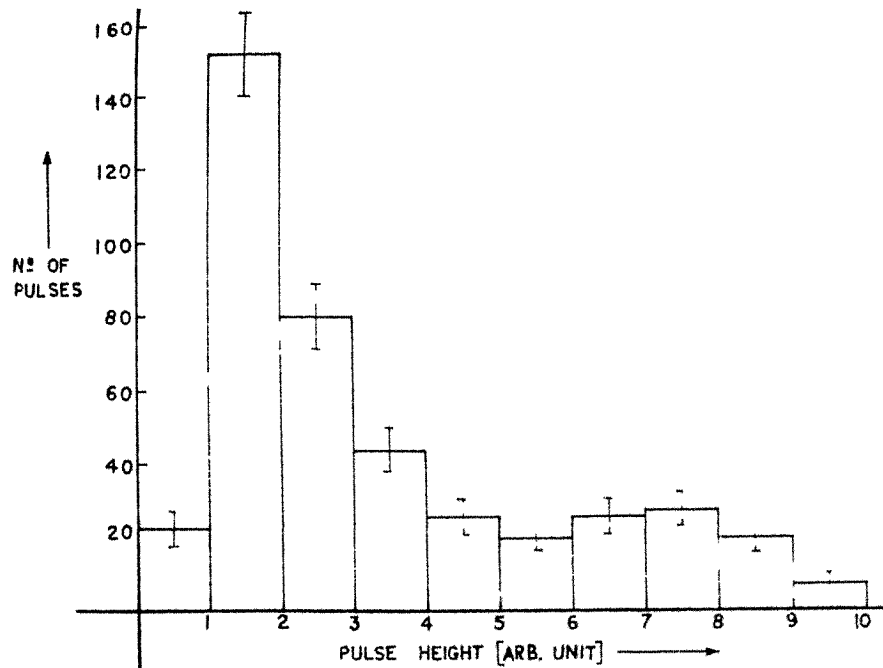


Fig.5 Pulse height distribution of all the optical Cerenkov pulses of Figs.3 and 4 taken together.

In Fig.6, a differential pulse height distribution $C(H)/H$ vs. H predicted by equation (9) is shown. Further on this graph the data of the present experiment are superimposed. Experimental data are normalised at an arbitrary point $H = 2$.

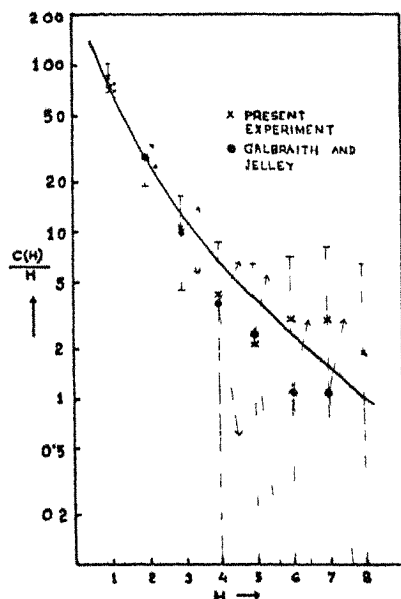


Fig.6. Differential pulse height distribution of optical Cerenkov pulses predicted by equation (9). (x) - data of the present experiment. (o) - data of Galbraith and Jelley². The experimental data are normalised at an arbitrary point, $H = 2$.

The differential pulse height distribution obtained in the present work agrees fairly well, within experimental error, with the theoretical curve. The differential frequency decreases steadily with the increase of pulse height, that is to say that the number of large pulses are fewer. An observed Cerenkov pulse is a cumulative effect of Cerenkov radiation due to individual particles in a particular shower. Thus the pulse height due to a shower is a function of the number of particles in a shower as has been deduced in the theory as well. Jelley¹⁵ also showed that the Cerenkov intensity was just proportional to the number of particles in a shower. The large pulse height therefore represents large shower, i.e., shower with high primary energy. Since the differential frequency distribution of primary energy vs. intensity shows a rapid decrease towards high energy side, the number of large showers should also fall off rapidly, and consequently, the number of large Cerenkov pulses should also fall off. This conclusion seems to be corroborated by the theoretical as well as the experimental differential pulse height distributions. On the other hand, on the low energy side the frequency of occurrence of showers being higher, the corresponding frequency of Cerenkov pulses is also higher.

These observations reasonably lead to the conclusion that the observed optical pulses are due to direct contributions from Cerenkov radiation from the particles in LAS. This conclusion can further be substantiated if the results of the present work be compared with that of Galbraith and Jelley², as in Fig.6. These workers did a similar experiment, of course, mainly to study the Cerenkov pulses from LAS, unlike the present experiment wherein Cerenkov pulses were studied along with radio pulses from EAS.

7. Acknowledgements

The authors wish to thank Professor A.W. Wolfendale and Dr. K.E. Turver of Durham University, U.K. for their encouraging advice. They are also thankful to the former for helping them with some apparatus. They would like to thank the authorities of the University of Gauhati, Assam, India, for providing them with the necessary laboratory facilities.

References

1. Blackett, P.M.S.: Physical Society Gassiot Committee Report, 34 (1948).
2. Galbraith, W. and Jelley, J.V.: Nature, 171, 349 (1953).
3. Galbraith, W. and Jelley, J.V.: J. Atmos- Terr. Phys., 6, 250 (1955).
4. Jelley, J.V. and Galbraith, W.: J. Atmos. Terr. Phys., 6, 304 (1955).
5. Fomin, Yu. A. and Khristiansen, G.B.: Sov. J. Nuc. Phys., 14, 361 (1972).
6. Smith, G.J. and Turver, K.E.: J. Phys. A., 6, L-121 (1973).
7. Askaryan, G.A.: Sov. Phys. JETP, 14, 441 (1962).
8. Kahn, F.D. and Lerche, I.: Proc. R. Soc., A 289, 206 (1966).
9. Allan, H.R.: J. Atmos. Terr. Phys., 29, 1103 (1967).
10. Fujii, M. and Nishimura, J.: 12th Int. Conf. Cosmic Rays, Hobart, 7, 2753 (1971).
11. Galbraith, G.: Extensive Air Showers, Butterworths Scientific Publications, London, p.98 (1958).
12. Greisen, K. Progr. Cosmic Ray Physics, 3, 68 (1956).
13. Olbert, as cited by G. Clark, Earl, J., Kraushaar, W., Linsley, J., Rossi, B., and Scherb, F.: Nature 180, 353 (1957).
14. Zatsepin, V.T. and Chudakov, A.E.: Sov. Phys. JETP, 15, 1126 (1962).
15. Jelley, J.V.: Proc. Int. Conf. Cosmic Rays, London, 2, 698 (1965).

CHARGE RATIO OF ELECTRONS IN EXTENSIVE AIR SHOWERS

S.W. Fong and L.K. Ng

Physics Department, University of Hong Kong,
Hong Kong.

One possible source of radio emission from extensive air showers is believed to be the negative charge excess of the showers. Measurement of the positron-electron ratio in the extensive air showers may therefore reveal the relative contribution to radio emission.

In the present experiment, a small air-gap magnet is being used to identify the positrons and electrons, the tracks of which are then located by means of a stack of spark chambers. So far, about 6000 pictures have been taken, of which about 10% give tracks with significant deflections by the magnet field.

Detailed analysis of the events shall include (a) the study of the total charge ratio, (b) the east-west effect, and (c) the dependence of the charge ratio on the average electron energy.

1. Introduction

Since the discovery of radio emission from extensive air showers by Jelley et al.^{1,2}, scientists have started extracting information from the radio signals detected and investigating the mechanisms causing the radiation. Of the many possible emission mechanism proposed, the Cerenkov radiation due to the negative charge excess as well as the dipole current and dipole moment due to separation of charge by geomagnetic field are the most probable ones⁵. In the present work, the amount of negative charge excess and the extend to which the charge are separated will be measured.

2. Theory

The average energy of each particle in a typical shower is of the order of 30 MeV, and an excess of negative charge is expected as a

result of three processes namely, annihilation of positrons with atmospheric electrons, Compton effect and δ -ray process. Theoretical calculations have been made by Guzhavin et al.³ and Fujii et al.⁴ on the negative excess due to these processes and their results are shown in Figure 1. Furthermore, shower particles travel in earth's magnetic field and a separation of the positrons and electrons is expected due to the Lorentz force $e\mathbf{v} \times \mathbf{B}$. The amount of displacement r of a charged particle depends on the energy E of that particle and is given approximately as

$$r = \frac{5000}{E} \text{ metres,}$$

with E in MeV at shower maximum⁵. Therefore the low-energy particles will be at larger distances from the shower axis spreading towards the east and the west, and the differences in the number of particles of opposite charges should be more pronounced there.

3. The shower array

Shower events are selected by the coincidence of four scintillation counters placed near the top corners of an air-conditioned room. The relative separations are shown in Figure 2. The roof of the room is made of a thin layer of wood so that absorption of particles is neglected. Each of the scintillation counters consists of a piece of plastic scintillator (50 cm x 50 cm x 5 cm) viewed by a five-inch photomultiplier tube (Du Mont 6364) from the above. The photomultiplier tube is supported by a pyramidal reflector made of thin sheets of galvanised iron coated internally with aluminium foil. Two output signals are taken from each photomultiplier tube. The negative pulses from the anode are shaped and sent to the coincidence circuits while the amplitudes of the positive pulses from the last dynode are digitised and recorded by a camera. Each digitising channel consists of a sample-and-hold amplifier, which catches the peak value of the pulse, and a ten-bit analogue-to-digital converter. The digital outputs are displayed by 7-segment LED's and photographed by a motor-driven camera. These figures then give a measure of the particle densities at the four sites of the scintillation counters. The dynamic range of each digitising unit is about 80 equivalent vertical minimum ionising particles. A block diagram of the triggering

and recording electronics is shown in Figure 4. As can be seen, no discrimination level is being set for each of the scintillation counters. This is because of the fact that low particle density is desired for good correlation between the tracks of the two pairs of spark chambers which is described in the next paragraph. The probability of chance coincidence is practically eliminated by the four-fold coincidence. Furthermore, the negative excess is expected to be more pronounced at large distances from the shower axis, where the particle density is low.

4. The positron-electron analyser

The analyser is essentially a simple air-gap magnet spectrometer. As shown in Figure 3, spark chambers are used for the particle track location. The area of the gap opened to 'vertical' particles is 30 cm x 10 cm and the length of the magnetic path is 10 cm. The field produced is about 500 gauss. The m.d.m. is estimated to be 80 MeV. Two pairs of spark chambers are placed on top and under the magnet. Their internal dimensions are 1.5 cm x 26 cm x 12 cm. The thickness of the glass plates used is 4 mm. The chamber gas is a mixture of Neon (90%) and Helium (10%) at atmospheric pressure. Thin aluminium plates of thickness 1.2 mm are used as electrodes for the application of high tension pulses delivered from a spark gap. The pulse is of amplitude 27 KV, with 0.3 μ s and rise time about 15 ns. Charged particles of suitable energy are deflected by the magnet and the deflected tracks are located by the spark chambers. This analyser is placed at the centre of the area bounded by the scintillation counters. The spark chambers are viewed by an open-shutter camera loaded with TriX film (ASA 400) and some of the tracks taken are shown in Figure 5.

5. Procedure of the measurement

The position of the shower core relative to the apparatus is determined by the four digitised amplitudes. The amplitude corresponding to a single vertical minimum-ionising particle is obtained by calibrating against single vertical muons. The particle tracks recorded are scanned using a projector. The incident direction is determined by the upper pair of spark chambers and the emerging direction, by the lower pair. The angle of deflection is measured for each event so that the momentum of the particle can be estimated. Muons are too energetic to be deflected and so will not give bias to the result.

The main objective of this experiment are divided into three parts. The first part is the study of the total charge ratio which is the ratio of the number of particles deflected by the magnet in opposite directions. The second part is the east-west effect. This provides a check on the spreading of the electrons and positrons towards the east and west and gives the extent of the spreading. Finally, the charge ratio will be found for the successive energy intervals and will be compared with the theoretical results obtained by the previous authors.^{3,4}

So far, about 6000 photographs have been taken, of which about 10% give tracks with significant deflections by the magnetic field. The experiment is still at the stage of data accumulation analysis.

6. Acknowledgement

The authors would like to thank Dr. P.K. MacKeown for the useful discussion, and the technical staff of the Physics Department, University of Hong Kong for their valuable assistance.

7. References

1. Jelley J.V., 1965, Proc. 9th IUPAP Conf. on Cosmic Rays, London, Vol. 2, 698.
2. Jelley, J.V., 1967, Progress in Elementary Particle and Cosmic Ray Physics, Vol. IX, 41.
3. Guzhavin V.V., I.P. Ivanenko and A.E. Levitin, 1968, Can. J. Phys. 46, S209.
4. Fujii M. and J. Nishimura, 1969, Proc. 11th IUPAP Conf. on Cosmic Rays, Budapest, Vol. 3, 709.
5. Allan H.R., 1971, Progress in Elementary Particle and Cosmic Ray Physics, Vol. X, 169.

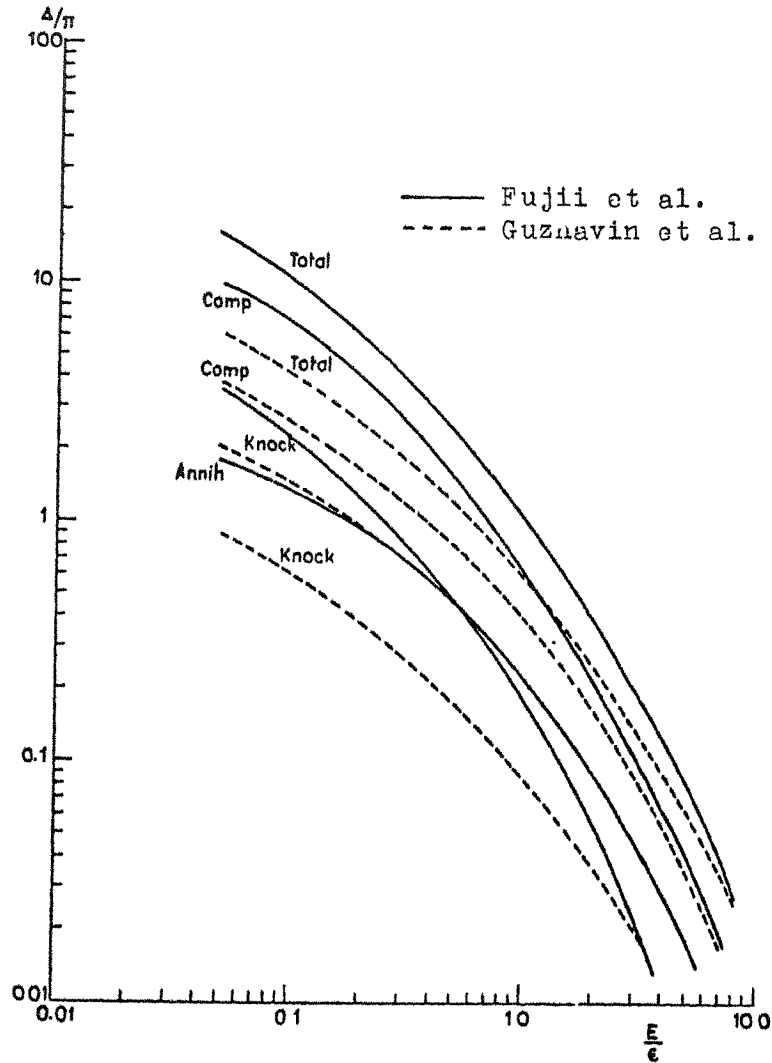


Fig. 1. Contributions to the negative charge excess from various processes. The ordinate shows the fraction of the total number of shower particles constituting the negative excess for particles with energy higher than the specified value

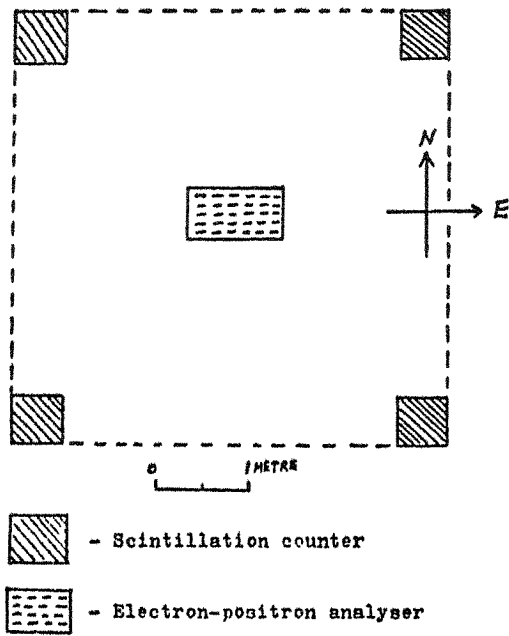


Fig 2. The shower array.(top view)

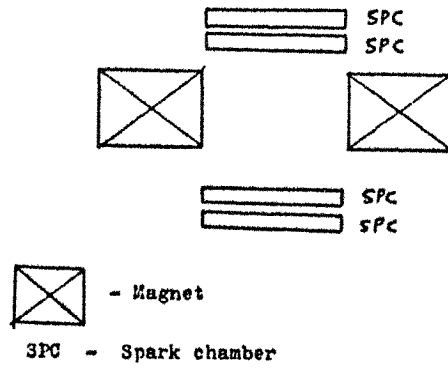
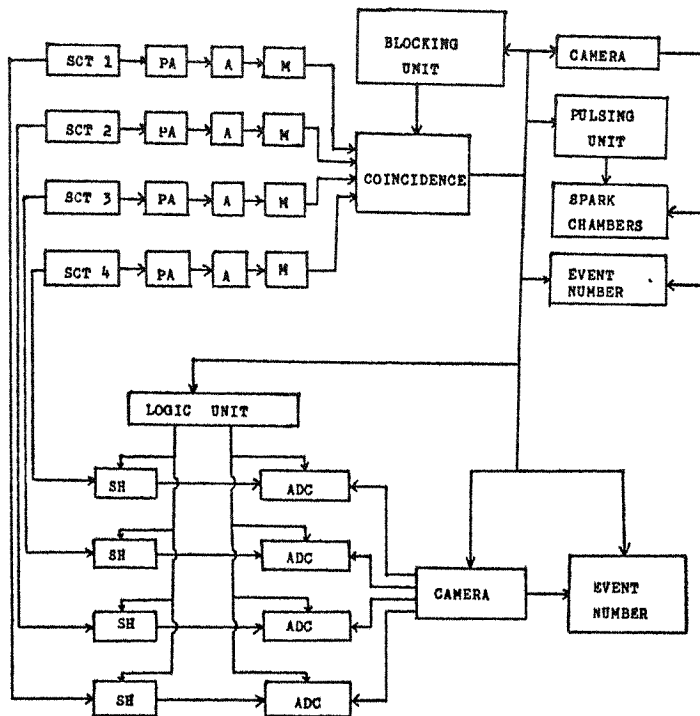


Fig 3. The electron-positron analyser.



- SCT - Scintillation counter
- PA - Pre-amplifier
- A - Main amplifier
- M - Monostable multivibrator
- SH - Sample and hold amplifier
- ADC - Analogue to digital converter with LED display

Fig 4. Block diagram of the electronics.

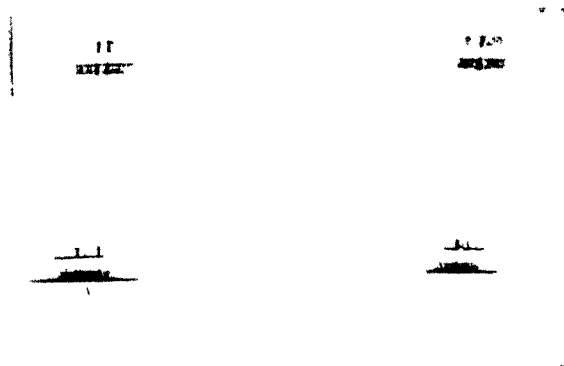


Fig.5 Shower tracks from the spark chambers. The left picture shows an electron track and a positron track, while the right picture shows an electron track.

CERENKOV AND SCINTILLATION COSMIC RAY COUNTERS DEVELOPED
IN THE PHYSICS DEPARTMENT OF THE UNIVERSITY OF
SINGAPORE

M. Huq
Department of Physics, University of Singapore

Abstract

This paper describes two cosmic ray counters developed in the Physics Department of the University of Singapore, viz:

- (A) A focussing type of Cerenkov counter using water as radiator, and
- (B) A large area non-focussing scintillation-cum-Cerenkov counter.

Both counters have been developed with simplicity and ease of construction as the guiding principles, so that small laboratories with limited workshop facilities may easily adopt them. Both the counters are suitable for cosmic ray showers with Vertical incidence, though counter (A) being of focussing type is capable of making discrimination both in energy and direction, within a somewhat limited range. Both the counters have been developed with the help of graduate students of the author. Counter (A) has been developed with the assistance of Miss Chin Sook Hong while counter (B) has been developed by Mr. Wong Sing Wan.

- (A) A focussing type of Cerenkov counter suitable for the study of the directional properties of cosmic rays.

Summary

In this counter water has been used as a simple and readily available Cerenkov radiator, though other types of denser optical media like glycerene may easily be substituted if it is desired.

To focuss the Cerenkov cone of light a parabolic mirror like the ones used in search lights was used. The mirror was placed at the bottom of a cylindrical light tight steel cylinder, painted black. These dimensions of the cylinder were chosen so that sufficient latitude was available to displace the photomultiplier both laterally and vertically to test the optimum focussing condition. The photomultiplier was mounted on a sliding plate attached in a light-tight manner to the lid of the cylindrical container (See Fig.1.).

The Detector

To investigate the performance of this detector it would be ideal to have a well-defined parallel beam of monoenergetic particles of controllable energy. As this is not available in this laboratory, we have made use of cosmic ray particles to test the performance of the detector, depending on the fact that cosmic ray intensity is maximum in the vertical direction.

The main components of the detector are a light-tight chamber, a concave mirror, a photomultiplier and its associated circuits (Fig.2). The chamber is partially filled with distilled water which is the radiator in this detector. High energy cosmic ray particles whose velocity is greater than the phase velocity of light in the radiator will, when traversing the radiator, emit Cerenkov light in the form of a solid cone which is reflected upwards and focussed into a ring by a concave mirror placed at the bottom of the Chamber. A photomultiplier is placed with its photocathode at the focal plane of the mirror such that a maximum portion of the ring focus is intercepted. The photomultiplier pulses are fed into a fast amplifier the output of which is recorded in a scaler.

At the later stage of this work an improved optical system using sectors of a mirror instead of a single mirror to reflect the Cerenkov light was designed. (Fig.6). By this system it is possible to make the whole of the ring focus of Cerenkov light fall within the area covered by the photocathode, and thus improve the efficiency of the detector greatly.

Optical Considerations of the Detector

Two parabolic mirrors, one 10.5 inch in diameter and the other 20 inch were used in two detectors of the same type but different dimensions.

In order to get an idea about the spread of the ring focus of a Cerenkov cone formed by the mirror, we simulated a ray of the cone by a narrow parallel beam of light passing through a small aperture from a galvanometer lamp, and studied how the ray was reflected by the mirror.

Taking the value of β for mu-mesons, the predominant component of cosmic ray at sea level, to be unity, the Cerenkov angle in distilled water was found to be approximately 41° . To find the spread in the Cerenkov cones generated by particles of different energies, the experiment described above was carried out with several values of the angle θ up to a maximum of 41° .

On-Axis Particles

Looking at Fig.3 we see that the focus of Cerenkov rays emitted by particles travelling along the axis and making an angle of 41° with the direction of the particle track (these rays correspond to those emitted by cosmic-ray-mu-mesons traversing the axis of the detector under consideration) is rather diffused due to astigmatism. A sharper image can be obtained if we exclude the rays striking the central portion of the mirror up to a radius of about 3.5 cm.

Off-Axis Particles

The Cerenkov cone of light is equivalent to, as far as the mirror is concerned, rays from an annular source of light at infinity. The axis of this annular source of light coincides with the track of the particle. Hence for particles travelling parallel to the axis but displaced from it by a few cm., the position of the equivalent annulus at infinity will be practically the same, and its image which corresponds to the ring focus of Cerenkov rays from off-axis particles will not be appreciably displaced from the ring focus of Cerenkov rays from on-axis particles. This was checked experimentally (compare figs. 3 and 4). Thus the lateral displacement of the particles does not affect the position of the ring focus.

Particles incident at an angle to the optic axis

There will be an angular displacement of the ring focus corresponding to the angle of incidence of the particle (in relation to the optic axis). Fig.5.illustrates the phenomena.

Energy and Angular Resolution

The calculated angular resolution is 2° , and the energy resolution is given by a spread β ($= \frac{v}{c}$)

$$\delta\beta = \pm 0.025$$

Improved Optical System

The efficiency and resolution of the system may be vastly improved by cutting the mirror into four quadrants and filling them inwards so that almost all the Cerenkov rays are focussed into a small ring within the area covered by the photomultiplier placed along the axis of the detector, (Fig.6).

Results

The detector was tested with cosmic rays, in the absence of mono-energetic charged particle beam in the laboratory. It was assumed that the cosmic-ray intensity did not vary significantly during the test period. In any case, count rates, vastly different from the usual were ignored.

First of all bias curves were obtained both with a discriminator and a single-channel pulse-height analyser, to see if the signals were well separated from the noise-level. This was done for both the single mirror and the split-mirror arrangements using a 2" and a 5" photomultiplier (Fig.7).

The discriminator was then set to exclude noise and readings were taken for vertical and horizontal transverse for both single mirrors and the split-mirror arrangement (Figs.8 to 11).

The results conclusively show that the detector is a fairly efficient cosmic ray telescope, with the split-mirror arrangement yielding greater efficiency.

The detector was then set for the optimum operating condition and cosmic ray intensity monitored for several days (Fig.12). The reader would readily agree that there is room for further improvement of the detector without getting into too much complexity.

Acknowledgements

The author would like to express his gratitude to Miss Chin Sook Hong for her invaluable assistance and the members of the staff of the Physics Department, University of Singapore for their encouragement and critical discussions.

B. A Large Area non-focussing Cerenkov-cum-liquid Scintillation Counter for Cosmic Rays

A large area (1m x 1m x 0.5m) counter was developed to detect cosmic ray showers in Singapore.

The apparatus consisted of a large steel tank (1m x 1m x 0.5m) painted white inside-topped with a tapered umbrella of aluminium also painted white inside.

A photo-multiplier (Philips 54 AVP) was placed at an opening at the apex of the umbrella.

The whole system was made light-tight and for double protection the assembly was placed in light tight wooden hut. Fig.13 shows the experimental arrangement.

When used as Cerenkov counter the tank was filled with distilled water. Several liquid scintillators were used instead of water when the system was used as a liquid scintillation detector. Some new materials like kerosene and gasoline were also tested for their scintillation properties and the relative outputs are shown in Fig.14.

With distilled water the estimated light intensity incident on the photo-cathode is $\sim 4 \times 10^2$ photons. With scintillators the light output, however was several orders higher.

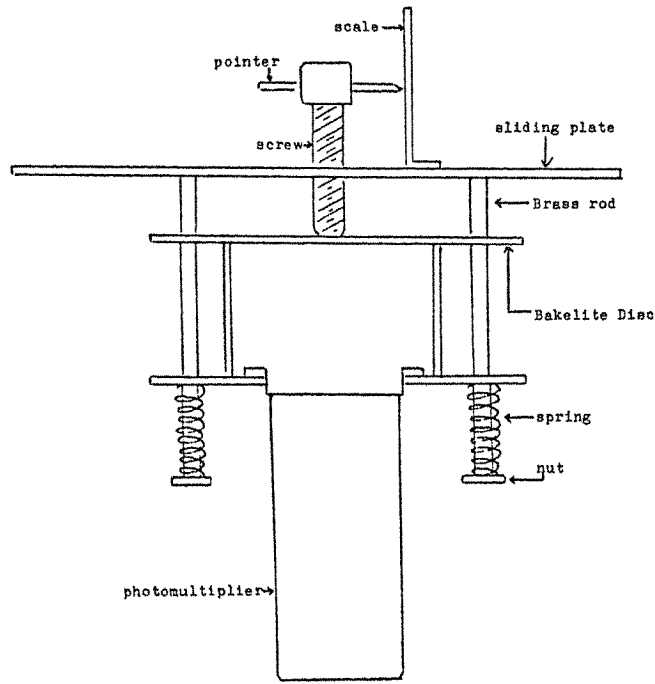


Figure 1. Section of the photomultiplier mounted on the sliding plate

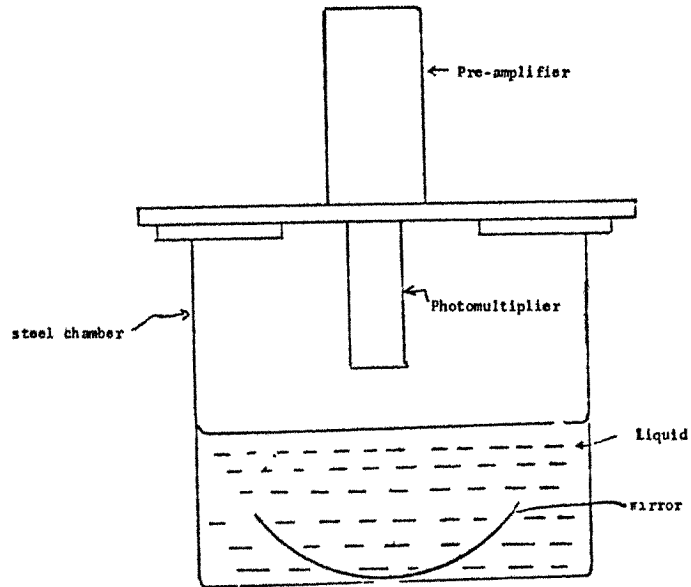


Fig. 2

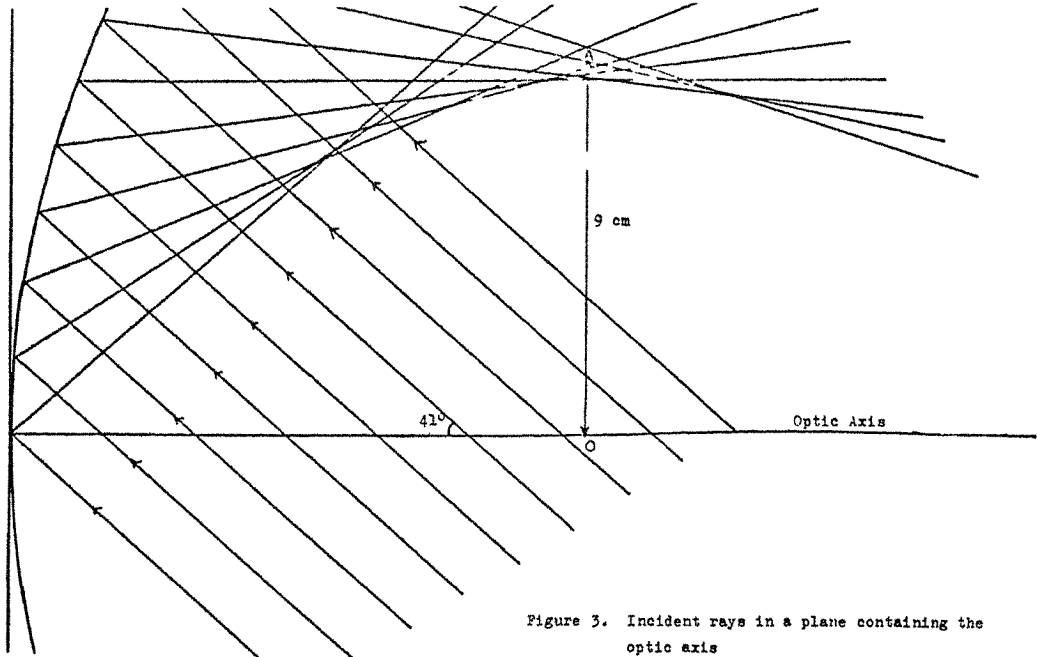


Figure 3. Incident rays in a plane containing the optic axis

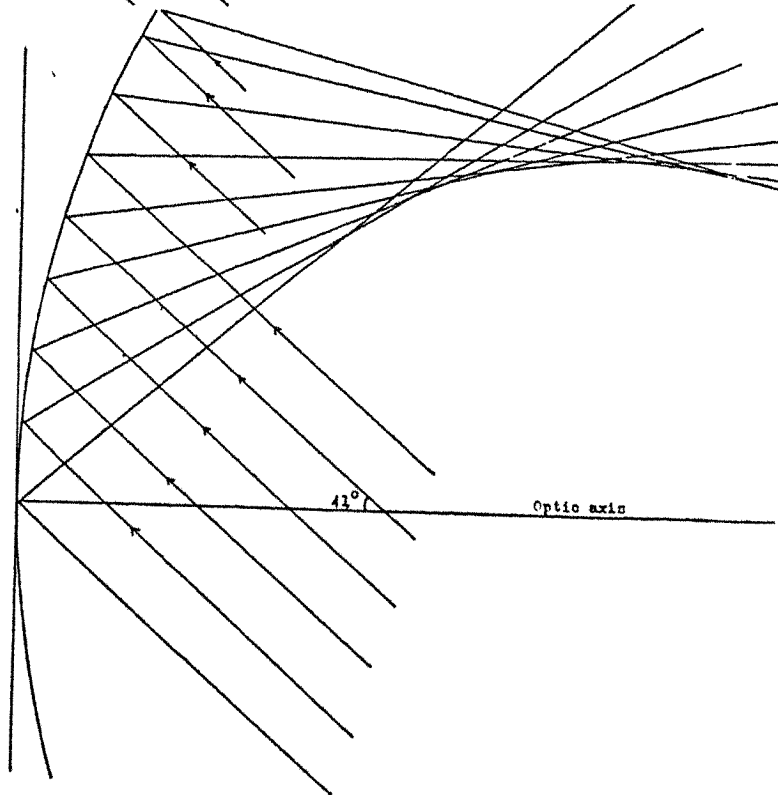


Fig. 4

Ray diagram (incident rays lie in a plane 3 cm above the optic axis)

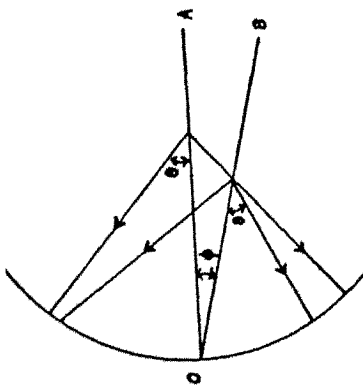


Figure 5a. Cerenkov cones generated by an on-axis particle and an off-axis particle.

Ring focus of Cerenkov rays from particles arriving at an angle ϕ_2 to the optic axis $\phi_2 > \phi_1$

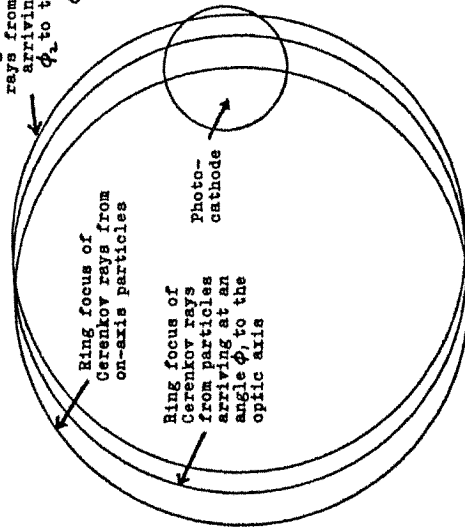


Figure 5b. Ring foci of Cerenkov rays from particles of different angles of incidence.

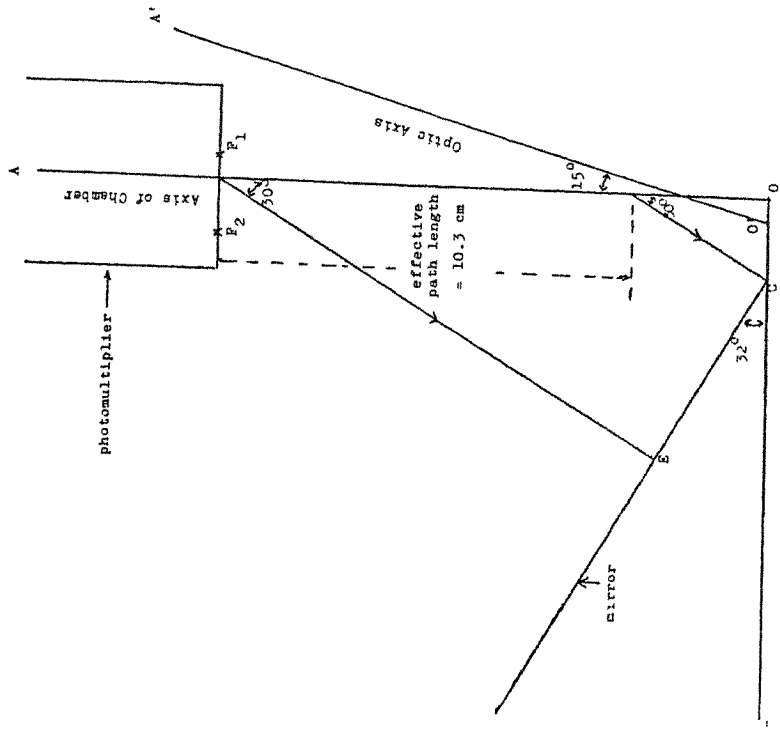


Figure 6. Improved focusing by split mirror

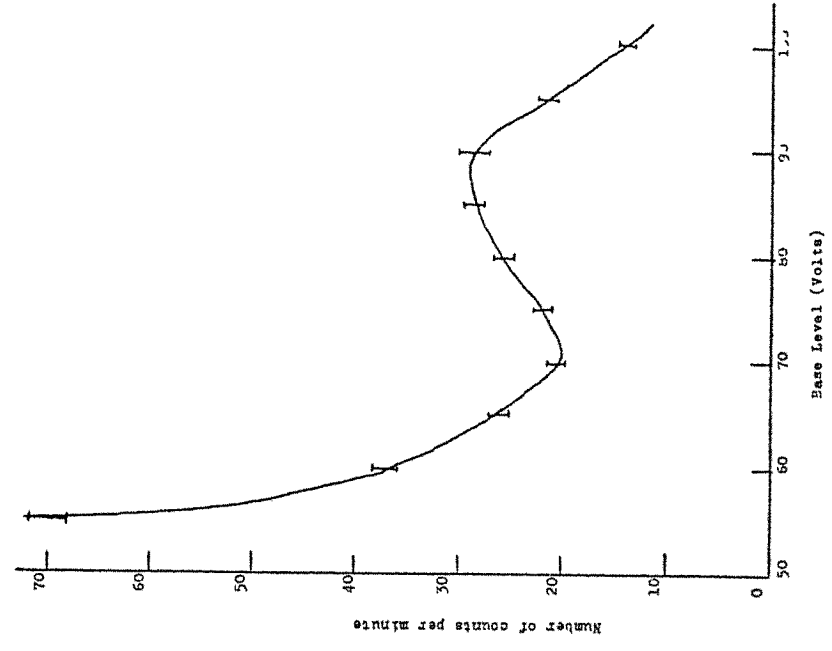


Figure 7. Bias curve (differential counting, small chamber, split mirror)

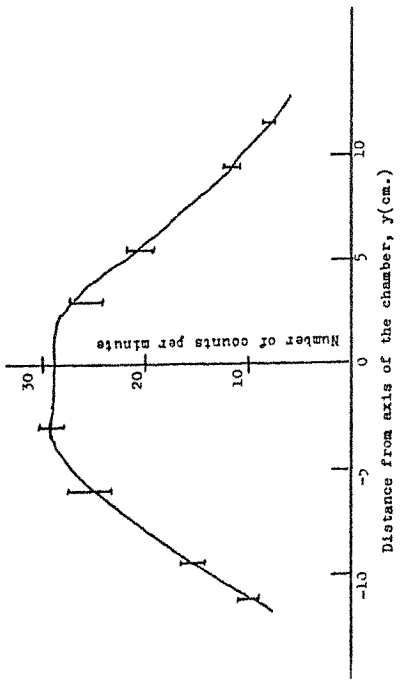


Figure 8. Horizontal traverse curve (small chamber and single mirror)

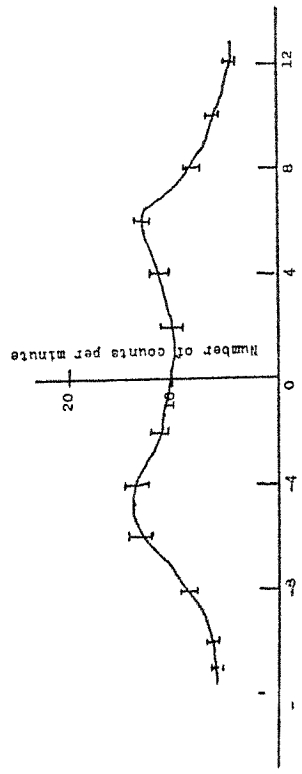


Figure 9. Horizontal traverse curve (small chamber, single mirror, plus the use of a stop)

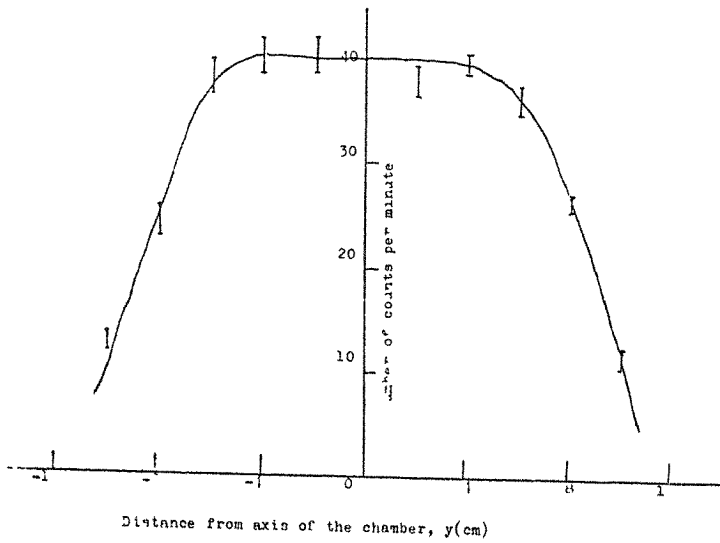


Figure 10 Horizontal traverse curve (small chamber and split mirror)

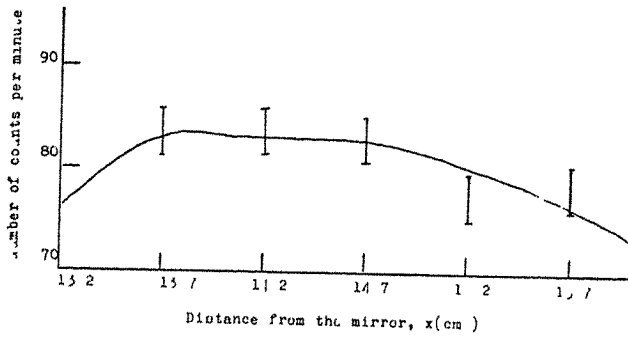


Figure 11 Vertical traverse curve (split mirror and bifurcated detector)

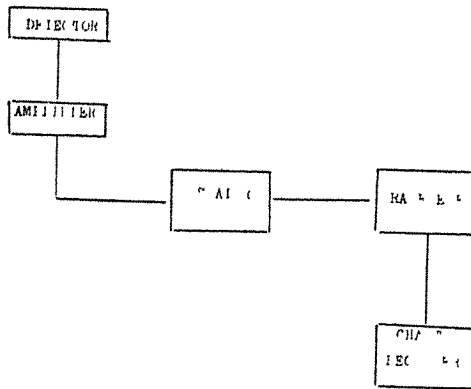


Figure 12 Block diagram (monitoring of cosmic rays)

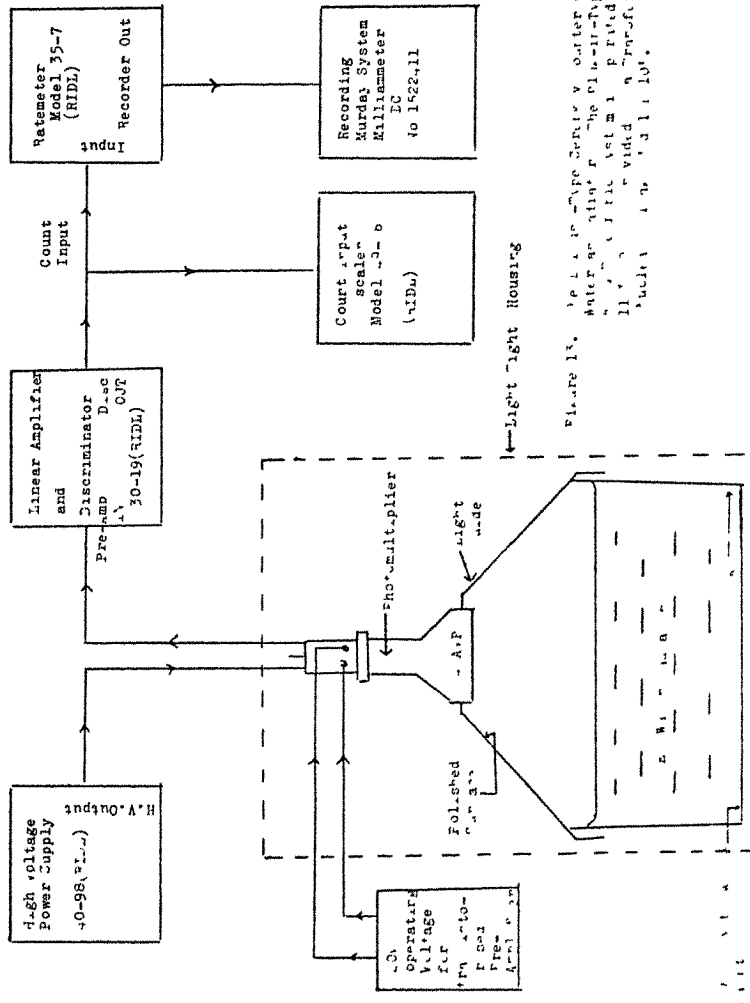


Fig. 1. Photomultiplier counter with
 discriminator for the photo-type
 scale. The scale is provided at
 the output of the photomultiplier
 Model 3-6 (RIDL).

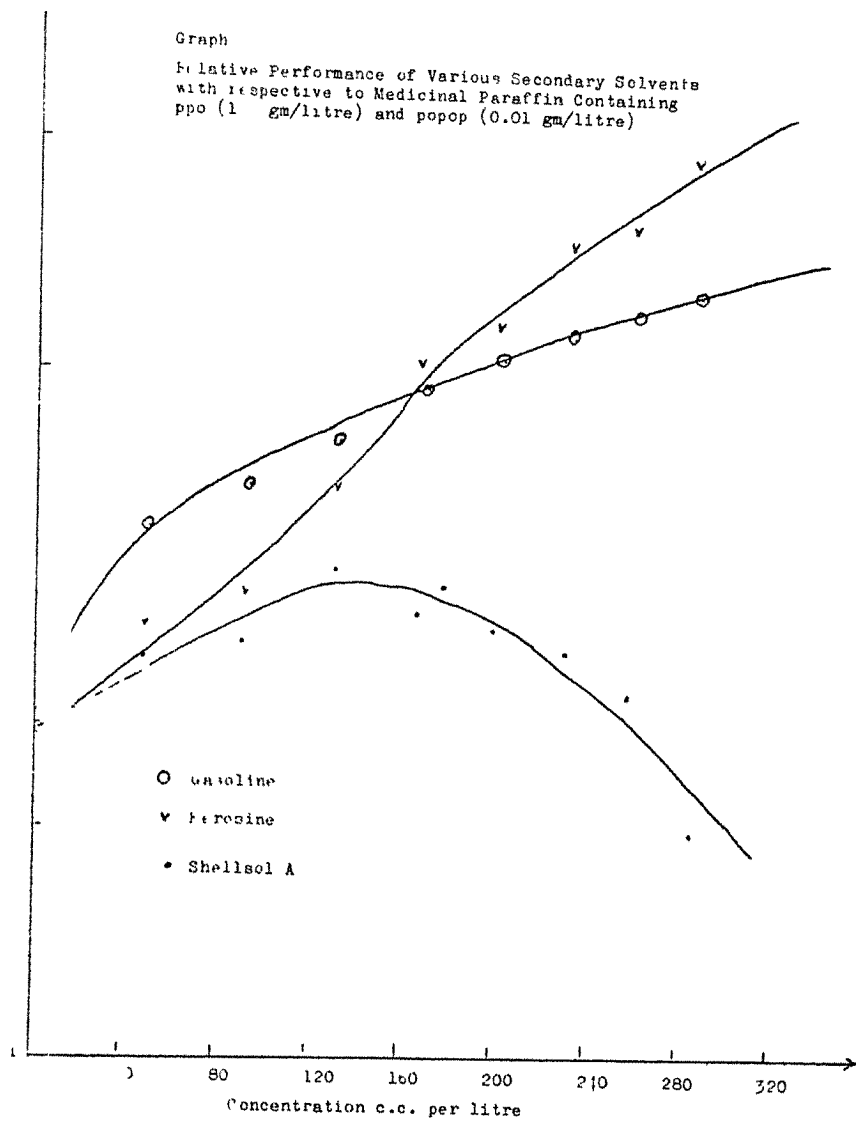


Figure 14.

Numerical Solution of Ingegro Differential
Equation

— Early Development of Cascade Shower —

Akeo Misaki and Iwao Mito*

Department of Physics, Saitama University,
Urawa, Japan

*Department of Electric Engineering,
Shibaura Institute of Technology,
Tamachi, Tokyo, Japan

Abstract

As an illustration of numerical salution of differential (and integral) eqvation, we treat the problem of cascade shower under approximation A.

Then we show that this method is powerful in clarifying an average behaviour of early development of cascade shower.

A Computer Experiment in Cosmic Rays Physics

— Monte Carlo Simulation of Cascade Shower —

Eiichi Konishi, Akeo Misake* and Gengiro Watanabe**

C/O Cosmic Ray Laboratory, University of Tokyo,
Tanashi, Tokyo, Japan

*Department of Physics, Saitama University ,
Urawa, Japan

**Department of Physics, Hirosaki University.
Hirosaki, Japan

Abstract

How to carry out a method of Monte Carlo simulation is explained in great detail.

The Akeno EAS Project

K. Kamata
Cosmic Ray Laboratory, University of Tokyo
Tanashi, Tokyo, Japan

I. Introduction

The new experimental project on extensive air showers started last year in Japan as an inter-university collaboration project. This project aims at studying the interaction characteristics of elementary particles as well as the nature of primary cosmic rays at energies 10^{14} - 10^{18} ev. This paper will describe the outline of this project.

Despite of many experimental and theoretical studies so far accumulated, we have not been able to draw a definite conclusion on EAS physics, and many subjects on super high energy physics are still remained to be done in future. On the other hand, the development of accelerators has gave us the new information on elementary particles up to about 2 Tev, and it is expected that accelerator energies will go up to 10^{14} ev within 10 years.

At the moment, the comparison of EAS data with those of accelerators tells us that the characteristics of particle interaction probably changes with energies. For example, the development of air shower through the atmosphere is hardly explained by scaling hypothesis, which then must be no more valid at EAS energies.

As to the nature of primary cosmic rays, no definite answer has not given yet to such subjects as the chemical composition, the distribution of arrival direction, and so on. Especially at energies above 10^{17} ev, the total energy spectrum has not been established as well as the unsolved question about the high energy end of cosmic ray spectrum.

Our project intends to give answer to such problems more clearly than now, trying to find the ways and means to overcome the difficulties met in the present EAS studies.

In order to clarify the complicated air shower phenomena, it is important to observe at a fixed level of observation the different components of each shower simultaneously, and to minimize option in the interpretation of observed data.

For that purpose, we are planning to build a complex shower array composed of a few hundred electron detectors, large area muon detectors, composite core detector, and air Cherenkov detectors. The details of each detector will be given in the following sections.

The construction of shower array, covering the detection area of 1 km^2 , started in January 1976 on a hill of an altitude of 900 m a.s.l. in Akeno village, about 100 km to the west of Tokyo.

2. Electron component

It seems that now the common agreement was reached in that the electron lateral distribution can not be represented by a single age parameter over the wide range of the distance from the core, but becomes flatter than NKG function at larger distance than one Moliere unit. (1) Moreover, some experiments show that the shape of lateral distribution varies with size of shower (2), though the reason of such variation is not clear now. So far we have understood that the sidewise spread of shower electron is entirely due to multiple Coulomb scattering in the atmosphere, but the development pattern of nuclear cascade and subsequent electron cascade in the atmosphere may have some effects on the lateral distribution of electrons.

Besides its own physical significance, the electron lateral distribution is important to give an electron size, the total number of electrons in a shower at an observation level, which give a rough measure of primary energy of each shower.

Together with the measurement of electron density, the measurement of arrival direction of electron has had increasing importance, because it gives an incident angle of each observed shower, front structure of electron disk, and the radius of curvature of electron front.

In general, it is needless to say that the electron component is one of the most important constituent of shower. Therefore, in our shower array, a few hundred scintillation counters of various sizes will be arranged in a lattice shape to measure the lateral distribution of shower electrons for sizes 10^4 - 10^9 .

Fig.1 shows the map of Akeno experimental site. The lattice shaped lines are the farmers roads. The road side is used to put scintillation counters and to lay cables over the entire area. The shaded area is used for the laboratory building, lodging house, other facilities, and also for the dense arrangement of electron detectors. In these area, both at central part and

at north-east part, showers of sizes less than 10^7 will be observed, while the whole area (1 km^2) will be used for the observation of shower of sizes larger than 10^7 with shower array located on road side.

With these arrangement of scintillation counters, the lateral distribution and subsequently the electron size, and the incident angle of each shower will be observed. The fast timing method will be applied to measure the incident zenith and azimuth with an accuracy of $5^0 \text{ sec } \theta$.

3. Muon component

As muons, once created, do not interact in the atmosphere, they are good probe to study the longitudinal development of showers above the observation level. Already a large number of data has been published on (a) lateral distribution, (b) size, (c) arrival time distribution, (d) fluctuation in muon density (e) zenith angle distribution, (f) momentum distribution, (g) charge ratio, and so on, of muons in EAS. Recently, an increasing attention has been paid to the characteristics of EAS muons, especially for large air showers, as it has been made clear that the muons are the powerful tool to study shower development, interaction characteristics, primary mass number, and primary energy.

Monte Carlo calculation shows that the total number of muons could give a better estimation of primary energy than electron size, as muon number suffers from less fluctuation than electron number for a fixed primary energy (3).

To get the muon number, however, it has been generally accepted that the muon lateral distribution has on the average a constant functional form (4). Recently, some experiments indicated that the lateral distribution of muons fluctuate from shower to shower, and probably varies with age parameter, of electron distribution (5). In this case, the measurement of a local muon density would not be good enough to give the muon size, and the observation of lateral distribution of muons for each shower would be necessary. The Monte Carlo simulation also shows that muon lateral distribution depends on the age of shower (3).

Besides a good measure to the primary energy, the muon number and its relation to electron number are important means to study the interaction characteristics and primary mass number at EAS energies. For example, the ratio, N_μ/N_e , is related to various parameter of interaction model, such as multiplicity, cross section,

production of nucleon pair, as well as the primary mass number (6). Furthermore, muons and its relation to electrons are interesting to study inclined shower, say with an incident angle greater than 60° . These showers are the mixture of tail of ordinary shower which should show high N_μ/N_e ratio and near-horizontal muon induced shower (7). The systematic study of these inclined shower is an interesting subject to be left in future.

The muon density is known to vary much more slowly than electrons with distance from the core, and at the distance of about 1 km from the core muon density overcomes electron density. At shorter distances, muon density is so low compared with electrons we need large shielded detector to observe muons. Near the core much thicker shielding is necessary to eliminate the contamination of energetic hadrons, and the observation of muons is limited to very high energy, scarce muons.

Accordingly, in our project, the lateral distribution of muons of each shower will be measured for showers of sizes larger than 10^7 , while muon densities at a few different distances will be observed for sizes less than 10^7 .

The arrangement of muon stations is shown in Fig. 1. There are two kinds of muon stations. One has a concrete roof of a thickness of 2 m, and energy of observed muons must be higher than 1 Gev with detector area of 25m^2 . The other has a concrete roof of a thickness of 1 m, and the detector area is 100m^2 . The structure of 1 Gev muon station is shown in Fig. 2. The detectors are arrays of proportional counters made of iron, the dimension of each counter being 10cm x 10cm x 500cm. In some stations, besides proportional counters, neon flash tubes and scintillation counters will be added.

As is shown in Fig. 1, eight 1 Gev stations and four 0.5 Gev stations will be built with mutual spacing of a few hundred meters, namely roughly equivalent to median distance of muon lateral distribution.

The 0.5 Gev stations, with 100m^2 detection area and thickness of absorber corresponding to 3 m.f.p will function as core detector when hit by energetic shower core. From the consideration of shower intensity, the cores of showers of sizes less than 10^7 will be effectively observed.

be

4. Atmospheric Cherenkov light

As Cherenkov light, once emitted by shower particles in the upper atmosphere, arrives at our observation level without suffering from serious absorption, it may give us a powerful means to study the longitudinal development of shower. The intensity of Cherenkov light is well above the background level for large showers, although the observation is limited to moonless clear night. It was pointed out that the lateral distribution of visible Cherenkov light is a function of shower maximum, and photon density at 300m from the core is a good measure of primary energy (3)(8).

The Cherenkov light is emitted by shower electrons above a certain threshold energy along shower axis continuously as shower develops through the atmosphere. Accordingly, if one can observe the time sequence of Cherenkov light, its pulse profile must directly connected to the shower curve in the atmosphere. The calculation shows that if we put an array of photomultipliers at about 2 km from the center, and record the sequential pulses with time resolution of about 100 ns, we could observe the shower curve with a depth resolution of 100 g cm^{-2} of air. Though the signal to noise ratio limit us to observe showers with energies higher than 10^{17} ev, and the expected on-time fraction is only a few percent throughout the year, it is worthwhile to carry out this observation.

In our project, such a time sequential observation of Cherenkov light will be added in future as well as the observation of total intensity of photons. The latter was already installed at the position shown in Fig. 1.

5. Data Recording and Monitoring System

The shower data (pulse height and timing data) and monitor data of all detectors are once buffered at the local substation and sent to central recording system via coaxial cables. The scanning and collection of data will be made fully automatically and all the recording system will be controlled by a computer at the center.

The shower data will then be stored in magnetic tape, and monitor data will be stored in magnetic disc, which is later used when correction of data is necessary.

6. Expected Intensity and Schedule of Construction

The expected intensity of showers to be observed by Akeno

array is estimated from the size spectrum at sea level(9) assuming that the attenuation length of electron size is 120 g cm^{-2} of air. The following table shows expected number of showers observed in the central part (shaded area in Fig.1) and the whole array, assuming that the core location of each shower can be determined within 60 % of each respective area.

size	Expected Intensities/year.gr			
	10^5	10^6	10^7	10^8
central area(dense array)	3×10^6	7×10^4	800	10
whole area(rough array)			4×10^4	500

At the moment, a part of shower array and laboratory building, lodging house, muon stations are being constructed at Akeno. The whole array will be completed in 1979. Since then, the whole project will be operated by the inter-university cooperation, and the array will be opened to those who are interested in carrying out EAS experiment.

References

- (1) N.A. Porter; Conf. Papers 13th Int. Cosmic Ray Conf, 5 3656(1973)
G.B. Khristiansen et al; Conf. Papers 14th Int. C.R. Conf. 8 2801 (1975)
T. Kaneko et al; *ibid* 8 2747 (1975)
- (2) S. Miyake et al; Conf. Papers 13th Int. C.R. Conf. 5 3220(1973)
C. Aguirre et al; *ibid* 4 2592(1973)
G.B. Khristiansen, Super High Energy Cosmic Rays, Moscow University Press, (1974) 96
- (3) H.E. Dixon et al; Proc. Roy. Soc. Lond. A339 133(1974)
- (4) For example, K. Greisen, Ann. Rev. Nucl. Sci. (1960)
- (5) S. Miyake et al; Conf. Papers 14th Int. C.R. Conf. 8 2783(1975)
G.B. Khristiansen et al; *ibid* 8 2801(1975)
T. Kaneko et al; *ibid* 12 4343(1975)
- (6) Kalmybov et al; Conf papers 13th Int. C.R. Conf. 4 2633(1973)
T.K. Gaisser et al; *ibid* 4 2652(1973)
Fishbane et al; Phys. Rev. D9 3083(1974)
- (7) M. Nagano et al; CRL Report 20 104(1976)
- (8) M.N. Dyakonov et al; Conf. Papers 13th Int. C.R. Conf. 4 2384(1973)
- (9) Data published by Tokyo, Yakutsk, Moscow and Kiel group

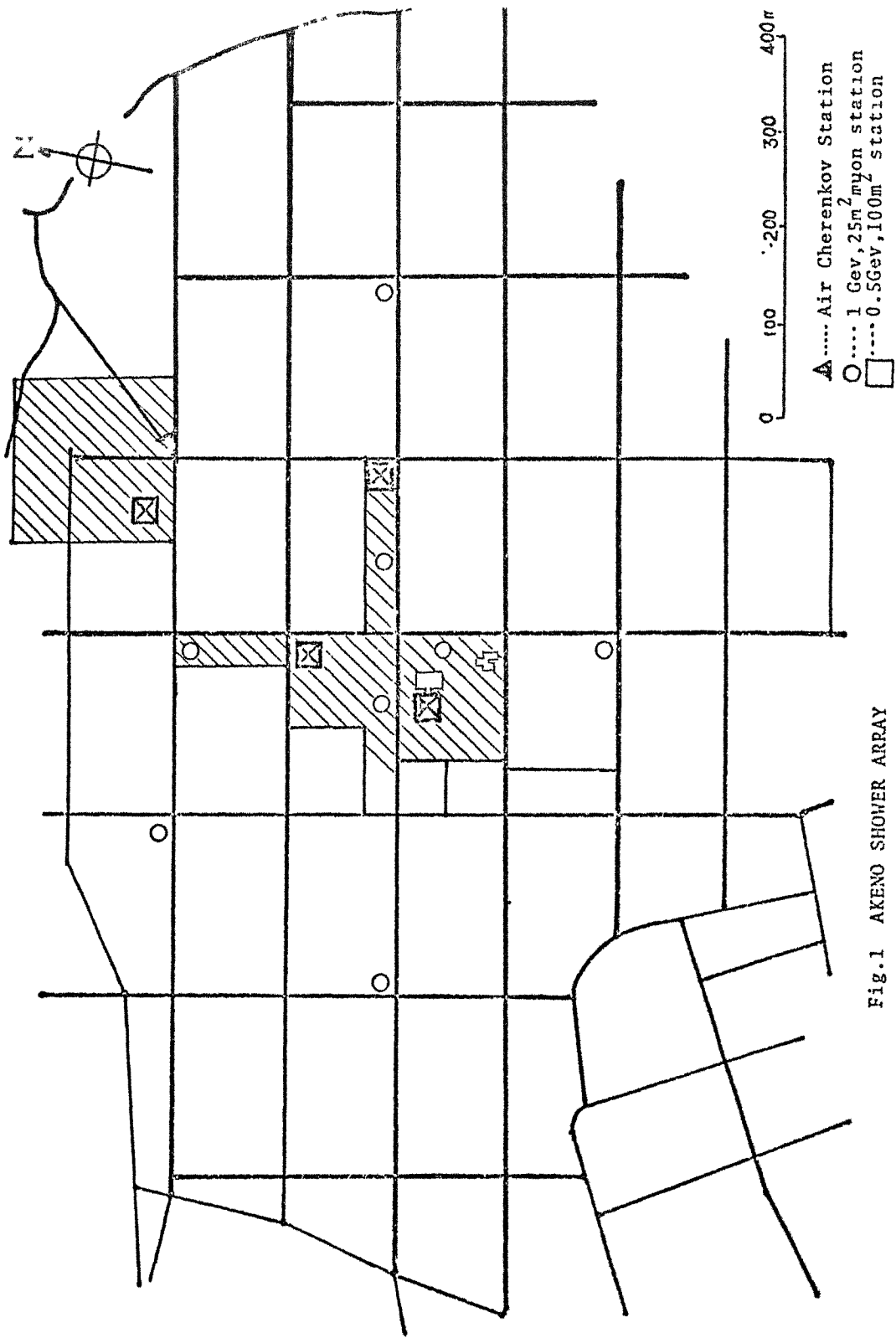


Fig. 1 AKENO SHOWER ARRAY

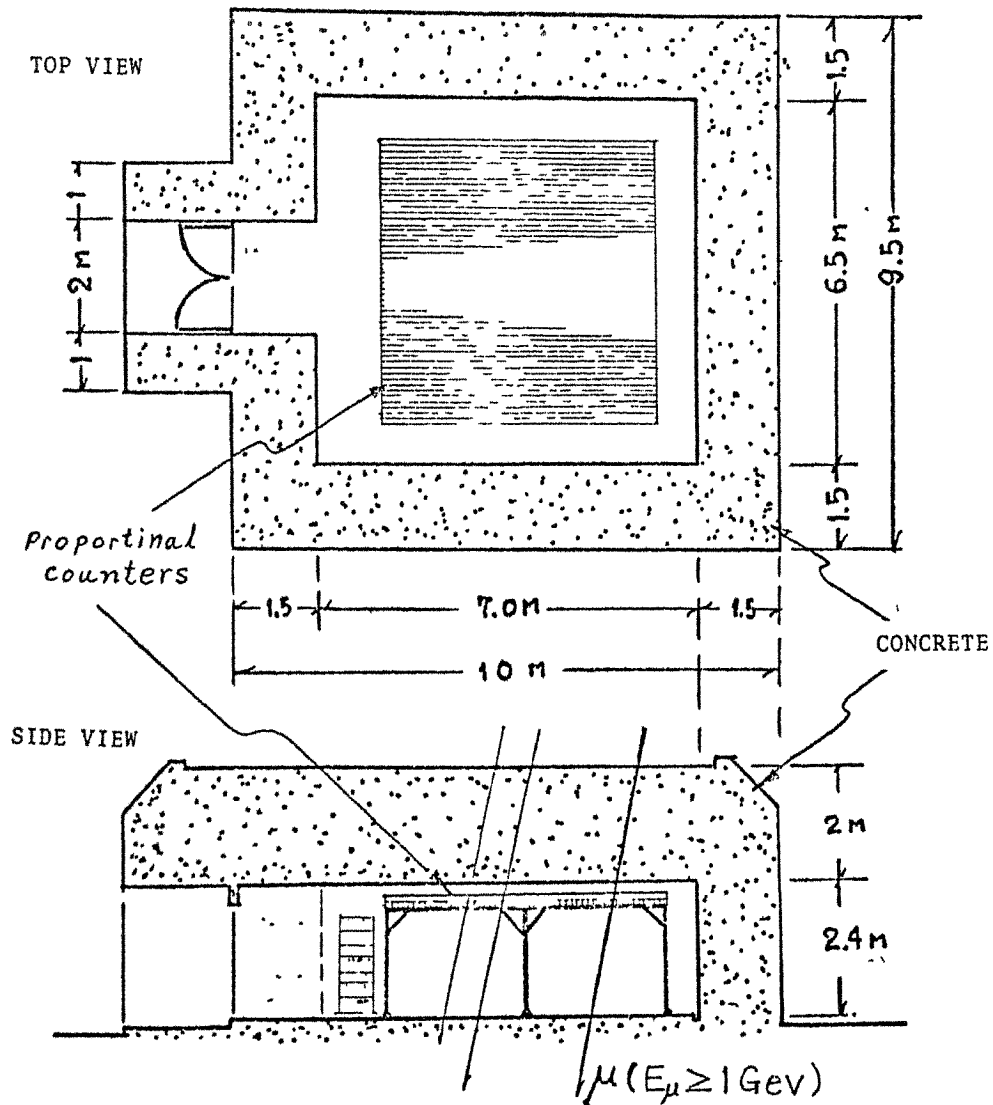


Fig.2 Structure of 1 GeV, 25m² muon station

ENERGY SPECTRA OF SPLASH ALBEDO ELECTRONS
OF COSMIC RADIATIONS

Satya Dev Verma

Department of Physics
University School of Sciences
Gujarat University
Ahmedabad 380 009
INDIA

ABSTRACT

The flux and energy of the splash albedo electrons of Cosmic Rays moving upwards in the upper atmosphere, are calculated in the 0.1 to 10,000 MeV energy interval. These are compared with the only measured flux and energy spectra of splash albedo electrons in the 10 to 1200 MeV energy interval, observed (Verma, 1967)* in a high altitude ballon experiment carried over Palestine, Texas (geomagnetic cut off 4.9 bv).

These splash albedo electrons return back due to earth's dipole field and appear as re-entrant albedo electrons moving downward in the upper atmosphere, approximately having the same flux and energy spectra. Therefore, calculations are also compared with the various observed fluxes and energy spectra of re-entrant albedo electrons. The agreement is good.

The calculated flux and energy spectra in the 0.1 to 10 MeV energy interval await experimental work for verification.

These low energy electrons will be a substantial source of the production of ionisation in the lower D-region of the ionosphere.

* Satya Dev Verma, J. Geophys. Res. 72, 915, (1967).

SECTION C

RESOURCE LETTER ON COSMIC RAY
EXPERIMENTS IN THE UNDERGRADUATE LABORATORY

K.B. Luk
Heep Yunn School, Kowloon, Hong Kong

Introduction

At the beginning of this century, cosmic rays were discovered in investigations of the residual electrical conductivity of gases. Thereafter, the subject stimulated activities in many other fields and created new ones also. This is particularly true for high energy physics and astrophysics. So far, cosmic ray researches are confined to the professional workers or well-trained graduate students. Nevertheless, many of the early cosmic ray experiments can be repeated today rather easily and inexpensively in the undergraduate laboratory. These experiments certainly will add interest to the normal physics courses and enable students to gain some experience with laboratory technique.

This Resource Letter attempts to give a short outline of the literature in secondary cosmic ray experiments which can be performed in the undergraduate laboratory. No effort is made to include references on history or theories of cosmic rays. This Resource Letter is by no means exhaustive and complete, the author should like to apologise for this.

1. Instrumentation

A. Detectors

To perform experiments using cosmic rays, it is necessary in general that the passage of a charged particle can be detected. There are many devices capable of achieving this task. The following references are concentrated on the construction of various detectors.

Cloud Chambers

A cloud chamber is a kind of visual detector, and is simple in construction. It is suitable for class demonstrations. There are two types of cloud chambers, namely, the Wilson cloud chamber and the diffusion cloud chamber. A diffusion cloud chamber can be operated continuously whereas a Wilson cloud chamber cannot.

1. Wilson Cloud Chamber. Christensen, F.E. Am. J. Phys. 18 (1950) 149. The chamber is 12-inch in diameter. The compression and expansion of the chamber is controlled by an electromagnetic valve.
2. Wilson Cloud Chamber. Sci. Am. 194 (1956, April), 156. A self-made chamber is described using two 12 oz peanut-butter jars, a coffee can, tubing and a balloon.
3. Plumber's Friend Cloud Chamber. Sci. Am. 195 (1956, Dec.), 176. The chamber is a modified Wilson cloud chamber with photographic accessory. The expansion is performed by a plunger and a lever system.
4. Wilson Cloud Chamber From Disposable Petri Dish. Johnston, T.C. Sch. Sci. Rev. 56 (1975, Mar.), 588.
5. An Advanced Laboratory Project, Construction of a Wilson Cloud Chamber. Tanner, R.L. Am. J. Phys. 26 (1958), 12.
6. Simplified Wilson Cloud Chamber. Llowarch, W. Sch. Sci. Rev. 31 (1949, Oct.) 106.
7. Diffusion Cloud Chamber. Ingalls, A.G. Sci. Am. 187 (1952, Sept.) 179.
8. Recipe for Cloud Chamber. Sci. Am. 184 (1951, Jan.), 29. A home-made diffusion cloud chamber is described.
9. Diffusion Cloud Chamber with Magnet. Sci. Am. 200 (1959, Jan.), 173. A more sophisticated set up is described. It can be employed to measure the velocity, the mass, and so on, of a charged particle.
10. Classroom Diffusion Type Cloud Chamber. Eich, A.M. Am. J. Phys. 24 (1956) 176. The sweeping field is not required for this chamber.
11. Efficient Method for Cooling a Diffusion Type Cloud Chamber. Snyder, E.S. & Heilmann, J.J. Am. J. Phys. 22 (1954) 38.
12. Diffusion Cloud Chamber with a Vacuum Jacket. Scividi, A.A. & Marn, D. Am. J. Phys. 29, (1961) 99. By means of a vacuum jacket surrounding the walls of the chamber, the effective area of observing tracks is increase.

An unusual type of cloud chamber is described in the following book:

13. Demonstrations in Modern Physics. Nokes, M.C. (Heinemann, London, 1963) 91-98. The constructions of two different projection cloud chambers are given in detail. The image of the tracks of the radiations, especially alpha particles, can be projected on a screen so as to be visible to a large audience.

Geiger Counters.

These are the commonest type of counter used in undergraduate cosmic ray experiments. The construction of a Geiger counter can be referred to the following:

14. Procedures in Experimental Physics. Strong, J. ed. (Prentice-Hall, New York, 1953). In the article 'Geiger Counters' written by H.V. Neher, the Geiger counter and the proportional counter are described in detail. The relating circuitries, probabilities and errors in Geiger counter work, voltage regulators, high-voltage sources, coincidence circuits and Geiger tubes for special uses are also given. The electronic circuits may be a little bit out of date.
15. Thin-Windowed Miniature Geiger-Müller Counter. Rae, E.R. J. Sci. Instr. 27 (1950) 143.
16. Electron and Nuclear Counters. Korff, S.A. (Van Nostrand, New York, 1955, Second Edition). Besides the Geiger counters, ionization chambers and proportional counters are also discussed. Chapter 5 on the student experiments is particularly useful, the making and filling of counters are presented. In addition, experiments on the zenith angle distribution of cosmic rays, and the absorption of cosmic ray particles are included.
17. Epoxy-Resin Seals for Geiger Müller Counter Construction. Davis, W.P. & Worthington, W.C. Am. J. Phys. 29 (1961) Apparatus Notes XV. The construction of a Geiger Müller counter sealed by Epoxy-Resin is discussed.
18. Ethyl Formate as a Quenching Agent in Geiger Müller Counter Tubes. Jenkins, R.O. J. Sci. Inst. 27 (1950) 254.
19. Bibliography of Geiger and Proportional Counters. Nucleonics. 1 (1947) Dec. 68. A selective listing of articles on the Geiger and proportional counters.

Spark Chambers.

The spark chamber is a simple and flexible device. It has a good time resolution and spatial resolution.

20. Spark Chamber for Cosmic Ray Demonstrations. Earl, J.A. Am. J. Phys. 31 (1963) 571. A small spark chamber design is given. An inexpensive electronic circuit used to trigger the spark chamber is also described.
21. Spark Chambers: A Simplified System for the Observation of Particle Trajectories in Two Types of Chambers. Sachs, A.M. Am. J. Phys. 35 (1957) 582. Excellent description on the operation and construction

of (a) multiplate (b) Curtain-discharge chamber. Included are the construction of scintillation counters, photomultiplier bases, coincidence circuit, high-voltage pulser, power supply and testing.

Scintillation Counters.

These are characterized by their efficiency, simple construction and large sharp output pulses. However, the spatial resolution is poor.

22. Scintillation Counters, Construction of. Sci. Am. 188 (1953, Mar.) 104. The design is simple and the relating electronic components are also given in detail; but may be out-dated.

Ionization Chambers and Proportional Counters.

See also reference 14, 16 and 19.

23. Ionization Chamber. Marcley, R.G. Am. J. Phys. 29 (1961) 845.
A simple parallel-plate ionization chamber of the integrating type is designed for undergraduate investigations.
24. Proportional Counter. Marcley, R.G. Am. J. Phys. 30 (1962) 60.
A cylindrical longitudinal cathod-coaxial anode proportional counter is described. Detailed information on the construction of the counter and gas handling system is given.

B. Electronic Circuitry

Nearly all modern detector systems contain electronic components as integrated elements. Apart from counting purposes, the electronic units can be used to determine the speed and/or the direction of a particle. For the design of coincidence circuits, article 14, 20, 21, 22, 28, 29, 30, 32 and 33 can also be included for reference.

25. Coincidence Circuit. Donnally, B.L. Am. J. Phys. 31 (1963) 133.
This circuit is simple, compact, reliable and cheap.
26. Scintillation Counter Preamplifier and Power Supply.
Bradley, G., Dewitt, J. and Mickle, K. Am. J. Phys. 36 (1968) 920.
The preamplifier is an integrated circuit video amplifier RCA type CA-3001, rated for a supply of +6 and -6V. The linearity is adequate for output pulses of less than 0.5V.
27. The Taylor Manual - Advanced Undergraduate Laboratory Experiments in Physics. Brown, T.B. ed. (Addison-Wesley, London, 1961) 527-534.
A coincidence circuit and methods to measure the counter dead time, to determine the counter efficiency, resolving time and chance coincidences are included. Furthermore, determination of the cosmic

ray flux, experiments on cosmic ray showers and absorption measurements using a cosmic ray telescope can also be found in this book.

28. Geiger Counter, Construction of. Sci. Am. 202 (1960, May)192. No construction is given, but the electronic circuit for a Geiger counter is drawn.

2. Experiments

Several interesting cosmic ray experiments can be performed in the laboratory by using two or three counters and a suitable coincidence circuit i.e. by means of a cosmic ray telescope. In this way, some aspects of particle physics or other effects (say, the time-dilation effect) can be studied. A few experiments are also included in references 16 and 27.

29. An Experiment on Cosmic Rays. Guest, P.G. and Simmons, W.A. Am. J. Phys. 21 (1953) 357. The apparatus is a two-counter telescope in conjunction with a Rossi-type coincidence circuit. The experiment is designed to form an introduction to the technique of coincidence counting and also to study the Poisson distribution of the rate of arrival of cosmic ray particles.
30. Integrated Circuit Counter for Cosmic Ray Experiments Gould, C.R. Am. J. Phys. 43 (1975) 918. The detection system consists of two Geiger Counters and a coincidence scaling and LED digital display circuit. This provides a good example of the use of digital electronics in a physics experiment. The telescope thus formed can be employed to demonstrate the directional intensity of cosmic rays, geomagnetic effect, long term intensity variation and the range of components of cosmic rays; using one Geiger counter, this could be used for studies of statistical distributions.
31. Design and Construction of a Cosmic-Ray Telescope for a Sophomore Modern Physics Laboratory. Zafiratos, C.D. Am. J. Phys. 35 (1967) 62. The telescope consists of 3 paddles of plastic scintillator and a triple-coincidence. The zenith angle dependence of cosmic ray intensity, the E-W effect and the attenuation coefficients of muons in various materials are investigated.

32. Cerenkov Telescope for Cosmic Rays. Rice-Evans, P. and Mishra, S.R. Am. J. Phys. 35 (1967) 357. The telescope is used to study the zenithal variation in cosmic ray intensity.
33. A Cosmic Ray Telescope used to Search for Massive and/or Fractionally Charged Particles. Alcock, C.R. et. al. Nuc. Inst. Meth. 115 (1974) 245. The telescope uses plastic scintillators, wide gap spark chambers and iron/lead absorbers. The construction, calibration and operation of the telescope are described. The set up is designed to search for stable or long-lived cosmic ray particles.
34. Electromagnetic Shower Transition Curve. Bartlett, A.A. Am. J. Phys. 23 (1955) 286. An experiment is described to observe the Rossi shower curve. The coincidences of two or three halogen-filled Geiger tubes are registered by a two-channel coincidence circuit. Theory and the procedure are mentioned.
35. Selected Topics From Cosmic Ray Physics. Rastin, B.C. Phys. Ed. 5 (1970) 349. Totally five experiments are described in detail, namely, (1) resolving time of the coincidence unit, (2) nature of the radiation at sea level, (3) geomagnetic effect, (4) shower producing particles at sea level, and (5) extensive air shower.
- The following experiments are related to the properties of muons:
36. A Simplified Muon Lifetime Experiment for the Instruction Laboratory. Hall, R.E. et al. Am. J. Phys. 38 (1970) 1196. The lifetime of the muon is measured by using a single rectangular plastic scintillator-photomultiplier system.
37. Development of Some New Experiments in Nuclear and Particle Physics. Am. J. Phys. 34 (1966) 15. The lifetime of muons is measured by a plastic scintillator coupled to a photomultiplier. The other experiment is the energy spectrum of electrons from muon decay determined by a multigap spark chamber triggered by a scintillator telescope above the chamber in anticoincidence with a scintillator below the chamber.
38. The Determination of the Muon Magnetic Moment from Cosmic Rays. Amsler, C. Am. J. Phys. 42 (1974) 1067. Principle of the experiment is given. The angular distribution of the decay positrons is measured as a function of time by using plastic scintillators.

39. Measurement of the Relativistic Time Dilation Using μ meson.
Frisch, D.H. and Smith, J.H. Am. J. Phys. 31 (1963) 342. A very detailed account of the whole experiment.
40. Special Relativity. French, A.P. (Thomas Nelson and Sons, London, 1972) 97-105. A summary of the experiment performed by D.H. Frisch and J.H. Smith in reference 39.
41. Muonium. Gillespie, E.S. Phys. Ed. 9 (1974) 34. The theory of muonium is presented and then followed by the description of the experiment, determining the lifetime of a muonium atom. The apparatus used is a system of two scintillation counters, sandwiching a chamber of argon gas.

ON THE TEACHING OF COSMIC RAY PHYSICS FOR UNDERGRADUATE
STUDENTS IN A PRIVATE UNIVERSITY IN JAPAN

Masaomi OHTA

Department of Physics, Kinki University

Higashi-Osaka, Japan 577

Some experiences using the cosmic radiation in teaching physics for undergraduate students in a private university in Japan are stated. In most universities in Japan, the textbooks of physics are usually written in Japanese. The description of cosmic ray physics in the textbooks is comparatively little.

In the Faculty of Science and Technology of Kinki University, the second year (sophomore) students are required to take the physical experiments, in which measurements of radioactivity are carried out using a G-M counter. This choice of the experiments is for the purpose of teaching the statistical treatment of data in experimental physics, in which the cosmic radiation is used as the random source instead of radioactive isotopes.

I think that the most important role of cosmic radiation as a tool in teaching physics is to offer the students a source as mentioned above. And by counter experiments students are taught the Poisson distribution, Gauss distribution, etc..

All the 4th year (senior) students can be engaged in the study for graduation under a professor's personal guidance. Fof 1976, following three items have been taken up;
I) Cosmic ray observation by proportional counters,
II) Studies on nuclear interactions in nuclear emulsion,
and III) Thermoluminescent dating.

I) Until the scintillation counters have been available, many G-M counters had been used for a long time. So we have many old G-M counters and these counters are now being changed to proportional counters by the 4th year (senior) students who chose the study of cosmic ray physics as their major. The changing processes consist of high evacuation of G-M counters and filling them with PR gas (90%Argon + 10 % Methane).

In order to teach the electronics and the detection of high energy charged particles, the measurement of ionisation loss in proportional counters (particularly multiwire-proportional counters) may be very useful. This is because the output pulse of proportional counters represents the

ionisation loss of incident particles in PR gas, and this ionisation loss increases relativistically with increasing energy of incident particles. Therefore, the pulse height distribution of proportional counters has been studied in order to investigate the applicability of gas counters for energy estimation of relativistic elementary particles (for example muons).

For practical teaching, a report of our previous research is used as the textbook. ¹⁾ The following are the outline of our teaching using our experimental data.

Fundamental characteristics of proportional counters filled with PR gas are studied and the counting rate as a function of high voltage by using cosmic rays and Cesium 137 is reproduced in Fig.1. The pulse height distribution of the proportional counters is illustrated in Fig.2. In Fig.3 the dependence of the resolution of single layer counter on the layer thickness obtained by many investigators is shown, and our data imply that for the mono-energetic cosmic rays the corrected full width at half maximum (FWHM) is expected to be 51% for the counter of 5 cm layer thickness.

Since it seems very important to improve the resolution, the use of multilayer proportional counters are tested.

The distribution of pulse height of 46 cosmic ray muons is presented in the bottom histogram(d) in Fig.4. From this, it may be said that in the case of 3 layers of 5 cm thickness counters the experimental FWHM becomes 37%.

To reduce the fluctuation of energy loss, we should increase the number of counters. So that the MONTE CARLO simulation is done on the assumption that the pulse height distribution of each counter is similar to the bottom histogram(d). The expected distribution width of mean pulse height thus calculated are shown in Fig.5. Here, N_0 is the number of proportional counters and N is the number of counters used to calculate the mean values. Therefore, N/N_0 represents the ratio of number of small pulses adopted to the calculation of the mean values among N_0 pulses. And from the same calculation, we obtain the relation between the pulse height resolution and number of layers of counters, which is illustrated in Fig.6.

Finally, the expected separation of momentum by ionisation measurements in the region of relativistic rise with 60 layers of 5 cm thickness proportional counters is shown in Fig.7.

My opinion is that the MONTE CARLO calculation is one of the most suitable research method for the graduate students, particularly in the private university with limited financial and manpower resources.

II) The second item is concerning the nuclear emulsions. I have engaged myself in the investigation of nuclear emulsions exposed to cosmic radiation, so that there are 4 binocular microscopes for the study of cosmic radiation. But they are now used to scan and analyse nuclear interactions

induced by high energy protons and muons produced in accelerators.

This year, we are investigating the Ilford K-5 emulsions exposed to 400 GeV proton beam in Fermi National Accelerator Laboratory. The scanning along the tracks is being carried out.

By accelerators so many high energy particles are produced that the role of cosmic rays as a tool for studying the elementary particle physics seems to be replaced by the particles artificially produced.

III) When cosmic rays enter the earth's atmosphere, high energy neutrons are produced. These neutrons, slowed down by collision processes, are highly effective in transmuting atmospheric nitrogen into carbon-14 (radiocarbon).

Because its chemical properties are the same as those of stable carbon, Libby hypothesized that carbon-14 should form carbon dioxide molecules, which mix in with the ordinary carbon dioxide of the atmosphere. In 1947, Libby confirmed the existence of natural carbon-14 in the atmosphere. Plant-life grows by photosynthesis of atmospheric carbon dioxide and in turn animals eat plants; consequently all the living animal and vegetable world should be very weakly radioactive owing to the presence of a small proportion of carbon-14. After the death of the living things, the carbon 14 in the dead body decay at a rate of the isotope carbon-14 and independent of all external conditions, this ratio is 1% per 83 years, equivalent to a half-life 5730 years.

This fact is well known and is used for "Radiocarbon dating". Cosmic ray group of Institute for Nuclear Study, University of Tokyo found that the intensity of cosmic rays, precisely the production rate of carbon-14, has shown small variation during last 2000 years.²⁾ If the intensity of the geomagnetism changes, the intensity of cosmic rays and, hence, the quantity of carbon-14 should change. The change of the geomagnetism during last 2000 years has already been confirmed by the measurements of archaeomagnetism in the laboratory of Prof. Thelie in France and of Prof. Nagata in Japan.³⁾

Japanese archaeologists studied the Jomon pottery and estimated the early period of this Jomon pottery to be 7000 to 8000 years old by constructing the transition history of types of pottery on the relative age axis. However, since the radiocarbon dating measurement gave the date of Natsushima shell mound to be more than 9000 years old, some objections have been proposed by Japanese archaeologists against the methods of dating and the hypotheses used.

Contrary to the situation with radiocarbon, the thermoluminescent signal increases with age of sample, ancient pottery. Therefore, the comparison of the two data from radiocarbon and thermoluminescence may be quite important. Important differences are that the relevant radioisotopes are long-lived natural impurities in clay and soil, and that

any effect due to variation of cosmic ray intensity is insignificant.

A student has constructed the apparatus for thermoluminescent dating referring to the textbook written by Aitken.⁴⁾

Stimulating discussions with Dr.K.Tsuji are gratefully acknowledged.

REFERENCES

- 1) K.Tsuji and M.Ohta; Journal of the Faculty of Science and Technology, Kinki University. 11 (1976) 315
- 2) S.Hayakawa; Cosmic Ray Physics (Wiley-Interscience) (1969)
- 3) T.Nagata et al., Journal of Geophysical Research, 68 (1963) 5277.
- 4) M.J.Aitken, Physics and Archaeology. (Clarendon press Oxford 1974)

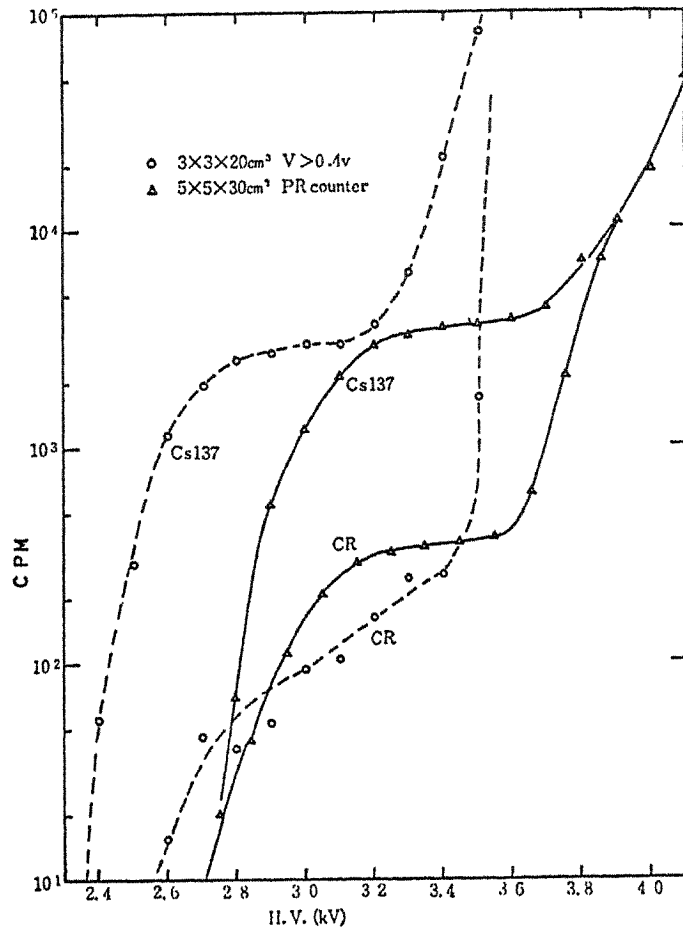


Fig. 1 Counting rate as a function of high voltage.
 Cosmic-ray muons and Cs 137 source are used.

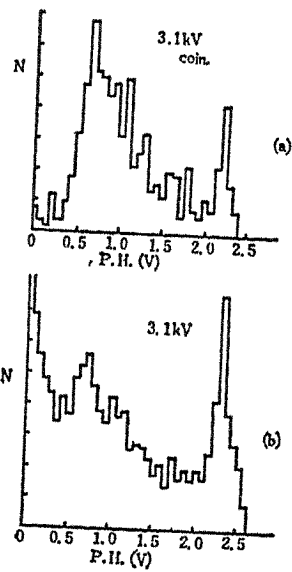


Fig. 2 Pulse height distribution of the proportional counter.
 (a) coincidence with an identical counter,
 (b) coincidence method is not used.

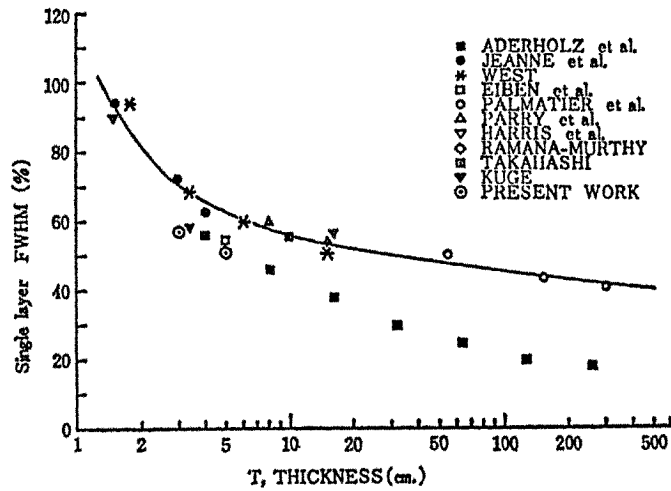


Fig. 3 Distribution width of ionization losses in a proportional counter as a function of the layer thickness.

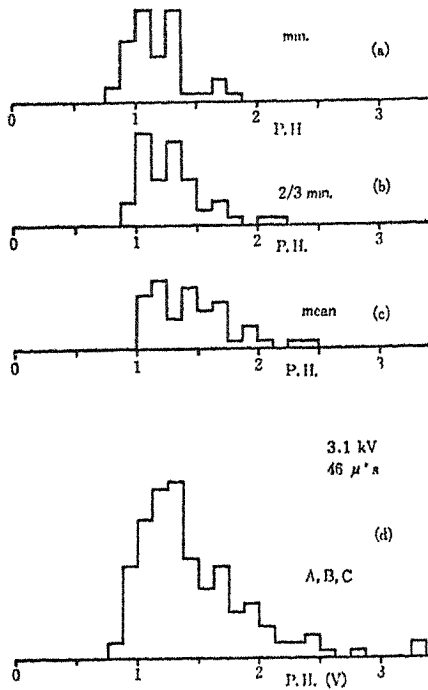


Fig. 4 Distributions of (a) minimum pulse heights among three counter pulses, (b) mean pulse heights of two smallest pulses, (c) mean pulse heights of three pulses, (d) pulse heights of each counter itself

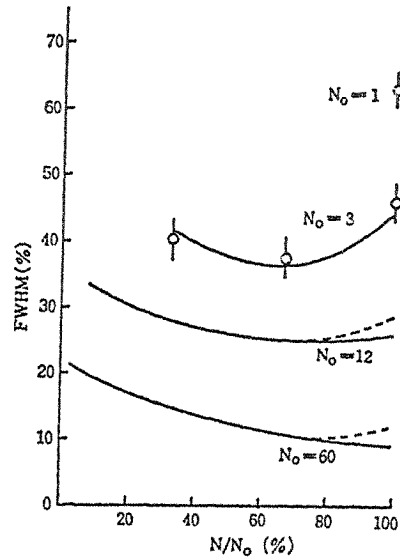


Fig. 5 Expected distribution width of mean pulse heights as a function of the percentage of values taken for the mean, and the experimental values.

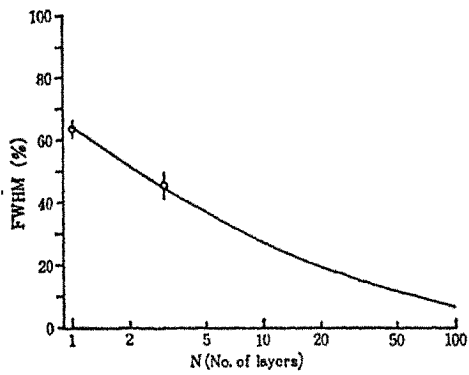


Fig. 6 Pulse-height resolution versus number of layers of proportional counters.

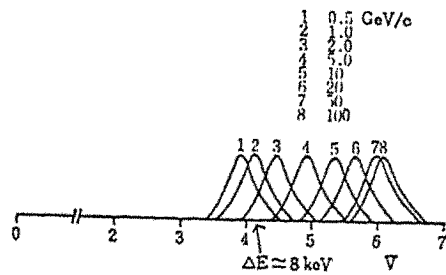


Fig. 7 Separation of momentum by ionization measurements in the region of the relativistic rise with 60 layers of 5 cm proportional counters.

UP DATING A RESEARCH LABORATORY FOR SOCIAL DEMAND
(A case in Nuclear Sciences)

L.S. Chuang
Department of Physics
The Chinese University of Hong Kong
Hong Kong

ABSTRACT

Social demand for a direct contribution from efforts in modern university research, especially in the natural sciences, calls for the change of research attitude from that based on traditional concepts to the modern one of study for society's sake.

As modern academic workers in Hong Kong, a scientifically remote and isolated commercial community, we have to be more practical in our research work. Careful selection of our research topics, collaboration with other groups and institutions are essential in order to solve some of the difficulties involved in researching in Hong Kong, in particular the problems of shortage of finance and manpower.

Illustrative examples for the justification of research in the modern society, are presented from our own experience in the field in nuclear sciences.

As the economy retreats, as a result of the oil crisis, in the industrial nations and those nations without natural resources, the luxury of study for the sake of study in the fields of natural sciences has been taken away. We have been forced to steer ourselves toward the attitude of study, especially in research, for the sake of the betterment of the society and human well-being. This tendency may continue for some time until the societies resume their economic power and are able to provide the money for research which can aim at a less practical goal; ideas. The adjustment may seem, in the initial stages, unscholarly in terms of the traditional concepts of the role of the university teacher and researcher. But, then, the traditional concept too was formed in the past through social demands and experiences. Therefore, it is reasonable for a modern university teacher or researcher to be practical, in the sense that his work has to be directly connected to the problems of human society. It should be noted, to avoid misunderstanding, that to be practical does not imply to stop working on the fundamental problems which are essential for the generation of these new ideas from which betterments of the society can be effectively developed. It is only a question of balancing the efforts, and it is generally understood that only a few of us can contribute to the generation of creative ideas.

Unfortunately, most of us in the universities in Hong Kong feel it difficult to count ourselves among the few who

can contribute to the generation of creative ideas. Realizing the difficulty of being a creative scientist in Hong Kong, a scientifically remote and isolated commercial community, I have, since the late sixties, been trying to become a practical scientist. Although the case, which I will be presenting below, may not be considered as a general or even a successful one, nevertheless, I think it is one way in which we can justify ourselves as academic workers in modern society. I wish to emphasize, with the illustration, the importance of finding research topics suitable for the social environment to which we are responsible, as well as the important roles played by collaboration and exchanges among groups in order to carry out research with a limited financial and manpower supply.

In my research group, besides myself, there are usually a full-time technician, a part-time technician-in-training, one to two graduate students who are working toward their M.Phil. degree and two to three fourth year undergraduate students who are working on their projects. Other associates are from the other groups engaged in the collaborative research projects. There are five fields of my own interest in nuclear sciences namely, cosmic ray, neutron activation analysis, neutron dosimetry and spectrometry, nuclear spectroscopy and Mössbauer spectrometry. As the years passed, we accumulated a few fundamental pieces of equipment essential for a research laboratory in the mentioned fields of our interests. Among them, the following equipment was obtained through the University grants:

a 400 channel pulse height analyzer, a liquid-scintillator incorporated with a pulse-shape analyzer system, a 1024 channel pulse height analyzer, a few coinc-anti-coinc. circuits, single channel pulse height analyzers, scalars, timers, an Am-Be neutron source (2.5×10^6 n/s), some reference radioactive sources, a Cary Vibrating Reed Electrometer with a Beckman five-inch recorder, and various types of radiation detectors and surveymeters. In response to our request, The International Atomic Energy Agency in Vienna has provided us with a 14 MeV neutron generator and a complete set of Ge(Li) gamma-ray spectrometer under its 1972 and 1975 regular programme of Technical Assistance. Under a research collaboration scheme between our laboratory and the Cosmic Ray Laboratory of The Institute of Physical and Chemical Research in Tokyo, a Nishina-type cosmic-ray ionization chamber and two plastic scintillators were loaned to us. It should be noted here that an elaborate iron shielding for the Ge(Li) detector was given to us through the kindness of the Island Navigation Corp. Ltd. in Hong Kong.

In the following, I will try to give a brief survey of the present status of the projects in the mentioned areas:

1. Cosmic Ray: Since 1969, in collaboration with the Cosmic Ray Laboratory of The Institute of Physical and Chemical Research in Tokyo, we have set up a cosmic-ray station which is equipped with a Nishina type ionization chamber incorporated with the Cary vibrating reed electrometer-Beckman five inch recorder system (ref. "Ground-Based

Cosmic-Ray Instrumentation Catalog", M.A. Shea, AFCRL-72-0411, 1972, Air Force Survey in Geophysics, No. 243, Air Force Systems Command, United States Air Force, Page 111). Routine measurement of the cosmic-ray intensity in Hong Kong has since been in operation. The data, after computer processing, have been supplied to the World Data Center for Cosmic Rays.

Other cosmic-ray research using the plastic scintillators, a muon telescope, have also been going on in parallel with the ionization chamber work for quite some years. There have been the following joint publications resulting from our collaborative efforts in cosmic ray research:

- (a) Spectra and Zenith Angle Dependence of Slow Muons in Hong Kong, Conference Papers - 12th International Conf. on Cosmic Rays, Vol. 3 pp.897-902 (1971);
- (b) August 1972 Cosmic Ray Event as observed at Different Stations by Identical Ionization Chambers, Sci. Papers I.P.C.R., Vol. 67, No.1, pp.1-6(1973);
- (c) Cosmic Ray Hourly Intensities during August 1-10, 1972, Report UAG-28, WDC-A for Solar-Terrestrial Physics, NOAA, USA (1973) pp.476-78;
- (d) Observation of Atmospheric Effects on Slow Muons, Proceedings on the 14th International Cosmic Ray Conference, pp.1387-92 (1975);
- (e) A Possibility of Underground Observation in Hong Kong, The Second International Cosmic Ray Symposium in Japan

(High Energy Cosmic Ray Modulation), Modulation (1976).

Presently, the muon telescope is used for cross-checking of the ionization chamber measurements on diurnal variation of cosmic-ray intensity in Hong Kong.

2. Neutron Activation Analysis: The neutron generator facility is equipped with sufficient specialized instrumentation for doing research in the areas of neutron activation analysis and gamma-ray spectrometry, radiation biology and dosimetry, and others. In addition to the 14 MeV neutron generator and the Ge(Li) gamma-ray spectrometer which are provided by the International Atomic Energy Agency, there are, a pulse-shape analyzer system incorporated with a liquid scintillator, a 3"x3" NaI(Tl) scintillation detector system and a fast pneumatic sample transfer system which was designed and fabricated with the collaboration of Tsing Hua University in Taiwan.

As this was the first neutron generating machine ever installed in the University, the radiation shielding scheme had been considered very carefully. A rigorous study of neutron leakage through a concrete-paraffin shielding which was built around the neutron generator was made (ref. 1. Shielding of Neutrons Generated by a 14 MeV Neutron Generator Installed in The Chinese University of Hong Kong, The First Asian Regional Congress on Radiation Protection, IARP 3/72, Bombay (1974); 2. Use of Monte Carlo Method in the Estimation of Fast Neutrons Leaked Through a Concrete-

Paraffin Shielding, Proceedings on the Conference on Nuclear Cross Sections and Technology, Washington D.C. Special Publication No.425, National Bureau of Standards, pp.426-30).

In order to benefit the community of Hong Kong careful consideration has been paid to what projects we should work on. The first project undertaken concerned the measurement of oxygen in steel. The accurate determination of Oxygen in steel is essential because oxygen-containing compounds, precipitated during solidification, have significant effects on the properties of some steels. Following the presently established method, analysis of one steel sample with ten repeated runs could be completed in 20 min. with a sensitivity high enough to determine an oxygen concentration of about 1 ppm in a 100 g steel sample. (ref. "Analysis of Oxygen Content in Steel by Means of 14 MeV Neutrons, Nuclear Engineering and Design, Vol. 34, No. 2 pp.255-67 (1975)). We then studied, partly in collaboration with the Chemistry Department of the University, a method to establish a rapid means for analyzing Chinese foodstuffs for protein information using 14 MeV neutron activation analysis. It was hoped that a rapid, reliable method of analysis could provide a significant first-step in a scientific study of such foodstuffs, which are becoming more readily accepted throughout the world, but of which little is known. A procedure requiring less than seven min

per sample, with a precision of about 2%, was developed. It was applied to the analysis of a wide variety (over 40) of foodstuffs (ref. "The 14 MeV Neutron Activation Analysis of Chinese Foodstuffs for Protein Content". Proceedings on Modern Trends in Activation Analysis, Vol 2, pp.938-46, Munich (1976)). Applying similar procedures used in the work with the Chinese foodstuffs, determination of nitrogen, and phosphorus and potassium in Chinese medicines of over 60 kinds has just recently been completed. We hope that this sort of information on the elemental constituents in Chinese medicines may serve as a reference to the study in biochemical aspects of Chinese medicines which is in progress at the Chinese Medicine Research Unit of the University. The 14 MeV neutron activation analysis for the protein content of various species of rice grains is now in process. Considering the large portion of the world population who eat rice and the need for proper nutrition, we feel our study will be of value if it can provide such information as, for instance what species of rice are more profitable to be grown. In collaboration with the Biology Department of the University, work on the effect of fire on nutrient cycling in a scrubby community is initiated. The part playable in our laboratory is analysis of the major nutrients e.g. N, P, K, in soil, plant tissues, and rain-water. Another project of collaboration is the study involving irradiation of *Monascus purpureus* with the 14 MeV neutrons. This study is to investi-

gate whether the physical factor, effect of neutrons, is also inhibitory or mutagenic to *Monascus purpureus*, a fungus used in Chinese medicine centuries ago.

In collaboration with the Art Gallery of the University work on study of the elemental contents of Chinese Bronze seals and coins using 14 MeV neutron activation analysis has been initiated. The chief advantage to this form of analysis is that it is non-destructive - something crucial in the study of such artifacts. From the study thus far obtained, we believe that in addition to providing general information which may prove useful to the archaeologist, there is a feasibility of categorizing such artifacts on the basis of their composition, or more likely, of using composition as a basis for establishing the authenticity of an artifact.

In collaboration with the Nuclear Reactor Group of Tsing Hua University of Taiwan, a study which concerns itself with environmental pollution, and in particular, involving the analysis of air particulates, is in progress. In this connection, arrangements have been made with the Government authority and the Professor of Chemistry of Hong Kong University to obtain air particulate samples collected under the present monitoring programmes. The samples will be irradiated in a nuclear reactor in Tsing Hua University and analyzed using the gamma-ray spectrometer system in our laboratory. Similar analysis have been carried out in other

major cities around the world, and on this basis it is expected that some 20-30 elemental concentrations could be measured including many elements that would be of particular interest to health authorities and environmentalists.

A new programme component "Nuclear Method in Environmental Research" has been introduced by the International Atomic Energy Agency. We have been asked, by the authority of IAEA, to participate in the project "Neutron activation analysis of pollutants in human hair using research reactors" which is the first step in implementing the mentioned component. It is believed that of all the components of the human organism hair has some peculiarities which make it an object of choice in starting a programme on environmental health research and monitoring. In this regard, collaboration with Tokyo Metropolitan University has been at sight in extending the work to cover the study for the natural radioactive components Sr-90, Ra-226, Th-232, etc., in the hairs.

3. Neutron Spectrometry and Dosimetry: For an appropriate use of the neutron generator, such as neutron activation analysis, study of biological effects of neutron irradiation and neutron radiotherapy, etc., a study of the energy distribution of the output neutrons from the neutron generator has to be made. We used a neutron spectrometer which is composed of an organic liquid scintillation detector and a pulse shape analyzer system for the measurements of the relative neutron energy spectra

around the target area. To determine an absolute neutron energy spectrum by means of the relative one measured, various kinds of threshold detectors were then applied for the determination of the differential neutron flux density. The analysis of the data for the final spectrum is in the final stage now.

When the neutron spectrum is known, a tissue-equivalent neutron dosimeter can be conveniently used for the determination of neutron dosage around the target where neutron irradiation of samples is to be made. We are trying to build a multiwire proportional counter type tissue-equivalent neutron dosimeter which has a merit of high sensitivity. Construction of the dosimeter has been made and we are now studying its characteristics and the possible uses for our neutron generator projects.

4. Nuclear Spectroscopy: In collaboration with the Department of Physics of the University of Hong Kong, we are looking into the possibility of refining the old data in nuclear spectroscopic works. This pursuit is thought to be possible by using the Ge(Li) gamma-ray spectrometer available in our laboratory. A work in gamma-gamma coincidence on the study of the level scheme of the nucleus Sb-125 is now in progress.
5. "Mössbauer Spectrometer: In collaboration with the Mössbauer Group of the Institute for Solid State Physics of The University of Tokyo we are starting on work in dosimetry by means of Mössbauer effects. The high radiation sources installed

in the University of Tokyo is essential in this type of work. Although, it is still not in the stage of action, we plan to extend our efforts, with collaboration of the Biochemistry Department of the University, on "Hemoglobin" and, with collaboration of the Art Gallery of the University, on archaeological problems both of them require much higher activity of the Mössbauer radioactive source which is still out of our financial range.

It has been illustrated that, presently, any research program is rather limited because of a shortage of finances and, more importantly, a shortage of manpower. It has also been illustrated that the possible solutions to the difficulties are by attracting financial suppliers with meaningful research topic and by collaboration with other groups and institutions with which partial solutions to the lack of manpower and equipments can be reached.

Fundamental Idea which is derived from the Concept of
Collaboration among Asian Countries

Akeo Misake, Yasushi Muraki* and Itaru Ohta**

Department of Physics, Saitama University, Urawa, Japan

*Cosmic Ray Laboratory, University of Tokyo

**Department of Physics, Utsunomiya University.
Utsunomiya, Japan

Abstract

Related to the concept of collaboration among Asian countries,
fundamental ideas are discussed.

LIST OF PARTICIPANTS

CHAN, S.K., Dept. of Physics,
University of Hong Kong.

CHUANG, L.S., Dept. of Physics,
Chinese University of Hong Kong.

COXELL, H., Dept. of Physics,
University of Hong Kong.

FONG, S.W., Dept. of Physics,
University of Hong Kong.

HUQ, M., Dept. of Physics,
University of Singapore.

KAKIMOTO, F., Dept. of Physics,
Tokyo Institute of Technology.

KAMATA, K., Cosmic Ray Laboratory,
University of Tokyo.

KAMIYA, Y., Dept. of Physics,
University of Nagoya.

KITAMURA, T., Cosmic Ray Laboratory,
University of Tokyo,

KONG, D.F.L., Hong Kong Telephone Co.,
Hong Kong.

LAU, K.S., Dept. of Applied Sciences,
Hong Kong Polytechnic.

LAU, S.Y., Dept. of Applied Sciences,
Hong Kong Polytechnic.

LEE, A.K. Dept. of Physics,
University of Hong Kong.

LEUNG, S.K., Dept. of Physics,
University of Hong Kong.

LI, Y.M., Dept. of Physics,
University of Hong Kong.

LUK, K.B. Heep Yun School,
Kowloon, Hong Kong.

MACKEOWN, P.K., Dept. of Physics,
University of Hong Kong.

MISAKI, A., Dept. of Physics,
Saitama University.

MIYAZAKI, Y., Institute of Physical and
Chemical Research, Tokyo.

MIZUTANI, K., Dept. of Physics,
Saitama University.

MURAKAMI, K., Institute of Physical and
Chemical Research, Tokyo.

NG, L.K., Dept. of Physics,
University of Hong Kong.

NISHIMURA, J., Institute of Space Science,
University of Tokyo.

OHTA, M., Dept. of Physics,
Kinki University, Osaka.

OKADA, A., Cosmic Ray Laboratory,
University of Tokyo.

PATHAK, K.M., Dept. of Physics,
University of Gauhati.

POON, C.H., Dept. of Physics,
University of Hong Kong.

POON, K.H., Dept. of Physics,
University of Hong Kong.

SHIN, F.G., Dept. of Applied Sciences,
Hong Kong Polytechnic.

WALKER, G.O., Dept. of Physics,
University of Hong Kong.

YEN, E., Dept. of Physics,
National Taiwan University.

YOUNG, K.K.H., Dept. of Physics,
Chinese University of Hong Kong.

AUTHOR INDEX

Aguirre C.	147	MacKeown P.K.	126, 147
Akashi M.	4	Mejia G.R.	147
Aoki T.	94,	Mikamo S.	94, 133
Basu D.	50, 57	Minorikawa Y.	94, 133
Bhattacharyya D.P.	50, 157, 141	Misaki A.	4, 73, 216, 217, 252
Chan S.K.	5	Mishima Y	34
Chaudhuri N.	44, 70	Mito I.	4, 216
Chuang L.S.	25, 240	Mitsui K.	94, 95, 133
Fong S.W.	117, 197	Miyake S.	94, 133
Goswami D.C.	117, 188	Mizumoto Y.	147
Higashi S.	94, 133	Mizutani K.	4, 64
Honda K.	94, 133	Murakami K.	34, 147
Huq M.	204	Muraki Y.	94, 133, 252
Iida S.	94, 133	Nayano M.	147
Inoue A.	34	Nagashima K.	34
Kakimoto F.	147	Nakamura I.	94, 133
Kamata K.	148, 218	Ng L.K.	74, 112, 117, 197
Kamiya Y.	94, 133	Nishi K.	147
Kaneko T.	147	Nishimura J.	73, 96
Karmakar N.L.	44, 70	Ohashi Y.	94, 133
Kasahara K.	4	Ohta I.	4, 64, 252
Kawashima H.	94, 133	Ohta M.	234
Kitamura T.	81, 94, 133	Okada A.	94, 95, 133
Kobayakawa K.	94, 133	Ozaki S.	94, 133
Komori H.	65	Pathak K.M.	177, 188
Konishi E.	217	Paul C.R.	44, 70
Lai C.C.	117	Poon C.H.	112
Lau K.S.	5	Roychoudhury R.K.	50, 141
Lau S.Y.	74	Sagisaka S.	34
Lee A.K.	160	Sarkar K.	57, 141
Leung S.H.	117	Shibata H.	94, 133
Leung S.K.	117	Shibata M.	4, 95, 133
Luk K.B.	227		

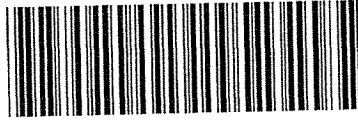
Shirai T.	4
Singhal K.P.	111
Suga K.	147
Taira K.	4
Taira T.	4
Takahashi T.	133
Takahashi Y.	4, 94
Tateyama N.	4
Teramoto Y.	94, 133
Torii S.	4
Toyoda Y.	147
Verma S.D.	226
Wada M.	25
Watanabe G.	4
Watanabe Z	217
Yoshii H.	147
Yuda T.	4

M25919415

539.7223 A83

X 539 7223 A83

M25919415



539.7223

1259194

Asian Cosmic Ray Symposium on
Secondary Cosmic Rays, Hong Kong,
1976.

Proceedings ... [1977]

Date Due	1259194
5/11/78	22 MAY 1978
6/27/78	27 JUN 1978
18 AUG 1978	
18 OCT 1978	
20 NOV 1978	
